THE UNIVERSITY OF CHICAGO

COUPLED-CLUSTER RESPONSE THEORY: PARALLEL ALGORITHMS AND NOVEL APPLICATIONS

A DISSERTATION SUBMITTED TO
THE FACULTY OF THE DIVISION OF THE PHYSICAL SCIENCES
IN CANDIDACY FOR THE DEGREE OF
DOCTOR OF PHILOSOPHY

DEPARTMENT OF CHEMISTRY

BY
JEFFREY RICHARD HAMMOND

CHICAGO, ILLINOIS
JUNE 2009

TABLE OF CONTENTS

LIST OF FIGURES

LIST OF TABLES

ABSTRACT

The parallel implementation of coupled-cluster response theory within NWChem and its subsequent application to novel chemical problems is reported. Linear-response dipole polarizabilities of polyacenes, the 60-carbon buckyball, and larger water clusters were computed with coupled-cluster singles and doubles (CCSD) and compared to density-functional results. The complete treatment of coupled-cluster response theory including up to triples (CCSDT) was applied to diatomic molecules using large basis sets and this method was used to evaluate a newly-developed perturbative approximation for triples. Hyperpolarizabilities and Lennard-Jones coefficients were implemented at the CCSD level of theory by extending the linear response code in two different ways. Benchmark hyperpolarizabilities are reported for molecules as large as para-nitroaniline using large basis sets. Tensor transpose algorithms are shown to be an important component in a coupled-cluster property code and automatic code generation successfully identified faster algorithms for these.

ACKNOWLEDGEMENTS

My academic success would not have been possible if not for an the efforts of many, many people. The support of my family and friends as well as the tireless effort of many teachers, professors and scientists provided me with the means by which I have come to the end of 22 years of formal education.

My wife Meghan has been integral part of my success in graduate school. She patiently guided me through the most difficult periods in my graduate career and continues to put up with my enthusiastic nerdiness when things go well. Meghan also proofread this thesis, a heroic task for a cultural anthropogist. My family — Alice, Betsy Greg, Rich and Vance[1] — has been extremely supportive during graduate school, some of them even so far as to suffer through reading my papers. My parents have supported throughout my life in all things, but particularly my scientific pursuits. My mom went to extraordinary lengths to saturate my thirst for scientific knowledge as a child, going so far as to read me the John Deere product line technical specifications and taking me to see every piece of large mechanical equipment being operated in the Seattle area. My dad has always encouraged me to do extraordinary things but also tries to keep me humble.

Karol Kowalski has been a wonderful teacher, collaborator and friend during the past three years. He taught me everything I know about coupled-cluster theory and supervised the majority of the research presented in this thesis. Bert de Jong supervised the early stages of my work on NWChem during the summer of 2006

[1] All lists of names in this chapter are given in alphabetical order.

and has supported my work in numerous ways since then, not the least of which is allowing me developer access to NWChem. I am especially grateful to Tim Carlson and Dunyou Wang at PNNL for their help with numerous hardware and software issues. These four and others at PNNL — Eric Bylaska, Steve Elbert, Peng-Dong Fan, Kevin Glass, Niri Govind, Pat Nichols and Sotiris Xantheas — were the source of many enlightening scientific discussions as well as my only friends during the four months I lived in Richland. The EMSL MSCF consultants played an integral role in my work, not the least of which was their patience on the numerous occasions that my jobs brought down some or all of Chinook during its pre-acceptance stage.

I thank Karl Freed and Ridg Scott for their encouragement and support, both administratively and intellectually; I could not have asked for better advisors. While I did not solve all of the interesting problems they presented me with during graduate school, I hope to elucidate at least some of them in the near future. Rajat Chaudhuri and Glen Hocky group provided me enlightening discussions as well as technical assistance during my time in the Freed group. Ridg and his confederates — Peter Brune, Matt Knepley and Andy Terrel — deserve much credit for their immense patience with my ignorance of computer science and applied mathematics and for helping me to overcome it. Benoît Roux provided me with a number of interesting scientific problems which push the limits of theory and computation in quantum chemistry; sadly, time did not permit me to describe progress on those fronts in this thesis. I learned a great deal about chemistry and about life from my classmates in the chemistry department, especially Benj FitzPatrick, Greg Gidofalvi, Margaret Herschberger, Stefan Kilyanek, Jason Montgomery and Shannon Stewman. Finally, I thank Aaron Dinner and Greg Engel for serving on my committee with Karol and Karl. Comments from my committee members greatly improved the readability and

correctness of the forthcoming text.

Many people have encouraged my work in science. I greatly appreciated encouragement from Rod Bartlett and Fritz Schaefer, as much of my work was accomplished by standing on their shoulders. Garnet Chan, Robert Harrison, Chris Rinderspacher and Ed Valeev have been good friends and taught me a great deal about computational chemistry. The CSGF program has provided with numerous friends and talented colleagues who have broadened my intellectual outlook and made yearly visits to Washington, D.C. quite fun.

I am grateful for the many excellent science teachers I have had over the years. Ed Beardslee and math team coaches like Mr. Edmunds and Ms. Smith (now Mrs. Clymer) provided me with the foundation in mathematics which made my career in science possible. Mrs. Richards and Mrs. Fitzgerald forced me to write properly,[2] which is just a valuable a skill for a professional scientist as integral calculus or computer programming. Mr. Zink at Highline High School inspired me to be a chemist by showing me that chemistry is the essence of some many essential and amusing events. At the University of Washington, Nic Epiotis inspired me to become a theoretical chemist, Bill Reinhardt inspired me to become a physical chemist and Eric Brown inspired me to be quantum chemist. The advice Bill and Eric gave me in regards to graduate school and other career choices was invaluable. Finally, Wes Borden and Dave Hrovat showed me what it means to do research and providing me with the foundation upon which my graduate career has been built. I have been especially fortunate to have as supervisors for both my undergraduate (Wes Borden) and graduate (Karl Freed) theses two of the most principled scientists I have ever known.

[2]Any deviations from proper writing in this thesis are exclusively the fault of the author.

I would be a fool not to thank the people in this world with real power. In addition to their invaluable assistance in practical matters, Pegg Anderson, Don Bradley and John Phillips displayed superlative kindness to me throughout my tenure in the James Franck Institute. Vera Dragisich and Melinda Moore work tirelessly on behalf of graduate students in my department and while I have no basis for comparison, I cannot imagine my graduate studies would have gone so smoothly if not for them. Xena Anderson and Rosemary Garrison provide equally zealous support for graduate students in the James Franck Institute. Finally, I thank Martina Munsters, Rick Hefley and Christopher Myers for their help during the darkest period of my graduate career.

My graduate studies were supported by a Department of Energy Computational Science Graduate Fellowship (DE-FG02-97ER25308), administered through the Krell Institute, and by a Harvey Fellowship from the Mustard Seed Foundation. Administrators of these fellowships — Martin Edelson, Duane Grobman, Rachel Huisman, Mary Ann Leung and John Ziebarth — were a source of encouragement and support throughout my time at the University of Chicago. After meeting my wife, the CSGF program was the best thing to happen to me during graduate school.

Computational resources at Pacific Northwest (PNNL) and Argonne (ANL) National Laboratries and the National Energy Research Scientific Computing Center (NERSC) were critical to the completion of my work. Some of these resources were provided under the following allocations:

- *High accuracy modeling of frequency-dependent polarizabilities: exploring the cutting edge limits of NWChem* (PNNL).

- *QM/MM simulation of nonlinear optical and Raman spectroscopy of molecules*

in solution using coupled-cluster response theory (NERSC).

- *Testing and tuning NWChem for BlueGene/P and studies of nonlinear optical properties of conjugated chromophores* (ANL).
- *Development of accurate methods for non-bonded interactions in biological and acqueous environments* (PNNL).
- *Ultra-high accuracy simulations for large molecular systems: Exploring the Cutting Edge Limits of NWChem* (PNNL).

In addition, I benefited from access to computational resources at the National Center for Supercomputing Applications (NCSA) at the University of Illinois, the Ohio Supercomputing Center (OSC) and the Sony-Toshiba-IBM Center of Competence at Georgia Institute of Technology as well as the Department of Chemistry, the Department of Computer Science and the Computational Institute (CI) at the University of Chicago

In total, I used close to ten million hours of computing time during the course of my thesis research.

Development of my NWChem codes for molecular properties was greatly assisted by the no-cost and open-source distribution of three computational chemistry programs:

- DALTON 2.0, see http://www.kjemi.uio.no/software/dalton/dalton.html.
- Aces II (Mainz-Austin-Budapest), see http://www.aces2.de.
- PSI3, see http://www.psicode.org.

ECCE, JMol and Molden were used extensively to create and interpret the structures of complex molecules.

The research reported in this thesis would not have been possible without no-cost licenses to the following software: OpenMPI, MPICH, BLAS, ATLAS, GotoBLAS and, most importantly, the GNU/Linux collection, particularly GCC. The code described herein was written using VI and KDevelop. This thesis has been typeset exclusively in LaTeX with Kile using the thesis template of Bryan Clair and Nathan Dunfield provided to me by Greg Gidofalvi. All plots have been generated using Gnuplot. OpenOffice and Python were used extensively in the analysis data. Firefox and Google Scholar were invaluable in almost every aspect of my research.

Some men see things as they are and say why —

I dream things that never were and ask, "Why not?"

Robert Kennedy

(paraphrasing George Bernard Shaw)

CHAPTER 1

INTRODUCTION

This thesis focuses on the computation of electric properties of molecules using massively-parallel computers. While significant effort has been devoted to the development of software for computing the ground-state energy at various levels of approximation, proportionally little effort has been spent on software for molecular properties, particularly those corresponding to higher-order derivatives. Over the last three years, I have implemented coupled-cluster linear response polarizabilities for singles and doubles (CCSD), singles, doubles and triples (CCSDT), and singles, doubles, triples and quadruples (CCSDTQ) within the massively-parallel chemistry software package NWChem. In each case, mine was the first parallel implementation of coupled-cluster response theory reported, and it has allowed the study of chemical problems of unprecedented scale. In addition, code for CCSD quadratic response hyperpolarizabilities and linear response C_6 coefficients was developed. The following chapters describe these chemical applications and the associated theory which was implemented to compute the response properties of interest.

Despite the obvious fact that experiments are the only direct means to probe the physical world, there are numerous reasons to simulate models of reality. It is important to recognize that computational chemistry only simulates models of reality, but within a particular model, the results are directly interpretable. When a variational calculation of the water molecule for a fixed geometry within a specified basis produces a value for the ground-state energy, that is the exact ground-state

energy *within that model of reality*. In contrast, experiments directly probe reality but are only indirectly interpretable. Physical chemistry experiments do not produce as output bond-lengths or energy differences, experiments produce electrical signals which are converted into spectra by the apparatus. Only when the scientist interprets this spectra using a model for the system subject to interrogation does s/he obtain the data of interest. Because of the difficulty associated with interpreting spectra, there is a long history of synergy between experimental and theoretical work in this regard. Three experiments where theory was critical to attain the correct interpretation of molecular spectra are:

- methylene (CH_2) — is it bent or linear? (Ref. [1])
- methylene — ground-state singlet or triplet? (Ref. [2])
- benzaldehyde — what is the barrier to internal rotation? (Ref. [3])

Additional evidence for the importance of this type of synergy is that the two quantum chemistry papers most recently published in *Science* were authored jointly by theorists and experimentalists [4]. Additional examples of the important role of interplay between theory and experiment are too numerous to list.

The second role of theory is to explain *why* nature behaves a certain way. Any chemist can state authoritatively that water is a liquid at room temperature, since regular encounters with liquid water are necessary to sustain human life. However, why is water a liquid at room temperature? Ammonia and hydrogen fluoride are not, despite having the same number of electrons (10) and protons (10) as water. Hydrogen sulfide is also not a liquid at room temperature, despite having a similar valence character. More importantly, why is water necessary for human life while ammonia,

hydrogen fluoride and hydrogen sulfide are quite contrary to it? Experiments can provide data on these phenomena, but only theory can explain why. Computation allows us to test theories in ways experiment cannot, either due to genuine impossibility or impracticality.

Consider, for example, the question of where a metal atom is positioned when complexed with a fullerene [5]. Experimental data reveals a massive dipole polarizability but does not produce relative coordinates for the metal with respect to the fullerene. Computation, however, provides us an opportunity to test three possible hypotheses for the geometric configuration of the aforementioned system: (1) the metal sits on the outside surface of the fullerene, (2) the metal sits on the inside surface of the fullerene, or (3) the metal floats near the center of the fullerene. For each of these three configurations, one can compute the dipole polarizability and compare the results to the experiment. Provided the computed approximation is sufficiently accurate for this instance, it can conclusively resolve which geometric configuration is present in the experiment. This approach will fail, however, if the computation is not able to resolve the structures from each other with fine enough resolution, of if the theoretical model used in the computation is inadequate.

The aforementioned scenario is one of many motivations for developing the computational tools reported in this thesis. When I first started writing the coupled-cluster property code in NWChem in the summer of 2006, the largest molecular system which had been treated with the coupled-cluster singles and doubles approximation (CCSD) was benzene [6], and then only using a modest basis set. Although CCSD was known to produce accurate results for diatomic molecules, it was not known at that time if CCSD was a sufficiently complete theoretical model of electron correlation for the computing dipole polarizabilities of benzene. I became aware of serious

deficiencies in the density-functional formalism for electric-field properties (see Ref. 1 of Ch. 2) around that time and set out to try and understand what the necessary and sufficient computational approximations were for computing polarizabilities. Subsequently, it was discovered that for larger systems (including benzene), the role of triple excitations was small for polarizabilities. In addition, benchmark calculations were performed starting with benzene and eventually reaching C_{60}, nearly an order of magnitude larger, a significant feat given the CCSD model scales to the sixth-power in the system size. These results were used to evaluate numerous approximate methods with lower computational cost, particularly density-functional theory (DFT). Because of the large-scale benchmarks performed using my code, DFT property calculations can now be performed with greater confidence on larger chemical systems, enabling exploration of an ever greater set of experimental questions.

Unlike for experimental work, for computational models in chemistry, calibration is significantly more difficult than the application of those models to the systems of interest. An experimental apparatus might be calibrated with a pure solvent before studying solvent rearrangement in the vicinity of a photo-excited chromophore, but the pure solvent experiment takes very little time if the machine is functioning properly. However, what is the "pure solvent" of computational chemistry? The conventional view is that one should perform high-level calculations on a model system to determine the sufficient approximation required for use with a more complex system not amenable to accuracy, expensive approximations. However, if the model system does not adequately represent the complex system, the calibration step is meaningless. The most common excuse for inadequate calibration is that the computational expense of a thorough benchmark study is infeasible. That the acquisition of many of the computational results reported in the following chapters required a supercom-

puter was one of the most important reasons why they were performed. After decades of study, the coupled-cluster approximation has emerged one of the pillars of quantum chemistry [7] and is a universally respected benchmark method for many kinds of chemical phenomena. The implementation of coupled-cluster property methods within a massively-parallel software package has already revealed new insight into the computation of electric-field properties and will continue to do so for many years. My work has shown that it is possible to accurately reproduce experimental values for large systems using the same systematic approach employed for small molecules. There is also some evidence that this task is actually easier for larger systems because the complexity of the experiments grows rapidly, whereas the computational approach willfully exclude the phenomena which keep experimentalists up at night. Resolving which level of electron correlation treatment or basis set is necessary for a certain level of accuracy can be addressed separately from vibrational effects, optical dispersion or sample purity. The absence of such luxuries in experimental methods indicates that the synergy between theory and experiment will increase as experiments grow increasingly complex and computational methods grow in utility due to advances in software and hardware.

The exploitation of ever-more-powerful supercomputers by developing massively-parallel scientific software is one of the fundamental goals of this work. As more supercomputers are installed at colleges and universities around the world, the impressive results reported here will become pedestrian. The transformation of rare and difficult scientific tasks into ubiquitous and easy ones is a central theme in computational chemistry and one to which I hope my work contributes.

1.1 Overview

A reasonably complete presentation of coupled-cluster response theory and its implementation within NWChem is provided in Chapter 2. Chapter 3 presents the application of coupled-cluster response theory to polyacenes. Chapter 4 is a natural extension of the polyacene study to the C_{60} fullerene. Polarizabilities of water clusters are the subject of Chapter 5. Chapter 6 reports on the extension of coupled-cluster response theory to the CCSDT level of theory, while Chapter 7 discusses a non-iterative approximation for triples.

In Chapter 8, I move outside of realm of polarizabilities to the computation of C_6 coefficients. Hyperpolarizabilities are the subject of Chapter 9. The integration of coupled-cluster response theory into the NWChem QM/MM module is the focus of Chapter 10. Finally, Chapter 11 analyzes the bottleneck serial operations in the NWChem coupled-cluster property code and presents a rudimentary auto-tuning library to generate these kernels. Chapter 12 summarizes the conclusions while Chapter 13 includes some of my vision for the future of computational chemistry.

1.2 Omissions

This thesis focuses exclusively on response properties and their implementation within NWChem. As such, I have omitted the following material which I also completed during graduate school.

- R. K. Chaudhuri, J. R. Hammond, K. F. Freed, S. Chattopadhyay and U. S. Mahapatra, *J. Chem. Phys.* **129**, 064101 (2008). "Reappraisal of *cis* effect in 1,2-dihaloethenes: An improved virtual orbital (IVO) multi-reference approach."

- J. R. Hammond and D. A. Mazziotti, *Physical Review A***73**, 062505 (2006). "Variational reduced-density-matrix calculation of the one-dimensional Hubbard model."

- J. R. Hammond and D. A. Mazziotti, *Physical Review A***73**, 012509 (2006). "Variational reduced-density-matrix calculations on small radicals: a new approach to open-shell ab initio quantum chemistry."

- J. R. Hammond and D. A. Mazziotti, *Physical Review A***71**, 062503 (2005). "Variational two-electron reduced-density-matrix theory: Partial 3-positivity conditions for N-representability."

In additional to the aforementioned omissions, Raman cross-sections computed by numerical differentiation of the linear-response polarizability are not reported, nor is a comparative study of density-functional and coupled-cluster polarizabilities for molecules relevant to the pharmaceutical industry.

1.3 Background Material

The coupled-cluster (CC) method — which will be described in detail in the next chapter — solves the electronic — i.e., Born-Oppenheimer [8] — Schrödinger equation [9] in the basis set of one-electron orbitals which are produced by a Hartree-Fock [10] calculation performed in a finite atomic-orbital basis set [11]. Although CC can be used to solve the Schrödinger equation for other types of Hamiltonians [12, 13], these applications will not be considered.

The reader is encouraged to consult some or all of the following material, which contain introductory presentations of second-quantization, Hartree-Fock theory and electron-correlation methods:

- A. Szabo and N. S. Ostlund, *Modern Quantum Chemistry: Introduction to Advanced Electronic Structure Theory*, (McGraw-Hill, New York, 1989).

- T. Helgaker, P. Jørgensen and J. Olsen, *Molecular Electronic-Structure Theory*, (Wiley, Chichester, 2000).

- D.R. Yarkony, ed., *Modern Electronic Structure Theory*, (World Scientific, Singapore, 1995).

1.4 Unit conventions

Unless otherwise noted, all quantities are given in atomic units. The convention that Planck's constant ($\hbar$) and the permittivity of free space (ϵ_0) are unity will be used throughout. As these quantities have no impact on the mathematics within this convention, they will be omitted.

REFERENCES

[1] C. F. Bender and H. F. Schaefer, *J. Am. Chem. Soc.* **92**, 4984 (1970); H. F. Schaefer, *Science* **231**, 1100 (1986).

[2] P. J. Hay, W. J. Hunt and W. A. Goddard III, *Chem. Phys. Lett.* **13**, 30 (1972); L. B. Harding and W. A. Goddard III, *J. Chem. Phys.* **67**, 1777 (1977); W. A. Goddard III, *Science* **227**, 917 (1985).

[3] L. D. Speakman, B. N. Papas, H. L. Woodcock and H. F. Schaefer III, *J. Chem. Phys.* **120**, 4247 (2004).

[4] O. Geβner, A. M. D. Lee, J. P. Shaffer, H. Reisler, S. V. Levchenko, A. I. Krylov, J. G. Underwood, H. Shi, A. L. L. East, D. M. Wardlaw, E. t. H. Chrysostom, C. C. Hayden and Albert Stolow, *Science* **311**, 219 (2006); M. H. Kim, L. Shen, H. Tao, T. J. Martinez and A. G. Suits, *Science* **315**, 1561 (2007).

[5] D. Rayane, R. Antoine, Ph. Dugourd, E. Benichou, A. R. Allouche, M. Aubert-Frécon, and M. Broyer, *Phys. Rev. Lett.* **84**, 1962 (2000).

[6] A. Rizzo, C. Cappelli, B. Jansík, D. Jonsson, P. Sałek, S. Coriani, and H. Ågren, *J. Chem. Phys.* **121**, 8814 (2004).

[7] R. J. Bartlett and M. Musiał, *Rev. of Mod. Phys.* **79**, 291 (2007).

[8] M. L. Born and R. Oppenheimer, *Ann. Phys.* **84**, 457 (1927).

[9] E. Schrödinger, *Phys. Rev.* **28**, 1049 (1926); E. Schrödinger, *Ann. Phys.* (Paris) **386**, 109 (1926).

[10] V. Fock, *Z. Phys.* **61**, 126 (1930); C. C. J. Roothaan, *Rev. Mod. Phys.* **23**, 69 (1951); D. R. Hartree, *The Calculation of Atomic Structures*, (Wiley, New York, 1957).

[11] S. F. Boys, *Proc. Roy. Soc. Lond.* **A258**, 402 (1960).

[12] J. H. Heisenberg and B. Mihaila, *Phys. Rev. C* **59**, 1440 (1999); K. Kowalski, D. J. Dean, M. Hjorth-Jensen, T. Papenbrock, and P. Piecuch, *Phys. Rev. Lett.* **92**, 132501 (2004).

[13] O. Christiansen, *J. Chem. Phys.* **120**, 2149 (2004).

CHAPTER 2

COUPLED-CLUSTER RESPONSE THEORY AND NWCHEM

2.1 Coupled-cluster theory

The coupled-cluster (CC) method was first developed in the nuclear physics community [1, 2], but was subsequently adopted for atomic and molecular problems [3, 4, 5, 6, 7, 8, 9, 10, 11]. It is one of the most popular methods in quantum chemistry, and has been implemented within all major software packages, including Aces II [12, 13], Dalton [14], GAMESS [15, 16], Gaussian [17], Molpro [18, 19], NWChem [20, 21], PSI3 [22] and QChem [23] as well as the very recently released Aces III [24] and CFOUR [25]. Some of the earliest implementations of CC within software packages were Aces [26] (developed in Rod Bartlett's group), PSI [27, 28] (developed in Fritz Schaefer's group) and TITAN [29]. This is not meant to be a complete historical record of software development for CC; the interested reader is encouraged to investigate the literature for possible omissions.

2.1.1 The coupled-cluster energy equations

The CC wavefunction ansatz is

$$|\Psi_{CC}\rangle = \exp(T)|\Phi\rangle \tag{2.1}$$

where $|\Phi\rangle$ denotes the reference functions, usually chosen as the Slater determinant obtained from a Hartree-Fock SCF calculation, and the cluster operator, T, is given by

$$T = T_1 + T_2 + \cdots + T_M \tag{2.2}$$

$$T_m = \frac{1}{(m!)^2} \sum_{i_1,\ldots,i_m} \sum_{a_1,\ldots,a_m} t_{i_1\ldots i_m}^{a_1\ldots a_m} \hat{a}_{a_1}^\dagger \ldots \hat{a}_{a_m}^\dagger \hat{a}_{i_m} \ldots \hat{a}_{i_1} \ , \tag{2.3}$$

where $\hat{a}_p^\dagger$ ($\hat{a}_p$) are the creation (annihilation) operators. The $i_1, i_2, \ldots$ ($a_1, a_2, \ldots$) indices refer to occupied (unoccupied) spin-orbitals in the reference $|\Phi\rangle$. For the exact theory the N parameter corresponds to the total number of correlated electrons (N), while all practical approximate formalisms use $M \ll N$. The quantities $t_{i_1\ldots i_m}^{a_1\ldots a_m}$ are referred to as the cluster amplitudes. With the exception of CCSD ($M = 2$), the CC method is limited by the computational storage of the cluster amplitudes, which scales as $o^m v^m$, and the associated floating point computation, which scales as $o^m v^{(m+2)}$. For CCSD, the memory bottleneck is the storage of the two-electron integrals in the molecular orbital basis, which requires $(o + v)^4$ storage when using the conventional method. Algorithms which are based partially or fully upon atomic integrals have different performance characteristics (See [19, 30].

The standard CC energy expression is obtained by projecting the standard energy eigenvalue relationship onto $\langle 0| \exp(-T)$,

$$E_{CC} = \langle \Phi| \exp(-T) H \exp(T) |\Phi\rangle. \tag{2.4}$$

The CC similarity-transformed Hamiltonian, $\overline{H} = \exp(-T) H \exp(T)$, will be used to simplify subsequent equations. From the Baker-Campbell-Hausdorff expansion, we

see that

$$\overline{H} = H + [H,T] + \frac{1}{2!}[[H,T],T] + \frac{1}{3!}[[[H,T],T],T] + \frac{1}{4!}[[[[H,T],T],T],T] \; , \quad (2.5)$$

where the expansion in commutators stops at four when there are only two-body interactions. In this case, there are only four indices on H and thus it can be connected with no more than four cluster operators, T.

Projection of the $\overline{H}$ onto m-fold ($m = 1, \ldots, M$) excitation manifolds defines the CC energy equations:

$$\begin{aligned} 0 &= \langle \Phi^{a_1 \ldots a_m}_{i_1 \ldots i_m} | \overline{H} | \Phi \rangle & (2.6) \\ |\Phi^{a_1 \ldots a_m}_{i_1 \ldots i_m}\rangle &= \hat{a}^\dagger_{a_1} \ldots \hat{a}^\dagger_{a_m} \hat{a}_{i_m} \ldots \hat{a}_{i_1} |\Phi\rangle \; . & (2.7) \end{aligned}$$

Choosing $m = 1, \ldots, M$ ensures that the number of equations is the same as the number of unknowns.

The effective Hamiltonian within the CCSD approximation is

$$\begin{aligned} \overline{H} &= H + [H, T_1 + T_2] + \frac{1}{2!}[[H, T_1 + T_2], T_1 + T_2] \\ &\quad + \frac{1}{3!}[[[H, T_1 + T_2], T_1 + T_2], T_1 + T_2] \\ &\quad + \frac{1}{4!}[[[[H, T_1 + T_2], T_1 + T_2], T_1 + T_2], T_1 + T_2] \; , \quad (2.8) \end{aligned}$$

which leads to the following set of equations,

$$
\begin{aligned}
E_{CCSD} &= \langle\Phi|H + [H, T_1 + T_2] + \frac{1}{2}[[H, T_1], T_1]|\Phi\rangle && (2.9)\\
0 &= \langle\Phi_i^a|H + [H, T_1 + T_2]|\Phi\rangle + \frac{1}{2}\langle\Phi_i^a|[[H, T_1], T_1]|\Phi\rangle \\
&\quad + \langle\Phi_i^a|[[H, T_1], T_2]|\Phi\rangle + \frac{1}{6}\langle\Phi_i^a|[[[H, T_1], T_1], T_1]|\Phi\rangle && (2.10)\\
0 &= \langle\Phi_{ij}^{ab}|H + [H, T_1 + T_2]|\Phi\rangle + \frac{1}{2}\langle\Phi_{ij}^{ab}|[[H, T_1 + T_2], T_1 + T_2]|\Phi\rangle \\
&\quad + \frac{1}{2}\langle\Phi_{ij}^{ab}|[[[H, T_1], T_1], T_2]|\Phi\rangle \\
&\quad + \frac{1}{24}\langle\Phi_{ij}^{ab}|[[[[H, T_1], T_1], T_1], T_1]|\Phi\rangle\ , && (2.11)
\end{aligned}
$$

which define the CCSD method. Many terms from $\overline{H}$ disappear upon projection onto singles and doubles. For example, $[[[[H, T_2], T_2], T_2], T_2]|\Phi\rangle$ can only be projected only the hextuply-excited manifold (Eqn. 2.7 for $m = 6$). Further simplications can be made if H is separated into the Fock operator F and the fluctuation potential V. The CCSD equations are carefully derived in the review by Crawford and Schaefer [9].

Even though Eqn. 2.6 represents a set of nonlinear equations, they are almost exclusively solved via linearization. Eqns. 2.10 and 2.10 are solved via Jacobi iteration [31], frequently combined with the DIIS method of Pulay [32], which is closely related to Krylov-subspace methods [33]. Recently, a conjugate residual method for solving the CC equations was reported [34] which has the potential to require less memory than the Jacobi-DIIS method as well as converge more robustly for non-canonical (i.e. local) formulations of CC. Because the residual of Eqn. 2.6 can be formed with $o^m v^{(m+2)}$ computational cost and $o^m v^m$ storage even though the Jacobian thereof is dimension $o^m v^m \times o^m v^m$ and dense, it is impractical to employ methods which require the explicit formation of the Jacobian for solving the CC

equations.

2.1.2 First derivatives of the energy

Molecular property calculations require energy derivatives, which can be symbolically represented by dE/dx where x is a parameter that defines the electronic Hamiltonian $H(x)$ (for simplicity, we will denote this Hamiltonian by H). For example, x can correspond to the nuclear coordinate in the case of gradients or an external electric-field in the case of dipole moments. Straightforward differentiation of the CC energy functional in Eq. 2.4,

$$\frac{dE_{CC}}{dx} = \langle 0|\overline{\frac{\partial H}{\partial x}}|0\rangle + \langle 0|\left[\overline{H}, \frac{\partial T}{\partial x}\right]|0\rangle \ , \tag{2.12}$$

requires amplitude derivatives for every perturbation parameter, x. We obtain the equations for the first-derivative amplitudes by differentiating Eq. 2.6,

$$0 = \langle X|\overline{\frac{\partial H}{\partial x}}|0\rangle + \langle X|\left[\overline{H}, \frac{\partial T}{\partial x}\right]|0\rangle \ , \tag{2.13}$$

where $|X\rangle$ denotes an arbitrary excited-state manifold (Eqn. 2.7). In the case of CCSD, $|X\rangle = |S\rangle + |D\rangle$ where $|S\rangle$ and $|D\rangle$ are the singles and doubles manifold, respectively, which correspond to $m = 1$ and $m = 2$ in Eqn. 2.7. Upon insertion of the resolvent[1] becomes

$$\langle X'|\frac{\partial T}{\partial x}|0\rangle = -\left\{\langle X|\overline{H}|X'\rangle\right\}^{-1}\langle X|\overline{\frac{\partial H}{\partial x}}|0\rangle. \tag{2.14}$$

[1]The resolvent is $|X'\rangle\langle X'|$ for all relevant excited-state manifolds X'. Insertion of the resolvent preserves the connectedness previously enforced via the commutator.

This equation can be inserted into Eq. 2.12 along with the resolvent to give

$$\frac{dE_{CC}}{dx} = \langle 0|\overline{\frac{\partial H}{\partial x}}|0\rangle - \langle 0|\overline{H}|X'\rangle \left\{\langle X|\overline{H}|X'\rangle\right\}^{-1} \langle X|\overline{\frac{\partial H}{\partial x}}|0\rangle \ , \tag{2.15}$$

which leads to the perturbation-independent Λ-equations [35],

$$\langle 0|\Lambda|X\rangle = -\langle 0|\overline{H}|X'\rangle \left\{\langle X|\overline{H}|X'\rangle\right\}^{-1} \ . \tag{2.16}$$

The amplitudes defined by Eqn.2.16 are Lagrange multipliers that provide a new energy functional which satisfies the generalized Hellman-Feynman theorem [36],

$$\widetilde{E}_{CC} = \langle \Phi|(1+\Lambda)\overline{H}|\Phi\rangle, \tag{2.17}$$

where

$$\Lambda = \Lambda_1 + \Lambda_2 + \cdots + \Lambda_M \tag{2.18}$$

$$\Lambda_m = \frac{1}{(m!)^2} \sum_{i_1,\ldots,i_m} \sum_{a_1,\ldots,a_m} \lambda^{i_1\ldots i_m}_{a_1\ldots a_m} \hat{a}^\dagger_{i_1} \ldots \hat{a}^\dagger_{i_m} \hat{a}_{a_m} \ldots \hat{a}_{a_1} \ . \tag{2.19}$$

Thus, any first-order property can be computed using an expectation-value like equation; for example, the dipole moment is computed with

$$\mu = \langle \Phi|(1+\Lambda)\hat{\overline{\mu}}|\Phi\rangle \ , \tag{2.20}$$

where $\overline{\mu} = \exp(-T)\mu\exp(T)$. The density matrices [37] required for CC analytic gradients [35] are also computable with this approach when the dipole operator μ is replaced with the 1- and 2-particle reduced-density-operators (RDOs).

The Lagrange multipliers are solved via projection onto n-fold excitation manifolds on the right

$$0 = \langle \Phi | (1 + \Lambda) \overline{H} | \Phi^{a_1 \ldots a_m}_{i_1 \ldots i_m} \rangle. \tag{2.21}$$

The first-derivatives of the energy with respect to any parameter can now be written

$$\frac{dE_{CC}}{dx} = \langle \Phi | (1 + \Lambda) \overline{\frac{dH}{dx}} | \Phi \rangle. \tag{2.22}$$

2.1.3 Second derivatives of the energy

Second derivatives of the CC energy functional can be obtained from the original energy formula (Eq. 2.4),

$$\begin{aligned} \frac{d^2 E_{CC}}{dx\ dy} &= \hat{P}(x,y) \langle \Phi | \left[\overline{\frac{\partial H}{\partial y}}, \frac{\partial T}{\partial x} \right] | \Phi \rangle + \langle \Phi | \left[\overline{H}, \frac{\partial^2 T}{\partial x\ \partial y} \right] | \Phi \rangle \\ &\quad + \langle \Phi | \left[\left[\overline{H}, \frac{\partial T}{\partial y} \right], \frac{\partial T}{\partial x} \right] | \Phi \rangle \ , \end{aligned} \tag{2.23}$$

where $\hat{P}(x,y) f(x,y) = f(x,y) + f(y,x)$ and we discard $\overline{\frac{\partial^2 H}{\partial x\ \partial y}}$ because it will be zero for all properties considered subsequently. This use amplitude second derivatives requires the solution of $|\{x\}||\{y\}|$ additional sets of linear equations. Alternatively, second-derivatives can be obtained from the CC-Λ energy functional (Eq. 2.17) using the symmetric formulation,

$$\begin{aligned} \frac{d^2 \widetilde{E}_{CC}}{dx\ dy} &= \langle 0 | (1 + \Lambda) \left[\overline{\frac{\partial H}{\partial x}}, \frac{\partial T}{\partial y} \right] | 0 \rangle + \langle 0 | (1 + \Lambda) \left[\overline{\frac{\partial H}{\partial y}}, \frac{\partial T}{\partial x} \right] | 0 \rangle \\ &\quad + \langle 0 | (1 + \Lambda) \left[\left[\overline{H}, \frac{\partial T}{\partial y} \right], \frac{\partial T}{\partial x} \right] | 0 \rangle \ , \end{aligned} \tag{2.24}$$

or the asymmetric formulation,

$$\frac{d^2\widetilde{E}_{CC}}{dx\ dy} = \langle 0|(1+\Lambda)\left[\overline{\frac{\partial H}{\partial x}}, \frac{\partial T}{\partial y}\right]|0\rangle + \langle 0|\frac{\partial \Lambda}{\partial y}\overline{\frac{\partial H}{\partial x}}|0\rangle\ , \tag{2.25}$$

which require the solution of $|\{x\} \cap \{y\}|$ or $2 \cdot |\{y\}|$ additional sets of linear equations, respectively. The optimal choice between these two depends on the type of perturbation x and y correspond to.

The asymmetric formulation of second-derivatives is obtained from the symmetric formulation in a manner similar to the derivation of Eqn. 2.20. Because the goal is to eliminate the need for the $\frac{\partial T}{\partial x}$ amplitudes, we consider only the second and third terms from Eqn. 2.24 and define a the following intermediate quantity,

$$\left(\frac{d^2\widetilde{E}_{CC}}{dx\ dy}\right)_{2,3} = \langle 0|(1+\Lambda)\left[\overline{\frac{\partial H}{\partial y}}, \frac{\partial T}{\partial x}\right]|0\rangle + \langle 0|(1+\Lambda)\left[\left[\overline{H}, \frac{\partial T}{\partial y}\right], \frac{\partial T}{\partial x}\right]|0\rangle\ . \tag{2.26}$$

By inserting the resolvent and using Eqn. 2.14, we see that

$$\begin{aligned}
\left(\frac{d^2\widetilde{E}_{CC}}{dx\ dy}\right)_{2,3} &= \langle 0|(1+\Lambda)\left[\overline{\frac{\partial H}{\partial y}} + \frac{1}{2}\left[\overline{H}, \frac{\partial T}{\partial y}\right], \frac{\partial T}{\partial x}\right]|0\rangle & (2.27)\\
&= \langle 0|(1+\Lambda)\left\{\overline{\frac{\partial H}{\partial y}}|X\rangle + \left[\overline{H}, \frac{\partial T}{\partial y}\right]|X\rangle\right\}\langle X|\frac{\partial T}{\partial x}|0\rangle & (2.28)\\
&= \langle 0|(1+\Lambda)\left\{\overline{\frac{\partial H}{\partial y}}|X\rangle + \left[\overline{H}, \frac{\partial T}{\partial y}\right]|X\rangle\right\}\\
&\qquad \times \left\{\langle X'|\overline{H}|X\rangle\right\}^{-1}\langle X'|\overline{\frac{\partial H}{\partial x}}|0\rangle\ . & (2.29)
\end{aligned}$$

The connection to Eqn. 2.25 is obvious after we define a new set of amplitudes,

$$\langle 0|\frac{\partial \Lambda}{\partial y}|X\rangle = \langle 0|(1+\Lambda)\left\{\overline{\frac{\partial H}{\partial y}}|X\rangle + \left[\overline{H}, \frac{\partial T}{\partial y}\right]|X\rangle\right\}\left\{\langle X'|\overline{H}|X\rangle\right\}^{-1}\ . \tag{2.30}$$

The first-order Lagrange-multipliers $\frac{\partial \Lambda}{\partial y}$ are obtained by solving

$$\begin{aligned} 0 &= \langle \Phi | \frac{\partial \Lambda}{\partial y} \overline{H} | X \rangle - \langle \Phi | (1+\Lambda) [\overline{H}, \frac{\partial T}{\partial y}] | X \rangle \\ &\quad - \langle \Phi | (1+\Lambda) \overline{\frac{\partial H}{\partial y}} | X \rangle \; . \end{aligned} \tag{2.31}$$

One advantage of using Eqn. 2.25 to compute properties is that one can compute response densities $D_y^{(1)}$ by replacing $\overline{\frac{\partial H}{\partial y}}$ by the 1- and 2-particle RDOs and obtain the second-derivatives by contracting these densities with $\frac{\partial H}{\partial y}$. For properties where $\frac{\partial H}{\partial y}$ is the dipole operator, this is particularly simple since only the 1-particle density-matrix is required. However, computing properties via Eqn. 2.25 requires that $\frac{\partial \Lambda}{\partial y}$ be computed. For dipole polarizabilities, it is more efficient use Eqn. 2.24, but for properties corresponding to perturbations which depend on the nuclear centers (geometric Hessians and NMR properties), it is advantageous to use the asymmetric formalism for polyatomic molecules because there $|\{x\} \cap \{y\}| \gg 2 \cdot |\{y\}|$.

2.1.4 Third derivatives of the energy

Third-order properties are obtained by simple differentiation of Eqn. 2.25:

$$\begin{aligned} \frac{d^3 \widetilde{E}_{CC}}{dx\, dy\, dz} &= \hat{P}_{xyz} \Big\{ \langle \Phi | (1+\Lambda) \left[\left[\overline{\frac{\partial H}{\partial x}}, \frac{\partial T}{\partial y} \right], \frac{\partial T}{\partial z} \right] | \Phi \rangle \\ &\quad + \langle \Phi | \frac{\partial \Lambda}{\partial x} \left[\left[\overline{H}, \frac{\partial T}{\partial y} \right], \frac{\partial T}{\partial z} \right] | \Phi \rangle \\ &\quad + \langle \Phi | (1+\Lambda) \left[\left[\left[\overline{H}, \frac{\partial T}{\partial x} \right], \frac{\partial T}{\partial y} \right], \frac{\partial T}{\partial z} \right] | \Phi \rangle \\ &\quad + \langle \Phi | \frac{\partial \Lambda}{\partial x} \left[\overline{\frac{\partial H}{\partial y}}, \frac{\partial T}{\partial z} \right] | \Phi \rangle \Big\} \end{aligned} \tag{2.32}$$

where $\hat{P}$ enforces the appropriate permutation symmetry of the x, y and z components. Computing third-derivatives requires T, Λ, $\frac{\partial T}{\partial x}$, $\frac{\partial T}{\partial y}$, $\frac{\partial T}{\partial z}$, $\frac{\partial \Lambda}{\partial x}$, $\frac{\partial \Lambda}{\partial y}$ and $\frac{\partial \Lambda}{\partial z}$, but no second-derivative amplitudes or multipliers. This is because Eqn. 2.17 satisfies satisfies Wigner's $2n+1$ and $2n+2$ rules [38] for the T and Λ amplitudes, respectively. Previous derivations are consistent with this rule, as second-order properties can be computed with T, Λ, $\frac{\partial T}{\partial x}$, $\frac{\partial T}{\partial y}$ and $\frac{\partial T}{\partial z}$ and it was just demonstrated that third-order properties require only first derivatives of the amplitudes and Lagrange multipliers. Without deriving equations for fourth-order properties, it can be stated that they will require, in addition to the amplitudes required for third-order properties, the solution of second-derivative amplitudes of T but not of Λ.

2.1.5 From energy derivatives to response theory

Once the Hamiltonian $H(x)$ can be represented in a simple form $H(x) = H_0 + xO$, where H_0 is the original electronic Hamiltonian for isolated system, x is a scalar, and operator O is considered as a perturbation (in our case, O is the dipole operator to model the effect of an weak external electric-field), then the derivatives of energy and cluster operator can be easily related to the coefficients in the perturbative expansion for the energy and cluster operator,

$$E(x) = E^{(0)} + \lambda E^{(1)} + \lambda^2 E^{(2)} + \cdots \tag{2.33}$$

$$T(x) = T^{(0)} + \lambda T^{(1)} + \lambda^2 T^{(2)} + \cdots . \tag{2.34}$$

Straightforward algebra leads to

$$E^{(1)} = \langle \Phi | \exp(-T) O \exp(T) | \Phi \rangle + \langle \Phi | \exp(-T) \left[H, T^{(1)} \right] \exp(T) | \Phi \rangle \tag{2.35}$$

and the connection to Eq. 2.12 is obvious. The projected response equations to be solved are

$$0 = \langle \Phi^{a_1 \ldots a_m}_{i_1 \ldots i_m} | \exp(-T) O \exp(T) | \Phi \rangle + \langle \Phi^{a_1 \ldots a_m}_{i_1 \ldots i_m} | \exp(-T) \left[H, T^{(1)} \right] \exp(T) | \Phi \rangle \tag{2.36}$$

which can be written as $A\mathbf{x} + \mathbf{b} = 0$, with $\mathbf{x}$ corresponding to the perturbed amplitudes, as stated by Monkhorst [39].

While the original CC response theory of Monkhorst is simple and effective for computing low-order properties, it is not suitable for higher-order properties since it requires tedious elimination of phase-factors. In 1990, Koch and coworkers rederived CC response theory in a more useful fashion [40]. The general theory of quasi-energy Lagrangians, which provides a means to derive arbitrary order time-dependent properties for variational and non-variational wavefunctions, is the subject of an exhaustive review [41]. A detailed presentation of that subject will not be repeated here.

The working equations for CC response theory for second- and third-order dynamic properties presented transparently in Refs. [42] and [43]. For $\omega = 0$, the zeroth-order cluster operator (T), the zeroth-order Lagrange multipliers ($\Lambda^{(0)}$), first-order cluster amplitudes ($T^{(1)}$), and first-order Lagrange multipliers ($\Lambda^{(1)}$) are obtained by solving,

$$0 = \langle \Phi^{a_1 \ldots a_n}_{i_1 \ldots i_n} | \overline{H} | \Phi \rangle \tag{2.37}$$

$$0 = \langle \Phi | (1 + \Lambda) \overline{H} | \Phi^{a_1 \ldots a_n}_{i_1 \ldots i_n} \rangle \tag{2.38}$$

$$0 = \langle \Phi^{a_1 \ldots a_n}_{i_1 \ldots i_n} | [\overline{H}, T^{(1)}_\gamma] | \Phi \rangle + \langle \Phi^{a_1 \ldots a_n}_{i_1 \ldots i_n} | \overline{\mu}_\gamma | \Phi \rangle \tag{2.39}$$

$$\begin{aligned} 0 = {} & \langle \Phi | \Lambda^{(1)}_\gamma \overline{H} | \Phi^{a_1 \ldots a_n}_{i_1 \ldots i_n} \rangle + \langle \Phi | (1 + \Lambda) [\overline{H}, T^{(1)}_\gamma] | \Phi^{a_1 \ldots a_n}_{i_1 \ldots i_n} \rangle \\ & + \langle \Phi | (1 + \Lambda) \overline{\mu}_\gamma | \Phi^{a_1 \ldots a_n}_{i_1 \ldots i_n} \rangle \end{aligned} \tag{2.40}$$

for the excitation manifold ($\Phi^{a_1 \ldots a_n}_{i_1 \ldots i_n}$) used to define the cluster and Λ operators and appropriate components of the dipole moment operator, μ_γ, where $\gamma = x, y, z$ in the nonsymmetric case.

2.2 NWChem and the Tensor Contraction Engine

The CC equations are not easily to program efficiently, particularly in parallel. Due to the exhaustive coverage of various ways that CC has been programmed available in the literature, this topic will not be covered here. A straightforward presentation of the CC equations in algebraic form is Ref. [16] while Ref. [9] present the working equations in both algebraic and diagrammatic form.

A breakthrough for programming CC for parallel computers was the Tensor Contraction Engine (TCE) [44, 45]. The TCE combined a number of advanced topics in programming, including automatic code generation, complex algorithmic transformations and strategies for achieving parallelism, such as tiling. The TCE was not the first project to employ these techniques, but it was the first to combine them and solve a complex programming problem like CC. Despite all its advantages, signficant hand-tuning was required to enable to code to scale to thousands of nodes on modern supercomputers. Some of these developments are reported in Ref. [46].

The structure of NWChem as a whole has been reviewed many times [47], so we will not describe the Global Array tools [48], NWChem's object-oriented design[2], or any of the modules besides the TCE module, which contains the CC property code. The TCE module in NWChem includes more than 80,000 lines of hand-written code

[2]Object-oriented (OO) design is not the same as using an OO language such as C++. NWChem is written almost exclusively in Fortran 77, with the remaining code written in C, but the design is modular and data-encapsulation is implemented to the extent permitted by the language.

Table 2.1: Line counts for various components of the NWChem CC code. The equations in the text corresponding to each procedure are given.

		Lines of code[a]		
Procedure	Corresponding Equations	CCSD	CCSDT	CCSDTQ
T-equations	2.37	46325	50010	52236
Λ-equations	2.38	41365	83936	225466
EOM (CC Jacobian)	2.39.1 & 2.40.1	91308	201036	364325
Linear response	2.39.2 & 2.24	40975	269053	340652
Quadratic response	2.40.2, 2.40.3 & 2.32	151158	332198[b]	-

[a] Line counts for linear and quadratic response are for the response functions as EOM procedures are reused for the solution of the response equations.
[b] This feature is not yet interfaced to the main driver.

and approximately 2.75 million lines written by the TCE code generator. Table 2.1 gives an accounting of the lines of code used at each level of CC approximation (CCSD, CCSDT and CCSDTQ) for the procedures necessary to compute properties.

The code generated by TCE is exclusively for computing tensor contractions. A large number of procedures are necessary because of many different types of contractions possible between tensors of various rank. For example, there are only four ways to contract two rank-2 tensors[3], but hundreds of ways to contract a rank-2 and rank-3 tensor, for example. It is not possible to provide code for all of the tensor contractions used in the TCE[4], but it is instructive to consider one case to understand how parallelism is achieved. Consider the procedure for computing a simple contraction,

$$J_{p_3p_4}^{h_1h_2} = \sum_{p_5} T_{p_3p_5}^{h_1h_2} \cdot I_{p_4}^{p_5} \ , \tag{2.41}$$

[3]Matrices are rank-2 tensors. The four ways to contract matrices A and B to a third matrix C are $C = AB$, $C = A^TB$, $C = AB^T$ and $C = A^TB^T$.

[4]The code can be downloaded for free as part of NWChem. See `http://www.emsl.pnl.gov/docs/nwchem/`.

where I is a singles intermediate ($m = 1$), J is a doubles intermediates ($m = 2$), T is the array of doubles amplitudes and p and h are indices representing particles and holes, respectively. The procedure to compute this tensor contraction is described in Figure 2.1. Tiles are sets of indices for molecular orbitals which all have the same spin- and spatial-symmetry properties. The conditionals `C1`, `C2`, `C3`, `C4` and `C5` are all related to spatial and spin symmetry at the tile level. Details for the local computation (`compute Jb += Tb*Ib`) can be found in Chapter 10. The `put` and `get` are one-sided communication operations performed using Global Arrays.

A very important feature in Figure 2.1 is `my_turn`, which determines if a given node will perform the subsequent local operations. It queries a global counter which runs over all possible tasks in a given contraction and provides for parallel load-balancing.

2.2.1 NWChem parallelism in non-technical language

A simple analogy for the parallel load-balancing strategy in the TCE would be 1000 workers transcribing the United States Declaration of Independence (USDI) onto stone blocks, one for each word. A chalk board visible to all works has the number "1" written on it. The first worker claims the word "When" and then replaces the "1" on the chalk board with "2" and begins to carve "When" into his stone block. The next worker in line sees the number "2" and knows to carve "in" into her stone block. She also increments the chalkboard counter. This proceeds until all words are carved in stone blocks. When stone block is finished, it is placed in the appropriate location on the ground such that when all blocks are finished, the USDI will be reproduced correctly. The management of the layout of stone blocks is done by a wizard who has previously determined the location of all blocks and can provide exact coordinates for where all finished stone blocks should be placed. When a worker finishes a block, a

Figure 2.1: Procedure for computing a particular contraction. See text for details.

```
for P3 in all P tiles:
  for P4 in all P tiles:
    for H1 in all H tiles:
      for H2 in all H tiles:
        if my_turn:
          if C1 and C2 and C3:
            create and zero buffer Jb
            for P5 in all P tiles:
              if C5 and C6:
                create and zero buffer Tb
                get Tb from global T
                reorder Tb
                create and zero buffer Ib
                get Ib from global I
                reorder Ib
                compute Jb += Tb*Ib
              endif
            endfor
            reorder Jb
            put Jb to global J
          endif
        endif
      endfor
    endfor
  endfor
endfor
```

trained gorilla takes the block and puts into the appropriate location, having received the proper instructions from the wizard. Because the gorillas are well-trained, workers need not be concerned with the fate of their stone block one the gorilla takes it. It is the responsibility of the wizard, not the worker, to ensure that all blocks end up in the proper place.

In the previous analogy, the workers are local compute nodes, the wizard is the Global Array library, the chalkboard is the ARMCI `NXTVAL` operation and the gorillas are one-sided communication operations in ARMCI. For details, see the documentation for the Global Array tools [49]. It is important to recognize that NWChem uses one-sided communication, not two-sided communication or message-passing. It is far more difficult to implement the complex algorithms of CC using MPI [50].

The necessary conditions for good parallel performance in NWChem can be inferred from the previous analogy. If the text to be transcribed to stone was not the USDI, but rather a 14-word sentence, 986 of the 1000 workerss would do absolutely nothing, as their would be no words available for them to carve. In parallel computing, this condition is called data-starvation. A condition known as load-imbalance also leads to poor parallel performance. Consider the transcription to stone of the list of states — carving "Mississippi" takes much longer than "Iowa." Thus, the worker who carves the shorter state name will finish much quicker. If the next name that worker carves is also short, he or she may finish around the same time as the worker with the longer name. However, if those two names are the last names carved by both workers, then one worker sits idle while the other finishes. Hence, it is optimal to rearrange the list of names such that long names come first and short names are last. Another solution is to combine into a single task the carving of "Iowas" and another short name. The consequences of a load-imbalance grow with the size of the

computer used. It is not terrible for 2 of 4 processors to sit idle for 30 seconds, but if half the processors in BlueGene/P sit idle for 30 seconds, that is almost 1 day of wasted processor time in total.

The connection of the analogy to quantum chemistry is that when the tiles of orbitals vary greatly in size or are too few in number (i.e. $N_{tasks} \gg N_{processors}$ is false) the parallel performance will be poor. This can occur for molecules with high-symmetry or when one uses too many processors for a particular problem. On the positive side, when a molecular system — usually large and lacking any spatial symmetry — produces set of tiles which align well to the number of processors used, near-perfect scaling is attained [46].

2.2.2 Summary

NWChem is parallel framework for developing computational chemistry because it is built upon a powerful set of tools which implement basic functionality required for many algorithms. While it is not possible to describe all of the useful features in NWChem, or even all of the components of the TCE module, the code example given above provides provides the necessary foundation for understanding the parallel structure of the TCE CC code in more detail. The interested reader is encouraged to download NWChem and peruse the source code, as this is the only way to obtain a thorough understanding of how the algorithms work.

REFERENCES

[1] F. Coester, *Nucl. Phys.* **7**, 421 (1958).

[2] F. Coester and H. Kümmel, *Nucl. Phys.* **17**, 477 (1960).

[3] J. Čížek, *J. Chem. Phys.* **45**, 4256 (1966); J. Čížek and J. Paldus, *Int. J. Quantum Chem.* **5**, 359 (1971).

[4] J. Paldus, J. Čížek, and I. Shavitt, *Phys. Rev. A* **1972**, *5*, 50.

[5] J. Paldus, in *New Horizons of Quantum Chemistry*, edited by P.-O. Löwdin and B. Pullman (Reidel, Dordrecht, 1983), pp. 31-60.

[6] R.J. Bartlett, C.E. Dykstra, and J. Paldus, in *Advanced Theories and Computational Approaches to the Electronic Structure of Molecules*, edited by C.E. Dykstra (Reidel, Dordrecht, 1984), pp. 127-159.

[7] R. J. Bartlett, in *Modern Electronic Structure Theory*, Part I, edited by D.R. Yarkony (World Scientific, Singapore, 1995), pp. 1047-1131.

[8] J. Paldus and X. Li, *Adv. Chem. Phys.* **110**, 1 (1999).

[9] T. D. Crawford and H. F. Schaefer III, *Rev. Comp. Chem.* **14**, 33 (2000).

[10] R.J. Bartlett, in *Theory and Applications of Computational Chemistry: The First Forty Years*, edited by C.E. Dykstra, G. Frenking, K.S. Kim, and G.E. Scuseria (Elsevier, 2005), pp. 1191-1221.

[11] R. J. Bartlett and M. Musiał, *Rev. of Mod. Phys.* **79**, 291 (2007).

[12] ACES II is a program product of the Quantum Theory Project, University of Florida. Authors: J. F. Stanton, J. Gauss, J. D. Watts, M. Nooijen, N. Oliphant, S.A. Perera, P.G. Szalay, W.J. Lauderdale, S. A. Kucharski, S. R. Gwaltney, S. Beck, A. Balková D. E. Bernholdt, K. K. Baeck, P. Rozyczko, H. Sekino, C. Hober, and R. J. Bartlett. Integral packages included are VMOL (J. Almlöf and P. R. Taylor); VPROPS (P. Taylor) ABACUS; (T. Helgaker, H. J. Aa. Jensen, P. Jørgensen, J. Olsen, and P. R. Taylor).

[13] *Aces II*, a quantum chemical program package written by J. F. Stanton, J. Gauss, J .D. Watts, P. G. Szalay, R. J. Bartlett with contribution from A. A. Auer, D. B. Bernholdt, O. Christiansen, M. E. Harding, M. Heckert, O. Heun, C. Huber, D. Jonsson, J. Juselius, W. J. Lauderdale, T. Metzroth, K. Ruud and the integral packages *MOLECULE* (J. Almlöf and P. R. Taylor),Props (P. R. Taylor), and ABACUS (T. Helgaker, H. Aa. Jensen, P. Jørgensen, and J. Olsen). See also J. F. Stanton, J. Gauss, J. D. Watts, W. J. Lauderdale, R.J. Bartlett, *Int. J. Quantum Chem. Symp.* **26**, 879 (1992) as well as: `http://www.aces2.de` for the current version.

[14] *DALTON, a molecular electronic structure program, Release 2.0* (2005), see `http://www.kjemi.uio.no/software/dalton/dalton.html`.

[15] M. W. Schmidt, K. K. Baldridge, J. A. Boatz, S. T. Elbert, M. S. Gordon, J. H. Jensen, S. Koseki, N.Matsunaga, K. A. Nguyen, S. Su, T. L. Windus, M. Dupuis, J. A. Montgomery, *J. Comp. Chem.* **14**, 1347 (1993); M.S.Gordon and M.W.Schmidt, in *Theory and Applications of Computational Chemistry: The*

First Forty Years, edited by C.E. Dykstra, G. Frenking, K.S. Kim, and G.E. Scuseria (Elsevier, 2005), pp. 1167-1189.

[16] P. Piecuch, S. A. Kucharski, K. Kowalski and M. Musiał, *Comp. Phys. Comm.* **149**, 71 (2002).

[17] *Gaussian 03*, M. J. Frisch, G. W. Trucks, H. B. Schlegel, G. E. Scuseria, M. A. Robb, J. R. Cheeseman, J. A. Montgomery, Jr., T. Vreven, K. N. Kudin, J. C. Burant, J. M. Millam, S. S. Iyengar, J. Tomasi, V. Barone, B. Mennucci, M. Cossi, G. Scalmani, N. Rega, G. A. Petersson, H. Nakatsuji, M. Hada, M. Ehara, K. Toyota, R. Fukuda, J. Hasegawa, M. Ishida, T. Nakajima, Y. Honda, O. Kitao, H. Nakai, M. Klene, X. Li, J. E. Knox, H. P. Hratchian, J. B. Cross, V. Bakken, C. Adamo, J. Jaramillo, R. Gomperts, R. E. Stratmann, O. Yazyev, A. J. Austin, R. Cammi, C. Pomelli, J. W. Ochterski, P. Y. Ayala, K. Morokuma, G. A. Voth, P. Salvador, J. J. Dannenberg, V. G. Zakrzewski, S. Dapprich, A. D. Daniels, M. C. Strain, O. Farkas, D. K. Malick, A. D. Rabuck, K. Raghavachari, J. B. Foresman, J. V. Ortiz, Q. Cui, A. G. Baboul, S. Clifford, J. Cioslowski, B. B. Stefanov, G. Liu, A. Liashenko, P. Piskorz, I. Komaromi, R. L. Martin, D. J. Fox, T. Keith, M. A. Al-Laham, C. Y. Peng, A. Nanayakkara, M. Challacombe, P. M. W. Gill, B. Johnson, W. Chen, M. W. Wong, C. Gonzalez, and J. A. Pople, Gaussian, Inc., Wallingford CT, 2004.

[18] MOLPRO is a package of ab initio programs written by H.-J. Werner, P. J. Knowles, R. Lindh, F. R. Manby, M. Schütz, P. Celani, T. Korona, A. Mitrushenkov, G. Rauhut, T. B. Adler, R. D. Amos, A. Bernhardsson, A. Berning, D. L. Cooper, M. J. O. Deegan, A. J. Dobbyn, F. Eckert, E. Goll, C. Hampel, G. Hetzer, T. Hrenar, G. Knizia, C. Köppl, Y. Liu, A. W. Lloyd, R. A. Mata,

A. J. May, S. J. McNicholas, W. Meyer, M. E. Mura, A. Nicklaβ, P. Palmieri, K. Pflger, R. Pitzer, M. Reiher, U. Schumann, H. Stoll, A. J. Stone, R. Tarroni, T. Thorsteinsson, M. Wang, A. Wolf.

[19] C. Hampel, K. A. Peterson, H.-J. Werner, *Chem. Phys. Lett.* **190**, 1 (1992).

[20] E. J. Bylaska, W. A. de Jong, N. Govind, K. Kowalski, T. P. Straatsma, M. Valiev, D. Wang, E. Apra, T. L. Windus, J. Hammond, J. Autschbach, P. Nichols, S. Hirata, M. T. Hackler, Y. Zhao, P.-D. Fan, R. J. Harrison, M. Dupuis, D. M. A. Smith, J. Nieplocha, V. Tipparaju, M. Krishnan, A. Vazquez-Mayagoitia, Q. Wu, T. Van Voorhis, A. A. Auer, M. Nooijen, L. D. Crosby, E. Brown, G. Cisneros, G. I. Fann, H. Fruchtl, J. Garza, K. Hirao, R. Kendall, J. A. Nichols, K. Tsemekhman, K. Wolinski, J. Anchell, D. Bernholdt, P. Borowski, T. Clark, D. Clerc, H. Dachsel, M. Deegan, K. Dyall, D. Elwood, E. Glendening, M. Gutowski, A. Hess, J. Jaffe, B. Johnson, J. Ju, R. Kobayashi, R. Kutteh, Z. Lin, R. Littlefield, X. Long, B. Meng, T. Nakajima, S. Niu, L. Pollack, M. Rosing, G. Sandrone, M. Stave, H. Taylor, G. Thomas, J. van Lenthe, A. Wong, and Z. Zhang. "NWChem, A Computational Chemistry Package for Parallel Computers, Version 5.1.1" (2009), Pacific Northwest National Laboratory, Richland, Washington 99352-0999, USA. A modified version.

[21] R. Kobayashi and A. P. Rendell, *Chem. Phys. Lett.* **265**, 1 (1997).

[22] T. Daniel Crawford, C. David Sherrill, Edward F. Valeev, Justin T. Fermann, Rollin A. King, Matthew L. Leininger, Shawn T. Brown, Curtis L. Janssen, Edward T. Seidl, Joseph P. Kenny, and Wesley D. Allen, *J. Comp. Chem.* **28**, 1610 (2007).

[23] Y. Shao, L. Fusti-Molnar, Y. Jung, J. Kussmann, C. Ochsenfeld, S. T. Brown, A. T. B. Gilbert, L. V. Slipchenko,S. V. Levchenko, D. P. O'Neill, R. A. Distasio Jr., R. C. Lochan, T. Wang, G. J. O. Beran, N. A. Besley, J. M., Herbert, C. Y. Lin, T. Van Voorhis, S. H. Chien, A. Sodt, R. P. Steele, V. A. Rassolov, P. E. Maslen, P. P. Korambath, R. D. Adamson, B. Austin, J. Baker, E. F. C. Byrd, H. Dachsel, R. J. Doerksen, A. Dreuw, B. D. Dunietz, A. D. Dutoi, T. R. Furlani, S. R. Gwaltney, A. Heyden, S. Hirata, C.-P. Hsu, G. Kedziora, R. Z. Khalliulin, P. Klunzinger, A. M. Lee, M. S. Lee, W. Liang, I. Lotan, N. Nair, B. Peters, E. I. Proynov, P. A. Pieniazek, Y. M. Rhee, J. Ritchie, E. Rosta, C. D. Sherrill, A. C. Simmonett, J. E. Subotnik, H. L. Woodcock III, W. Zhang, A. T. Bell, A. K. Chakraborty, D. M. Chipman, F. J. Keil, A. Warshel, W. J. Hehre, H. F. Schaefer III, J. Kong, A. I. Krylov, P. M. W. Gill, M. Head-Gordon, *Phys. Chem. Chem. Phys.* **8**, 3172 (2006).

[24] V. Lotrich, N. Flocke, M. Ponton, A. Yau, A. Perera, E. Deumens and R. J. Bartlett, *J. Chem. Phys.* **128**, 194104 (2008).

[25] CFOUR, Coupled Cluster techniques for Computational Chemistry, a quantum-chemical program package by J.F. Stanton, J. Gauss, M.E. Harding, P.G. Szalay with contributions from A.A. Auer, R.J. Bartlett, U. Benedikt, C. Berger, D.E. Bernholdt, Y.J. Bomble, O. Christiansen, M. Heckert, O. Heun, C. Huber, T.-C. Jagau, D. Jonsson, J. Juslius, K. Klein, W.J. Lauderdale, D.A. Matthews, T. Metzroth, D.P. O'Neill, D.R. Price, E. Prochnow, K. Ruud, F. Schiffmann, S. Stopkowicz, M.E. Varner, J. Vzquez, F. Wang, J.D. Watts and the integral packages MOLECULE (J. Almlf and P.R. Taylor), PROPS (P.R. Taylor), ABACUS (T. Helgaker, H.J. Aa. Jensen, P. Jrgensen, and J. Olsen), and ECP routines by

A. V. Mitin and C. van Wllen. For the current version, see http://www.cfour.de.

[26] ACES, a program system for ab initio electronic structure calculations, authored by R. J. Bartlett, G. D. Purvis III, D. E. Bernholdt, S. J. Cole, G. B. Fitzgerald, R. J. Harrison, W. D. Laidig, Y. S. Lee, D. H. Magers, L. Meissner, M. Rittby, E. A. Salter, H. Sekino, C. Sosa, J. F. Stanton, G. W. Trucks, and J. D. Watts.

[27] No citation can be found although subsequent works attribute PSI 1.0, particularly the CC code, to Scuseria.

[28] G. E. Scuseria, A. C. Scheiner, T. J. Lee, J. E. Rice and H. F. Schaefer III, *J. Chem. Phys.* **86**, 2881 (1987).

[29] TITAN is a vectorized coupled-cluster program written by T. J. Lee, A. P. Rendell and J. E. Rice.

[30] M. Schütz, R. Lindh and H.-J. Werner, *Mol. Phys.* **96**, 719 (1999); P. Knowles, M. Schütz and H.-J. Werner, in *Modern Methods and Algorithms of Quantum Chemistry* (2nd ed.), NIC Series Vol. 3, edited by J. Grotendorst, D. Marx, and A. Muramatsu (John von Neumann Institute for Computing, Jülich, 2000), pp. 1-83.

[31] J. W. Demmel, *Applied Numerical Linear Algebra*, (SIAM, Philadelphia, 1997).

[32] P. Pulay, *Chem. Phys. Lett.* **73**, 393 (1980); P. Pulay, *J. Comp. Chem.* **3**, 556 (1982).

[33] R. J. Harrison, *J. Comp. Chem.* **25**, 328 (2004).

[34] M. Ziólkowski, V. Weijo, Poul Jørgensen and J. Olsen, *J. Chem. Phys.* **128**, 204105 (2008).

[35] E. A. Salter, G. W. Trucks and R. J. Bartlett, *J. Chem. Phys.* **90**, 1752 (1989).

[36] P.-O. Löwdin, *Journal of Molecular Spectroscopy*, **13**, 326 (1964).

[37] E. R. Davidson, *Reduced density matrices in quantum chemistry* (Academic Press, New York, 1976).

[38] E. A. Hylleraas, *Z. Phys.* **65**, 209 (1930); E. Wigner, *Math. Natur. Anz. Budapest* **53**, 477 (1935); A. Dalgarno and A. L. Stewart, *Proc. R. Soc. London, Ser. A* **238**, 269 (1956); J. O. Hirschelder, W. Byers-Brown and S. Epstein, *Adv. Quantum Chem.* **1**, 255 (1964); V. Kvasnička, V. Laurinc and S. Biskupič, *Mol. Phys.* **39**, 143 (1980); W. Kutzelnigg, *Theor. Chim. Acta.* **83**, 263 (1992); X. Gonze, *Phys. Rev. A* **52**, 1086 (1995).

[39] H. J. Monkhorst, *Int. J. Quantum Chem.* **S11**, 421 (1977); E. Dalgaard, H.J. Monkhorst, Phys. Rev. A **28**, 1217 (1983).

[40] H. Koch and P. Jørgensen, *J. Chem. Phys.* **93**, 3333 (1990).

[41] O. Christiansen, C. Hättig and P. Jørgensen, *Int. J. Quantum Chem.* **68**, 1 (1998).

[42] M. Kállay and J. Gauss, *J. Mol. Struct. (THEOCHEM)* **768**, 71 (2006).

[43] D. P. O'Neill, M. Kállay and J. Gauss, *J. Chem. Phys.* **127**, 134109 (2007).

[44] A. A. Auer, G. Baumgartner, D. E.Bernholdt, A. Bibireata, V. Choppella, D. Cociorva, X. Gao, R.Harrison, S. Krishnamoorthy, S. Krishnan, C.-C. Lam, Q. Lu, Nooijen, M. R. Pitzer, J.Ramanujam, P. Sadayappan, A. Sibiryakov, *Mol. Phys.* **104**, 211 (2006).

[45] S. Hirata, *J. Phys. Chem. A* **107**, 9887 (2003); *J. Chem. Phys.* **121**, 51 (2004); *Theor. Chem. Acc.* **116**, 2 (2006).

[46] K. Kowalski, J. R. Hammond, W. A. de Jong, P.-D. Fan, M. Valiev, D. Wang and N. Govind, in *Computational Methods for Large Systems: Electronic Structure Approaches for Biotechnology and Nanotechnology*, edited by J. R. Reimers (Wiley, 2010, Hoboken).

[47] R. A. Kendall, E. Aprà, , D. E. Bernholdt, E. J. Bylaska, M. Dupuis, G. I. Fann, R. J. Harrison, J. Ju, J. A. Nichols1, J. Nieplocha, T. P. Straatsma, T. L. Windus and A. T. Wong, *Comp. Phys. Comm.* **128**, 260 (2000); E. Aprà, , D. E. Bernholdt, H. A. Früchtl, M. F. Guest, R. J. Harrison, R. A. Kendall, R. A. Kutteh, X. Long, J. B. Nicholas, J. A. Nichols, H. L. Taylor, A. T. Wong, G. I. Fann, R. J. Littlefield and J. Nieplocha, *Int. J. Quantum Chem.* **56**, S29 475 (2004); M. F. Guest, E. Aprà, D. E. Bernholdt, H. A. Früchtl, R. J. Harrison, R. A. Kendall, R. A. Kutteh, X. Long, J. B. Nicholas, J. A. Nichols, H. L. Taylor, A. T. Wong, G. I. Fann, R. J. Littlefield and J. Nieplocha, in *Lecture Notes in Computer Science* (Springer, Berlin, 1996), Vol. 1041, pp. 278-294; T. L. Windus, E. J. Bylaska, M. Dupuis, S. Hirata, L. Pollack, D. M. Smith, T. P. Straatsma and E. Aprà, in *Lecture Notes in Computer Science* (Springer, Berlin, 2003), Vol. 2660, pp. 168-177.

[48] J.Nieplocha, R. J. Harrison and R. J. Littlefield, *J. Supercomputing* **10**, 169 (1996).

[49] `http://www.emsl.pnl.gov/docs/parsoft/`

[50] `http://www.mpi-forum.org/`

CHAPTER 3

DYNAMIC POLARIZABILITIES OF POLYAROMATIC HYDROCARBONS USING COUPLED-CLUSTER LINEAR RESPONSE THEORY

This chapter has been previously published in the following article: J. R. Hammond, K. Kowalski and W. A. de Jong, "Dynamic polarizabilities of polyaromatic hydrocarbons using coupled-cluster linear response theory," *J. Chem. Phys.* **127**, 144105 (2007). Copyright 2007 by the American Institute of Physics.

3.1 Introduction

Density-functional-theory (DFT) faces well-known challenges in accurately describing the polarizabilities and hyperpolarizabilities of conjugated systems [1], and accurate calculations require both a proper description of the correlation effects and judicious choice of the orbital basis set. Accuracy for smaller oligomers using a given combination of functional and basis set does not necessarily extend to larger oligomers. Because DFT is used to model organic chromophores and nanographene, which contain many aromatic rings, it is important to understand the accuracy of these methods in detail and to evaluate the role of exact-exchange and electron correlation in achieving quantitative accuracy in large conjugated systems. The availability of coupled-cluster results would be invaluable in quantifying the accuracy of different density-functional methodologies for these systems. Using our newly developed coupled-cluster singles

and doubles (CCSD) linear response theory codes, we calculate static and dynamic dipole polarizabilities for large aromatic hydrocarbons, including benzene, pyrene and linear oligoacenes as large as hexacene.

Because the dipole polarizability is related to many other molecular properties, the benchmark coupled-cluster calculations can be used to evaluate the potential accuracy of other approximate methods for properties other than the polarizability. The polarizability at complex frequencies is used to calculate C_6 parameters [2, 3] while the Raman scattering cross section is obtained from derivatives of the polarizability with respect to vibrational modes according to the Placzek theory [4, 5]. The accuracy of the polarizability is directly related to the accuracy of the linear response function, the poles of which are electronic excitations. Hyperpolarizabilities are obviously derivatives of the polarizability, and finally, the microscopic polarizability is related to to the dielectric constant via the Clausius-Mossotti equation [6]. Some of these issues are discussed in this chapter.

Previous comparisons of density-functional and coupled-cluster polarizabilities employed finite field techniques [7], suitable only for static properties, or were constrained to diatomic molecules or minimal basis sets [8]. Comparison of density-functional and *ab initio* methods for extended systems have been performed by Champagne and coworkers [1] by focusing on hydrogen chains and linear polyenes using simple *ab initio* methods, such as Hartree-Fock (HF) and second-order perturbation theory (MP2), for comparison.

3.2 Theory and computational details

Coupled-cluster theory and its linear response extension have been described in a number of papers [9, 10, 11]; in this section we present only salient features of this methodology (for details regarding the implementation used for this paper see Ref. [12]).

Results in this chapter employ the asymmetric formulation of the second-derivative of the energy:

$$\begin{aligned}\frac{d^2\widetilde{E}_{CC}}{dxdy} &= \langle 0|(1+\Lambda)\exp(-T)\frac{\partial^2 H}{\partial x \partial y}\exp(T)|0\rangle \\ &+ \hat{P}(x,y)\langle 0|(1+\Lambda)\exp(-T)\left[\frac{\partial H}{\partial y},\frac{\partial T}{\partial x}\right]\exp(T)|0\rangle \\ &+ \langle 0|(1+\Lambda)\exp(-T)\left[\left[H,\frac{\partial T}{\partial y}\right],\frac{\partial T}{\partial x}\right]\exp(T)|0\rangle,\end{aligned} \tag{3.1}$$

where $\hat{P}(x,y)f(x,y) = f(x,y) + f(y,x)$. Three iterative steps: (1)the CCSD equations (defining the CCSD cluster operator $T = T_1 + T_2$); (2) the CCSD-Λ equations (defining the CCSD de-excitation operator $\Lambda = \Lambda_1 + \Lambda_2$); and (3) the first order CCSD response equations (defining the first order linear response CCSD cluster amplitudes $T^{(1)} = T_1^{(1)} + T_2^{(1)}$), were implemented in NWChem [13] using the Tensor Contraction Engine [14] suite of programs. All CC codes include the more efficient handling of two-electron integrals and improved offset tables [15].

For benzene, the geometry used was the same as that of Rizzo and coworkers [16]. All-electron (ae) HF/cc-pVTZ, B3LYP/cc-pVTZ and PBE0/cc-pVTZ and frozen-core (fc) MP2/cc-pVTZ optimized geometries were calculated within NWChem. All optimized geometries were done assuming a D_{2h} geometry and singlet ground state, which is consistent with the earlier work of Kadantsev, et al. [17].

Density-functional linear response calculations were performed within the Dalton

2.0 suite of programs [18] using the direct SCF method [19]. Basis sets were obtained from the Dalton basis set library. Parameters for the density-functionals used (PBE, PBE0, BLYP, B3LYP) were set using the specifications given in the manual [20]. A single set of data was calculated within Gaussian 03 [21] to extend the results of Schlegel and coworkers [22] to complete Table 3.9.

To investigate the effect of truncating the cluster expansion at doubles, the CC3 model is applied to the benzene molecule using small basis sets. Coupled-cluster calculations at the CCSD and CC3 levels of theory were performed using the Aces II quantum chemistry package [23]. The convergence criteria was 10^{-9} for SCF and 10^{-6} for CC iterations. Because of the steep scaling of CC3 and the serial nature of the Aces code, polarizabilities for benzene could only be calculated using 6-31+G*, 6-31++G** and aug-cc-pVDZ. A more complete study of the role of triples is underway using the massively parallel implementation of CCSDT-LR polarizabilities within NWChem [24].

All NWChem CCSD calculations were performed fully in-core on MPP2 [25]. All CCSD calculations used an RHF reference wavefunction and no core orbitals were frozen. Basis sets were obtained from the NWChem basis set library. Spherical *d*-functions were used for calculations reported in this chapter. The effect of using Cartesian *d*-functions instead of spherical ones is ~ 0.01 a.u. for both energies and polarizabilities of the 6-31+G*, 6-31++G**, 6-311+G*, 6-311++G**, aug-cc-pVDZ and Sadlej pVTZ basis set calculations shown in Table 3.2. The SCF iterations were converged to 10^{-7} and CCSD iterations were converged to 10^{-4}. This lower convergence threshhold was employed for the coupled-cluster iterative steps to reduce the wall time on larger calculations. To ensure that this level of convergence was sufficient for meaningful results, calculations using a higher convergence threshhold

Figure 3.1: Convention for the tensor components of the polarizability. In both cases the N component comes out of the plane of the page.

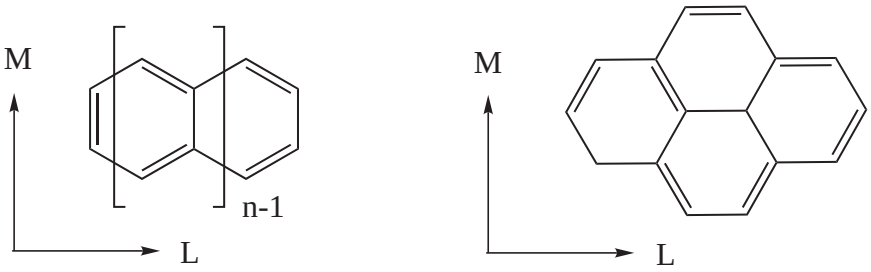

(10^{-8}) were performed for the aug-cc-pVDZ and Sadlej pVTZ basis set calculations shown in Table 3.2. The change in convergence threshhold had a negligible effect (~ 0.05 a.u.) on polarizabilities and energies ($\sim 5 \cdot 10^{-6}$ a.u.), particularly given that the errors due to basis set and the incompleteness of the CCSD model are at least an order of magnitude larger than the effect due to convergence (see Section 3.3 for a complete discussion).

All energies and polarizabilities reported in this chapter are reported using atomic units. Geometry parameters are in Angstroms. For benzene, the polarizability tensor components are $\alpha_{LL} = \alpha_{MM}$ in the plane of the molecule, and α_{NN} perpendicular to it. For pyrene and the oligoacene series, the α_{LL} component is the longest axis of the molecule, α_{MM} the other axis in the plane defined by the aromatic rings, and α_{NN} the axis normal to the plane. See Figure 3.1 for a visual representation.

3.2.1 Performance analysis

The performance of the CCSD-LR in NWChem is demonstrated in Table 3.1. The relative timings for for CCSD, CCSD-Λ and CCSD-LR are approximately $2 : 4 : 3$. The unfavorable scaling of the CCSD-Λ equations with respect to the CCSD ones is mainly caused by the need of using the most expensive four-virtual-index 2-electron

Table 3.1: Timing data for parallel CCSD-LR calculations. All calculations were performed using the Sadlej TZ basis set in D_{2h} symmetry. The CCSD-LR timings refers to the Z-axis and were taken from iteration 5 for all cases. Timings are in seconds.

			CPU Timings Per Iteration		
Molecule	Atomic Basis Set Rank	Processors	CCSD	CCSD-Λ	CCSD-LR
C_6H_6	198	64	9.8	20.2	15.7
$C_{10}H_8$	312	128	45.6	82.3	68.7
$C_{14}H_{10}$	426	256	82.4	160.6	116.0
$C_{18}H_{12}$	540	256	399.1	925.5	621.7
$C_{22}H_{14}$	654	512	359.2	746.7	478.5
$C_{26}H_{16}$	768	640	1001.8	2053.2	1236.0

integrals twice: in the equations for doubly excited Λ amplitudes and in the equation for singly excited Λ amplitudes (the $\langle\Phi|\Lambda_2 V_N T_1|\Phi_i^a\rangle$ term). In the CCSD equations these integrals are used only once in the equations for doubly excited amplitudes. The timings of the CCSD-LR part are generally the same as the timings of the EOM-CCSD approach for a single root since solving the CCSD-LR response equations is equivalent to solving the right-eigenvalue equations, except for the term corresponding to the similarity transformed dipole operator. Evaluation of the last term in the polarizability in the form of Eq. 3.1 is approximately as expensive as one iteration of CCSD-Λ. In the symmetric formulation, the evaluation of the polarizability would be computationally trivial, as it requires only the dipole integrals, although that requires iterative solution of $\Lambda^{(1)}$, which is at least as expensive as CCSD-Λ.

There appears to be no significant decrease in performance for many hundreds of processors, indicating that the ceiling on CCSD property calculations is much greater than 1000 spatial orbitals, which opens the door to a whole new size regime for accurate calculation of molecular properties.

3.3 Results

We compare CCSD to four common density-functionals (PBE, PBE0, BLYP, B3LYP) in two ways: (i) dynamic polarizabilities of oligoacenes $n = 1 - 6$ and (ii) dynamic polarizabilities of benzene and pyrene for a wide range of frequencies. The basis set dependence of CCSD static polarizabilities and the role of triples is evaluated using benzene. Sources of error with respect to experiment come from the incompleteness of the one-particle and many-particle basis sets, both of which are addressed below, and vibrational effects, which are not considered in this study.

3.3.1 Basis set convergence

Because of the computational cost of coupled-cluster calculations, it is important to find the most efficient basis set for obtaining accurate polarizabilities. To evaluate the basis set convergence for oligoacenes, we considered the smallest reasonable subunit, benzene, which permitted calculations employing very large basis sets (see Table 3.2). Static dipole polarizabilities of benzene were calculated using a number of Pople [28] and Dunning [27] basis sets as well as the Sadlej pVTZ basis set [26]. The largest basis set used, aug-cc-pVQZ, is used as the standard for comparison.

For benzene, Dunning basis sets greatly outperform Pople basis sets of similar size for polarizability calculations at the CCSD level of theory. The aug-cc-pVDZ basis, with only 192 functions, produces equivalently accurate results to the largest Pople basis considered, 6-311++G(3df,3pd), which has 342 functions. Smaller basis sets in the Pople family greatly underestimate both polarizability components. For quantitative results, the smallest Pople basis set that can be used is 6-311++G(2d,2p). Smaller basis sets which include only one d-function underestimate the polarizability

Table 3.2: Static dipole polarizabilities of Benzene calculated with CCSD and a variety of basis sets. Energies and polarizabilities are given in atomic units.

Basis Set	Atomic Basis Set Rank	E_{CCSD}	α_{LL}	α_{NN}
6-31+G*	120	-231.5146	75.06	39.87
6-31++G**	144	-231.5640	75.53	40.51
6-311+G*	150	-231.6896	75.32	40.16
6-311++G**	174	-231.7352	75.99	40.70
6-311++G(2d,2p)	222	-231.7923	78.22	42.96
6-311++G(3df,3pd)	342	-231.8935	79.63	44.17
aug-cc-pVDZ	192	-231.5894	80.13	44.89
aug-cc-pVTZ	414	-231.8807	80.26	44.51
aug-cc-pVQZ	756	-232.0006	80.14	44.25
d-aug-cc-pVDZ	270	-231.5915	80.53	45.00
d-aug-cc-pVTZ	564	-231.8841	80.35	44.49
Sadlej TZ	198	-231.6826	80.57	44.66

by more than 5% for benzene. The error in 6-311++G(2d,2p) can be understood by comparing the exponents of the two *d*-functions of carbon and the two *p*-functions of hydrogen with those from aug-cc-pVDZ. In the former, the exponents are 1.252 and 0.313 for carbon and 1.500 and 0.375 for hydrogen while in the latter they are 0.550, 0.151, 0.727 and 0.141, respectively. The approximately two-fold decrease in the *d*-function exponent for aug-cc-pVDZ produces polarizabilities nearly equivalent to aug-cc-pVQZ, although the total energy is more than 0.2 a.u. higher. The 6-311++G(3df,3pd) basis includes another diffuse ($\zeta = 0.1565$) *d*-function, at which point the polarizabilities are close to those of aug-cc-pVQZ.

The Pople basis sets systematically converge to the aug-cc-pVQZ polarizability from below, while the Dunning basis sets appear to converge from above, if we neglect the smallest case, aug-cc-pVDZ, although certainty as to the convergence in the basis set cannot be obtained without calculations at even larger basis sets. The singly-

augmented Dunning basis sets are suitable for polarizabilities because they all include two *d*-functions, which allows a balanced convergence in the correlation energy as well as properties. The Pople basis sets were optimized for thermochemistry before correlated methods became commonplace and one should not expect a similar rate of convergence in the basis set for energies and properties.

The Sadlej pVTZ basis set produces accurate results with a small number of functions and was specifically designed for polarizability calculations [26]. For that reason, it is the only basis set used for extremely large calculations where using more functions is computationally intractable.

3.3.2 Importance of iterative triples

While the CCSD model obtains a large percentage of correlation effects for a wide variety of molecules, the contribution of triples is important for both energies and properties. For energies, the CCSD(T) model [29] is widely used for the inclusion of triples, but this method has no corresponding response function, and cannot be used to obtain dynamic properties. For calculating response functions, the CC3 model [30] has been shown to be an excellent approximation to full iterative triples [31]. The effect of triple excitations is important for dynamic polarizabilities [32]; computational limitations permitted evaluating the effect of triples using the CC3 model only for static polarizabilities of benzene using three small basis set, 6-31+G*, 6-31++G**, and aug-cc-pVDZ. The results are listed in Table 3.3. Because the use of small basis sets mitigates the full manifesting of triples and the accuracy of CC3 has not been calibrated for molecules with more than two atoms, future investigation is necessary to fully understand the role of triples in aromatic molecules.

For benzene, the absolute difference between α_{LL} polarizabilities for the CCSD

Table 3.3: Benzene dipole polarizabilities calculated with CCSD and CC3 and the three small basis sets. Energies and polarizabilities are given in atomic units.

Method	E_{CC}	α_{LL}	α_{NN}
	6-31+G*		
CCSD	-231.514693	75.05	39.81
CC3	-231.552142	74.47	39.88
Δ	-0.037449	-0.58	0.07
	6-31++G**		
CCSD	-231.564128	75.50	40.43
CC3	-231.602965	74.81	40.43
Δ	-0.038837	-0.69	0.00
	aug-cc-pVDZ		
CCSD	-231.589824	80.09	44.83
CC3	-231.631672	79.24	44.59
Δ	-0.041848	-0.85	-0.24

and CC3 models increases with the flexibility of the basis set, from 0.58 to 0.69 with the singly and doubly augmented Pople basis sets to 0.85 for aug-cc-pVDZ. The difference in the α_{NN} polarizability is negligible for the Pople basis sets and 0.24 for aug-cc-pVDZ. While the small basis sets make definitive conclusions impossible, the effect of triples for static polarizabilities of benzene is not large enough to justify concern as to the validity of the CCSD calculations. A more complete investigation of the role of triples in aromatic molecules, particularly for dynamic polarizabilities, is in progress [24].

3.3.3 Geometry effects

When studying long conjugated systems, one must carefully select the method with which to optimize the geometry. In this section, we compare optimized carbon-carbon bond lengths from B3LYP to SCF, PBE0 and MP2 (See Table 3.4 for details).

Kadantsev, et al. [17] previously found that for naphthalene, anthracene, tetracene and pentacene, B3LYP/6-311++G(d,p) agrees well with experiment compared to PBE and LSDA. Martin and coworkers studied polyaromatic hydrocarbons including naphthalene and anthracene and found the B3LYP/cc-pVDZ was generally accepted for understanding the structural properties of these molecules, but that due to bond-length-alternation (BLA), B3LYP/cc-pVTZ is desirable [33]. Houk and coworkers found that B3LYP/6-31G* reproduced crystallographic geometries to within 0.01 Å for benzene through pentacene [36]. An experimental geometry for hexacene is not available because it is not stable [37].

The optimized geometries in this study employ a larger basis set than previously used for these molecules and include frozen-core MP2 calculations as well, which have not been reported for most of these molecules. For anthracene, none of the methods reproduce all of the bond lengths accurately. There are many reasons why this could be the case. The accuracy of geometries for larger polyacenes, where BLA is more likely to occur, is of greater concern. Fortunately, the B3LYP and PBE0 for anthracene agree well with the corrected B3LYP/cc-pVDZ values of Martin and coworkers [33]. Both DFT methods agree with the tetracene and pentacene experimental geometries to within 0.01Å, except for three bonds in tetracene. SCF and MP2 are noticeably less accurate. Because no experimental geometry is available for hexacene, a complete evaluation of optimized geometries is not possible.

Because the B3LYP/cc-pVTZ optimized geometries agree well with the experimental ones, polarizability calculations were not run at other geometries. Further justification is the excellent agreement of CCSD polarizabilities with experiment for naphthalene using the B3LYP geometry.

Figure 3.2: Numbering scheme for carbon atoms in (a) anthracene, (b) tetracene, (c) pentacene, (d) hexacene. The presence of double bonds indicates only that all carbons are sp^2 hybridized.

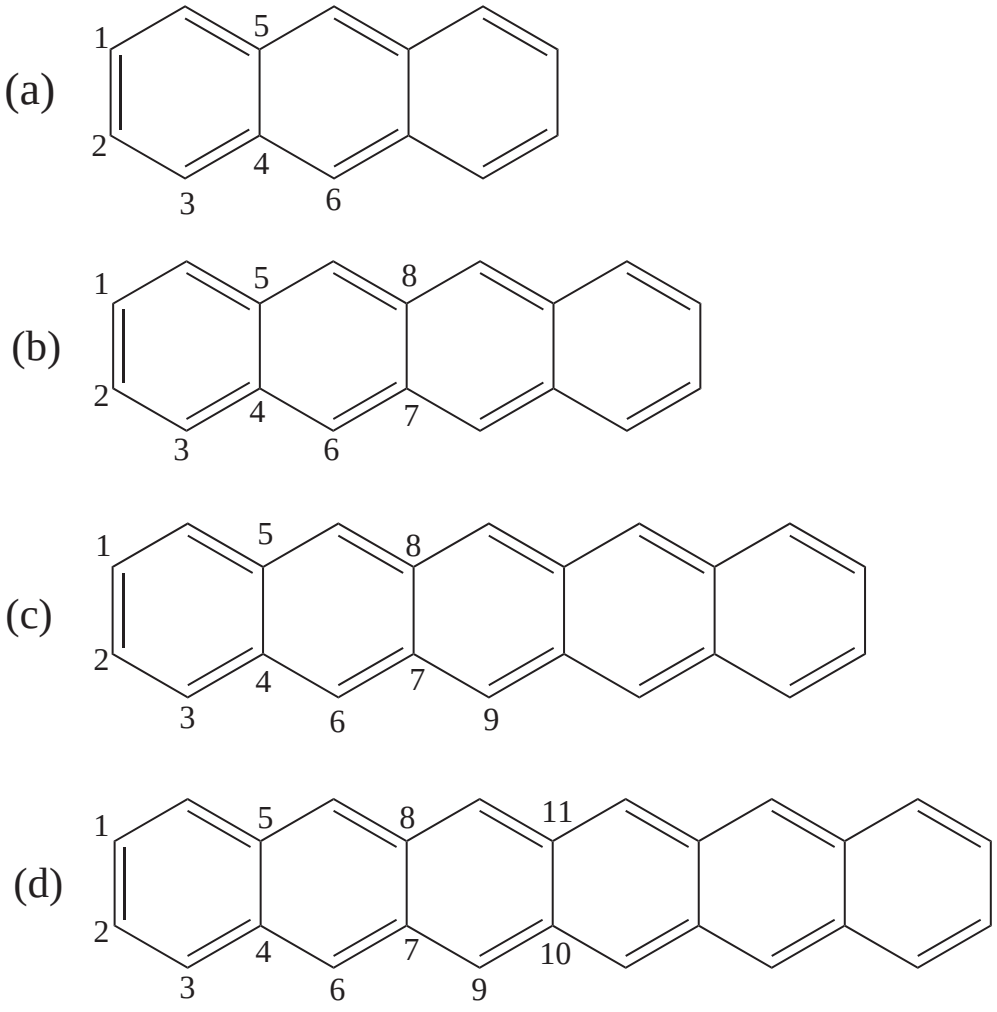

Table 3.4: Geometry data for anthracene, tetracene, pentacene and hexacene. All calculations were performed using the cc-pVTZ basis set. For MP2 only, the core orbitals were frozen. All bond lengths are given in Angstroms.

Bond	SCF	B3LYP	PBE0	MP2	Expt.[a]
			Anthracene		
d(C_1−C_2)	1.43040	1.42144	1.41826	1.41268	1.442(8)
d(C_2−C_3)	1.34339	1.36331	1.36058	1.36664	1.397(4)
d(C_3−C_4)	1.43298	1.42548	1.42178	1.41380	1.437(4)
d(C_4−C_5)	1.42047	1.43970	1.43399	1.43214	1.437(4)
d(C_4−C_6)	1.38567	1.39499	1.39170	1.39093	1.392(6)
			Tetracene		
d(C_1−C_2)	1.43993	1.42622	1.42302	1.41540	1.46
d(C_2−C_3)	1.33792	1.36025	1.35748	1.36509	1.35
d(C_3−C_4)	1.44143	1.42963	1.42593	1.41585	1.42
d(C_4−C_5)	1.43454	1.44670	1.44091	1.43553	1.42
d(C_4−C_6)	1.36918	1.38677	1.38359	1.38714	1.39
d(C_6−C_7)	1.40493	1.40509	1.40188	1.39682	1.40
d(C_7−C_8)	1.42316	1.44685	1.44121	1.44257	1.46
			Pentacene		
d(C_1−C_2)	1.44576	1.42871	1.42563	1.41619	1.43
d(C_2−C_3)	1.33484	1.35873	1.35603	1.36477	1.35
d(C_3−C_4)	1.44638	1.42871	1.42795	1.41619	1.42
d(C_4−C_5)	1.44472	1.43594	1.44452	1.45044	1.44
d(C_4−C_6)	1.35946	1.38669	1.37966	1.38287	1.38
d(C_6−C_7)	1.41747	1.41009	1.40679	1.39785	1.40
d(C_7−C_8)	1.43057	1.44650	1.44593	1.45180	1.45
d(C_7−C_9)	1.38718	1.39691	1.39359	1.39328	1.39
			Hexacene		
d(C_1−C_2)	1.44948	1.43011	1.42700	1.42233	
d(C_2−C_3)	1.33293	1.35789	1.35514	1.37040	
d(C_3−C_4)	1.44949	1.43273	1.42908	1.42384	
d(C_4−C_5)	1.45198	1.45244	1.44658	1.42261	
d(C_4−C_6)	1.35340	1.38078	1.37756	1.39478	
d(C_6−C_7)	1.42580	1.41265	1.40944	1.40489	
d(C_7−C_8)	1.43830	1.45465	1.44875	1.45456	
d(C_7−C_9)	1.37491	1.39270	1.38942	1.40146	
d(C_9−C_{10})	1.40089	1.40195	1.39872	1.40162	
d(C_{10}−C_{11})	1.43241	1.45577	1.44981	1.45960	

[a] Experimental geometries are from Ref. [38] for anthracene (electron diffraction) and Ref. [39] for tetracene and pentacene (x-ray crystallography).

3.3.4 Comparison of density-functional and coupled-cluster polarizabilities for linear oligoacenes

Comparison of CCSD to four common density-functionals has been made for benzene using the aug-cc-pVTZ basis and for naphthalene through hexacene using Sadlej pVTZ (calculations for naphthalene and anthracene find that Sadlej pVTZ and aug-cc-pVDZ produce nearly identical results). For benzene, naphthalene, anthracene and pentacene we compare polarizabilities at $\omega = 0.0$ a.u. and $\omega = 0.072$ a.u. (632 nm).

For benzene, as seen in Table 3.5, none of the calculated static polarizabilities fall within the experimental error bars, although an explanation for this was already noted in [16]. The agreement with experiment for dynamic polarizabilities is much better; however, none of the functionals can produce polarizabilities which are within the error bars for both the planar and perpendicular values. The PBE0 value of α_{LL} agrees very well with CCSD and experiment, although the α_{NN} value is underestimated by $\sim 5\%$. The other three functionals agree well with the experimental α_{NN} value but exaggerate the α_{LL} value. Only CCSD produces values which fall within the error bars for both components of the polarizability.

In the case of naphthalene (see Table 3.6), the DFT errors for static polarizabilities with respect to the experimental values are consistently larger than the CCSD ones. In this case the CCSD provides the most balanced description of α_{LL}, α_{MM}, and α_{NN} quantities for $\omega = 0.0$. For example, the discrepancy between CCSD and BLYP values for α_{LL} amounts to 8.64 a.u. At the same time the α_{LL} value at the CCSD level (166.61 a.u.) is located close to the one of the experimental value 164.6 a.u. It is clear for naphthalene that functionals which include some exact exchange (B3LYP and PBE0) outperform those which do not (BLYP and PBE). The role of exact exchange

Table 3.5: Benzene dipole polarizabilities calculated with the aug-cc-pVTZ basis set and various methods. Polarizabilities and frequencies are given in atomic units.

Method	$\omega = 0.0$		$\omega = 0.072$	
	α_{LL}	α_{NN}	α_{LL}	α_{NN}
HF	78.87	45.20	81.78	46.28
BLYP	82.79	43.76	86.27	44.86
B3LYP	81.20	43.02	84.46	44.04
PBE	82.11	43.08	85.47	44.10
PBE0	80.26	42.27	83.37	43.19
CCSD	80.26	44.51	83.12	45.48
Experiment [42][a]	82.36±0.79	49.13±1.09	82.73±0.91	44.94±1.33

[a] Data taken from Ref. [16].
[b] Polarizability obtained from Buckingham effect measurements.

in polarizabilities and excited states for DFT has been noted by [34] and others. For frequency-dependent polarizabilities (in Table 3.5 we discuss results obtained only for $\omega = 0.072$) discrepancies between DFT and CCSD results are bigger. A good illustration is again provided by a difference of the BLYP and CCSD α_{LL} values which equals 12.26 a.u. Also the PBE0 results are significantly above the CCSD ones for α_{LL} polarizabilities. While for $\omega = 0.0$ these method differ by 1.94 a.u. for $\omega = 0.072$, this difference reaches 3.75 a.u. A similar trend in accuracy of polarizabilities is seen for anthracene (Table 3.7), although comparison with experimental data (even on the CCSD level) is more problematic.

For larger oligoacenes we compare dynamic polarizabilities for pentacene using CCSD, PBE and PBE0. All results are collected in Table 3.8. In both DFT calculations, the α_{MM} component of the dynamic polarizability is erroneous due to approaching or crossing a pole. Consistent with the results for smaller oligoacenes, the presence of exact exchange makes PBE0 significantly closer to CCSD than PBE, and the error in PBE increases substantially for finite frequency.

Table 3.6: Dipole polarizabilities of naphthalene for various levels of theory. Polarizabilities and frequencies are given in atomic units.

	$\omega = 0.0$			$\omega = 0.072$		
Method	α_{LL}	α_{MM}	α_{NN}	α_{LL}	α_{MM}	α_{NN}
BLYP	175.25	127.77	66.23	188.40	134.19	67.86
B3LYP	170.92	124.88	65.37	182.90	130.79	66.88
PBE	173.60	126.48	65.21	186.27	132.65	66.70
PBE0	168.55	123.11	64.37	179.89	128.71	65.73
CCSD	166.61	123.39	66.43	176.14	128.14	67.79
Experiment [44][a,b]	164.6	122.8	64.8			
Experiment [45][a,c]	161.9	119.4	70.8			

[a] Data taken from Ref. [40].
[b] Crystal refraction.
[c] Laser Stark spectroscopy using a static field.

Table 3.7: Dipole polarizabilities of anthracene for various levels of theory. Polarizabilities and frequencies are given in atomic units.

	$\omega = 0.0$			$\omega = 0.072$		
Method	α_{LL}	α_{MM}	α_{NN}	α_{LL}	α_{MM}	α_{NN}
BLYP	303.53	171.78	86.43	338.75	185.48	88.43
B3LYP	294.19	168.15	85.32	325.26	180.16	87.17
PBE	301.11	170.16	85.13	335.20	183.29	86.96
PBE0	290.11	165.91	84.03	319.48	177.18	85.71
CCSD	281.60	166.00	87.58	305.21	173.95	89.33

Method	α_{LL}	α_{MM}	α_{NN}
Experiment [43][a,c]	237.54	172.76	102.57
Experiment [46][a,d]	242.27	165.33	107.30
Experiment [48][b,e]	367	174	154

[a] Data taken from Ref. [41].
[b] Data taken from Ref. [47].
[c] Cotton-Mouton effect in benzene.
[d] Kerr effect in benzene at 589 nm.
[e] Kerr effect in CCl_4.

Table 3.8: Static and dynamic polarizabilities of pentacene at different levels of theory using the Sadlej TZ basis set. The α_{MM} component of the dynamic polarizability (in parentheses) is erroneous for the both PBE and PBE0 since the frequency is greater than the first pole of the response function in the corresponding symmetry. Polarizabilities and frequencies are given in atomic units.

	$\omega = 0.0$			$\omega = 0.072$		
Method	α_{LL}	α_{MM}	α_{NN}	α_{LL}	α_{MM}	α_{NN}
PBE	642.22	259.61	120.20	773.43	(175.85)	122.59
PBE0	603.36	254.92	118.58	704.92	(373.30)	120.77
CCSD	589.97	254.92	129.58	672.07	284.54	132.06

Literature values were used to compared to static polarizabilities for oligoacenes $n = 1-6$ to determine the saturation rate with respect to ring size and to quantify the large error in the longitudinal polarizability component. We find that the difference between two common functionals (PBE0 and B3LYP) and CCSD is approximately 10% for $n = 6$, and the limited nature of the basis sets used for the DFT calculations reported suggests that difference would be larger if the Sadlej basis set was used.

3.3.5 Accuracy of frequency-dependent polarizabilities

The accuracy of DFT polarizabilities as a function of frequency is a less explored dimension than the size-related error. We compare both benzene and pyrene at a number of frequencies up to the first excitation energy. The results of our calculations are juxtaposed in Tables 3.8, 3.10 and 3.11. We find a significant overestimation of the polarizability for pyrene, especially the planar component, while the DFT values for benzene are fairly accurate.

At zero frequency, all three functionals examined (B3LYP, PBE, PBE0) underestimate the normal component of the polarizability, α_{NN} and both B3LYP and PBE

Table 3.9: Static dipole polarizabilities of linear oligoacenes for $n = 1 - 6$. The first set of data is the polarizability tensor components and the second is the values per ring, $\widehat{\alpha} = \alpha/n$, indicating the level of saturation with increasing n. Polarizabilities are given in atomic units.

	CCSD/Sadlej pVTZ[a]			B3LYP/6-311G+(2d,1p)[b]			PBE0/6-311G+(2d,2p)[c]		
Rings	α_{LL}	α_{MM}	α_{NN}	α_{LL}	α_{MM}	α_{NN}	α_{LL}	α_{MM}	α_{NN}
1	80.57	80.57	44.66	79.38	79.38	42.97	78.75	78.75	42.65
2	166.61	123.39	66.43	168.59	121.70	63.58	166.48	120.53	63.03
3	281.60	166.00	87.58	291.56	164.63	83.83	287.07	162.97	83.07
4	423.83	209.77	108.61	447.60	209.00	103.97	439.52	206.90	102.98
5	589.97	254.92	129.58	634.65	255.01	124.00	622.40	252.90	123.00
6	776.83	301.26	150.55	849.55	302.79	143.95	831.79	300.57	142.85
Rings	$\widehat{\alpha}_{LL}$	$\widehat{\alpha}_{MM}$	$\widehat{\alpha}_{NN}$	$\widehat{\alpha}_{LL}$	$\widehat{\alpha}_{MM}$	$\widehat{\alpha}_{NN}$	$\widehat{\alpha}_{LL}$	$\widehat{\alpha}_{MM}$	$\widehat{\alpha}_{NN}$
1	80.57	80.57	44.66	79.38	79.38	42.97	78.75	78.75	42.65
2	83.31	61.70	33.22	84.30	60.85	31.79	83.24	60.27	31.52
3	93.87	55.33	29.19	97.19	54.88	27.94	95.69	54.32	27.69
4	105.96	52.44	27.15	111.90	52.25	25.99	109.88	51.73	25.75
5	117.99	50.98	25.92	126.93	51.00	24.80	124.48	50.58	24.60
6	129.47	50.21	25.09	141.59	50.47	23.99	138.63	50.10	23.81

[a] Geometry optimized with B3LYP/cc-pVTZ.
[b] Geometry optimized with B3LYP/6-311G(2d,1p). All values taken from Ref. [47].
[c] Geometry optimized with PBE0/6-311G+(2d,2p). Values for $n = 1 - 4$ are from Ref. [22].

Table 3.10: Frequency-dependent dipole polarizabilities of benzene and the lowest excited state of any symmetry (denoted by ω_{pole}) at the respective levels of theory using the Sadlej basis set. Polarizabilities and frequencies are given in atomic units.

	PBE		PBE0		B3LYP		CCSD	
ω	α_{LL}	α_{NN}	α_{LL}	α_{NN}	α_{LL}	α_{NN}	α_{LL}	α_{NN}
0.000	82.31	42.48	80.25	41.74	81.53	42.54	80.55	44.64
0.020	82.55	42.55	80.48	41.81	81.77	42.62	80.76	44.72
0.040	83.30	42.79	81.18	42.02	82.50	42.86	81.41	44.96
0.060	84.60	43.19	82.38	42.39	83.78	43.26	82.54	45.36
0.080	86.54	43.78	84.18	42.92	85.68	43.85	84.21	45.95
0.100	89.27	44.60	86.69	43.65	88.34	44.66	86.51	46.76
0.150	101.68	48.05	97.89	46.63	100.39	48.08	96.56	50.05
ω_{pole}	0.193		0.202		0.199		0.189[a]	

[a] Taken from Ref. [49].

slightly exaggerate the planar component. At $\omega = 0.100$, all three functionals display similar differences with respect to CCSD as for the static values. At $\omega = 0.150$, α_{LL} is exaggerated on account of proximity to a pole.

For pyrene, the accuracy is far worse at all values of ω. Again, PBE0 is fairly close to the CCSD values. However, as the frequency approaches the ultraviolet region, the errors with respect to CCSD exceed 10% for the planar component. PBE and B3LYP are erroneous by 20.6% and 13.4%, respectively, for $\omega = 0.100$. The BLYP functional was found to produce the least accurate polarizabilities of the four functionals compared so calculations for that functional are not reported.

3.4 Conclusions

In this chapter, the first massively parallel implementation of coupled-cluster linear response theory is applied to large aromatic molecules and comparison of both static and dynamic dipole polarizabilities with respect to common DFT functionals is made.

Table 3.11: Frequency-dependent dipole polarizabilities of pyrene and the lowest excited state of any symmetry (denoted by ω_{pole}) for the four DFT methods. Polarizabilities and frequencies are given in atomic units.

	PBE		PBE0		B3LYP		CCSD	
ω	α_{LL}	α_{MM}	α_{LL}	α_{MM}	α_{LL}	α_{MM}	α_{LL}	α_{MM}
0.000	299.12	217.51	290.74	210.40	294.42	213.18	285.94	210.12
0.020	301.31	218.38	292.71	211.15	296.63	214.09	287.58	210.86
0.040	308.95	221.39	299.38	213.80	303.68	216.88	292.69	213.13
0.060	323.72	226.86	311.97	218.56	317.08	221.91	301.97	217.14
0.080	350.99	235.73	333.90	226.08	340.74	229.92	316.97	223.32
0.100	411.32	250.23	375.18	237.79	386.84	242.52	341.10	232.46
ω_{pole}	0.125		0.138		0.134		-	

The BLYP and PBE functionals do not include exact-exchange, while PBE0 and B3LYP include 25% and 20% exact-exchange, respectively. Because of the importance of exact-exchange in maintaining the proper physical behavior of delocalized electron distributions, the performance of the functionals for the systems considered here is $PBE0 > B3LYP > PBE > BLYP$. These four functionals outperformed other functionals considered (BP86, B3P86, OLYP) but data for these other functionals is not reported here. These conclusions are not restricted to the molecules considered here, but have been found to be true when many types of functional groups perturb the aromatic ring [50].

For benzene, the CCSD/aug-cc-pVTZ level of theory is found to reproduce both the planar and normal component of the dynamic polarizability to within experimental precision, which cannot be said for any of the functionals considered. The agreement with the static experimental values is not as good, and this is attributed to the neglect of vibrational contributions to the polarizability, which are more important in static polarizabilities. For naphthalene, the CCSD/Sadlej pVTZ level

of theory accurately reproduces the experimental values while common functionals exaggerate the longitudinal component. For larger oligoacenes, comparison to gas-phase experimental data cannot be made, although the four functionals considered all overestimate the longitudinal component of the polarizability, with the error growing towards 15% of the total value.

Evaluation of the frequency-dependence of the dynamic polarizability has been made for both benzene and pyrene. For benzene, the accuracy of DFT functionals follows the trend that PBE0 accurately reproduces the planar polarizability while underestimating the normal component, while B3LYP and PBE are less accurate. The deviation with respect to CCSD grows with frequency in spite of the fact that the DFT methods reproduce the location of the first pole quite well. For pyrene, the error with respect to CCSD grows significantly with frequency and it is clear that there is a significant breakdown in all of the DFT methods, although again, PBE0 is the most accurate of those considered. The magnitude of the error as a function of frequency grows significantly from benzene to pyrene, indicating that optical properties of larger polyaromatic hydrocarbons will be treated even less accurately by DFT methods. Considering that the breakdown in the nonlinear polarizabilities is much greater than the linear polarizability for conjugated systems, it is quite clear that the use of the conventional DFT methods requires special caution in studying the nonlinear optical properties of organic chromophores with more than a few conjugated rings.

REFERENCES

[1] B. Champagne, E. A. Perpète, S. J. A. van Gisbergen, E. J. Baerends, J. G. Snijders, C. Soubra-Ghaoui, K. Robins, and B. Kirtman, *J. Chem. Phys.* **109**, 10489 (1998); **110**, 11664(E) (1999); S. J. A. van Gisbergen, P. R. T. Schipper, O. V. Gritsenko, E. J. Baerends, J. G. Snijders, B. Champagne, and B. Kirtman, *Phys. Rev. Lett.* **83**, 694 (1999); B. Champagne, E. A. Perpète, D. Jacquemin, S. J. A. van Gisbergen, E. J. Baerends, C. Soubra-Ghaoui, K. Robins, and B. Kirtman, *J. Phys. Chem. A* **104**, 4755 (2000); B. Champagne, F. A. Bulat, W. Yang, S. Bonness and B. Kirtman, *J. Chem. Phys.* **125**, 194114 (2006).

[2] A. Dalgarno, *Adv. Chem. Phys.* **12**, 143 (1967).

[3] J. F. Stanton, *Phys. Rev.* **A49**, 1698 (1994).

[4] G. Placzek, in *Handbuch der Radiologie*, edited by E. Marx (Akademische Verlagsgesellschaft, Leipzip, 1934), Vol. 6, p. 205.

[5] M. Pecul and A. Rizzo, *J. Chem. Phys.* **116**, 1259 (2002).

[6] M. Born and E. Wolf, *Principles of Optics*, 6th ed. (Pergamon, New York, 1980).

[7] H. Sekino, Y. Maeda, M. Kamiya and K. Hirao, *J. Chem. Phys.* **126**, 014107 (2007).

[8] P. Sałek, T. Helgaker, O. Vahtras, H. Ågren, D. Jonsson, and J. Gauss, *Mol. Phys.* **103**, 439 (2005).

[9] H. J. Monkhorst, *Int. J. Quantum Chem.* **S11**, 421 (1977).

[10] H. Koch and P. Jørgensen, *J. Chem. Phys.* **93**, 3333 (1990); O. Christiansen, P. Jørgensen, C. Hättig, *Int. J. Quantum Chem.* **68**, 1 (1998); R. Kobayashi, H. Koch and P. Jørgensen, *Chem. Phys. Lett.* **249**,30 (1994); C. Hättig, O. Christiansen, H. Koch and P. Jørgensen, *Chem. Phys. Lett.* **269**,428 (1997); C. Hättig, O. Christiansen and P. Jørgensen, *Chem. Phys. Lett.* **282**,139 (1998).

[11] M. Kállay and J. Gauss, *J. Mol. Struct. (THEOCHEM)* **768**, 71 (2006).

[12] J. R. Hammond, M. Valiev, W. A. de Jong and K. Kowalski, *J. Phys. Chem. A*, **111**, 5492 (2007).

[13] E. J. Bylaska, W. A. de Jong, K. Kowalski, T. P. Straatsma, M. Valiev, D. Wang, E. Apra, T. L. Windus, S. Hirata, M. T. Hackler, Y. Zhao, P.-D. Fan, R. J. Harrison, M. Dupuis, D. M. A. Smith, J. Nieplocha, V. Tipparaju, M. Krishnan, A. A. Auer, M. Nooijen, E. Brown, G. Cisneros, G. I. Fann, H. Früchtl, J. Garza, K. Hirao, R. Kendall, J. A. Nichols, K. Tsemekhman, K. Wolinski, J. Anchell, D. Bernholdt, P. Borowski, T. Clark, D. Clerc, H. Dachsel, M. Deegan, K. Dyall, D. Elwood, E. Glendening, M. Gutowski, A. Hess, J. Jaffe, B. Johnson, J. Ju, R. Kobayashi, R. Kutteh, Z. Lin, R. Littlefield, X. Long, B. Meng, T. Nakajima, S. Niu, L. Pollack, M. Rosing, G. Sandrone, M. Stave, H. Taylor, G. Thomas, J. van Lenthe, A. Wong, and Z. Zhang, "NWChem, A Computational Chemistry Package for Parallel Computers, Version 5.0" (2006), Pacific Northwest National Laboratory, Richland, Washington 99352-0999, USA.

[14] S. Hirata, *J. Phys. Chem. A*, **107**, 9887 (2003); S. Hirata, *J. Chem. Phys.* **121**, 51 (2004); S. Hirata, *Theor. Chem. Acc.* **116**, 2 (2006); `http://www.csc.lsu.edu/~gb/TCE/`.

[15] K. Kowalski and W. A. de Jong, in preparation.

[16] A. Rizzo, C. Cappelli, B. Jansík, D. Jonsson, P. Sałek, S. Coriani, and H. Ågren, *J. Chem. Phys.* **121**, 8814 (2004).

[17] E. S. Kadantseva, M. J. Stott and A. Rubio, *J. Chem. Phys.* **124**, 134901 (2006).

[18] *DALTON, a molecular electronic structure program, Release 2.0* (2005), see `http://www.kjemi.uio.no/software/dalton/dalton.html`.

[19] H. Ågren, O. Vahtras, H. Koch, P. Jørgensen, and T.Helgaker, *J. Chem. Phys.* **98**, 6471, (1993); K. Ruud, D. Jonsson, P. Norman, H. Ågren, T. Saue, H. J. Aa. Jensen, P. Dahle, and P. Dahle, *J. Chem. Phys.* **108**, 7973 (1998).

[20] C. Angeli, K. L. Bak, V. Bakken, O. Christiansen, R. Cimiraglia, S. Coriani, P. Dahle, E. K. Dalskov, T. Enevoldsen, B. Fernandez, C. Hättig, K. Hald, A. Halkier, H. Heiberg, T. Helgaker, H. Hettema, H. J. Aa. Jensen, D. Jonsson, P. Jørgensen, S. Kirpekar, W. Klopper, R. Kobayashi, H. Koch, A. Ligabue, O. B. Lutnæs, K. V. Mikkelsen, P. Norman, J. Olsen, M. J. Packer, T. B. Pedersen, Z. Rinkevicius, E. Rudberg, T. A. Ruden, K. Ruud, P. Sałek, A. Sanchez de Merás, T. Saue, S. P. A. Sauer, B. Schimmelpfennig, K. O. Sylvester-Hvid, P. R. Taylor, O. Vahtras, D. J. Wilson, and H. Ågren, *DALTON Release 2 Program Manual.*

[21] *Gaussian 03, Revision C.02*, M. J. Frisch, G. W. Trucks, H. B. Schlegel, G. E. Scuseria, M. A. Robb, J. R. Cheeseman, J. A. Montgomery, Jr., T. Vreven, K.

N. Kudin, J. C. Burant, J. M. Millam, S. S. Iyengar, J. Tomasi, V. Barone, B. Mennucci, M. Cossi, G. Scalmani, N. Rega, G. A. Petersson, H. Nakatsuji, M. Hada, M. Ehara, K. Toyota, R. Fukuda, J. Hasegawa, M. Ishida, T. Nakajima, Y. Honda, O. Kitao, H. Nakai, M. Klene, X. Li, J. E. Knox, H. P. Hratchian, J. B. Cross, V. Bakken, C. Adamo, J. Jaramillo, R. Gomperts, R. E. Stratmann, O. Yazyev, A. J. Austin, R. Cammi, C. Pomelli, J. W. Ochterski, P. Y. Ayala, K. Morokuma, G. A. Voth, P. Salvador, J. J. Dannenberg, V. G. Zakrzewski, S. Dapprich, A. D. Daniels, M. C. Strain, O. Farkas, D. K. Malick, A. D. Rabuck, K. Raghavachari, J. B. Foresman, J. V. Ortiz, Q. Cui, A. G. Baboul, S. Clifford, J. Cioslowski, B. B. Stefanov, G. Liu, A. Liashenko, P. Piskorz, I. Komaromi, R. L. Martin, D. J. Fox, T. Keith, M. A. Al-Laham, C. Y. Peng, A. Nanayakkara, M. Challacombe, P. M. W. Gill, B. Johnson, W. Chen, M. W. Wong, C. Gonzalez, and J. A. Pople, Gaussian, Inc., Wallingford CT, 2004.

[22] S. M. Smith, A. N. Markevitch, D. A. Romanov, X. Li, R. J. Levis, H. B. Schlegel, *J. Phys. Chem. A* **108**, 11063 (2004).

[23] *Aces II*, a quantum chemical program package written by J. F. Stanton, J. Gauss, J .D. Watts, P. G. Szalay, R. J. Bartlett with contribution from A. A. Auer, D. B. Bernholdt, O. Christiansen, M. E. Harding, M. Heckert, O. Heun, C. Huber, D. Jonsson, J. Juselius, W. J. Lauderdale, T. Metzroth, K. Ruud and the integral packages *MOLECULE* (J. Almlöf and P. R. Taylor),Props (P. R. Taylor), and ABACUS (T. Helgaker, H. Aa. Jensen, P. Jørgensen, and J. Olsen). See also J. F. Stanton, J. Gauss, J. D. Watts, W. J. Lauderdale, R.J. Bartlett, *Int. J. Quantum Chem. Symp.* **26**, 879 (1992) as well as : `http://www.aces2.de` for the current version.

[24] J. R. Hammond and K. Kowalski, *J. Chem. Phys.* **128**, 224102 (2008).

[25] `http://mscf.emsl.pnl.gov/hardware/config_mpp2.shtml`.

[26] A. J. Sadlej, Collec. *Czech. Chem. Commun.* **53**, 1995 (1988); A. J. Sadlej and M. Urban, *J. Mol. Struct. (THEOCHEM)* **234**, 147 (1991); A. J. Sadlej, *Theor. Chim. Acta* **79**, 123 (1992); A. J. Sadlej, *Theor. Chim. Acta* **81**, 45 (1992); A. J. Sadlej, *Theor. Chim. Acta* **81**, 339 (1992).

[27] T. H. Dunning Jr., *J. Chem. Phys.* **90**, 1007 (1989); R. A. Kendall, T. H. Dunning Jr. and R. J. Harrison, *J. Chem. Phys.* **96**, 6796 (1992); D. E. Woon and T. H. Dunning Jr., *J. Chem. Phys.* **98**, 1358 (1993); D. E. Woon and T. H. Dunning Jr., *J. Chem. Phys.* **100**, 2975 (1994).

[28] P. C. Hariharan and J. A. Pople, *Theor. Chimica Acta* **28**, 213 (1973); R. Krishnan, J. S. Binkley, R. Seeger and J. A. Pople, *J. Chem. Phys.* **72**, 650 (1980); M. M. Francl, W. J. Petro, W. J. Hehre, J. S. Binkley, M. S. Gordon, D. J. DeFrees and J. A. Pople, *J. Chem. Phys.* **77**, 3654 (1982); T. Clark, J. Chandrasekhar and P. v. R. Schleyer, *J. Comp. Chem.* **4**, 294 (1983); P. M. W. Gill, B. G. Johnson, J. A. Pople and M. J. Frisch, *Chem. Phys. Lett.* **197**, 499 (1992).

[29] J. A. Pople, M. Head-Gordon and K. Raghavachari, *J. Chem. Phys.* **87**, 5968 (1987).

[30] H. Koch, O. Christiansen, P. Jørgensen, A. M. Sanchez de Merás and T. Helgaker, *J. Chem. Phys.* **106**, 1808 (1997).

[31] H. Larsen, J. Olsen, C. Hättig, P. Jørgensen, O. Christiansen and J. Gauss, *J. Chem. Phys.* **111**, 1917 (1997).

[32] O. Christiansen, J. Gauss and J. F. Stanton, *Chem. Phys. Lett.*, **292**, 437 (1998).

[33] J. M. L. Martin, J. El-Yazal and J.-P. François, *J. Phys. Chem.* **100**, 15358 (1996).

[34] S. Grimme and M. Parac, *ChemPhysChem* **3** 292, (2003); M. Parac and S. Grimme, *Chemical Physics* **292** 11, (2003).

[35] B. Champagne and E. A. Perpète, *Int. J. Quantum Chem.*, **75** 441 (1999).

[36] K. N. Houk, P. S. Lee and M. Nendel, *J. Org. Chem.*, **66**, 5517 (2001).

[37] K. B. Wiberg, *J. Org. Chem.* **62** 5720 (1997).

[38] S. N. Ketkar, M. Kelley, M. Fink and R. C. Ivey, *J. Mol. Struct.* **77**, 127 (1981).

[39] R. Campbell and J. Robertson, *Acta Crystallogr.* **15**, 289 (1962).

[40] S. Millefiori and A. Alparone, *J. Mol. Struct. (THEOCHEM)* **422**, 179 (1998).

[41] Z. G. Soos, E. V. Tsiper and R. A. Pascal Jr., *Chem. Phys. Lett.* **342**, 652 (2001).

[42] G. L. D. Ritchie and J. N. Watson, *Chem. Phys. Lett.* **322**, 143 (2000).

[43] C. L. Cheng, D. S. N. Murthy and G. L. D. Ritchie, *Aust. J. Chem.* **25**, 1301 (1972).

[44] H. F. Vuks. *Opt. Spectrosc.* **20**, 361 (1966).

[45] S. Heitz, D. Weidauer, B. Rosenow and A. Hese, *J. Chem. Phys.* **96**, 976 (1992).

[46] R. J. W. Le Fèvre, L. Radom and G. L. D. Ritchie, *J. Chem. Soc. B*, 775 (1968).

[47] A. Hinchcliffe and H. J. S. Machado, *Int. J. Mol. Sci.* **1**, 8 (2000).

[48] H. G. Kuball and R. Gob, *Z. Physik. Chem.* **NF63**, 251 (1969).

[49] J. E. Del Bene, J. D. Watts and R. J. Bartlett, *J. Chem. Phys.* **106**, 6051 (1997).

[50] J. R. Hammond, K. Kowalski and W. A. de Jong, unpublished results.

[51] O. Christiansen, C. Hättig and J. Gauss, *J. Chem. Phys.* **109**, 4745 (1998).

CHAPTER 4

COUPLED-CLUSTER CALCULATIONS FOR STATIC AND DYNAMIC POLARIZABILITIES OF C_{60}

This chapter has been previously published in the following article: K. Kowalski, J. R. Hammond, W. A. de Jong and A. J. Sadlej, "Coupled-cluster calculations for static and dynamic polarizabilities of C_{60}," *J. Chem. Phys.* **129**, 226101 (2008). Copyright 2008 by the American Institute of Physics.

4.1 Introduction

Due to the role the C_{60} molecule plays in condensed phase studies and its possible application as a nonlinear optical material, the properties of C_{60} have been intensively studied over the last two decades. Two measurements have provided experimental values for the static [1] and dynamic [2] ($\lambda = 1064$ nm) dipole polarizability (α). Antoine *et al.* used a beam deflection technique to assess the static polarizability of the isolated C_{60} molecule. The obtained value of 76.5±8 $Å^3$ is characterized by significant uncertainty. Ballard *et al.* [2] measured 79±4 $Å^3$ for the optical polarizability at a wavelength of 1064 nm. Calculating electric properties of C_{60} is a significant challenge, which is best illustrated by the range of different theoretical estimates of its polarizability which vary from 36 to 154 $Å^3$ [3, 4, 5, 6].

Owing to the delocalized character of the electronic structure of C_{60}, the proper choice of the basis set and accurate inclusion of the correlation effects are paramount

for obtaining reliable results for dipole polarizabilities. Ruud *et al.* [7] generated results of 75.1 and 76.4 $Å^3$ in good agreement with the experimental values 76.5±8 and 79±4 $Å^3$ for $\lambda = \infty$ and $\lambda = 1064$ nm. However, the authors employed a rather small 6-31++G basis set and did not account for correlation effects. A later study by Pedersen *et al.* [8] clearly shows the strong basis set/correlation effect dependence of the polarizability. For example, for the static polarizability the difference between the 6-31++G and aug-cc-pVDZ [8] is as big as 5.5 $Å^3$ (37 a.u.). For dynamic polarizabilities, the differences are even larger. Due to the large size of the molecular system very few coupled-cluster (CC) calculations have been performed for C_{60}. Pedersen *et al.* used the CC2 method [9] with an aug-cc-pVDZ basis set and the Cholesky approximation for the two-electron integrals, to obtain polarizabilities equal to 92.33 $Å^3$ (623.70 a.u.) and 94.77 $Å^3$ (640.15 a.u.) for $\lambda = \infty$ and $\lambda = 1064$ nm [8], respectively, which are too high compared to experiment. These discrepancies may be caused by the incomplete treatment of correlation effects due to singles and doubles offered by the CC2 formalism. Moreover, the results by Pedersen *et al.* [8] appear to indicate that the CC2 method combined with sufficiently flexible basis sets may overestimate the electron correlation contribution to the dipole polarizability of C_{60}. To our knowledge the reported calculations are the first attempt to investigate the dipole polarizability of C_{60} within the non-truncated form of the linear response CC formalism with single and double excitations (CCSD-LR) [10, 11]. The present CCSD-LR studies provide also an estimate of the effect of terms neglected in the CC2 method. Simultaneously, the present calculations are carried out with property-tailored basis set suitable for calculations of electric dipole polarizabilities, yet small enough to make these calculations feasible. This leaves the basis set choice as the main factor which determines the accuracy of the theoretical value of the dipole polarizability of C_{60}.

4.2 Results

The present calculations use the recently developed reduced-size polarized basis sets [13, 14] denoted hereafter by ZPolX, where X is the element symbol. The ZPolC basis set used in this study corresponds to the Zm3PolC basis set of Ref. [14]. The ZPolX basis sets originate from earlier ideas [15] concerning the form of the electric-field-dependence of basis set functions and have lead to the development of the so-called PolX sets [16]. In comparison with PolX sets the ZPolX basis sets offer significant reduction (by about 1/3) of the basis set size with negligible $(1-2\%)$ loss of accuracy of the calculated polarizabilities. They are presumably the smallest basis sets which lead to reliable theoretical data for dipole polarizabilities.

Prior to our study of C_{60}, we checked the performance of both the LR-CCSD method and ZPolC basis set for benzene. Despite the significantly reduced dimension, the ZPolC results are in a good agreement with those obtained with the PolC basis set (Table 4.1). The differences between ZPolC and PolC data for static longitudinal, $\alpha_{LL}(0)$, and normal, $\alpha_{NN}(0)$, components of the polarizability tensor amount to 0.25 and 0.50 a.u., respectively. For the optical frequency $\omega = 0.072$, the respective numbers are 0.22 and 0.49 a.u. One should also add that the PolX basis sets give dipole polarizabilities which are of similar accuracy as those calculated with considerably larger aug-cc-pVTZ [17] basis sets.

The results for $\alpha(\omega)$ ($\alpha = \alpha_{XX} = \alpha_{YY} = \alpha_{ZZ}$) of C_{60} are shown in Table 4.2. Due to the size of the system, we converged all CCSD iterations to 10^{-4}. One may expect that the quality of our CC calculations primarily depends on the basis set choice, assumptions concerning the geometry, and on the level of including the electron correlation effects. The geometry dependence is not considered in this paper and for

Table 4.1: CCSD polarizabilities (in a.u.) of benzene.

	$\omega = 0.0$		$\omega = 0.072$	
Basis set	α_{LL}	α_{NN}	α_{LL}	α_{NN}
aug-cc-pVDZ	80.08	44.85	82.94	45.85
aug-cc-pVTZ	80.21	44.47	83.09	45.45
POLC	80.51	44.61	83.43	45.66
ZPolC	80.76	45.11	83.65	46.15
Experiment	82.36 ±0.79	49.13 ±1.09	82.73 ±0.91	44.94 ±1.33

Benzene geometry as in Ref. [12]; all electrons correlated.

the sake of direct comparisons with earlier studies we have used the same geometry of C_{60} as in Refs. [7, 8]. The study of the benzene molecule (Table 4.1) shows that the ZPolC basis set performs similarly to aug-cc-pVDZ and aug-cc-pVTZ sets. Hence, by comparing our results with the CC2 data of Pedersen *et al.* [8] we can estimate the importance of terms which are not included in the CC2 formalism. The CC2 value of $\alpha(0)$ for the aug-cc-pVDZ basis set is equal to 623.70 a.u. (92.33 Å^3) and increases to 640.15 (94.77 Å^3) for $\lambda = 1064$ nm (see Ref. [8]). Hence, for static and dynamic cases the differences between the CC2 data of Pedersen *et al.* [8] and present LR-CCSD values of α are equal to 10.13 Å^3 and 11.15 Å^3, respectively. This indicates that T_2-dependent terms, not included in CC2, play an important role in the evaluation of linear response properties in C_{60}. This conclusion is in line with the hierarchical structure of CC methods discussed by Christiansen, Koch, and Jørgensen in Ref. [9]. The calculated LR-CCSD static polarizability of C_{60} is well within error bars of the experimental value. The LR-CCSD dynamic polarizability for $\lambda = 1064$ nm is only marginally higher (by 0.62 Å^3) than the upper limit for the experimental estimate (see Table 4.2).

All calculations were performed with our CCSD-LR implementation in NWChem [18]. The observed speedup when going from 256 to 1024 CPUs is a factor of ~ 3.75. Indi-

Table 4.2: Polarizabilities of C_{60} in $Å^3$ (a.u.).

Wavelength (nm)	CCSD/ZPolC	Experiment
∞	82.20 (555.27 a.u.)	76.5±8
1064	83.62 (564.84 a.u.)	79±4
532	88.62 (598.64 a.u.)	-

C_{60} geometry from Ref. [7]; C 1s orbitals frozen.

vidual timings per CCSD iteration amount to 2924 and 776 seconds for 256 and 1024 CPUs, respectively (1080 basis set functions were used).

4.3 Conclusion

Using the complete form of the CCSD-LR theory and employing a perturbation-dependent basis set (ZPol), we obtained a theoretical estimate for the polarizabilities of C_{60} that fall into experimental error bars (static polarizability) or are above the experimental error bars by 0.62 $Å^3$. Our crude estimates indicate that the effect of full inclusion of T_2-dependent terms affects polarizabilities by $12 - 13\%$ when the treatment of electron correlation changes from CC2 to CCSD.

REFERENCES

[1] R. Antoine, Ph. Dugourd, D. Rayane, E. Benichou and M. Broyer, *J. Chem. Phys.* **110**, 9771 (1999).

[2] A.Ballard, K. Bonin and J. Louderback, *J. Chem. Phys.* **113**, 5732 (2000).

[3] H. Weiss, R. Ahlrichs and M. Häser, *J. Chem. Phys.* **99**, 1262 (1993).

[4] J. Cioslowski, *Electronic Structure Calculations on Fullerenes and Their Derivatives* (Oxford University Press, 1995).

[5] P. Norman, Y. Luo, D. Jonsson and H. Ågren, *J. Chem. Phys.* **106**, 8788 (1997).

[6] K. Bonin and V. Kresin, *Electric-Dipole Polarizabilities of Atoms, Molecules, and Clusters* (World Scientific, Singapore, 1997).

[7] K. Ruud, D. Jonsson and P. R. Taylor, *J. Chem. Phys.* **114**, 4331 (2001).

[8] T. B. Pedersen, A. J. Sánchez de Merás and H. Koch, *J. Chem. Phys.* **120**, 8887 (2004).

[9] O. Christiansen, H. Koch and P. Jørgensen, *Chem. Phys. Lett.* **243**, 409 (1995).

[10] H. J. Monkhorst, *Int. J. Quantum Chem.* **S11**, 421 (1977); E. Daalgard and H.J. Monkhorst, *Phys. Rev. A* **28**, 1217 (1983).

[11] H. Koch and P. Jørgensen, *J. Chem. Phys.* **93**, 3333 (1990).

[12] J. R. Hammond, K. Kowalski and W. A. de Jong, *J. Chem. Phys.* **127**, 144105 (2007).

[13] Z. Benkova, A. J. Sadlej, R. E. Oakes and S. E. J. Bell, *J. Comp. Chem.* **26**, 145 (2005);

[14] Z. Benkova, A.J. Sadlej, R.E. Oakes and S. E. J. Bell, *Theor. Chem. Acc.* **113**, 238 (2005); A. Baranowska, M. Siedlecka and A. J. Sadlej, *Theor. Chem. Acc.* **118**, 959 (2007).

[15] A. J. Sadlej, *Chem. Phys. Lett.* **47**, 450 (1977); A. Baranowska and A. J. Sadlej, *Chem. Phys. Lett.* **398**, 270 (2004).

[16] A. J. Sadlej, *Coll. Czech. Chem. Comm.* **53**, 1995 (1988); A. J. Sadlej and M. Urban, *J. Mol. Struct. (THEOCHEM)* **234**, 147 (1991); A. J. Sadlej, *Theor. Chim. Acta* **79**, 123 (1992); A. J. Sadlej, *Theor. Chim. Acta* **81**, 45 (1992); A. J. Sadlej, *Theor. Chim. Acta* **81**, 339 (1992); I. Černušák, V. Kellö and A. J. Sadlej, *Coll. Czech. Chem. Comm.* **68**, 211 (2003).

[17] T. H. Dunning, Jr., *J. Chem. Phys.* **90**, 1007 (1989); R. A. Kendall, T. H. Dunning, Jr. and R. J. Harrison, *J. Chem. Phys.* **96**, 6796 (1992); D. E. Woon and T. H. Dunning, Jr., *J. Chem. Phys.* **98**, 1358 (1993); D. E. Woon and T. H. Dunning, Jr., *J. Chem. Phys.* **100**, 2975 (1994).

[18] E. J. Bylaska, W. A. de Jong, N. Govind, K. Kowalski, T. P. Straatsma, M. Valiev, D. Wang, E. Apra, T. L. Windus, J. Hammond, P. Nichols, S. Hirata, M. T. Hackler, Y. Zhao, P.-D. Fan, R. J. Harrison, M. Dupuis, D. M. A. Smith, J. Nieplocha, V. Tipparaju, M. Krishnan, Q. Wu, T. Van Voorhis, A. A. Auer, M. Nooijen, E. Brown, G. Cisneros, G. I. Fann, H. Fruchtl, J. Garza, K. Hirao, R.

Kendall, J. A. Nichols, K. Tsemekhman, K. Wolinski, J. Anchell, D. Bernholdt, P. Borowski, T. Clark, D. Clerc, H. Dachsel, M. Deegan, K. Dyall, D. Elwood, E. Glendening, M. Gutowski, A. Hess, J. Jaffe, B. Johnson, J. Ju, R. Kobayashi, R. Kutteh, Z. Lin, R. Littlefield, X. Long, B. Meng, T. Nakajima, S. Niu, L. Pollack, M. Rosing, G. Sandrone, M. Stave, H. Taylor, G. Thomas, J. van Lenthe, A. Wong and Z. Zhang. "NWChem, A Computational Chemistry Package for Parallel Computers, Version 5.1" (2007), Pacific Northwest National Laboratory, Richland, Washington 99352-0999, USA.

CHAPTER 5
BENCHMARK CALCULATIONS OF DFT FUNCTIONALS FOR THE BINDING ENERGIES AND DIPOLE POLARIZABILITIES OF WATER CLUSTERS

5.1 Introduction

Liquid water is an ubiquitous solvent with many interesting chemical properties. Simulations of bulk liquid water come in two varieties: first-principles molecular dynamics simulations (FPMD) wherein the energies and forces are computed with density function theory (DFT) and those where an empirical potential (force field) is employed. The complexity of both types of models has increased significantly with time. Whereas in the past FPMD with LDA and the TIP3P water model were standard, the pursuit of greater chemical accuracy has led to models of ever increasing complexity. FPMD can now be done with GGA or GGA hybrids and water force fields have evolved from simple rigid-body models like TIP3P [1] to flexible models which incorporate various physically relevant effects (see Refs. [2, 3, 4, 5] for a few examples).

The microscopic interactions between water molecules have been investigating with high-resolution experiments on water clusters which have elucidated, among other things, the minimum-energy structures for small clusters [6, 7]. These experiments affirmed early benchmark quantum chemical studies for water clusters up to the hexamer [8]. Over the past 20 years, the synergy between theory and experiment has led to a detailed understanding of the competing physical effects at work, such as

the competition between hydrogen bond count and conformation strain therewithin as well as the vital role of zero-point vibrational energy in determining the minimum-energy hexamer.

Previous investigations [9, 10] of the performance of DFT for polarizabilities considered very small molecules which are not relevant to the evaluation of functionals for bulk properties. Subsequently, two groups considered the electric properties of water clusters [11, 12, 13]. This paper addresses shortcomings of previous work by considering the polarizability of water clusters at the CCSD-LR level of theory [14], which provides highly accurate polarizability [15], yet can be applied to very large molecular systems [16]. The role of basis set choice is evaluated by comparing results using basis sets from the Dunning, Pople and Sadlej families. Finally, we consider a variety of functionals (PBE0, B3LYP, X3LYP, HCTH120, Becke98, CAMB3LYP and CAMPBE0), not all of which have been evaluated for large molecular systems. Classic models like Hartree-Fock and MP2 are not considered since the shortcomings of the former for polarizabilities are well-documented and the accuracy of the latter is not sufficiently greater than DFT to justify the additional computational cost. Additionally, neither method is relevant to one of the purposes of this paper, which is to identify density functionals which should most accurately reproduce bulk polarization in liquid water.

5.2 Computational details

Coupled-cluster dipole polarizabilities were computed with the NWChem [17] TCE response property module as described in Refs. [16] and [18]. The largest CCSD-LR calculation — $(H_2O)_{12}$ with aug-cc-pVDZ (516 functions) — was run on 256 nodes

(4 cores per node) of the Chinook supercomputer with wall times per iteration of ~ 600, ~ 1300 and ~ 900 seconds, respectively for the T, Λ and $T^{(1)}$ equations, for a total wall time of ~ 33 hours.

Polarizability calculations at the DFT level, including asymptotically-corrected functionals [19], were also performed using NWChem using the approach of Autschbach and coworkers [20]. For comparison, the $(H_2O)_{12}$ job with CAMPBE0/aug-cc-pVDZ took less than an hour on 8 nodes (4 cores per node). Asymptotically-corrected functionals require approximately twice the wall time as conventional GGA hybrids under the current implementation.

Monomer polarizability calculations at the SCF, MP2, CCS, CC2 and CC3 level of theory were performed using Dalton 2.0 [21] and Aces II (MAB) [22].

5.3 Results

In order to understand polarizabilities and binding energies of water clusters, a hierarchy of benchmarks have been performed. First, polarizabilities of the water monomer were calibrated at the highest levels of theory permissible. Second, polarizabilities and binding energies were calibrated for small clusters using CCSD and CCSD(T) with aug-cc-pVNZ (N=D,T,Q). Third, basis sets from the Dunning, Pople and Sadlej families were compared at the DFT level of theory for all clusters. Finally, we compare polarizabilities and binding energies from DFT calculations to CCSD results. Water cluster labeling conventions used in the figures are given in Table 5.1.

The aug-cc-pVXZ (X=D,T,Q) basis sets [23] will be abbreviated to DZ, TZ and QZ when the usage is clear. No other basis sets will use these abbreviations.

Table 5.1: Labeling scheme for clusters with multiple isomers. W_n=$(H_2O)_n$.

W_6	b=Book	W_{11}	a=434	W_{20}	d=Dodecahedron
	c=Cage		b=4412		e=Edge-sharing
	y=cYclic		c=443		f=Face-sharing
	p=Prism		d=515		c=fused Cubes
			e=551		
W_8	d=D_{2d}	W_{17}	i=Interior		
	s=S_4		s=Surface		

5.3.1 Benchmarking the monomer

High-level calculations which approach the feasible limit for the treatment of both correlation and basis set were performed in order to understand the possible limitations in are cluster calculations. In Table 5.2, we compare wavefunction methods from SCF to CCSDT for Dunning's augmented DZ and TZ basis sets as well as CCSDTQ with just DZ. The polarizability of the water monomer has a strong dependence on the treatment of both correlation and the basis set. The MP2 results are somewhat close to those of CCSD but are clearly not a suitable replacement for high-accuracy calculations. Other low-order methods — SCF, CCS and CC2 — are much less accurate. The approximate triples method CC3 reproduces CCSDT to within 0.003 a.u. and in this case appears to be a very useful method for including triple excitations without the storage requirements of CCSDT. Lastly, the effect of quadruples (CCSDTQ-CCSDT) is almost one-third that of triples (CCSDT-CCSD) — -0.019 a.u. versus -0.065 a.u. — for the isotropic polarizability. While this is interesting in the context of theoretical benchmarking, higher-order correlation is not likely to play a significant role for larger clusters since their magnitude is dwarfed by lower-order effects. In addition, computation of clusters — even the dimer — at the

Table 5.2: Static dipole polarizabilities of the water monomer and the dimer. The isotropic (α_{iso}) and anisotropic components (α_{ani}) are reported for aug-cc-pVDZ (DZ) and aug-cc-pVTZ (TZ) using a variety of methods.

		α_{iso}		α_{ani}	
	Method	DZ	TZ	DZ	TZ
Monomer	SCF	8.163	8.465	1.484	1.208
	MP2	9.190	9.556	0.971	0.638
	CCS	8.596	8.905	1.666	1.375
	CC2	9.764	10.099	0.970	0.634
	CCSD	9.225	9.484	1.057	0.778
	CC3	9.158	9.477	1.048	0.744
	CCSDT	9.160	9.474	1.049	0.745
	CCSDTQ	9.141	-	1.051	-
Dimer	SCF	16.712	17.082	3.084	2.930
	MP2	19.051	-	3.524	-
	CCS	17.509	17.899	2.984	2.851
	CC2	20.197	20.584	3.578	3.390
	CCSD	19.107	19.357	3.471	3.238
	CCSDT	19.022	-	3.609	-

CCSDTQ/aug-cc-pVDZ level of theory is impossible.

As is suggested by the DZ and TZ results, none of the results in Table 5.2 are close to being converged in the basis set. Table 5.3 presents data only at the SCF, CCSD and CCSDT level of theory for very large basis sets. It is immediately obvious that SCF is inadequate for both the isotropic and anisotropic components of the polarizability, demonstrating the large role of electron correlation even for water near the equilibrium geometry. The difference in α_{iso} between CCSD and CCSDT appears large with the aug-cc-pVDZ basis (0.065 au) but it drops to 0.011 a.u. for the d-aug-cc-pVQZ basis, a trend observed previously for other small molecules [15]. For the anisotropy, the opposite trend occurs, with the effect of triples increasing from -0.008 a.u. with aug-cc-pVDZ to 0.046 a.u. for d-aug-cc-pVQZ. Comparison of CCSD

Table 5.3: Comparison of SCF, CCSD and CCSDT polarizabilities for the Dunning series of basis set.

	α_{iso}			α_{ani}		
Basis	SCF	CCSD	CCSDT	SCF	CCSD	CCSDT
aug-cc-pVDZ	8.163	9.225	9.160	1.484	1.057	1.049
aug-cc-pVTZ	8.465	9.484	9.474	1.208	0.778	0.745
aug-cc-pVQZ	8.523	9.531	9.540	1.132	0.662	0.620
aug-cc-pV5Z	8.530	9.538	9.554	1.123	0.623	0.577
aug-cc-pV6Z	8.534	9.541	-	1.117	0.608	-
d-aug-cc-pVDZ	8.535	9.789	9.725	1.032	0.448	0.445
d-aug-cc-pVTZ	8.546	9.669	9.665	1.116	0.543	0.502
d-aug-cc-pVQZ	8.540	9.593	9.604	1.115	0.578	0.532
d-aug-cc-pV5Z	8.539	9.565	-	1.114	0.589	-
t-aug-cc-pVDZ	8.533	9.785	9.722	1.033	0.436	0.432
t-aug-cc-pVTZ	8.545	9.672	9.668	1.112	0.541	0.500
t-aug-cc-pVQZ	8.540	9.593	9.605	1.114	0.578	0.531
t-aug-cc-pV5Z	-	9.565	-	-	0.589	-

to CCSDT for the isotropic polarizability of the water monomer indicates that the role of triples is less than 1% and that benchmarks at the CCSD level of correlation treatment are quite useful. Further evidence for the utility of CCSD is that the effect of triples are less noticeable for larger molecules, such as benzene [16, 24].

The role of the basis set is even more critical for the water monomer than correlation. For the singly-augmented Dunning series, the change in the polarizability, particularly the anisotropy, is still noticeable between quadruple- and quintuple-zeta for CCSDT. For the CCSD results out the hextuple-zeta, α_{iso} is close to converged but α_{ani} has not yet flattened out. The only aspect of the basis set which is observed to converge is the augmentation level, for which double augmentation is sufficient since the addition of a third set of diffuse functions (t-aug) has almost no effect.

5.3.2 Benchmarking of small clusters

Because of the strong method and basis set dependence for the monomer, small clusters were studied using high-level methods. In Table 5.4 we consider the CCSD and CCSD(T) total energies and CCSD-LR isotropic and anisotropic polarizabilities for aug-cc-pVNZ basis sets (N=D,T,Q) for small water clusters. As expected, the basis set dependence of the total energies is not small, nor is the role of electron correlation. However, the basis set dependence of the polarizabilities is quite small. Variance with the basis set size if the anisotropic component is larger than for the isotropic component. While the change from TZ to QZ of α_{ani} is larger than from DZ to TZ, α_{iso} changes negligibly in both cases for the dimer and trimer. From these results, the use of CCSD/aug-cc-pVDZ polarizabilities to calibrate water cluster polarizabilities is well justified.

The method dependence of the binding energies is expected to be much larger than that of the polarizability, but when DZ and TZ are compared, the basis set dependence appears relatively small (See Table 5.5). The difference between the DZ and TZ SCF binding energies of the dimer, trimer, tetramer and pentamer are 0.40, 0.69, 0.58 and 0.45 kJ/mol, respectively. For the hexamer, the basis set dependence of the binding energies varies with geometry, namely, the dimensionality of the hydrogen-bond network. The number of hydrogen bonds in the 6 hexamers (book, cage, cyclic and prism) are seven, eight, six and nine while the changes in the SCF binding energy from DZ to TZ are 0.763, 1.050, 0.423 and 1.293 kJ/mol, respectively. The heptamer, which resembles the cage hexamer, displays qualitatively similar basis set dependence to that structure.

Table 5.4: Comparison of basis sets for coupled-cluster energies and polarizabilities of small water clusters using aug-cc-pVNZ basis sets. $\Delta E = E_n - nE_1$.

E (Hartrees)	DZ		TZ		QZ	
n	CCSD	CCSD(T)	CCSD	CCSD(T)	CCSD	CCSD(T)
1	-76.271643	-76.277026	-76.335784	-76.344496	-76.355826	-76.365303
2	-152.551248	-152.562649	-152.679461	-152.697425	-152.719231	-152.738720
3	-228.839165	-228.857187	-229.031697	-229.059623	-228.839165	-
4	-305.128927	-305.153637	-305.385901	-305.423802	-	-
α (bohr^3)	CCSD/DZ		CCSD/TZ		CCSD/QZ	
n	Iso	Ani	Iso	Ani	Iso	Ani
1	9.26	1.03	9.54	0.71	9.56	0.61
2	19.11	3.47	19.36	3.24	19.31	2.83
3	28.94	5.28	29.02	5.21	28.94	4.87
4	39.06	7.46	38.96	7.51	-	-

The basis set dependence of the correlated methods follow a similar trend to the mean-field binding energies for the hexamer, albeit with the opposite sign. The changes in the second-order ($E_{MP2} - E_{SCF}$) contribution to the binding energy from DZ to TZ are -1.014, -1.144, -0.960 and -1.222 kJ/mol for the four W_6 isomers. The basis set dependence of the CCSD ($E_{CCSD} - E_{MP2}$) and CCSD(T) ($E_{CCSD(T)} - E_{CCSD}$) contributions (see Table 5.5) are significantly smaller, nearly equal in magnitude but opposite each other in sign, and follow the same trend as the MP2 contributions. That the CCSD and CCSD(T) contributions themselves are also nearly equal and but opposite in sign affirms the value of previous MP2 calculations for the binding energies of water [25].

5.3.3 Basis set evaluation for computing cluster polarizabilities

The basis set dependence of the cluster calculations was evaluated by comparing the results with DZ and TZ basis sets. For CCSD and all six DFT functionals, the absolute difference in the isotropic and anisotropic component of the polarizability was less than 0.5 a.u. and generally decreased with cluster size. For the isotropic component, the polarizability change from DZ to TZ was exclusively positive. The difference between DZ and TZ for the decamer was 0.21, 0.14 and 0.21 au, respectively, for B3LYP, PBE0 and B98. The effect of basis on the polarizability per molecules is thus very small for larger clusters when using the Dunning series.

In addition to verifying that the aug-cc-pVDZ basis was sufficient for the purposes of comparing methods, numerous other basis sets were evaluated using the B3LYP and PBE0 functionals. In Figure 5.1, four common Pople basis sets [27] (6-31+G*, 6-31++G**, 6-311+G* and 6-311++G**) are compared to aug-cc-pVQZ (where available). The data confirms what should be well known, which is that the

Table 5.5: Comparison coupled-cluster binding energies of small water clusters. $\Delta E = E_n - nE_1$.

ΔE (kJ/mol)	SCF	MP2-SCF	CCSD-MP2	CCSD(T)-CCSD
aug-cc-pVDZ				
2	-6.870	-4.340	0.624	-0.701
3	-13.711	-9.182	1.548	-1.506
4	-18.278	-11.840	2.184	-1.954
5	-19.456	-12.119	2.309	-1.994
6b	-19.892	-13.456	2.417	-2.232
6c	-19.330	-14.318	2.424	-2.382
6y	-20.424	-11.995	2.314	-1.970
6p	-19.498	-14.352	2.305	-2.406
7	-20.981	-15.268	2.580	-2.547
aug-cc-pVTZ				
2	-6.466	-4.573	0.678	-0.708
3	-13.025	-9.943	1.662	-1.566
4	-17.691	-12.664	2.285	-2.004
5	-19.005	-13.035	2.404	-2.047
6b	-19.129	-14.470	2.554	-2.300
6c	-18.280	-15.462	2.599	-2.478
6y	-20.002	-12.955	2.404	-2.025
6p	-18.204	-15.574	2.492	-2.513
7	-19.824	-16.461	2.767	-2.642
Difference				
2	0.404	-0.233	0.053	-0.007
3	0.686	-0.761	0.114	-0.060
4	0.587	-0.824	0.102	-0.050
5	0.451	-0.916	0.095	-0.054
6b	0.763	-1.014	0.137	-0.068
6c	1.050	-1.144	0.175	-0.095
6y	0.423	-0.960	0.090	-0.055
6p	1.293	-1.222	0.188	-0.106
7	1.157	-1.192	0.187	-0.095

Pople family of basis sets is inadequate for computing polarizabilities. Not only do the Pople basis sets not reproduce the magnitude of the polarizability per molecule, which is 9.9 for the Dunning basis sets but less than 9 for all Pople basis sets, but the qualitative trends in the relative magnitude of the polarizability for different isomers of clusters with the same cardinality. For the hexamer, the ordering of the polarizability for book and cyclic isomers changes between the Pople and Dunning sets, which is of consequence if one wishes to use the minimum polarizability principle from conceptual DFT to try and predict the stability of various isomers. The relative ordering of the polarizabilities is reversed for the two isomers of W_{17} between the Pople and Dunning basis sets. Similarly, the double-zeta Pople basis sets (6-31+G* and 6-31++G**) also improperly order the polarizabilities of W_{11} while the triple-zeta Pople sets (6-311+G* and 6-311++G**) agree with the ordering of aug-cc-pVDZ.

Comparison of Dunning and Sadlej basis sets [26] for water clusters was less interesting (see Figure 5.2). All four of the Sadlej basis sets considered (POL, HYPOL, Z2POL, Z3POL) closely reproduced the Dunning basis set polarizabilities. The POL and HYPOL basis sets were closer to aug-cc-pVTZ whereas Z2POL and Z3POL were closer to aug-cc-pVDZ. The excellent agreement of POL with aug-cc-pVQZ is consistent with other results (such as Ref. [16]), which of practical significance since POL has approximately the same rank as aug-cc-pVDZ. The only downside of using the computationally less expensive POL basis set is the absence of validation of convergence via a hierarchy of basis sets, as is available for the Dunning series.

Figure 5.1: Evaluation of Pople basis sets for water clusters (see text for details).

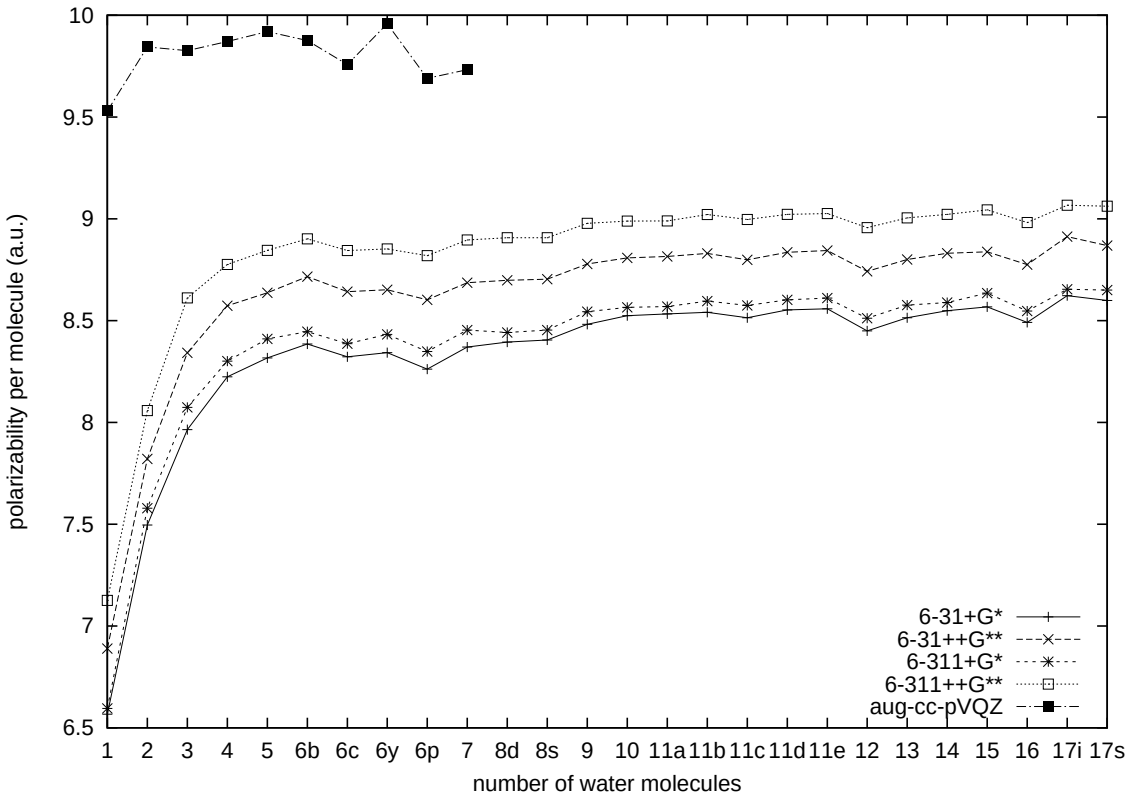

Figure 5.2: Evaluation of Sadlej basis sets for water clusters (see text for details).

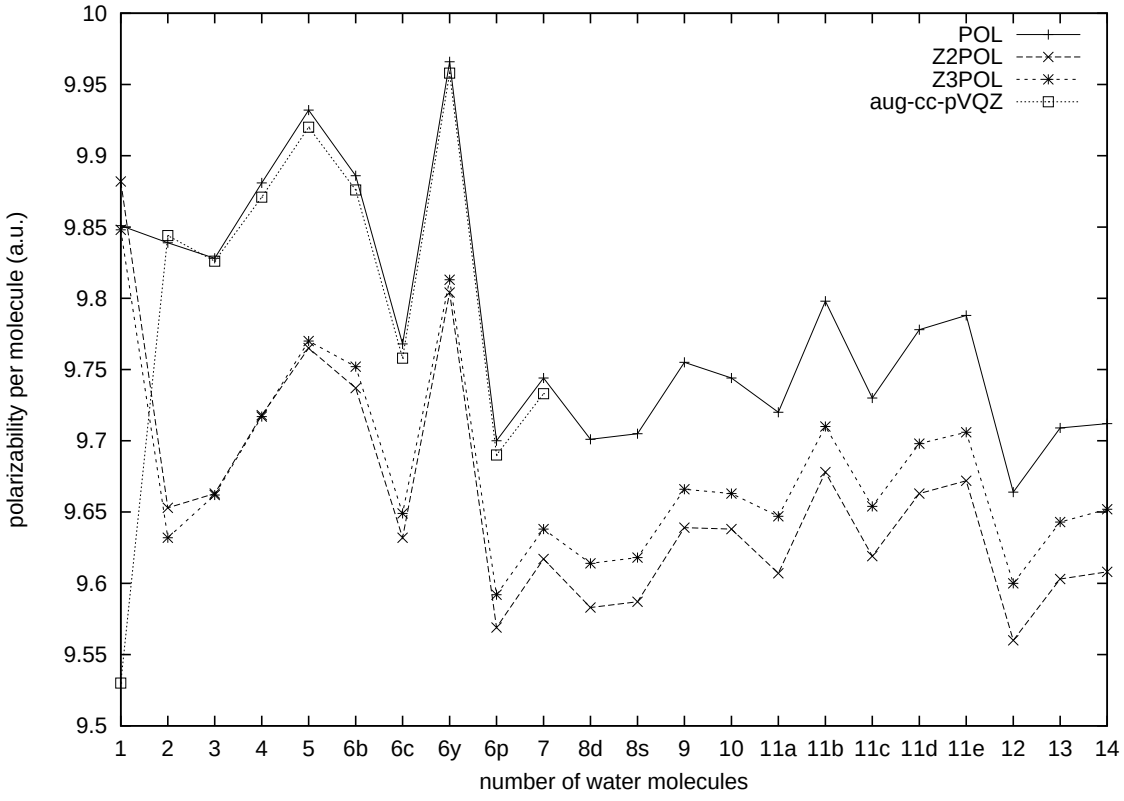

Figure 5.3: Isotropic polarizabilities of water clusters at the CCSD/aug-cc-pVDZ (frozen core) level of theory.

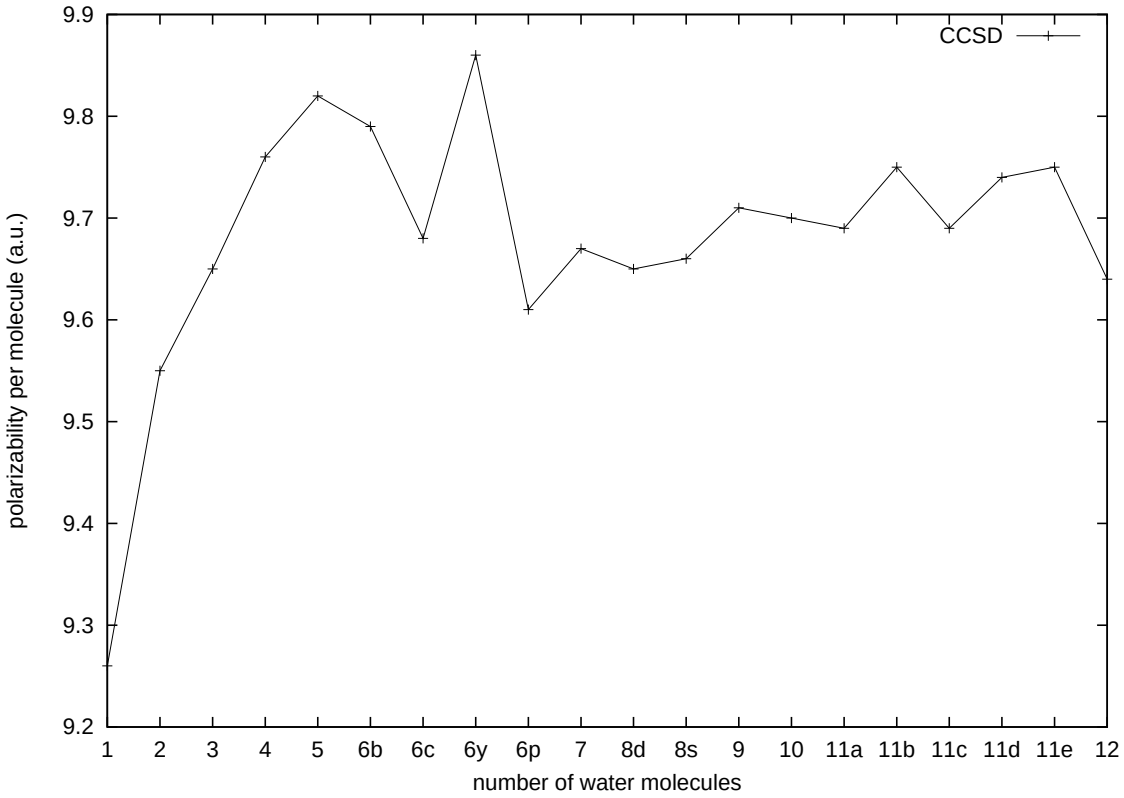

5.3.4 Comparison of density-functionals for computing cluster polarizabilities

Figure 5.3 shows the isotropic polarizability per molecule for water clusters up to W_{12} for CCSD with the DZ basis set. Errors with respect to CCSD for various density-functionals are reported in Figure 5.4. While all functionals display relatively similar trends, the rate at which each functional reaches the asymptotic value of its percent error with respect to CCSD varies. Both HCTH120 and B98 decrease in error rapidly from $N = 1 - 4$, where as PBE0, B3LYP and X3LYP are all around their asymptotic error from the start. While the asymptotic error is approximately reached at the hexamer, estimating the polarizability itself requires substantially larger clusters due to the fluctuations with respect to geometries. Starting at the heptamer, the polarizability per molecule is essentially flat as the cluster size increases suggesting asymptotic values for α_{iso}/N of ca. 9.2, 9.6, 9.7, 9.8 and 9.8 for B98, HCTH120, PBE0, B3LYP and X3LYP, respectively. The B3LYP and X3LYP functions produce essentially indistinguishable results for the polarizability, while the total energies are quite different. Finally, the PBE0 functional is clearly most able to reproduce the CCSD polarizabilities, with errors ranging from 0.17% to 0.42% for $4 \leq N \leq 21$.

The polarizability anisotropy, whose magnitude is highly dependent on the cluster geometry, is reported in Figure 5.5. Data is reported only up to $N = 15$ because large clusters have a substantially larger anisotropy which obscures the trends; also, CCSD results are only available for $N \leq 12$. The CCSD anisotropy is almost exclusively lower than the DFT results, the exceptions are where B98 and CCSD are essentially identical. Except for HCTH120, the DFT functionals considered are able to reproduce the anisotropy to within 10% of CCSD. This can be attributed the im-

Figure 5.4: Errors (with respect to CCSD) in the isotropic polarizability per molecule for a number of density-functionals.

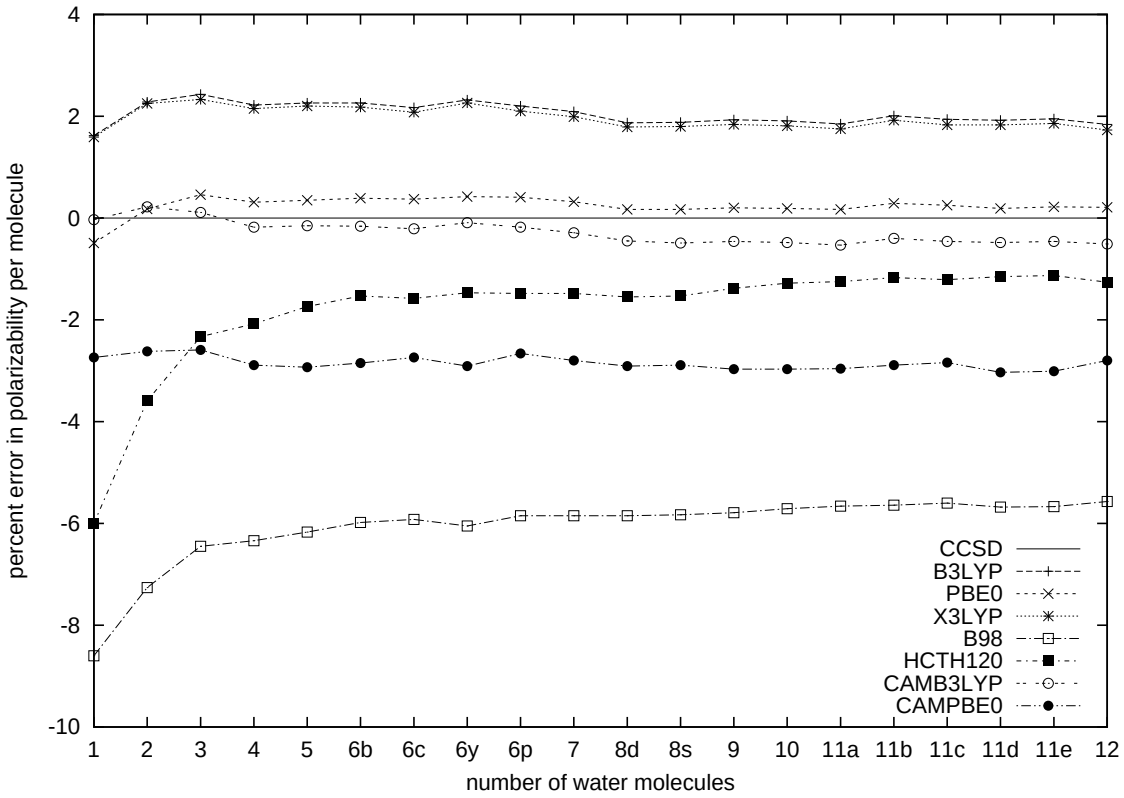

Figure 5.5: Errors (with respect to CCSD) in the anisotropic polarizability per molecule for a number of density-functionals.

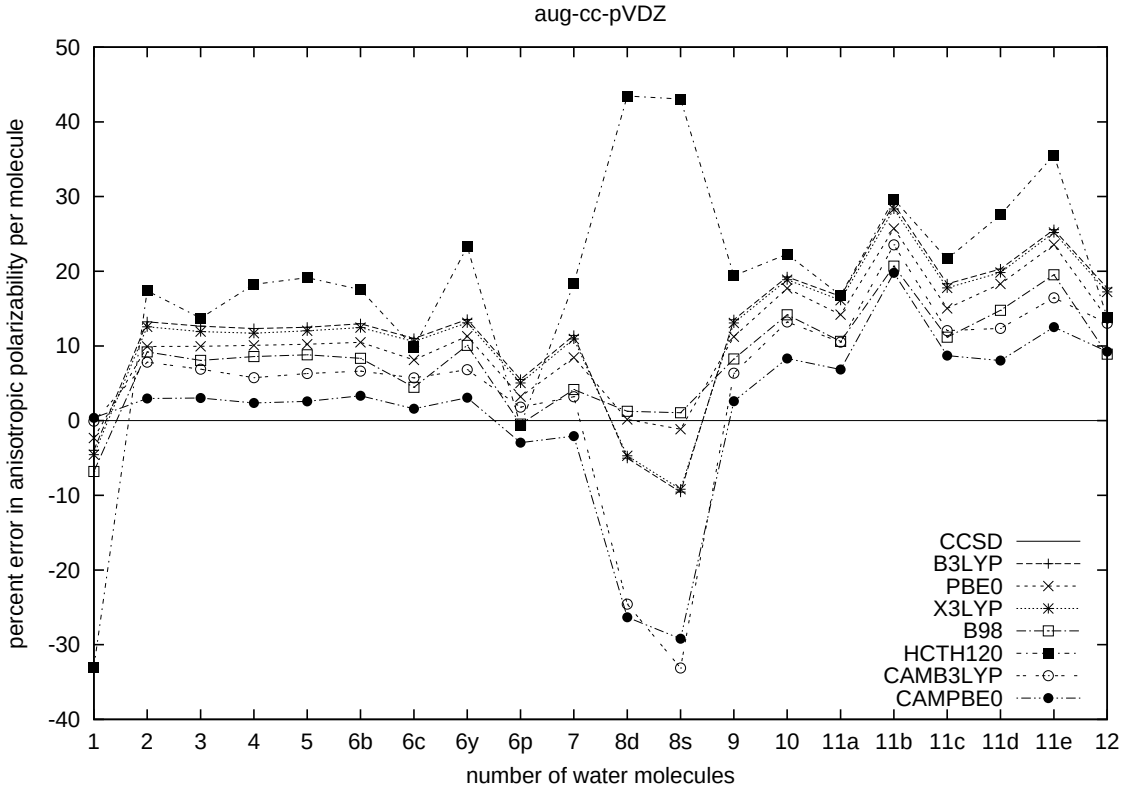

portance of exact-exchange in computing the anisotropy, since HCTH120 is a pure GGA functional.

5.3.5 Comparison of density-functionals for computing cluster binding energies

The binding energy per molecule is reported for SCF, MP2, CCSD and CCSD(T) with aug-cc-pVDZ in Table 5.6. The role of electron correlation is significant, as indicated by the large gap between the SCF data and the other methods. However, it is particularly interesting to note that the MP2 and CCSD(T) data points are

almost on top of each other. As previously noted for smaller clusters, MP2 accurately reproduces CCSD(T) for $N \leq 10$ with aug-cc-pVDZ due to a near-perfect cancellation of $\Delta E_{CCSD} - \Delta E_{MP2}$ and $\Delta E_{CCSD(T)} - \Delta E_{CCSD}$ ($\Delta E = E_n - n \cdot E_1$, that is, the binding energy). This is an important counterexample to the wisdom provided by order-by-order analysis of correlation models, which suggests that HF < MP2 < CCSD < CCSD(T) [28]. Both zeroth- and first-order terms are contained with Hartree-Fock theory while MP2 obviously contains only second-order terms. The CCSD approximation includes all third-order terms plus fourth-order terms in the space of singles, doubles and quadruples, but not triples [29]. The (T) correction to CCSD adds the missing fourth-order triples terms [30] as well as a subset of the fifth-order terms [31, 32, 33]. It is not clear why higher-order correlation effects cancel for waters clusters, such that $\Delta E_{MP2} \approx \Delta E_{CCSD(T)}$, but the numerical results suggest that it is possible to get highly accurate binding energies for water without an expensive correlation model. Because of its lower computational cost and increased parallel scalability, it is feasible to apply MP2 with a reasonable basis set to water clusters of sufficient size ($N > 100$) that it is possible to deduce bulk properties from them.

In Table 5.7, binding energies per molecule are reported for the density-functionals considered in this chapter. Both CAM functionals (CAMB3LYP and CAMPBE0) underestimate binding and are the only functionals to do so. Of the functionals which overestimate binding, the relative performance is HCTH120 < B3LYP < B98 < X3LYP < PBE0. The performance of X3LYP and PBE0 is quite similar; however, X3LYP was parameterized for water clusters whereas PBE0 contains no empirical fitting parameters [34, 35]. The error in binding per molecule of PBE0 is approximately 2 kJ/mol for clusters $N = 7 - 10$, which corresponds to $\sim 5\%$ error. In contrast, the

Figure 5.6: Binding energy per molecule for the SCF, MP2, CCSD and CCSD(T) methods with the aug-cc-pVDZ basis set.

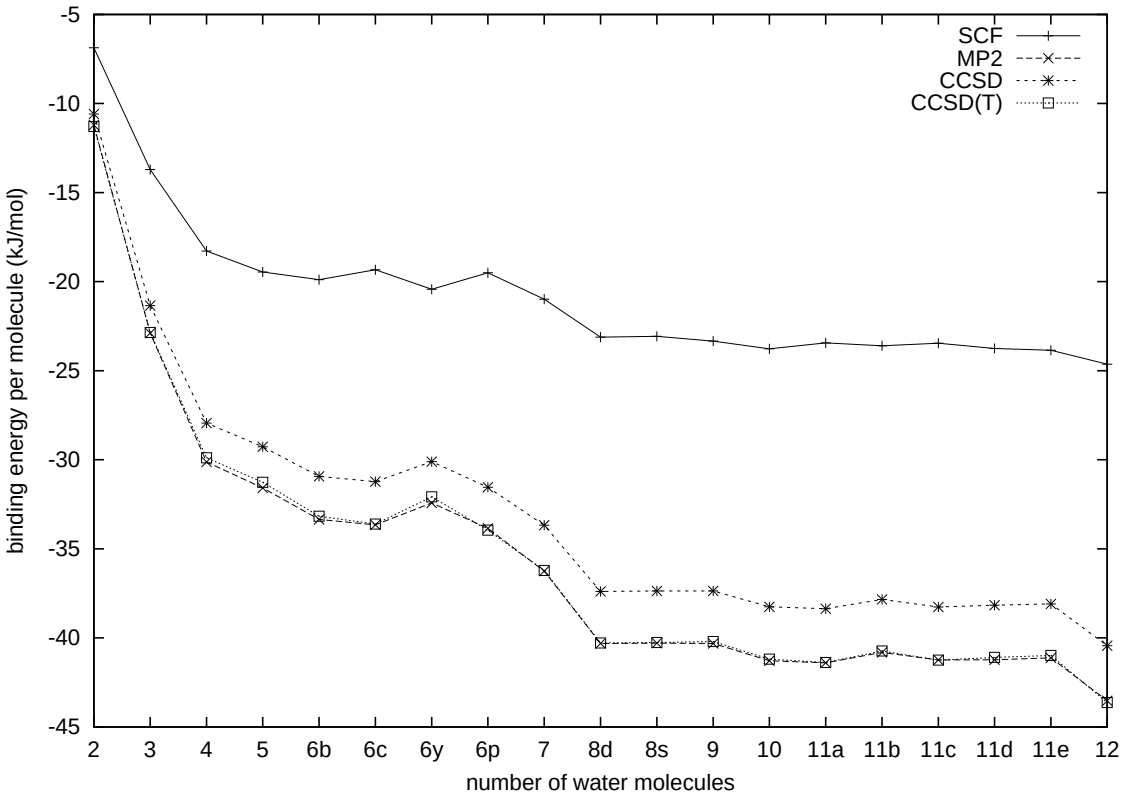

Figure 5.7: Error (with respect to CCSD(T)) in the binding energy per molecule for a number of density-functionals.

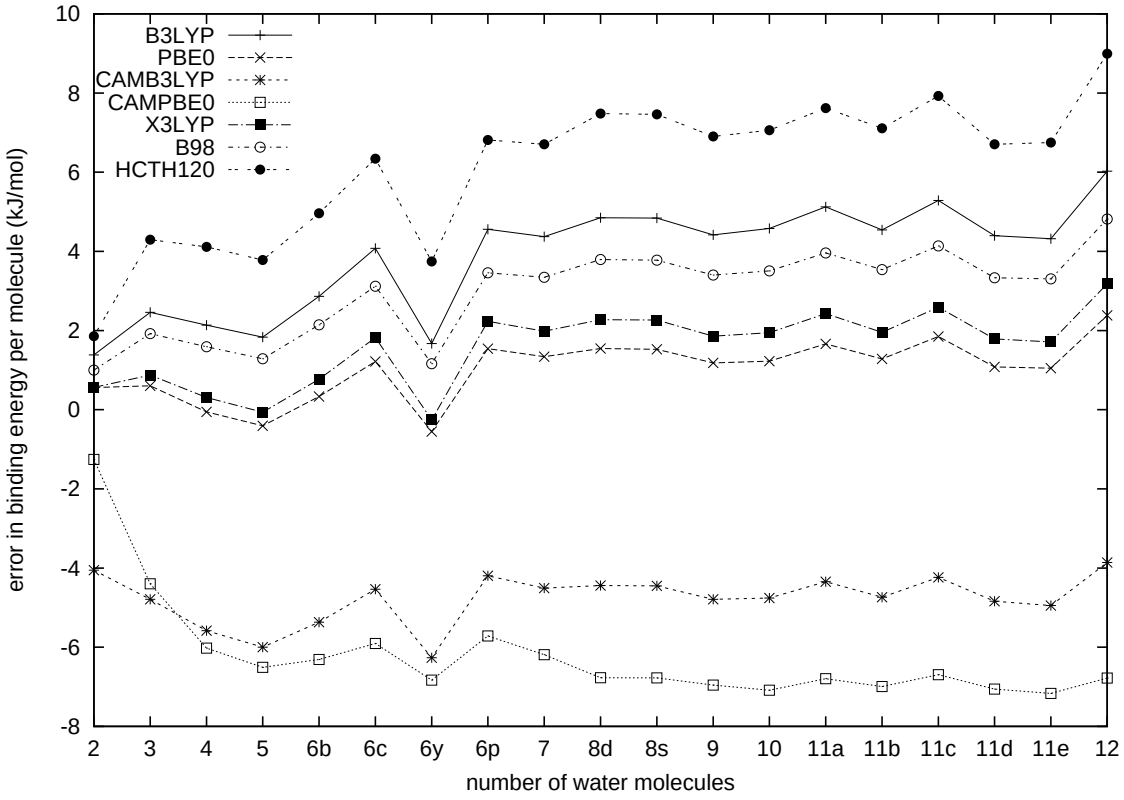

errors in MP2 are almost exclusively below 1% relative error.

A reasonable correlation is observed between the accuracy of polarizabilities and that of binding energies if the CAM functionals are excluded. The B98 and HCTH120 functionals are not particularly good for either quantity, while PBE0 is the best for both. CAMB3LYP is accurate for polarizabilities but poor for binding energies, while CAMPBE0 is poor for both. The X3LYP functional is very close to PBE0 for binding energies but nearly superimposed with B3LYP for polarizabilities. This should reveal the relative importance of difference exchange-correlation functional components.

5.4 Conclusions

The accuracy of six DFT functionals for static electric properties and binding energies of water clusters has been evaluated using coupled-cluster methods. The functionals considered were chosen from a much larger set based upon their ability to accurately predict the polarizability of a single water molecule and/or because they are common functionals used to simulate both water clusters and bulk water. In particular, the HCTH class of functionals has been touted within the CPMD community as capable of reproducing important bulk properties of water [36, 37]. However, the results of this paper demonstrate that PBE0 is superior to the other five functionals for both polarizabilities and binding energies, and by inference, superior to many other functionals not considered here since many functionals not chosen are known to be inadequate for the quantities considered. Any functional not containing some exact (Hartree-Fock) exchange is significantly less accurate for electric properties than their hybrid counterparts. Thus PBE0 is better than PBE, B3LYP is better than BLYP, and so forth. The ramifications — specifically, computational cost — of employing exact exchange in CPMD simulations are greater than in molecule simulations with Gaussian basis functions. However, at least for simulations which intend to directly quantify polarization, exact exchange cannot be neglected. It is quite clear that HCTH should not be immediately adopted as a substitute for BLYP in the CPMD community and that much more research into the development of density-functionals is necessary.

The results for MP2, however, were very encouraging and indicate that much can be learned about aqueous systems using this simple model for electron correlation, provided computational resources are available to treat sufficiently large model sys-

tems to infer bulk properties. The next important question to consider is whether or not the accuracy of MP2 for water is confined to pure water or if it is a sufficient model for treating ion solvation using cluster models. The polarizing effect of the solvated ion will be significant in such a system and extensive calibration will be necessary to determine what theoretical models are necessary to produce quantitative insight into these systems.

REFERENCES

[1] W. L. Jorgensen, J. Chandrasekhar, J. D. Madura, R. W. Impey and M. L. Klein, *J. Chem. Phys* **79**, 926 (1983).

[2] C. J. Burnham and S. S. Xantheas, *J. Chem. Phys.* **116**, 1479 (2002). S. S. Xantheas, C. J. Burnham and R. J. Harrison, *J. Chem. Phys.* **116**, 1493 (2002). C. J. Burnham and S. S. Xantheas, *J. Chem. Phys.* **116**, 1500 (2002) C. J. Burnham and S. S. Xantheas, *J. Chem. Phys.* **116**, 5115 (2002). G. S. Fanourgakis and S. S. Xantheas, *J. of Phys. Chem. A* **110**, 4100 (2006) G. S. Fanourgakis and S. S. Xantheas, *J. Chem. Phys.* **128**, 074506 (2008)

[3] G. Lamoureux, A. D. MacKerell Jr. and B. Roux, *J. Chem. Phys.* **119**, 5185 (2003).

[4] J. Chen and T. Martínez, *Chem. Phys. Lett.* **438**, 315 (2007).

[5] H. A. Stern, F. Rittner, B. J. Berne and R. A. Friesner, *J. Chem. Phys.* **115**, 2237 (2001).

[6] N. Pugliano and R. J. Saykally, *Science* **257**, 1937 (1992); J. D. Cruzan, L. B. Braly, K. Liu, M. G. Brown, J. G. Loeser and R. J. Saykally, *Science* **271**, 59 (1996); K. Liu, M. G. Brown, J. D. Cruzan and R. J. Saykally, *Science* **271**, 62 (1996); K. Liu, J. D. Cruzan and R. J. Saykally, *Science* **271**, 929 (1996); J. K. Gregory, D. C. Clary, K. Liu, M. G. Brown and R. J. Saykally, *Science* **275**, 814 (1997); J. B. Paul, R. A. Provencal, C. Chapo, K. Roth, R. Casaes and R. J.

Saykally, *J. Phys. Chem. A* 103, 2972 (1999); J. B. Paul, C. P. Collier and R. J. Saykally, *J. Phys. Chem. A* **101**, 5211 (1997); M. G. Brown, F. N. Keutsch and R. J. Saykally, *J. Chem. Phys.* **109**, 9645 (1998); Frank N. Keutsch and R. J. Saykally, *Proc. Nat. Acad. Sci.* **98**, 10533 (2001); F. N. Keutsch, M. G. Brown, P. B. Petersen, R. J. Saykally, M. Geleijns and A. van der Avoird, *J. Chem. Phys.* **114**, 3994 (2001); F. N. Keutsch, R. S. Fellers, M. R. Viant and R. J. Saykally, *J. Chem. Phys.* **114**, 4005 (2001).

[7] K. Nauta and R. E. Miller, *Science* **287**, 293 (2000).

[8] S. S. Xantheas and T. H. Dunning Jr., *J. Chem. Phys.* **99**, 8774 (1993); S. S. Xantheas, *J. Chem. Phys.* **100**, 7523 (1994); S. S. Xantheas, *J. Chem. Phys.* **102**, 4505 (1995).

[9] A. J. Cohen and Y. Tantirungrotechai, *Chem. Phys. Lett.* **299**, 465 (1999).

[10] C. Adamo, M. Cossi, G. Scalmani and V. Barone, *Chem. Phys. Lett.* **307**, 265 (1999).

[11] T. K. Ghanty and S. K. Ghosh, *J. Chem. Phys.* **118**, 8547 (2003).

[12] M. Yang, P. Senet and C. Van Alsenoy, *Int. J. of Quantum Chem.* **101**, 535 (2004).

[13] A. Krishtal, P. Senet, M. Yang and C. Van Alsenoy, *J. Chem. Phys.* **125**, 034312 (2006).

[14] H. J. Monkhorst, *Int. J. Quantum Chem.* **S11**, 421 (1977); H. Koch and P. Jørgensen, *J. Chem. Phys.* **93**, 3333 (1990); O. Christiansen, P. Jørgensen and C. Hättig, *Int. J. Quantum Chem.* **68**, 1 (1998).

[15] J. R. Hammond and K. Kowalski, *J. Chem. Phys.*, **128**, 224102 (2008).

[16] J. R. Hammond, K. Kowalski and W. A. de Jong, *J. Chem. Phys.*, **127**, 144105 (2007).

[17] E. J. Bylaska, W. A. de Jong, N. Govind, K. Kowalski, T. P. Straatsma, M. Valiev, D. Wang, E. Apra, T. L. Windus, J. Hammond, J. Autschbach, P. Nichols, S. Hirata, M. T. Hackler, Y. Zhao, P.-D. Fan, R. J. Harrison, M. Dupuis, D. M. A. Smith, J. Nieplocha, V. Tipparaju, M. Krishnan, A. Vazquez-Mayagoitia, Q. Wu, T. Van Voorhis, A. A. Auer, M. Nooijen, L. D. Crosby, E. Brown, G. Cisneros, G. I. Fann, H. Fruchtl, J. Garza, K. Hirao, R. Kendall, J. A. Nichols, K. Tsemekhman, K. Wolinski, J. Anchell, D. Bernholdt, P. Borowski, T. Clark, D. Clerc, H. Dachsel, M. Deegan, K. Dyall, D. Elwood, E. Glendening, M. Gutowski, A. Hess, J. Jaffe, B. Johnson, J. Ju, R. Kobayashi, R. Kutteh, Z. Lin, R. Littlefield, X. Long, B. Meng, T. Nakajima, S. Niu, L. Pollack, M. Rosing, G. Sandrone, M. Stave, H. Taylor, G. Thomas, J. van Lenthe, A. Wong and Z. Zhang. "NWChem, A Computational Chemistry Package for Parallel Computers, Version 5.1.1" (2009), Pacific Northwest National Laboratory, Richland, Washington 99352-0999, USA. A modified version.

[18] J. R. Hammond, M. Valiev, W. A. de Jong and K. Kowalski, *J. Phys. Chem. A*, **111**, 5492 (2007).

[19] N. Govind, M. Valiev, L. Jensen and K. Kowalski, *J. Phys. Chem. A*, Article ASAP (2009).

[20] M. Krykunov, A. Banerjee, T. Ziegler and J. Autschbach, *J. Chem. Phys.* **122**, 074105 (2005); L. Jensen, J. Autschbach and G. C. Schatz, *J. Chem. Phys.* **122**,

224115 (2005); M. Krykunov and J. Autschbach, *J. Chem. Phys.* **123**, 114103 (2005).

[21] *DALTON, a molecular electronic structure program, Release 2.0* (2005), see `http://www.kjemi.uio.no/software/dalton/dalton.html`.

[22] *Aces II*, a quantum chemical program package written by J. F. Stanton, J. Gauss, J .D. Watts, P. G. Szalay, R. J. Bartlett with contribution from A. A. Auer, D. B. Bernholdt, O. Christiansen, M. E. Harding, M. Heckert, O. Heun, C. Huber, D. Jonsson, J. Juselius, W. J. Lauderdale, T. Metzroth, K. Ruud and the integral packages *MOLECULE* (J. Almlöf and P. R. Taylor), Props (P. R. Taylor), and ABACUS (T. Helgaker, H. Å. Jensen, P. Jørgensen and J. Olsen). See also J. F. Stanton, J. Gauss, J. D. Watts, W. J. Lauderdale, R.J. Bartlett, *Int. J. Quantum Chem. Symp.* **26**, 879 (1992) as well as : `http://www.aces2.de` for the current version.

[23] T. H. Dunning Jr., *J. Chem. Phys.* **90**, 1007 (1989); R. A. Kendall, T.H. Dunning Jr. and R. J. Harrison, *J. Chem. Phys.* **96**, 6796 (1992); D. E. Woon and T.H. Dunning Jr., *J. Chem. Phys.* **98**, 1358 (1993); D. E. Woon and T.H. Dunning Jr., *J. Chem. Phys.* **100**, 2975 (1994).

[24] J. R. Hammond, W. A. de Jong and K. Kowalski, unpublished results.

[25] S. S. Xantheas, C. J. Burnham and R. J. Harrison, *J. Chem. Phys.* **116**, 1493 (2002); G. S. Fanourgakis, E. Aprá and S. S. Xantheas, *J. Chem. Phys.* **121**, 2655 (2004).

[26] A. J. Sadlej, *Coll. Czech. Chem. Comm.* **53**, 1995 (1988); A. J. Sadlej and M. Urban, *J. Mol. Struct. (THEOCHEM)* **234**, 147 (1991); A. J. Sadlej, *Theor.*

Chim. Acta **79**, 123 (1992); A. J. Sadlej, *Theor. Chim. Acta* **81**, 45 (1992); A. J. Sadlej, *Theor. Chim. Acta* **81**, 339 (1992).

[27] P. C. Hariharan and J. A. Pople, *Theor. Chimica Acta* **28**, 213 (1973); R. Krishnan, J.S. Binkley, R. Seeger and J. A. Pople, *J. Chem. Phys.* **72**, 650 (1980); M. M. Francl, W. J. Petro, W. J. Hehre, J. S. Binkley, M. S. Gordon, D. J. DeFrees and J. A. Pople, *J. Chem. Phys.* **77**, 3654 (1982); T. Clark, J. Chandrasekhar and P. v. R. Schleyer, *J. Comp. Chem.* **4**, 294 (1983); P. M. W. Gill, B. G. Johnson, J. A. Pople and M. J. Frisch, *Chem. Phys. Lett.* **197**, 499 (1992).

[28] R. J. Bartlett and M. Musiał, *Rev. Mod. Phys.* **79**, 291 (2007).

[29] R. J. Bartlett, *Ann. Rev. Phys. Chem.* **32**, 359 (1981).

[30] M. Urban, J. Noga, S. J. Cole and R. J. Bartlett, *J. Chem. Phys.* **83**, 4041 (1985).

[31] K. Raghavachari, G. W. Trucks, J. A. Pople and M. Head-Gordon, *Chem. Phys. Lett.* **157**, 479 (1989).

[32] K. Raghavachari, J. A. Pople, E. S. Replogle and M. Head-Gordon, *J. Phys. Chem.* **94**, 5579 (1990).

[33] J. F. Stanton, *Chem. Phys. Lett.* **281**, 130 (1997).

[34] X. Xu and W. A. Goddard III, *Proc. Nat. Acad. Sci.* **101**, 2673 (2004).

[35] C. Adamo and V. Barone, *J. Chem. Phys.* **110**, 6158 (1998).

[36] M. Sprik, J. Hutter and M. Parrinello, *J. Chem. Phys.* **105**, 1142 (1996).

[37] A. D. Boese, N. L. Doltsinis, N. C. Handy and M. Sprik, *J. Chem. Phys.* **112**, 1670 (2000).

CHAPTER 6

COUPLED-CLUSTER DYNAMIC POLARIZABILITIES INCLUDING TRIPLE EXCITATIONS

This chapter has been previously published in the following article: J. R. Hammond, W. A. de Jong and K. Kowalski, "Coupled-cluster dynamic polarizabilities including triple excitations," *J. Chem. Phys.* **128**, 224102 (2008). Copyright 2008 by the American Institute of Physics.

6.1 Introduction

Coupled-cluster (CC) theory [1] is one of the most successful black-box[1] methods for calculating properties of molecules. By combining a well-established hierarchy of CC methods [2] with hierarchical basis sets [3], one can obtain high accuracy for many molecular properties [4, 5, 6]. While CC algorithms to calculate static properties, which are calculated using energy derivative techniques, are well-developed and readily available in a number of programs, progress has been slower in the development of closely-related response-theoretic methods for calculating dynamic properties.

It is widely accepted that including the effect of triple excitations is vital for accurate results. For energies and static properties, the CCSD(T) [7] performs very

[1]The term "black-box" means that explicit determination of electronic configurations to be included in the correlation treatment is not necessary, in contrast to other high-accuracy techniques such as multi-reference configuration-interaction (MRCI) or perturbation-theory (MRPT).

well, often providing — for nuclear configurations not too far from equilibrium geometry — accuracy at the CCSDT level when compared to experiment. Because the perturbative treatment of triples in CCSD(T) does not provide a corresponding wave function (or response function), it cannot be used to calculate dynamic properties. For these calculations, the iterative approximate triples method CC3 [8] is very successful, in part because like CCSD(T), triples amplitudes can be calculated on-the-fly. The importance of triples for obtaining accurate dynamic polarizabilities and hyperpolarizabilities has been demonstrated using the CC3 model [9, 10]. Recently, Gauss and coworkers reported CCSDT polarizabilities [11] and hyperpolarizabilities [12], but only for double-zeta basis sets.

In this paper, we report an implementation of CC linear response theory [13, 14] within the complete manifold of single, doubles and triples (CCSDT-LR) in the spin-orbital representation, which permits calculations using RHF, UHF and ROHF references, in the NWChem [15] software suite. The present work reports CCSDT-LR dynamic polarizabilities for large basis sets and is implemented as part of the general purpose massively-parallel computational chemistry code NWChem. Using parallel computers to perform CCSDT-LR calculations with very large basis sets, we are able to explore a new accuracy regime for molecular properties. We focus exclusively on electronic polarizabilities, where vibrational effects are often quite small, usually smaller in magnitude than the errors in the purely electronic contributions. Thus, benchmarking how accurately these can be calculated will determine how much effort should be expended towards the remaining effects. The inclusion of vibrational effects — vibrationally averaged electric polarizabilities [17, 16] or pure vibrational polarizabilities [18] — is an independent topic.

To benchmark CC-LR dynamic polarizabilities, the neon atom and six diatomic

molecules (HF, N_2, CO, CN, NO and O_2) commonly used for benchmarking polarizabilities, are considered using a hierarchy of Dunning basis sets [19] with the well-known CCSD, CC3 and CCSDT models as well as the approximate non-iterative model known as PS(T) [20]. The PS(T) method is based upon the CCSD-LR approach except that the similarity-transformed Hamiltonian is corrected by shifting the location of poles in an approximate way to account for the effect of triply excited configurations. This type of correction is extremely important for dynamic polarizabilities because the cost of CC3 — N^7 versus N^6 for CCSD (N refers to the system size) — is compounded by the number of iterations which must be performed, which can be substantial for dynamic polarizabilities. In addition, CC3 requires additional storage due to computation of the triples; even when done on-the-fly, the memory cost is likely to be significant unless performance is severely compromised. In contrast, the single non-iterative N^7 step associated with PS(T) increases the accuracy of all subsequent N^6 CCSD-like response calculations, regardless of how many iterations are needed, frequencies or perturbations are considered, or even the order of response theory. Of course, the success of PS(T) method requires that the non-iterative correction produce better poles than CCSD. With this in mind, benchmarking electronic polarizabilities are essential for understanding the utility of various approximate triples methods and also the complex relationship between the one- and many-particle bases employed.

6.2 Theory and computational details

The coupled-cluster wavefunction is given by the following ansatz,

$$|\Psi_{CC}\rangle = \exp(T)|\Phi\rangle \tag{6.1}$$

where $|\Phi\rangle$ is the reference function and the cluster operator, T, is given by

$$T = T_1 + T_2 + \cdots + T_n, \tag{6.2}$$

where T_i represents the i-th many-body component of the exact cluster operator T, and n refers to the total number of correlated electrons. The coupled-cluster energy and cluster amplitudes can be defined by a nonlinear eigenvalue equation, $H|\Psi_{CC}\rangle = E_{CC}|\Psi_{CC}\rangle$, but it is more often represented in the fully connected energy-independent form

$$\langle \Phi^{a_1 \ldots a_n}_{i_1 \ldots i_n}| \exp(-T) H \exp(T) |\Phi\rangle = 0 \tag{6.3}$$

where excited configurations $|\Phi^{a_1 \ldots a_n}_{i_1 \ldots i_n}\rangle$,

$$|\Phi^{a_1 \ldots a_n}_{i_1 \ldots i_n}\rangle = \hat{a}^\dagger_{a_1} \ldots \hat{a}^\dagger_{a_n} \hat{a}_{i_n} \ldots \hat{a}_{i_1} |\Phi\rangle \tag{6.4}$$

corresponds to the excitation manifold included in the cluster operator T. The $\bar{H} = \exp(-T) H \exp(T)$ operator is referred to as the similarity transformed Hamiltonian. Having solved the above equations for cluster amplitudes, the energy can be obtained from the formula:

$$E = \langle \Phi| \exp(-T) H \exp(T) |\Phi\rangle \ . \tag{6.5}$$

This paper focuses on two common truncations of the cluster expansion, CCSD, where $T = T_1 + T_2$, and CCSDT, where $T = T_1 + T_2 + T_3$, as well as the approximate triples model, CC3, which cannot defined solely by a T expansion. For CCSD and CCSDT, second-order properties are calculated using the linear response function,

$$\langle\langle A; B \rangle\rangle_\omega = \frac{1}{2} \hat{C}^{\pm\omega} \hat{P}_{A,B} \langle \Phi | (1 + \Lambda) \left\{ \left[\overline{A}, T^{(1)}_{B,\omega} \right] + \left[\left[\overline{H}, T^{(1)}_{A,\omega} \right], T^{(1)}_{B,-\omega} \right] \right\} |\Phi\rangle \tag{6.6}$$

where $\hat{C}$ enforces time-reversal symmetry and $\hat{P}$ permutes A and B. Evaluating this quantity requires the Λ amplitudes of gradient theory and the first-order response with respect to operators A and B at both positive and negative frequency. In the case of dipole polarizabilities, A and B are both dipole moment operators, and the polarizability is given by

$$\alpha_{ij}(\omega) = -\langle\langle \mu_i; \mu_j \rangle\rangle_\omega. \tag{6.7}$$

For CCSD and CCSDT, Λ and response ($T^{(1)}$) amplitudes are obtained by solving

$$\langle \Phi | (1+\Lambda) \overline{H} | \Phi^{a_1 \ldots a_n}_{i_1 \ldots i_n} \rangle = 0 \tag{6.8}$$

$$\langle \Phi^{a_1 \ldots a_n}_{i_1 \ldots i_n} | [\overline{H}, T^{(1)}_{\gamma,\omega}] - \omega T^{(1)}_{\gamma,\omega} | \Phi \rangle = -\langle \Phi^{a_1 \ldots a_n}_{i_1 \ldots i_n} | \overline{\mu}_\gamma | \Phi \rangle, \ \gamma = x, y, z \tag{6.9}$$

for the appropriate excitation manifold. In the CC3 approximation, the CCSD equations are modified by adding terms corresponding to approximate triples which can be calculated on-the-fly from the singles and doubles amplitudes, which minimizes the memory requirements. The reader is referred to the literature for the specific details of CC3 [8]. In contrast to CC3, where the singles and doubles amplitudes are iterated in the presence of approximate triples, the PS(T) method iterates only the response amplitudes and the supplemental term adds no additional cost to the solution of the response equations (the supplemental term itself requires non-iterative N^7 work).

The implementation of the CC static/frequency-dependent polarizabilities at the CCSDT level creates a unique opportunity to test the pole-shift (PS) technique [20]. In particular we will discuss the case of the so-called PS(T)-CCSD(m) approaches, where the poles (excitation energies) of the CCSD linear response equations are corrected by adding the non-iterative corrections due to triples to m selected excited states. The selection rules to define the so-called m-space (or the set of excitation

energies to be corrected) are straightforward: we consider only those low-lying dipole-allowed excited states which are characterized either by a large value for the transition moment or have a non-negligible contribution to the triply excited configurations.

In a general case ($m \geq 1$) we can derive the following formula for the PS(T)-CCSD first order response operator $\tilde{T}_\gamma^{(1)}(\omega)$

$$\tilde{T}_\gamma^{(1)}(\omega)|\Phi\rangle = T_\gamma^{(1)}(\omega)|\Phi\rangle + \sum_{K=1}^{m} |R_K\rangle \frac{\Delta\omega_K^{(T)} \mu_{K,0}^\gamma}{(\omega - \omega_K^{CCSD} - \Delta\omega_K^{(T)})(\omega - \omega_K^{CCSD})} \ . \quad (6.10)$$

where $T_\gamma^{(1)}(\omega)$ is the frequency-dependent first order CCSD operator for the γ-th component of the dipole moment. The corrections $\Delta\omega_K^{(T)}$ account for the effect of triply excited configurations. In the first paper (Ref. [20]) we tested the PS(T)-CCSD(m) approaches based on the completely renormalized equation-of-motion CCSD(T) (CR-EOM-CCSD(T)) corrections [21, 22], which offer an elegant way of constructing the non-iterative corrections in terms of moments of EOM-CCSD equations (for details see Ref. [23]). In addition to the CR-EOM-CCSD(T) corrections in this paper we will also test the PS(T)-CCSD(m) formalism based on the reduced variant of CR-EOM-CCSD(T) correction (r-CR-EOM-CCSD(T)) [24], which is derived using slightly different reasoning that in the case of the CR-EOM-CCSD(T) approach, namely, the r-CR-EOM-CCSD(T) correction is derived from the embedding of the EOM-CCSD equations in the method of moments functional constructed for the EOM-CCSDT level of theory. The final form of the r-CR-EOM-CCSD(T) correction is:

$$\delta_K^{(\mathrm{r-CR-EOM-CCSD(T)})} = \frac{1}{D_K}[\langle\Phi|C_{K,1}^\dagger V_N \tilde{R}_{K,3}|\Phi\rangle + \langle\Phi|C_{K,2}^\dagger V_N \tilde{R}_{K,3}|\Phi\rangle] \ , \quad (6.11)$$

where D_K represents the overlap between EOM-CCSD and trial wavefunctions, V_N is

two body part of electronic Hamiltonian in normal-ordered form and $C_{K,1}$ and $C_{K,2}$ operators are defined in terms of CCSD/EOM-CCSD cluster (T_1, T_2) and excitation ($R_{K,0}$, $R_{K,1}$, $R_{K,2}$) operators:

$$C_{K,1}|\Phi\rangle = [R_{K,1} + R_{K,0}T_1]|\Phi\rangle \tag{6.12}$$

$$C_{K,2}|\Phi\rangle = [R_{K,2} + R_{K,1}T_1 + R_{K,0}(T_2 + \frac{1}{2}T_1^2)]|\Phi\rangle \; . \tag{6.13}$$

In the Eq.(6.11) the $\tilde{R}_{K,3}$ operator is expressed using simplified form of the triply excited EOM-CCSD moments (version II in Ref. [24]), which eliminates the need of calculating expensive terms involving four-particle two-body integrals.

For brevity we will refer to the PS(T)-CCSD(m) approaches based on the CR-EOM-CCSD(T) and r-CR-EOM-CCSD(T) methodologies as to PS(CR)-CCSD(m) and PS(r-CR)-CCSD(m) (or PS(CR,m)/PS(r-CR,m) for short). We will be also testing (as a proof of concept) the approach where the $\Delta\omega_K^{(T)}$ correction is replaced by the difference between EOM-CCSDT and EOM-CCSD excitation energies. In this situation the locations of the first m-poles in the PS(T)-CCSD(m) approach correspond to the CCSDT poles. This formalism will henceforth be referred to as PS(CCSDT)-CCSD(m).

The NWChem [15] implementation of CCSD linear response (CCSD-LR) polarizabilities is described in Ref. [26], while computational issues are discussed in Ref. [27]. The CCSDT code follows the same prescription and was implemented using the Tensor Contraction Engine [28], which mitigates the time-consuming task of writing parallel code for the CC equations. The CCSDT dynamic polarizabilities are obtained by solving for the CC amplitudes T_1, T_2 and T_3, the left eigenvectors Λ_1, Λ_2 and Λ_3, and the first-order response amplitudes, $T_1^{(1)}$, $T_2^{(1)}$ and $T_3^{(1)}$ for each unique

component of the dipole operator. The polarizability is evaluated using the symmetric formulation of the second-derivative of the energy. Dynamic polarizabilities were calculated using unrelaxed orbitals. All CC equations steps were converged to 10^{-7} or better. Some calculations were excluded due to slow convergence, which occurred for CCSDT calculations using larger basis sets at large frequencies. In the case of CN, higher convergence (10^{-9}) was necessary to obtain accurate results.

All electrons were correlated for coupled-cluster calculations on Ne, HF and N_2, while the $1s$ core orbitals were frozen for CO, CN, NO and O_2. Basis sets were obtained from the NWChem basis set library and use the spherical form of the angular functions. All energies, frequencies and polarizabilities are reported using atomic units. Polarizability tensor components for linear diatomics use the notation $\alpha_\perp = \alpha_{xx} = \alpha_{yy}$ and $\alpha_\parallel = \alpha_{zz}$, where z is the unique axis. For the NO radical, $\alpha_{xx} \neq \alpha_{yy}$ in D_{2h} symmetry, thus $\alpha_\perp = \frac{1}{2}(\alpha_{xx} + \alpha_{yy})$ is reported instead. The molecular geometry parameters used in this paper are $R_{HF} = 1.7328795$ bohr, $R_{NN} = 2.068$ bohr, $R_{CO} = 2.132$ bohr, $R_{CN} = 1.1718$ Å, $R_{NO} = 1.1718$ Å and $R_{OO} = 1.20752$ Å.

NWChem CC calculations were performed using various types of computer hardware, from single workstations to supercomputers. The success of disk-based algorithms for calculations with more than 300 spin-orbitals demonstrate that the implementation described herein is not limited in utility to chemists with access to extensive computer facilities. At the same time, no other implementation of coupled-cluster response properties has the ability to take advantage of the rapid proliferation of computers with hundreds or thousands of processors. As an example of the extensible nature of the CCSDT codes, an approximately two-fold speedup was obtained when doubling (256 to 512) the number of processors on a BlueGene/L system for the HF CCSDT/d-aug-cc-pVQZ calculation. For an even smaller problem where less

ideal scaling is expected, CN UCCSDT/d-aug-cc-pVDZ, the iteration time decreased by a factor 9 when the processor rank was increased from 16 to 256. These same jobs can be run on small clusters or even single workstations, provided they are equipped with sufficient memory or disk space, but good parallel scaling for small systems should translate to excellent parallel performance for larger systems which can only be run on parallel machines.

The CC3 calculations were performed using Aces II (MAB) [29].

6.3 Results

This paper reports dynamic polarizabilities at the CCSD, CC3, CCSDT and PS(T) levels of theory for a number of small molecules using large basis sets. In particular, Ne, HF, N_2 and CO were considered because they were previously explored using post-CCSD methods [17, 30, 31], and are common benchmarks for high-accuracy methods. Because the NWChem implementation of coupled-cluster theory uses the spin-orbital formalism, we also report open-shell calculations using both ROHF and UHF references for CCSD and CCSDT dynamic polarizabilities for CN, NO and O_2, which have previously been considered by Urban and coworkers [37] and, more recently, CN was considered by Kállay and Gauss [11]. Accurate dynamic polarizabilities have been obtained using MRCI techniques by Spelsberg and Meyer for N_2, CO and O_2 [32], but their choice of basis set prevents direct comparison.

Although most results here are presented in figures, the numerical values are available in table form in Appendix A, along with additional benchmark data not explicitly mentioned in the text.

6.3.1 Ne and HF

For the neon atom, for which correlation is purely dynamic, CC3 reproduces CCSDT dynamic polarizabilities to within 0.005 a.u. for all basis sets and frequencies considered, while CCSD is within 0.040 a.u. for all cases. The similarity of results from all methods can be seen in Figure 6.1. Differences between the CC3 and CCSDT did not increase substantially for larger frequencies, in part because the CC3 model very accurately reproduces the pole structure of the linear response function [33]. The presence of a second set of augmented functions is significantly more important than the correlation treatment. The numerical shortcomings of CCSD with respect to CC3 and CCSDT *decrease* as the basis set becomes more complete. Specifically, for $\omega = 0.0$ the difference between CCSD and CCSDT for the aug-cc-pVDZ and d-aug-cc-pVDZ basis sets are 0.020 a.u. and 0.026 a.u., while for aug-cc-pV5Z and d-aug-cc-pV5Z the differences are only 0.001 a.u. and 0.003 a.u., respectively. The basis set convergence of each theory was monotonic from TZ to 5Z, from below with single augmentation and from above with double augmentation. The results for doubly-augmented basis sets did not vary significantly with zeta-level, unlike the singly-augmented ones. Finally, both CC3 and CCSDT agree with the experimental value [30] to within 0.001 a.u. with the d-aug-cc-pV5Z basis, and the trends suggest that this difference would disappear at the sextuple-zeta level.

As seen in Figure 6.2, polarizabilities for the hydrogen fluoride molecule follow similar trends to the neon atom, with the CC3 model reproducing CCSDT to within 0.005 a.u. and the differences between CCSD and CCSDT in $\alpha_{\perp}(0)$ and $\alpha_{\parallel}(0)$ dropping from 0.043 a.u. and 0.058 a.u. at the aug-cc-pVDZ basis set to 0.013 a.u. and 0.009 a.u. for d-aug-cc-pVQZ. As for neon, the singly-augmented basis sets appear to converge from below and the doubly-augmented from above, with $\alpha_{\perp}$ displaying

Figure 6.1: The basis-set dependence of static polarizabilities of neon calculated using CCSD, CC3 and CCSDT. The aug-cc-pVNZ (aug in the key) and d-aug-cc-pVNZ (d-aug in the key) were employed. The nearly horizontal line represents the d-aug-cc-pVNZ series. In both cases, the method dependence is nominal compared to the basis set dependence.

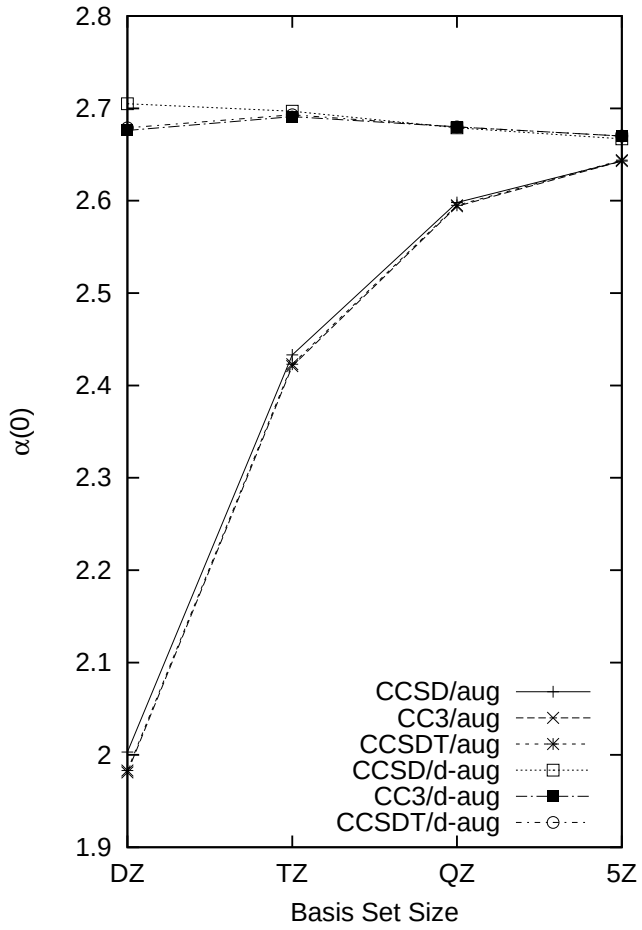

almost identical convergence in the basis set. In contrast, $\alpha_{\|}$ is still changing significantly with the basis set at the 5Z level. The differences in the dynamic polarizabilities with respect to CCSDT ($\Delta\alpha$) of CCSD and CC3 increase with frequency. The difference for CCSD is largest for aug-cc-pVDZ, decreases for both aug- and d-aug-cc-pVTZ, then increases again at the quadruple-zeta level. The error increases as the frequency approaches the first excited state in the appropriate symmetry; this affects $\alpha_{\perp}$ much more than $\alpha_{\|}$. Because of the outstanding agreement of CC3 and CCSDT, there is little purpose is reconsidering the agreement of theory and experiment for HF, since that was done — including the vibrational effects — in Reference [17].

The results for Ne and HF suggest that for molecules dominated by dynamic correlation, it is unnecessary to include full triples, as CC3 is more than sufficient and can be used in conjunction with much larger basis sets because it requires substantially less memory. Second, the basis set convergence in these systems is much more rapid for doubly-augmented basis sets than singly-augmented ones. This is a notable exception to the conclusion of Reference [17]: that increasing the zeta-level is more important than augmented functions beyond the first set.

6.3.2 N_2 and CO

In Table 6.1 static polarizabilities are given for CCSD, CC3, CCSDT and PS(T) [34] for different basis sets. The nitrogen molecule displays less basis set dependence than Ne or HF, as the aug-cc-pVTZ results are within 0.030 a.u. of those for d-aug-cc-pVQZ for both CCSD and CC3. For static polarizabilities, both CC3 and PS(T) are excellent approximations to CCSDT, with the latter slightly better in most cases. For example, with the largest basis set considered, aug-cc-pVQZ, CC3 differs from CCSDT by (0.029,0.109) while for PS(T) the difference is only (0.009,-0.015). The dynamic

Figure 6.2: Method and basis-set dependence of both the parallel and perpendicular components of the static polarizability tensor of HF. CC3 and CCSDT are indistinguishable for the perpendicular component.

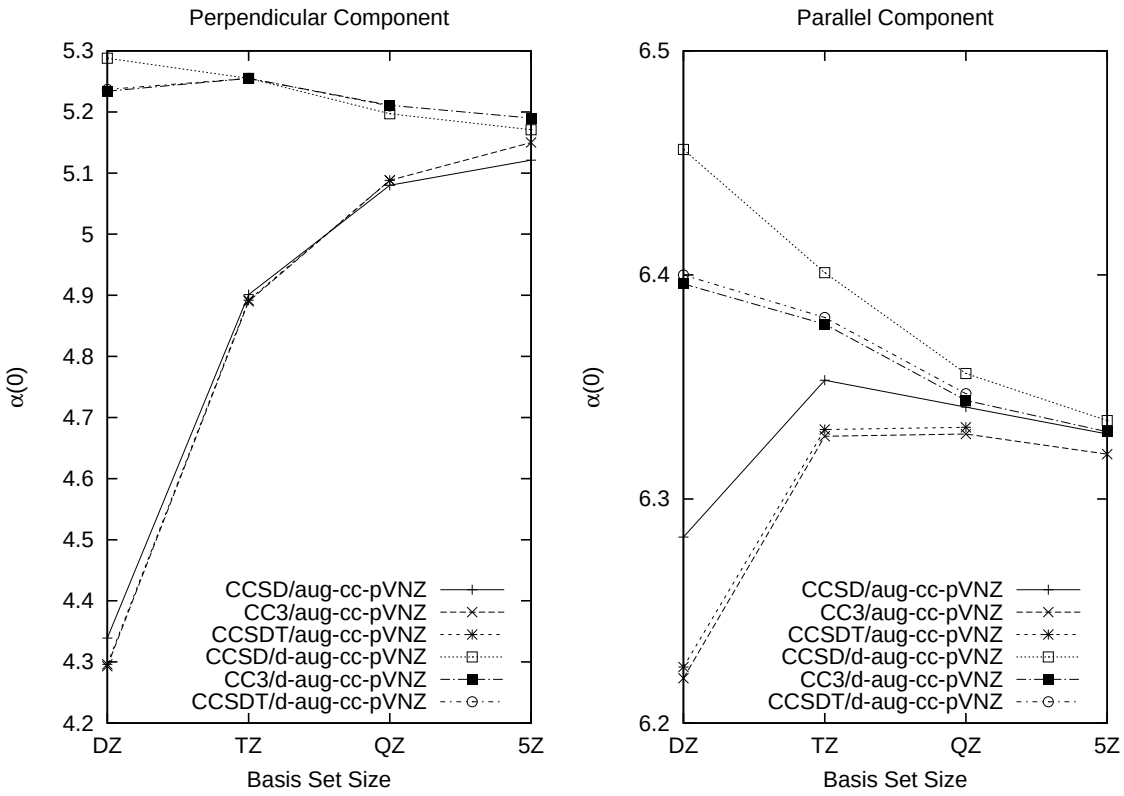

Table 6.1: Basis set dependence of static dipole polarizabilities of N_2 and dynamic polarizabilities using the aug-cc-pVQZ basis set. Calculations at the PS(T) level of theory used $m = 4$ and the CR-EOM-CCSD(T) approximation (see text for details). The n-aug-cc-pVXZ basis sets are abbreviated as naXZ in the table.

	CCSD		CC3[a]		PS(CR,$m = 4$)		CCSDT	
	$\alpha_\perp$	$\alpha_\parallel$	$\alpha_\perp$	$\alpha_\parallel$	$\alpha_\perp$	$\alpha_\parallel$	$\alpha_\perp$	$\alpha_\parallel$
Static								
aDZ	10.003	14.610	10.065	14.910	10.065	14.740	10.054	14.814
aTZ	10.126	14.578	10.213	14.860	10.202	14.730	10.187	14.753
aQZ	10.108	14.541	10.208	14.823	10.188	14.699	10.179	14.714
daDZ	10.191	14.739	10.274	15.039	10.254	14.809	10.257	14.944
daTZ	10.153	14.604	10.246	14.888	10.217	14.708	10.219	14.781
daQZ	10.109	14.548	10.210	14.831	10.179	14.665	-	-
Dynamic (aug-cc-pVDZ)								
0.00	10.108	14.541	10.208	14.823	10.188	14.699	10.179	14.714
0.10	10.349	14.926	10.459	15.248	10.440	15.105	10.430	15.128
0.20	11.180	16.256	11.328	16.728	11.314	16.514	11.297	16.566
0.30	13.101	19.320	13.366	20.223	13.375	19.827	13.337	19.956
0.40	18.619	27.917	19.529	30.694	19.696	29.737	19.581	29.961

[a] Data for CC3/aug-cc-pVQZ is from Ref. [9].

polarizabilities of N_2 using the aug-cc-pVQZ basis set (Table 6.1) show a very different trend from Ne and HF. The differences with respect to CCSDT of CCSD and CC3 grow significantly with frequency, to (-0.962,-2.044) and (-0.052,0.733), respectively, at $\omega = 0.4$.

At the aug-cc-pVQZ level of theory, the PS(T) method is accurate to within 0.015 a.u. for $\omega = 0.0$, while the CC3 method is more accurate for $\alpha_\perp$ values at large frequencies but overshoots $\alpha_\parallel$ by at least 0.100 a.u. for all frequencies. Unlike the previous cases, the difference between CCSD and CCSDT decreases only slightly, if at all, with increased basis set. This is most likely due to the presence of strong electron correlation effects not present in Ne or HF, although further investigation is

necessary to understand the dependence of polarizabilities on basis set and coupled-cluster excitation level. While the trends seen for N_2 are interesting from a theoretical perspective, they do not compel any reinterpretation of the conclusions of Ref. [9].

Carbon monoxide is similar to N_2 in that it has a triple bond, but is different in that it has a non-zero dipole moment, which has been the subject of much study [35]. While Scuseria and coworkers noted that "triples and g-type functions... are crucial to obtain satisfactory agreement with experiment," we find that the dipole polarizability is substantially less sensitive to method and basis set, in agreement with the results of Luis, et al. In Figure 6.2 dynamic polarizabilities of CO at the CCSD, CC3 and CCSDT levels of theory are presented for aug-cc-pVTZ. The effect of triples on the static polarizabilities is +0.042 a.u. for $\alpha_\perp$ and approximately -0.138 for $\alpha_\parallel$, by comparing the CCSD and CCSDT results with the aug-cc-pVTZ basis. The $\alpha_\perp(0.3)$ is substantially in error at the CCSD level due to overestimation of the first excited state of the corresponding symmetry. It is interesting to note that while Hartree-Fock does not even get the sign of the dipole moment correct for CO, the uncorrelated CCS model [36] produces polarizabilities very close to those of the correlated CC methods employed here for all but $\omega = 0.3$ au.

In Table 6.2 we evaluate the CC3 method and different forms of the PS(T) method for the CO molecule using the aug-cc-pVDZ basis set. The PS(CR,$m = 2$) approach experiences serious problems with adequate description of the $\alpha_\perp$ component especially for larger frequencies. For example, for $\omega = 0.3$ the PS(CR,$m = 2$) result significantly overestimates the CCSDT one by almost 7 a.u. In turn, the PS(r-CR,$m = 2$) approach for $\omega = 0.3$ underestimates the CCSDT α value by 5.7 a.u. In contrast, the PS(CCSDT,$m = 2$) approach reduces the 5.3 error of the CCSD formalism for $\alpha_\perp(\omega = 0.3)$ down to 0.98 a.u. While not a practical method, the PS(CCSDT) re-

Table 6.2: Comparison of frequency-dependent dipole polarizabilities of CO with the aug-cc-pVDZ basis set obtained with the PS(T)-CCSD(m) approach employing two approximate triples methods and the correction due to full triples, together with the CCSD, CC3 and CCSDT results.

				PS(T,$m=2$)			
	Frequency	CCSD	CC3	CR	r-CR	CCSDT	CCSDT
$\alpha_\perp$	0.00	11.618	11.685	11.694	11.619	11.659	11.663
	0.10	12.100	12.194	12.202	12.102	12.154	12.168
	0.20	14.169	14.423	14.442	14.166	14.304	14.371
	0.30	32.238	38.041	44.478	31.778	36.513	37.489
$\alpha_\parallel$	0.00	15.820	15.575	15.901	15.849	15.883	15.642
	0.10	16.342	16.101	16.438	16.376	16.416	16.169
	0.20	18.219	18.006	18.384	18.278	18.347	18.079
	0.30	23.164	23.151	23.657	23.339	23.545	23.219

sults demonstrate the fundamental principle of the PS(T) approach is correct: that the majority of the correlation effect due to triples in the linear response CC equations is achieved by pole shifting. Obviously, the inaccuracies in PS(T) using approximate triples are due to shortcomings in those methods for the molecule under consideration.

The experimental polarizability is reasonably well approximated by the composite method employed in Ref. [17]. The discrepancy in the estimated $\Delta\alpha = \alpha_\parallel - \alpha_\perp$ in that study would decrease significantly if a new estimated value for the electronic contribution is used. Whereas in that paper, the electronic contribution to $\Delta\alpha$ is 3.650 a.u., we estimate it to be 3.606 a.u., which is calculated from CCSD/d-aug-cc-pV5Z (3.790 au) plus the average of the differences between CCSD and CCSDT using the aug-cc-pVQZ and d-aug-cc-pVTZ basis sets (-0.184 au). This value is negligibly different from the experimental value of 3.59 au [43]. The same estimation method for the electronic contribution to $\alpha(0.072)$ value would decrease the error with respect to experiment of the value in Ref. [17] by one-third (0.007 au).

Figure 6.3: Frequency dependence of both the parallel and perpendicular components of the polarizability of CO using the CCSD, CC3 and CCSDT methods with the aug-cc-pVTZ basis set.

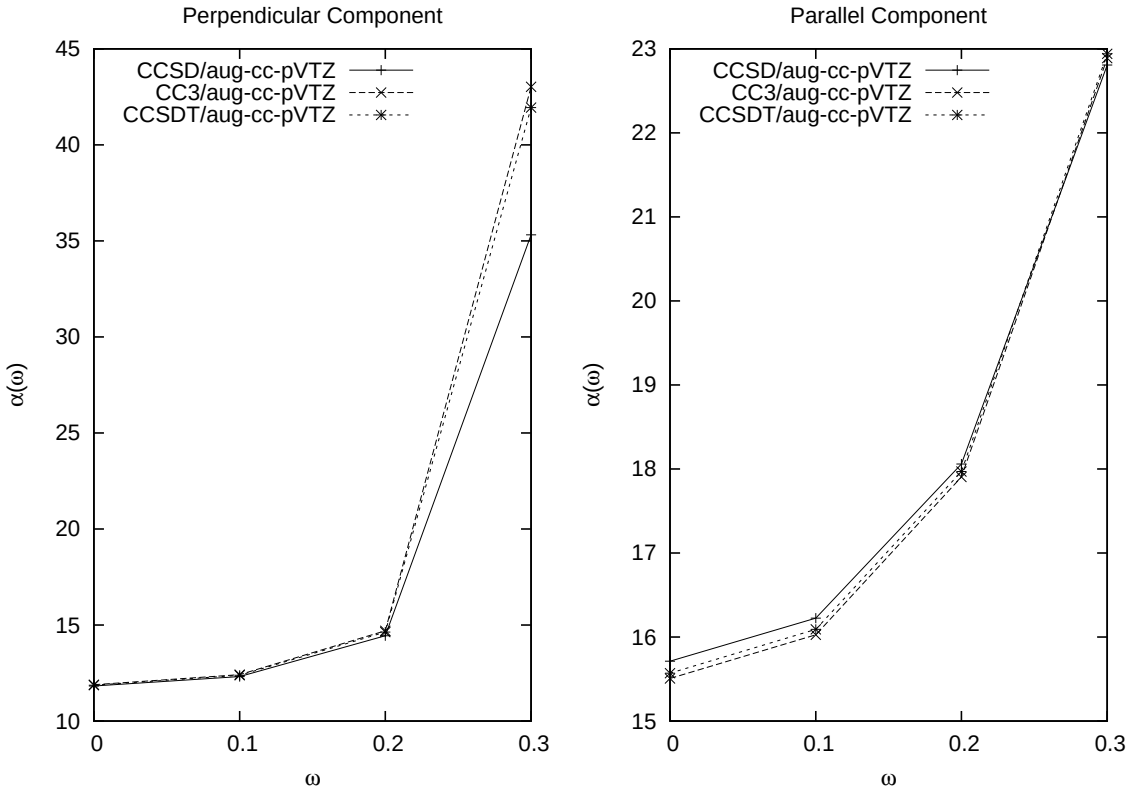

Figure 6.4: Basis-set dependence of both the parallel and perpendicular components of the static polarizability of CO using the CCSD, CC3 and CCSDT methods.

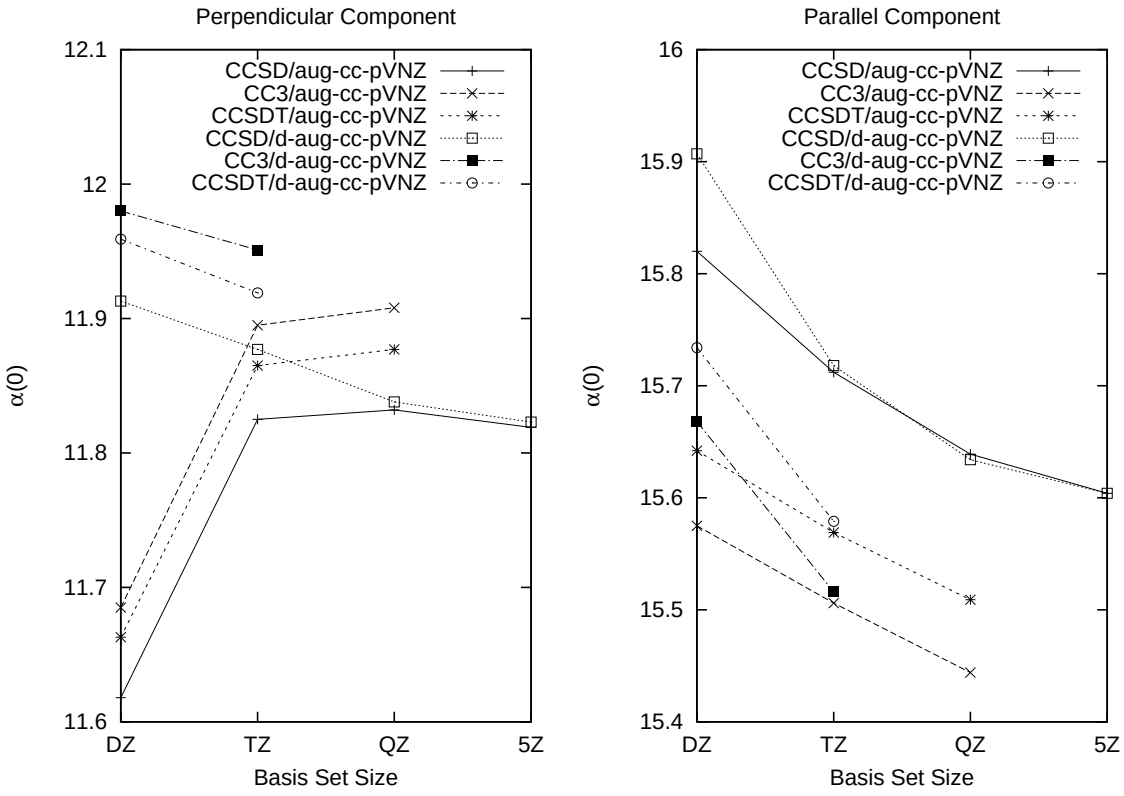

6.3.3 CN and NO

As observed by Kállay and Gauss, the effects of triple and quadruple excitations is important for obtaining accurate results for CN, particularly at larger frequencies [11]. That study used the d-aug-cc-pVDZ basis set and a UHF reference wavefunction, and the effect of both choices has been investigated. In Table 6.3 we compare CCSD and CCSDT dynamic polarizabilities based upon both ROHF and UHF references at the d-aug-cc-pVDZ and d-aug-cc-pVTZ basis sets. The difference between CCSD and CCSDT using an ROHF reference is often more than an order of magnitude less than with UHF. For the low frequencies, ROHF-CCSD is within 0.1 a.u. of ROHF-CCSDT and is closer to UHF-CCSDTQ than UHF-CCSDT, although it is not clear if the UHF-CCSDTQ result is better than the ROHF-CCSDT one. Because higher excitations mitigate the orbital dependence of coupled-cluster calculations and improve the spin-purity of the wavefunction, it is clear that UHF-CCSD calculations for CN are not suitable and that ROHF-based calculations would be preferred.

The basis set dependence of ROHF-CC dynamic polarizabilities is reported in Figure 6.5. There is almost no basis set dependence in $\alpha_{\perp}$ — the only notable effects are seen for the largest frequencies, as is to be expected since those values are affected by the location of the poles — while the basis set dependence of $\alpha_{\parallel}$ is large. It is important to notice that the basis set dependence (DZ vs. TZ) of the parallel component is much larger than the method dependence (CCSD vs. CCSDT), and that neither the basis set or method are particularly important for the perpendicular component when the ROHF reference is used.

Unfortunately, the spin-orbital implementation of CC cannot guarantee that the ROHF-CC wavefunction is a spin eigenfunction; that requires rigorously spin-adapted amplitude equations [37]. Spin-adapted or multireference CC-LR (see Refs. [41, 42])

Table 6.3: Comparison of frequency-dependent dipole polarizabilities of open-shell systems at the CCSD and CCSDT levels of theory using using UHF and ROHF references. All results are for the d-aug-cc-pVDZ basis set.

	ROHF Reference				UHF Reference			
	CCSD		CCSDT-CCSD		CCSD		CCSDT-CCSD	
Frequency	$\alpha_\perp$	$\alpha_\parallel$	$\alpha_\perp$	$\alpha_\parallel$	$\alpha_\perp$	$\alpha_\parallel$	$\alpha_\perp$	$\alpha_\parallel$
				CN				
0.00	16.319	26.398	-0.015	-0.049	15.878	25.587	0.333	0.680
0.01	16.472	26.458	-0.024	-0.046	15.982	25.637	0.364	0.692
0.02	17.017	26.641	-0.060	-0.037	16.335	25.789	0.486	0.730
0.03	18.377	26.963	-0.170	-0.019	17.118	26.056	0.847	0.797
0.04	22.851	27.449	-0.722	0.011	18.994	26.454	2.370	0.904
				NO				
0.00	9.844	15.546	0.048	-0.138	9.835	15.521	0.056	-0.115
0.05	9.922	15.699	0.052	-0.137	9.913	15.673	0.059	-0.113
0.10	10.177	16.199	0.064	-0.132	10.166	16.169	0.073	-0.106
0.15	10.707	17.228	0.096	-0.120	10.690	17.188	0.110	-0.085
				O_2				
0.00	8.349	15.520	0.005	0.079	8.352	15.505	0.002	0.089
0.10	8.527	16.251	0.007	0.134	8.530	16.235	0.004	0.144
0.20	9.163	19.524	0.014	0.492	9.166	19.503	0.012	0.500

Figure 6.5: Basis-set dependence of both the parallel and perpendicular components of the static polarizability of CN with CCSD and CCSDT. Only the parallel component is sensitive to the method and basis set, and much more so to the basis set than the method.

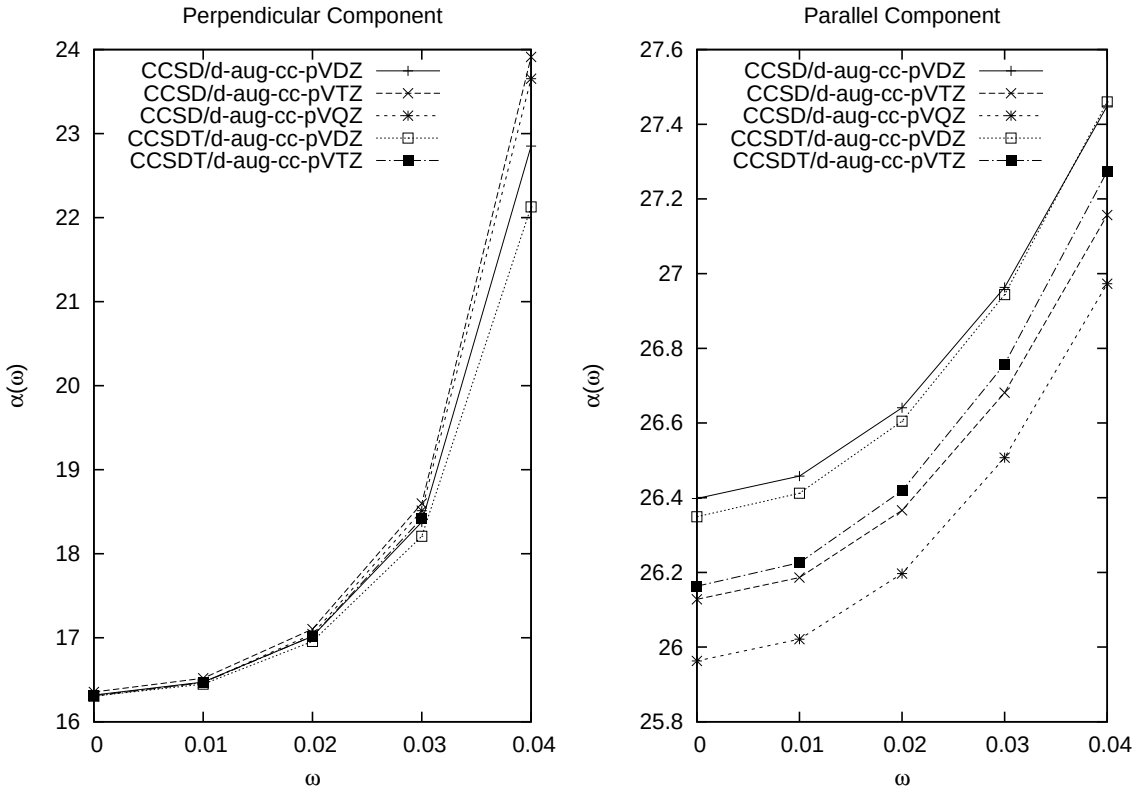

may be important for obtaining an accurate linear response function for CN, particularly given its role in obtaining accurate results for the dipole moment [37]. Given the difficulty of implementing post-CCSD coupled-cluster methods in general, it is unlikely that a spin-adapted CCSDT or higher linear response code will become available without the use automatic code generation [38, 39, 28] or string-based methods [40]. Until such an implementation exists, the ROHF-CCSDTQ results are likely to be the most authoritative since they will invariably be more spin-pure than the corresponding UHF results and are the highest order of CC method that can be reasonably computed. An investigation of these phenomena using our spin-orbital CCSDTQ-LR code is in progress.

To better understand the reference issues uncovered in the study of CN, we consider the NO radical due to its similarity to both CN, N_2 and CO. Both have an approximate bond order of 2.5 but NO has a radical electron in an anti-bonding orbital, whereas CN has a partially occupied bonding orbital. In contrast to CN, the dynamic polarizabilities obtained using ROHF and UHF references are quite similar at both the CCSD and CCSDT level of theory, as reported in Table 6.3. Similar trends were observed with both the aug-cc-pVDZ and aug-cc-pVTZ basis sets.

The experimental polarizabilities of NO are $\alpha_{\perp}(0.072) = 9.844$ a.u. and $\alpha_{\parallel}(0.072) = 15.539$ a.u. [43]. We estimate $\alpha_{\perp}(0.072) = 9.752 + 0.056 + 0.33 - 0.03 = 10.108$ a.u. and $\alpha_{\parallel}(0.072) = 15.840 - 0.124 + 0.03 - 0.04 = 15.706$ a.u. by adding the following contributions: (1) CCSD/d-aug-cc-pV5Z (2) the difference between CCSDT/aug-cc-pVTZ and CCSD/aug-cc-pVTZ (3) the core correlation and vibrational corrections of Urban and coworkers [37]. The over-estimating in both components with respect to experiment appears to be from the CCSD/d-aug-cc-pV5Z term since there was significant change in the CCSD results at the 5Z and 6Z levels. The estimated the-

Figure 6.6: Basis-set dependence of both the parallel and perpendicular components of the static polarizability of O_2 with CCSD and CCSDT.

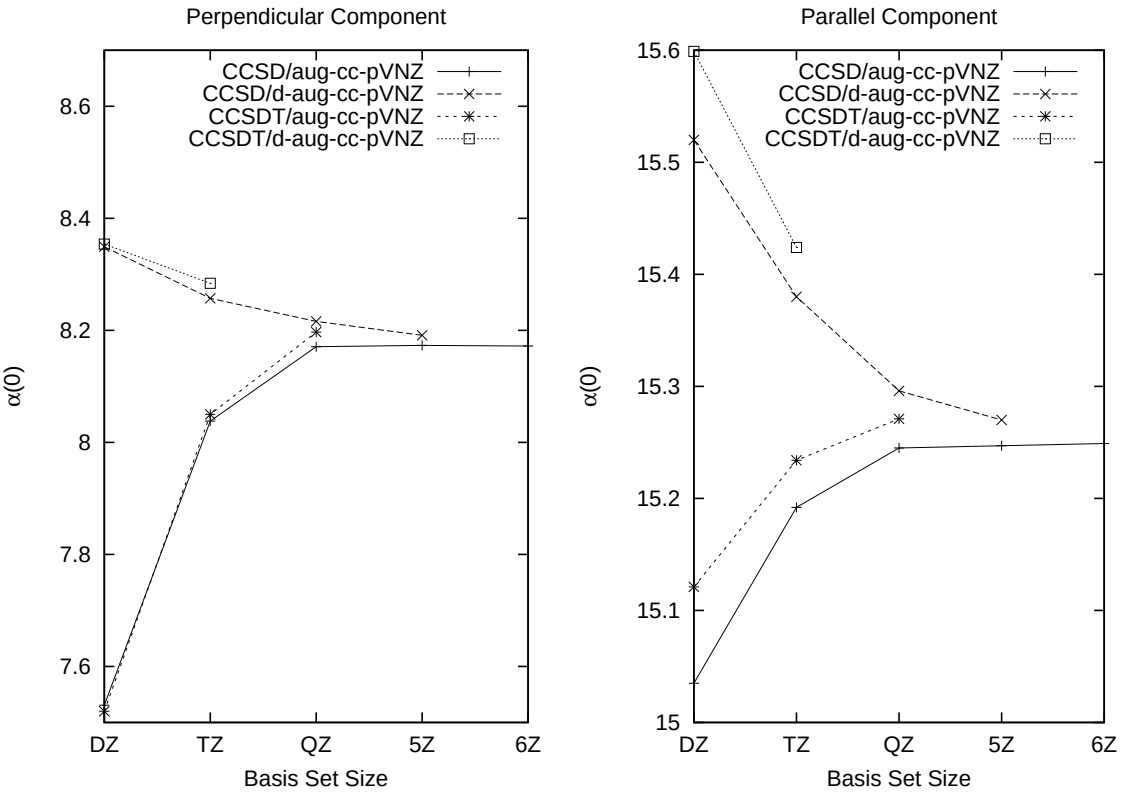

oretical value of $\alpha_{\|}$ becomes 15.340 when the aug-cc-pV6Z basis is used, while the $\alpha_{\perp}$ does not change significantly. Since it is not clear whether the basis dependence at the CCSD level is physical or a numerical artifact, we are hesitant to draw firm conclusions as to the reliability of the theoretical estimate.

6.3.4 O_2

To complete our study of dynamic polarizabilities of open-shell molecules, we consider the oxygen molecule, a ground-state triplet. The reference dependence of dynamic polarizabilities of O_2 (see Table 6.3) is negligible. We compare two forms of the PS(T)

Table 6.4: Frequency-dependent dipole polarizabilities of O_2 using various methods employing an ROHF refence. The aug-cc-pVTZ basis set was used in the calculations.

	CCSD		PS(CR,$m=4$)		PS(r-CR,$m=4$)		CCSDT	
Frequency	$\alpha_\perp$	$\alpha_\parallel$	$\alpha_\perp$	$\alpha_\parallel$	$\alpha_\perp$	$\alpha_\parallel$	$\alpha_\perp$	$\alpha_\parallel$
0.000	8.038	15.192	8.068	15.445	8.043	15.139	8.050	15.234
0.100	8.188	15.894	8.228	16.310	8.193	15.809	8.203	15.983
0.200	8.714	19.034	8.776	20.212	8.713	18.812	8.740	19.429

method with CCSD and CCSDT using an ROHF reference and the aug-cc-pVTZ basis sets in Table 6.4. To assess the accuracy of the CCSDT results, we explored the basis set convergence with CCSD out to d-aug-cc-pV5Z (see supplemental information). The perpendicular component — where triples seem less important — converges quickly in the d-aug-cc-pVNZ series and the effect of triples should increase the CCSD/d-aug-cc-pVNZ limit ($\alpha_\perp(0) \approx 8.18$) by less than 0.10 au. For the parallel component, the CCSD/d-aug-cc-pVNZ limit is $\alpha_\parallel(0) \approx 15.26$ a.u. and the difference between CCSD and CCSDT with d-aug-cc-pVTZ is less than ~ 0.05 au. This value appears reasonably converged in the basis set and does not vary significantly with frequency so that estimates for the static limit should also apply for the experimental frequency (0.072 a.u. = 632 nm).

The O_2 system can be also used the establish the accuracy of triples corrections. For this reason we performed several simple calculations with a one-dimensional m-space that contains the lowest state of symmetry of the corresponding dipole moment ($1^3\Pi_u$ state for μ_X and μ_Y components and $1^3\Sigma_u^+$ state for μ_Z component). Table 6.4 collects the results of various PS schemes obtained for the aug-cc-pVTZ basis set. As shown in the table, there are relatively large discrepancies between PS(CR,$m=4$)/PS(r-CR,$m=4$) and CCSDT results. This is true especially

for the $\alpha_{\|}$ component. To understand these differences, consider the EOM-CCSD, CR-EOM-CCSD(T), r-CR-EOM-CCSD(T), and EOM-CCSDT excitation energies of $1^3\Sigma_u^+$ state, which are equal to 6.371, 6.064. 6.404, 6.310 eV, respectively. While the EOM-CCSD excitation energy is very close to that of EOM-CCSDT (the CCSD results for $\alpha_{\|}(0.0)$ and $\alpha_{\|}(0.1)$ are in a good agreement with their CCSDT counterparts), CR-EOM-CCSD(T) underestimates the EOM-CCSDT excitation energy by 0.15 eV. In turn, r-CR-EOM-CCSD(T) overestimates EOM-CCSDT excitation energy nearly by 0.1 eV. Consequently, the PS(CR,$m = 4$) $\alpha_{\|}$ values are consistently above the CCSDT ones with errors equal to 0.212, 0.256 and 0.593 a.u. for ω=0.0, 0.1, 0.2, respectively, whereas the PS(r-CR) results are consistently below the CCSDT results with errors -0.095, -0.160 and -0.584 a.u. for ω=0.0, 0.1, 0.2. This explains why $\alpha_{\|}$ is systematically overestimated (underestimated) by the CR-EOM-CCSD(T) (r-CR-EOM-CCSD(T)) method and illustrates the reliance of the PS(T) method on the improvement of the poles upon inclusion of non-iterative triples corrections. In the case of O_2, a better non-iterative approximation is required to fully exploit the PS(T) approach.

Experimental polarizabilities are $\alpha_{\perp}(0.072) = 8.312$ and $\alpha_{\|}(0.072) = 15.728$ au [43]. We estimate $\alpha_{\perp}(0.072) = 8.276 + 0.029 - 0.02 + 0.03 = 8.315$ and $\alpha_{\|}(0.072) = 15.621 + 0.067 - 0.03 + 0.04 = 15.698$ a.u. by adding the following contributions: (1) CCSD/d-aug-cc-pV5Z (2) the difference between CCSDT/d-aug-cc-pVTZ and CCSD/d-aug-cc-pVTZ (3) the core correlation and vibrational corrections of Urban and coworkers [37]. The estimated values are quite close the measured ones, particularly $\alpha_{\perp}$, and the difference for $\alpha_{\|}$ should be almost entirely due to the effect of triples beyond the TZ basis. These values are close the MRCI values of Spelsberg and Meyer [32], who calculated $\alpha_{\perp}(0.072) = 8.310$ and $\alpha_{\|}(0.072) = 15.548$ a.u. using a

specially-constructed basis set, which affirms the correctness of our estimated $\alpha_{\perp}$ and lends credence to the conclusion that additional correlation effects are responsible for the shortcomings in $\alpha_{\parallel}$.

6.4 Conclusions

Benchmark coupled-cluster linear response calculations have been performed for Ne, HF, N_2, CO, CN, NO and O_2 using four correlated methods (CCSD, CC3, PS(T) and CCSDT). A few important conclusions can be drawn from these results. First, for systems with little or no static correlation, CC3 is nearly identical to CCSDT and the former should be used without hesitation given its marked efficiency with respect to computational storage. For strongly correlated systems, such as N_2 and CO, both approximate triples methods are more accurate than CCSD, but on the basis of accuracy alone, it is not always clear whether PS(T) or CC3 is better. The former is clearly better for N_2, while the latter is better for CO. The lower accuracy of PS(T) in the case of CO is not due to the PS(T) formalism, but rather the choice of approximate triples method used to calculate the EOM energies. Thus, with another choice of method for the triples correction, the PS(T) approach may be may be significantly more reliable in predicting response properties. This fact should provide yet another motivation for developing reliable non-iterative methods for excited states. In that event, computational cost strongly favors PS(T). However, unless systematic results can be achieved with a single non-iterative correction, the utility of the PS(T) approach will be limited. Unfortunately, a comparison of PS(T) and CC3 could not be made due to the absence of a publically-available implementation CC3-LR polarizabilities. The challenge posed by the ROHF Fockian has not been

explored except in the context of CC3 excited-state energies and may be a problem for polarizabilities [44]. Given the clear superiority of the ROHF reference for open-shell polarizabilities, it remains to be seen if the CC3 can deliver the same reliability for radicals as it does for closed-shell molecules.

For the same cases where CC3 performs well, the error with respect to CCSDT drops for both CCSD and CC3 as the basis set is increased. This may seem somewhat surprising given the conventional wisdom that the contribution of electron correlation increases commensurate with increasing the one-particle basis set rank. It is important to note this result when attempting benchmark correlated methods for polarizabilities, since a small basis may over-estimate the role of post-CCSD contributions in molecules like Ne and HF. The data would suggest that in these cases one should value a CCSD/d-aug-cc-pV5Z result over CCSDT/d-aug-cc-pVDZ one, for example, and that benchmarking the effect of higher excitations in coupled-cluster with double-zeta basis sets is not particularly valuable for molecules with little multireference character. In contrast, the data for N_2 has little variance between correlated methods and basis set except at large frequencies.

Despite the apparent similarity of the open-shell molecules considered — CN, NO and O_2 — the method and basis dependence of polarizabilities for these differed greatly. Dioxygen followed a similar trend to that of HF, with almost no difference between ROHF- and UHF-based calculations. A simple additive scheme produced results within ~ 0.02 a.u. of experiment, demonstrating that accurate polarizabilities are attainable for both the open-shell systems and closed-shell ones. In contrast, CN showed a huge discrepancy between the two Hartree-Fock references, which leads to a substantial overestimation of the contribution from the triples. The primary role of triples in UHF-CCSDT-LR polarizabilities is to more closely approximate the

proper spin state and not because of higher-order correlation effects, which are not seen in ROHF-based calculations, where the difference between CCSD and CCSDT is smaller by more than an order of magnitude. Because of the strong effects of reference, the conclusions of Ref. [11] should be viewed with some caution until spin-restricted (ROHF-, PSA- or SR-) CCSDTQ-LR results reaffirm the exact role of higher excitations.

The combination of high-level ab initio methods and powerful computers have allowed us to explore a new regime of accuracy in molecular properties calculations. The results of this paper demonstrate that the computational burden of CCSDT-LR is often unnecessary, and that two alternative methods for treating triples approximately can make a significant improvement over CCSD-LR. Lastly, a new complication emerges for open-shell systems: the spin-symmetry of the SCF reference can have a substantial impact on the accuracy of computed results. Thus, despite the additional complications of programming them by hand, ROHF-based CC-LR approaches should be favored over their UHF counterparts. The comparison of ROHF- and UHF-based approaches for modest basis sets should be an appropriate criteria for determining if higher-order UHF-based coupled-cluster methods can be employed.

REFERENCES

[1] J. Čížek, *Adv. Chem. Phys.* **14**, 35 (1969); J. Paldus, J. Čížek and I. Shavitt, *Phys. Rev. A* **5**, 50 (1972).

[2] R. J. Bartlett and M. Musiał, *Rev. Mod. Phys.* **79**, 291 (2007).

[3] T. H. Dunning Jr., *J. Phys. Chem. A*, **104**, 9062 (2000).

[4] T. Helgaker, J. Gauss, P. Jørgensen and J. Olsen, *J. Chem. Phys.* **106**, 6430 (1997).

[5] K. L. Bak, J. Gauss, P. Jørgensen, J. Olsen, T. Helgaker and J. F. Stanton, *J. Chem. Phys.* **114**, 6548 (2001).

[6] F. Pawłowski, A. Halkier, P. Jørgensen, K. L. Bak, T. Helgaker and W. Klopper, *J. Chem. Phys.* **118**, 2539 (2003).

[7] J. A. Pople, M. Head-Gordon and K. Raghavachari, *J. Chem. Phys.* **87**, 5968 (1987).

[8] O. Christiansen, H. Koch, P. Jørgensen, *J. Chem. Phys.* **103**, 7429 (1995); H. Koch, O. Christiansen, P. Jørgensen, A. M. Sanchez de Merás and T. Helgaker, *J. Chem. Phys.* **106**, 1808 (1997).

[9] O. Christiansen, J. Gauss and J. F. Stanton, *Chem. Phys. Lett.* **292**, 437 (1998).

[10] J. Gauss, O. Christiansen and J. F. Stanton, *Chem. Phys. Lett.* **296**, 117 (1998).

[11] M. Kállay and J. Gauss, *J. Mol. Struct. (THEOCHEM)* **768**, 71 (2006).

[12] D. P. O'Neill, M. Kállay and J. Gauss, *J. Chem. Phys.* **127**, 134109 (2007).

[13] H. J. Monkhorst, *Int. J. Quantum Chem.* **S11**, 421 (1977).

[14] H. Koch and P. Jørgensen, *J. Chem. Phys.* **93**, 3333 (1990); O. Christiansen, P. Jørgensen and C. Hättig, *Int. J. Quantum Chem.* **68**, 1 (1998).

[15] E. J. Bylaska, W. A. de Jong, N. Govind, K. Kowalski, T. P. Straatsma, M. Valiev, D. Wang, E. Apra, T. L. Windus, J. Hammond, P. Nichols, S. Hirata, M. T. Hackler, Y. Zhao, P.-D. Fan, R. J. Harrison, M. Dupuis, D. M. A. Smith, J. Nieplocha, V. Tipparaju, M. Krishnan, Q. Wu, T. Van Voorhis, A. A. Auer, M. Nooijen, E. Brown, G. Cisneros, G. I. Fann, H. Fruchtl, J. Garza, K. Hirao, R. Kendall, J. A. Nichols, K. Tsemekhman, K. Wolinski, J. Anchell, D. Bernholdt, P. Borowski, T. Clark, D. Clerc, H. Dachsel, M. Deegan, K. Dyall, D. Elwood, E. Glendening, M. Gutowski, A. Hess, J. Jaffe, B. Johnson, J. Ju, R. Kobayashi, R. Kutteh, Z. Lin, R. Littlefield, X. Long, B. Meng, T. Nakajima, S. Niu, L. Pollack, M. Rosing, G. Sandrone, M. Stave, H. Taylor, G. Thomas, J. van Lenthe, A. Wong and Z. Zhang. "NWChem, A Computational Chemistry Package for Parallel Computers, Version 5.1" (2007), Pacific Northwest National Laboratory, Richland, Washington 99352-0999, USA. A modified version.

[16] J. Kongsted and O. Christiansen, *J. Chem. Phys.* **125**, 124108 (2006).

[17] O. Christiansen, C. Hättig and J. Gauss, *J. Chem. Phys.* **109**, 4745 (1998).

[18] D. M. Bishop and B. Kirtman, *J. Chem. Phys.* 95, 2646 (1991); M. Torrent-Sucarrat, J. M. Luis and B. Kirtman, *J. Chem. Phys.* 122, 204108 (2005); J.

M. Luis, M. Torrent-Sucarrat, O. Christiansen and B. Kirtman, *J. Chem. Phys.* **127**, 084118 (2007).

[19] T. H. Dunning Jr., *J. Chem. Phys.* **90**, 1007 (1989); R. A. Kendall, T. H. Dunning Jr. and R. J. Harrison, *J. Chem. Phys.* **96**, 6796 (1992); D. E. Woon and T. H. Dunning Jr., *J. Chem. Phys.* **98**, 1358 (1993); D. E. Woon and T. H. Dunning Jr., *J. Chem. Phys.* **100**, 2975 (1994).

[20] K. Kowalski, J. R. Hammond and W. A. de Jong, *J. Chem. Phys.* **127**, 164105 (2007).

[21] K. Kowalski and P. Piecuch, *J. Chem. Phys.* **120**, 1715 (2004).

[22] P. Piecuch, K. Kowalski, I. S. O. Pimienta and M. J. McGuire, *Int. Rev. Phys. Chem.* **21**, 527 (2002).

[23] K. Kowalski and P. Piecuch, *J. Chem. Phys.* **113**, 18 (2000).

[24] K. Kowalski and M. Valiev, *Int. J. Quantum Chem.* **108**, 2178 (2008).

[25] O. Christiansen, H. Koch, P. Jørgensen, *J. Chem. Phys.* **105**, 1451 (1996).

[26] J. R. Hammond, M. Valiev, W. A. de Jong and K. Kowalski, *J. Phys. Chem. A*, **111**, 5492 (2007).

[27] J. R. Hammond, K. Kowalski and W. A. de Jong *J. Chem. Phys.* **127**, 144105 (2007).

[28] S. Hirata, *J. Phys. Chem. A*, **107**, 9887 (2003); *J. Chem. Phys.* **121**, 51 (2004); *Theor. Chem. Acc.* **116**, 2 (2006).

[29] *Aces II*, a quantum chemical program package written by J. F. Stanton, J. Gauss, J .D. Watts, P. G. Szalay and R. J. Bartlett; with contribution from A. A. Auer, D. B. Bernholdt, O. Christiansen, M. E. Harding, M. Heckert, O. Heun, C. Huber, D. Jonsson, J. Juselius, W. J. Lauderdale, T. Metzroth, K. Ruud and the integral packages *MOLECULE* (J. Almlöf and P. R. Taylor), Props (P. R. Taylor), and ABACUS (T. Helgaker, H. Å. Jensen, P. Jørgensen and J. Olsen). See also J. F. Stanton, J. Gauss, J. D. Watts, W. J. Lauderdale, R.J. Bartlett, *Int. J. Quantum Chem.* Symp. **26**, 879 (1992) as well as: `http://www.aces2.de` for the current version.

[30] K. Hald, F. Pawłowski, P. Jørgensen and C. Hättig , *J. Chem. Phys.* **118**, 1292 (2003).

[31] H. Larsen, J. Olsen, C. Hättig, P. Jørgensen, O. Christiansen and J. Gauss, *J. Chem. Phys.* **111**, 1917 (1997).

[32] D. Spelsberg and W. Meyer, *J. Chem. Phys.* **101**, 1282 (1994); **109**, 9802 (1998); **111**, 9618 (1999).

[33] H. Koch, O. Christiansen, P. Jørgensen and J. Olsen, *Chem. Phys. Lett.* **244**, 75 (1995).

[34] The PS(T) results reported in this paper differ slightly with respect to the first paper [20] for dynamic frequencies due to a bug in the code. The correct results corresponding to the original paper are given in the supplemental information, but no significant differences are observed.

[35] G. E. Scuseria, M. D. Miller, F. Jensen and J. Geertsen, *J. Chem. Phys.* **94**, 6660 (1991); L. A. Barnes, B. Liu and R. Lindh, *J. Chem. Phys.* **98**, 3972 (1993); J. M.

Luis, J. Marti, M. Duran and J. L. Andrés, *J. Chem. Phys.* **102**, 7573 (1995); K. A. Peterson and T. H. Dunning, *J. Mol. Struct. (THEOCHEM)* **400**, 93 (1997).

[36] O. Christiansen, H. Koch and P. Jørgensen, *Chem. Phys. Lett.* **243**, 409 (1995).

[37] P. Neogrády, M. Medveď; I. Černušák and M. Urban, *Mol. Phys.* **100**, 541 (2002); M. Medveď, M. Urban, V. Kellö and G. H. F. Diercksen, *J. Mol. Struct. (THEOCHEM)* **547**, 219 (2001).

[38] J. Paldus and H. C. Wong, *Comp. Phys. Comm.* **6**, 1 (1973); **6**, 9 (1973).

[39] C. L. Janssen and H. F. Schaefer III, *Theor. Chim. Acta* **79**, 1 (1991).

[40] M. Kállay and P. R. Surján, *J. Chem. Phys.* **115** 2945 (2001).

[41] A.E. Kondo, P. Piecuch and J. Paldus, *J. Chem. Phys.* **102**, 6511 (1995); P. Piecuch, A.E. Kondo, V. Špirko and J. Paldus, *J. Chem. Phys.* **104**, 4699 (1996); A.E. Kondo, P. Piecuch and J. Paldus, *J. Chem. Phys.* **104**, 8566 (1996); P. Piecuch and J. Paldus, *J. Math. Chem.* **21**, 51 (1997).

[42] P. Piecuch and J. Paldus, *J. Phys. Chem.* **99**, 15354 (1995).

[43] N. J. Bridge and A. D. Buckingham, *Proc. Roy. Soc. London, Ser. A* **295**, 344 (1966).

[44] C. E. Smith, R. A. King and T. Daniel Crawford, *J. Chem. Phys.* **122**, 054110 (2005).

CHAPTER 7

LINEAR RESPONSE COUPLED-CLUSTER SINGLES AND DOUBLES APPROACH WITH MODIFIED SPECTRAL RESOLUTION OF THE SIMILARITY TRANSFORMED HAMILTONIAN

This chapter has been previously published in the following article: K. Kowalski, J. R. Hammond and W. A. de Jong, "Linear response coupled-cluster singles and doubles approach with modified spectral resolution of the similarity transformed Hamiltonian," *J. Chem. Phys.* **127**, 164105 (2007). Copyright 2007 by the American Institute of Physics.

7.1 Introduction

The development of theoretical methods for calculating frequency-dependent properties such as dynamic polarizabilities or hyperpolarizabilities is an important component of the coupled-cluster (CC) formalism.[1, 2, 3, 4] Starting from seminal papers by Monkhorst and Dalgaard [5, 6] we have witnessed a steady progress both in the theoretical development and numerical implementations of the linear response CC theory (LR-CC). The cornerstone in the theoretical developments is marked by generalization of the time dependent CC formalism based on the quasi-energy Lagrangians by Koch and Jørgensen [7] (see also Ref. [8] by Christiansen, Hättig and Jørgensen), which led to a first implementations of the CCSD frequency-dependent

polarizabilities and hyperpolarizabilities. [9, 10, 11] This important development also paved the way for a number of the LR-CC formalisms to calculate vertical excitation energies and ground-state properties such as CC2[12, 13] and CC3 models [14, 15, 16, 17] (for review of these approaches see Ref. [18]). In excited-state calculations these approximations proved to be very efficient in describing the excitation energies of singly-excited states. Soon a hierarchy of approximations was established CC2, CCSD, CC3, CCSDT, etc. leading to increasingly more accurate vertical excitation energies as well as the static and dynamic properties.[12, 16] The full family of the LR-CC approaches, i.e., LR-CCSD, LR-CCSDT, LR-CCSDTQ, was recently implemented by Kállay and Gauss [19] (since the deficiencies of the CCSD approach quickly became clear, the need for methods accounting for triples was obvious). The CC3 method was especially design to meet the conflicting needs of approximate inclusion of triples and computational expenses. Because the triply-excited amplitudes in the CC3 approach can be easily expressed through the singly- and doubly- excited amplitudes this method is similar to the CCSDT-n models,[20, 21, 22] although the former approach is fully compatible with the linear response theory. Nowadays the CC3 method is applied not only in excited-state calculations but also in calculations for the frequency-dependent polarizabilities and hyperpolarizabilities [23, 24, 25, 26]. In view of success of iterative CC3 approach it is interesting to notice that a little attention (except for the non-iterative excited-state methods of the CCSDR(3) type [15, 27]) has been paid to develop the non-iterative approaches for static and frequency-dependent properties. Quite naturally, one would expect that these theories should be designed through the perturbative estimates of higher order effect in the first order response equations. Unfortunately, the typical values of the first order response singly-excited amplitudes in the CCSD model can assume values greater

than one, and constructing efficient perturbative estimates of triply-excited effects may be rather challenging task.

In this paper we propose an alternative way, which is based on the modification of the low-order linear-response equations (such as the linear response CC with singles and doubles equations (LR-CCSD)) by correcting the location of poles by adding corrections due to triples to CCSD (EOM-CCSD)[28, 29, 30] excitation energies. This approach can be derived by invoking the language of second quantization and ordinary projection techniques in configurational space, which makes this approach similar to the sum-over-state approach discussed by Stanton and Bartlett.[31] We hope that this method will partly fill the gap between iterative CC3 and CC2/CCSD approaches in calculating the static/dynamic properties. Due to its N^7 scaling (N symbolically refers to the system size) it can be used to handle the systems currently accessible by the CCSD(T)[32] like approaches for the ground state. The organization of the paper is as follows: in Section II we derive the pole-shifted CCSD equations. Section III discusses computational details and the results of calculations for two benchmark systems: the N_2 and $FHCH_3$ molecules.

7.2 Theory

The linear response CC theory is based on the combination of the exponential ansatz of CC with the time-dependent Schödinger equation. Since various linear response CC approaches were widely discussed in the literature we refer the reader to Ref. [18] and references therein. In this section we focus our attention only on the most widespread approach: the linear response CC methods with singles and doubles, which utilizes a simple parameterization of a time-dependent wavefunction in the presence of time-

dependent external perturbation. In the most cases the time dependent perturbation corresponds to an interaction of a given molecular system with external electric-field. On the CCSD level, the time-dependent wavefunction can be written:

$$|\Psi^{\mathrm{CCSD}}(t)\rangle = e^{-iP(t)} e^{T_1(t)+T_2(t)} |\Phi\rangle \ , \tag{7.1}$$

where $P(t)$ is time-dependent phase and $T_1(t)$ and $T_2(t)$ denotes time-dependent singly- and doubly-excited cluster operators defined through the time dependent cluster amplitudes $t_a^i(t)$ and $t_{ab}^{ij}(t)$ in the following way:

$$T_1(t) = \sum_{i,a} t_a^i(t) \hat{a}_a^\dagger \hat{a}_i \ , \tag{7.2}$$

$$T_2(t) = \frac{1}{4} \sum_{i,j,a,b} t_{ab}^{ij}(t) \hat{a}_a^\dagger \hat{a}_b^\dagger \hat{a}_j^\dagger \hat{a}_i^\dagger \ , \tag{7.3}$$

where $\hat{a}_p^\dagger$ ($\hat{a}_p$) is the creation (annihilation) operator and indices $i, j, k, \ldots$ $(a, b, c, \ldots)$ refer to occupied (unoccupied) spinorbitals in time-independent reference function (usually chosen as a Hartree-Fock (HF) determinant).

Usually, the $T_1(t)$ and $T_2(t)$ operators are expanded in terms of the strength of external time-dependent perturbation, i.e.,

$$T_i(t) = T_i^{(0)} + T_i^{(1)}(t) + T_i^{(2)}(t) + \ldots \ , \ (i = 1, 2). \tag{7.4}$$

The time independent (static) part $T_i^{(0)}$ is obtained in standard CCSD calculations. The higher order components of $T_i(t)$ (or their Fourier components) can be obtained from the variational principle applied to time averaged quasi-energy CCSD functional

Lagrangian [8] $\{L\}_T = \lim_{T\to\infty} \frac{1}{2T} \int_{-T}^{T} L(t)dt$ where

$$L(t) = \langle\Phi| \left(1 + \Lambda_1(t) + \Lambda_2(t)\right) \left\{ \left(H(t) - i\frac{\partial}{\partial t} \right) e^{T_1(t)+T_2(t)} \right\}_C |\Phi\rangle \ , \tag{7.5}$$

where the $\Lambda_i(t)$ (i=1,2) are the one- and two-body components of the time-dependent de-excitation operator $\Lambda(t)$ and $\{\cdot\}_C$ denotes that the quantity is connected (in the diagrammatic sense). In the most common situation when the time dependent perturbation corresponds to an interaction of electric dipole (μ) with oscillating external electric-field, the equations for the first-order CCSD cluster operator $T^{(1)} = T_1^{(1)}(\omega) + T_2^{(1)}(\omega)$ (actually its ω-dependent Fourier component) take the form

$$(Q_1 + Q_2)[\bar{H}_N - \omega]T_\gamma^{(1)}(\omega)|\Phi\rangle + (Q_1 + Q_2)e^{-T}\mu_\gamma e^T|\Phi\rangle = 0 \ , (\gamma = X, Y, Z) \ , \tag{7.6}$$

where $\bar{H}_N$ is a CCSD similarity transformed Hamiltonian ($\bar{H} = e^{-T}He^T$) in a normal product form ($\bar{H}_N = \bar{H} - \langle\Phi|\bar{H}|\Phi\rangle$) and $T = T_1^{(0)} + T_2^{(0)}$. The operators Q_1 and Q_2 are the projection operators on the subspace spanned by all singly- (Q_1) and doubly-excited (Q_2)determinants. Having solved these equations for plus and minus ω-values one can easily calculate the dipole frequency-dependent polarizabilities

$$\begin{aligned} \alpha_{\gamma,\delta}(\omega) \ = \ & -\langle\Phi|(1+\Lambda)[e^{-T}\mu_\delta e^T, T_\gamma^{(1)}(\omega)]|\Phi\rangle \\ & -\langle\Phi|(1+\Lambda)[e^{-T}\mu_\gamma e^T, T_\delta^{(1)}(-\omega)]|\Phi\rangle \\ & -\langle\Phi|(1+\Lambda)[[\bar{H}_N, T_\delta^{(1)}(-\omega)], T_\gamma^{(1)}(\omega)]|\Phi\rangle \ , \end{aligned} \tag{7.7}$$

where $\Lambda = \Lambda_1 + \Lambda_2$ is the CCSD de-excitation operator. The accuracy of the frequency- dependent polarizabilities calculated in this way heavily depends on the

location of the poles of the $(Q_1 + Q_2)\bar{H}_N(Q_1 + Q_2)$ matrix, which correspond to the EOM-CCSD excitation energies. The authors of Ref. [12] suggested a hierarchy of iterative CC models (CC2, CCSD, CC3, CCSDT) that provide a systematic improvements in accuracy of frequency-dependent properties mainly due to the better location of the poles. Obviously, the full inclusion of triples is rather expensive procedure. So far, only the iterative methods approximately accounting for the effect of triples such a CC3 were tested in the context of reducing the numerical cost. Unfortunately, the non-iterative methods for correcting the CCSD frequency-dependent polarizabilities for the effect of triples face severe problems. One of these problems should be attributed to the norm of the $T_1^{(1)}$ operator, whose amplitudes can easily go beyond 1.0 value. The cases where the maximum $T_1^{(1)}$ amplitudes exceed the value of 10.0 is not uncommon and for this reason the proper inclusion of due to triples effects is rather a challenging task.

In this section we outline the technique that allows us to incorporate the effect directly responsible for the changes in the locations of the EOM-CCSD poles caused by the inclusion of triply-excited configurations. The main idea behind this is to modify the spectral resolution of the similarity transformed Hamiltonian that enters the linear response CCSD equations. These considerations can be easily transferred to higher levels and higher orders of response equations of the CC formalism. In the next Section we will be trying to establish to what extent this approximation is justified and what kind of improvements should we expect.

The location of poles of the CCSD response theory can be identified with the EOM-CCSD excitation energies (ω_K^{CCSD}). This is best seen when the spectral decomposition of the $(Q_1+Q_2)\bar{H}_N(Q_1+Q_2)$ matrix (exactly this matrix is diagonalized in the EOM-

CCSD calculations), is invoked

$$(Q_1 + Q_2)\bar{H}_N(Q_1 + Q_2) = \sum_{K=1}^{N_{tot}} |R_K\rangle \omega_K^{\mathrm{CCSD}} \langle L_K| \tag{7.8}$$

where $|R_K\rangle$ and $\langle L_K|$ are the right and left eigenvectors of similarity transformed Hamiltonian $\bar{H}_N$ in normal product form diagonalized in the space spanned by singly- and doubly-excited configurations. The N_{tot} refers to the composite dimension of subspaces composed of singly- and doubly-excited configurations.

Our goal is to improve the location of the EOM-CCSD excitation energies or linear response CCSD poles. This can be easily achieved by adding to all (or to some) EOM-CCSD excitation energies ω_K^{CCSD} in Eq.(7.8) corresponding corrections that account for missing correlation effects. Such a correction should first include the effect of triply-excited configurations. Since its numerical cost is akin to that of the ground-state CCSD(T) approach,[32] we believe that completely renormalized EOM-CCSD(T) corrections (CR-EOM-CCSD(T))[3, 33]

$$\Delta\omega_K^{(T)} = \Delta\omega_K^{\mathrm{CR-EOM-CCSD(T)}} = \frac{\langle \Psi_K(3)|M_{K,3}(2)|\Phi\rangle}{\langle \Psi_K(3)|R_K e^T|\Phi\rangle} \,, \tag{7.9}$$

are ideally suited for this purpose, In the above formula the $M_{K,3}(2)$ operator corresponds to triply-excited moments of the EOM-CCSD equations for K-th state,[34] whereas the R_K operator represent the EOM-CCSD excitation operator $R_K = R_{K,0} + R_{K,1} + R_{K,2}$. The so-called trail wavefunction $|\Psi_K(3)\rangle$ can be defined as follows

$$|\Psi_K(3)\rangle = (P + Q_1 + Q_2 + Q_3)(R_{K,0} + R_{K,1} + R_{K,2} + \tilde{R}_{K,3}) e^{T_1^{(0)} + T_2^{(0)}} |\Phi\rangle \,, \tag{7.10}$$

where the $\tilde{R}_{K,3}$ is an approximation to the exact EOM-CCSDT $R_{K,3}$ operator and

the P and Q_3 operators are the projection operators onto the reference function $|\Phi\rangle$ and a subspace of all triply-excited configurations. Usually, the amplitudes defining the $\tilde{R}_{K,3}$ operator are expressed in terms of the triply-excited moments (see Refs. [3, 33] for details). As demonstrated in Refs. [35, 36], good estimates of vertical excitation energies are obtained by adding these corrections to corresponding EOM-CCSD energies. Alternatively, other non-iterative corrections due to triples can be used in correcting the EOM-CCSD poles. Among them the EOM-CCSD($\tilde{T}$)[37, 38] and CCSDR(3)[15, 27] approaches are the viable candidates. In many aspects these methods are similar, both CR-EOM-CCSD(T) and CCSDR(3) approaches use the EOM-CCSD amplitudes as building blocks. This fact entails some limitations in the usage of these non-iterative approaches. The most pronounced one is the size-intensive character of the EOM-CCSD methods. Unfortunately, the EOM-CCSD methods is not capable of producing size-consistent results for the dissociation process that involves the separation of the system into two subsystems each of those being in excited electronic states). In contrast to the CR-EOM-CCSD(T) formalism the CCSDR(3) corrections lead to rigorously size-intensive results (i.e.. This fact is caused by the presence of the denominator in Eq.(7.9). On the other hand, the CR-EOM-CCSD(T) approach includes important $Q_3(H_N T_2)_C R_{K,2}$ term which is important for a proper description of doubly-excited states. This term is missing in the CCSDR(3) as well as in the CC3 approach.

Now, the spectral resolution of the $(Q_1+Q_2)...(Q_1+Q_2)$ part of a new, redefined, Hamiltonian (we will refer to this Hamiltonian as the augmented Hamiltonian $\tilde{H}_N$) takes the form

$$(Q_1+Q_2)\tilde{H}_N(Q_1+Q_2) = \sum_{K=1}^{N_{tot}} |R_K\rangle(\omega_K^{\mathrm{CCSD}} + \Delta\omega_K^{(T)})\langle L_K| \qquad (7.11)$$

In order to get better location of the poles corresponding to the $T^{(1)}(\omega)$ we will replace the $((Q_1+Q_2)\bar{H}_N(Q_1+Q_2)$ matrix in Eq.(7.6) by the augmented Hamiltonian's matrix $((Q_1+Q_2)\tilde{H}_N(Q_1+Q_2)$. However, it is rather expensive to correct all the EOM-CCSD excitation energies. Instead we derive the criteria for a given EOM-CCSD excitation energy to be corrected. These criteria will help us to select only small subset of the excited states (composed of m EOM-CCSD roots, $m << N_{tot}$) whose excitation energies will be corrected in spectral resolution (7.11). From now on we will refer to this subspace as a m-space. It will also help us to establish a simple relation between $((Q_1+Q_2)\tilde{H}_N(Q_1+Q_2)$ and $((Q_1+Q_2)\bar{H}_N(Q_1+Q_2)$ matrices:

$$\begin{aligned} Q_{12}\tilde{H}_N Q_{12} &= \sum_{K=1}^{m} |R_K\rangle(\omega_K^{\mathrm{CCSD}} + \Delta\omega_K^{(T)})\langle L_K| + \sum_{K=m+1}^{N_{tot}} |R_K\rangle\omega_K^{\mathrm{CCSD}}\langle L_K| \\ &= Q_{12}\bar{H}_N Q_{12} + \sum_{K=1}^{m} |R_K\rangle\Delta\omega_K^{(T)}\langle L_K| \,. \end{aligned} \tag{7.12}$$

where $Q_{12} = (Q_1 + Q_2)$.

Let us analyze the modified (or pole shifted) linear response CCSD equation

$$(Q_1+Q_2)[\omega - \tilde{H}_N]\tilde{T}_\gamma^{(1)}(\omega)|\Phi\rangle = (Q_1+Q_2)e^{-T}\mu_\gamma e^{-T}|\Phi\rangle \ (\gamma = X,Y,Z), \tag{7.13}$$

where $\tilde{T}_\gamma^{(1)}(\omega)$ represents its solution. For simplicity we assume the easiest case $m = 1$, which means that only one excitation energy corresponding to some K-th excited state was a subject of adding the correction $\Delta\omega_K^{(T)}$ in the spectral resolution of the $((Q_1+Q_2)\bar{H}_N(Q_1+Q_2)$ matrix:

$$(Q_1+Q_2)\tilde{H}_N(Q_1+Q_2) = (Q_1+Q_2)\bar{H}_N(Q_1+Q_2) + |R_K\rangle\Delta\omega_K^{(T)}\langle L_K| \,. \tag{7.14}$$

We can easily find the inverse of $(Q_1+Q_2)[\omega-\tilde{H}_N](Q_1+Q_2)$ matrix once we know the inverse of $(Q_1+Q_2)[\omega-\bar{H}_N](Q_1+Q_2)$ matrix, i.e.,

$$[(Q_1+Q_2)[\omega-\tilde{H}_N](Q_1+Q_2)]^{-1} = [(Q_1+Q_2)[\omega-\bar{H}_N](Q_1+Q_2)]^{-1} + |R_K\rangle \frac{\Delta\omega_K^{(T)}}{(\omega-\omega_K^{CCSD}-\Delta\omega_K^{(T)})(\omega-\omega_K^{CCSD})}\langle L_K| \quad (7.15)$$

Now, premultiplying Eq.(7.13) from the left by $[(Q_1+Q_2)[\tilde{H}_N-\omega](Q_1+Q_2)]^{-1}$ and taking advantage of Eqs.(7.6) and (7.14) we obtain a simple result:

$$\tilde{T}_\gamma^{(1)}(\omega)|\Phi\rangle = T_\gamma^{(1)}(\omega)|\Phi\rangle + |R_K\rangle \frac{\Delta\omega_K^{(T)}\mu_{K,0}^\gamma}{(\omega-\omega_K^{\mathrm{CCSD}}-\Delta\omega_K^{(T)})(\omega-\omega_K^{\mathrm{CCSD}})} \quad (7.16)$$

where $\mu_{K,0}^\gamma = \langle L_K|e^{-T}\mu_\gamma e^T|\Phi\rangle$ is the right EOM-CCSD/LR-CCSD transition dipole moment from the ground to K-th excited state (in contrast to right transition moments the definition of the left transition moments are slightly different in EOM-CCSD and LR-CCSD approaches). This relationship between solution of the original LR-CCSD equation ($T_\gamma^{(1)}(\omega)$) and solution to the pole-shifted LR-CCSD equation ($\tilde{T}_\gamma^{(1)}(\omega)$) makes sense only for $\omega \neq \omega_K^{\mathrm{CCSD}}$. This means that in forming the m-space one should include:

- low-lying dipole-allowed excited states characterized by significant values of the due-to-triples corrections,

- dipole-allowed excited states characterized by large values of transition moment.

In a general case ($m \geq 1$) we can derive the following formula:

$$\tilde{T}_{\gamma}^{(1)}(\omega)|\Phi\rangle = T_{\gamma}^{(1)}(\omega)|\Phi\rangle + \sum_{K=1}^{m} |R_K\rangle \frac{\Delta\omega_K^{(T)} \mu_{K,0}^{\gamma}}{(\omega - \omega_K^{CCSD} - \Delta\omega_K^{(T)})(\omega - \omega_K^{CCSD})} \,. \quad (7.17)$$

where excited states that enter the above relationship are chosen based on the two criteria given above.

The most expensive part of the approximate pole shifted LR-CCSD approach (PS-LR-CCSD(m) or for brevity PS(T)-CCSD(m), where (T) indicates that the excitation energies of m EOM-CCSD states were corrected by adding CR-EOM-CCSD(T) or other due to triples corrections) is associated with the CR-EOM-CCSD(T) part (see next section for the numerical cost estimates). We believe that techniques based on the pole shift can be naturally applied to the higher order order response equations both for the T and Λ operators.

The PS(T)-CCSD(m) approach accounts only for the effect of the improved location of the poles. In contrast to approximate iterative approaches accounting for the effect of triples (the CC3 method) the PS(T)-CCSD(m) singly- and doubly-excited amplitudes are not iterated in the presence of genuine triply-excited amplitudes. We are aware that accommodating the effect of triples simply by shifting the location of poles may not be always sufficient in approximating full CCSDT results. We think that the presented algorithm along with the character of the CR-EOM-CCSD(T) correction gives us indication in what situations the PS(T)-CCSD(m) methodology has a chance to outperform the CCSD approach. Since usually the presence of low-lying excited states with doubly-excited component (for which the CR-EOM-CCSD(T) corrections take large values) is a sign of strong correlation effects taking place in the ground state, we expect the PS(T)-CCSD(m) formalism to work particularly well for

the strongly correlated systems. The examples in the forthcoming section will help us to figure out the extent of accuracy improvements of the PS(T)-CCSD(m) methods with respect to traditional LR-CCSD approach in the context of the static/dynamic polarizabilities calculations.

7.3 Computational details and results

Our core PS(T)-CCSD(m) algorithm was built upon the CCSD, LR-CCSD, EOM-CCSD, and CR-EOM-CCSD(T) Tensor Contraction Engine [39, 40, 41] implementation in NWChem.[42] The structure of the PS(T)-CCSD(m) code is as follows:

- The T amplitudes are obtained in standard CCSD calculations.
- The dipole allowed excitation energies ($\omega_K^{\rm CCSD}$ and corresponding left ($\langle L_K|$) and right ($|R_K\rangle$) eigenvectors of $\bar{H}_N$ are calculated in EOM-CCSD calculations.
- The CR-EOM-CCSD(T) corrections ($\Delta\omega_K^{\rm (T)}$) are formed from CCSD and EOM-CCSD amplitudes. In all our calculation we use the "IA" variant of the CR-EOM-CCSD(T) approach [33],
- The PS(T)-CCSD(m) equations are formed

$$[\mathbf{A}-\omega]\mathbf{x}_\gamma(\omega)+\sum_{K=1}^{m}\Delta\omega_K^{\rm (T)}(\mathbf{l}_K^+\mathbf{x}_\gamma(\omega))\mathbf{r}_K+\mathbf{b}_\gamma=\mathbf{0}\,, \tag{7.18}$$

  where the $\mathbf{A}$ matrix corresponds to $(Q_1+Q_2)\bar{H}_N(Q_1+Q_2)$ and the $\mathbf{x}_\gamma(\omega)$, $\mathbf{b}_\gamma$, $\mathbf{r}_K$ ($\mathbf{l}_K^+$) vectors correspond to $(Q_1+Q_2)\tilde{T}_\gamma^{(1)}|\Phi\rangle$, $(Q_1+Q_2)e^{-T}\mu_\gamma e^T|\Phi\rangle$, and right (left) eigenvector of $\bar{H}_N^{\rm CCSD}$, respectively. The PS(T)-CCSD(m) equations were implemented using LR-CCSD implementation of Ref. [43] by Hammond

et al.

All iterative steps (CCSD,EOM-CCSD, and PS(T)-CCSD(m)) are N^6 steps. The most expensive step is associated with calculating CR-EOM-CCSD(T) correction and scales as N^7. In order to reduce the scaling of CR-EOM-CCSD(T) corrections several approximate methods can be applied. Among those, the techniques based on the asymptotic extrapolation schemes (AES) [44] may be particularly attractive. Other choice is to construct the CR-EOM-CCSD(T) correction from the leading T_1, T_2, R_1, R_2 amplitudes only. The conceivable selection criterion of the leading cluster/excitation amplitudes can be based on the active-space concepts.

7.3.1 Static and dynamic polarizabilities for the N_2 molecule

The N_2 molecule was a subject of intensive studies with various level of CC response theory and basis sets. From Ref. [23], which discuss the effect of including triples on the accuracies of the frequency-dependent polarizabilities, the N_2 system emerges as a one posing significant challenge for theories based on singles and doubles. All CC3 static and frequency-dependent polarizabilities were obtained with the ACES2 [45] package. All static and dynamics CCSDT polarizabilities were obtained with our new CCSDT property code [46].

We decided to perform the PS(T)-CCSD(m) calculations for this system for basis set small enough that the exact CCSDT/EOM-CCSDT calculations are doable. For this purpose we chose the aug-cc-pVDZ [47] basis set. All calculations reported in this subsection were performed using spherical representation of the d functions and all core orbitals were kept frozen. Since the PS(T)-CCSD(m) approach heavily depends on the quality of excitation energies corresponding to the symmetry

Figure 7.1: Frequency dependent polarizability ($\alpha_{\|}(\omega)$) for the N_2 molecule in the aug-cc-pVDZ basis set (see text for details).

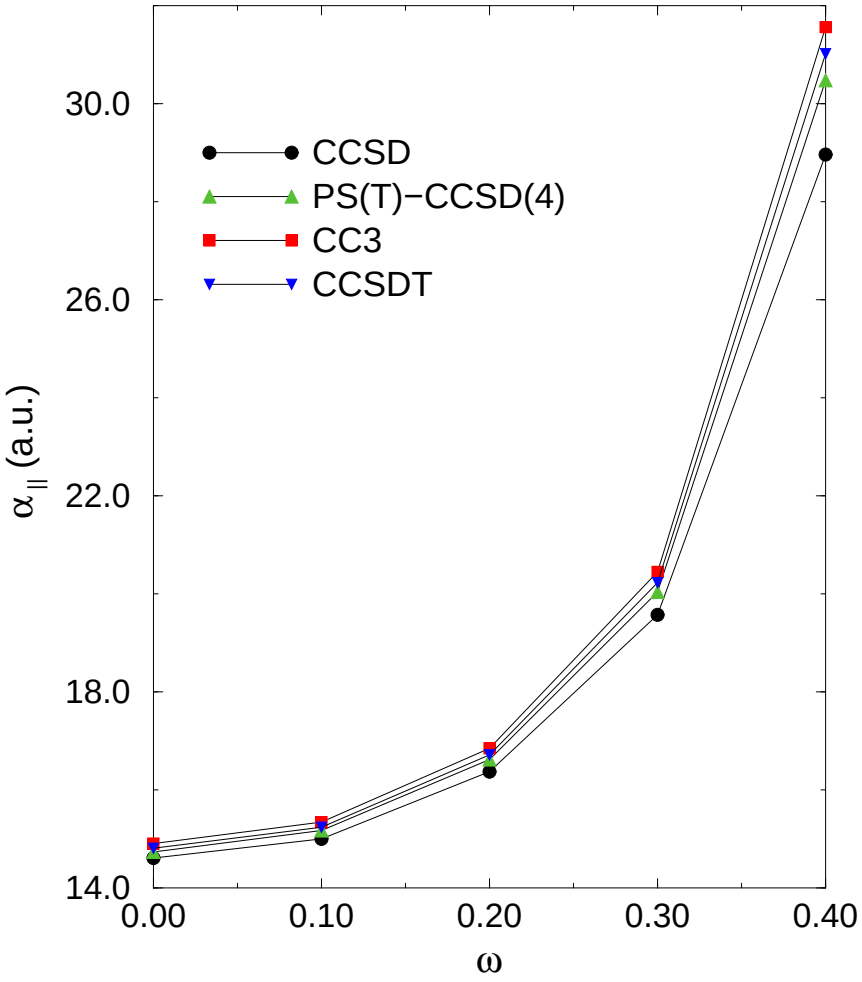

X,Y,Z components of the dipole moment μ operator (μ_X, μ_Y, and μ_Z), in Table 7.1 we collected EOM-CCSD, CR-EOM-CCSD(T), and EOM-CCSDT excitation energies and transition moment values obtained on the EOM-CCSD level of theory (at $R_{N-N} = 2.068$ a.u.). All calculations were carried out using D_{2h} symmetry. Although the CR-EOM-CCSD(T) excitation energies have tendency to slightly underestimate the EOM-CCSDT ones, they are located invariably closer to the EOM-CCSDT results than the EOM-CCSD excitation energies. In particular, the CR-EOM-CCSD(T) improvements upon the EOM-CCSD results take place for states such as 1^1B_{3u}, 1^1B_{2u}, 2^1B_{1u}, and 3^1B_{1u}, characterized by large transition moments. This fact play a key role in understanding of a good performance of the PS(T)-CCSD(m) approaches with suitably chosen m-states. For N_2 we discuss the m=2,3,4 cases (see Table 7.2). While m=2 case for $\alpha_{XX}(\omega)$ and $\alpha_{YY}(\omega)$ ($\alpha_{XX}(\omega) = \alpha_{YY}(\omega) = \alpha_{\perp}(\omega)$) incorporates degenerate 1^1B_{3u} and 1^1B_{2u} states characterized by a large values of the transition moment (0.894 a.u. on the EOM-CCSD level), for the B_{1u} representation (μ_z dipole moment) only the one state (2^1B_{1u}) corresponding to a large value for transition moments (0.975 a.u. given by the EOM-CCSD approach) is included. For this reason we can observe a significant improvements of the $\alpha_{\perp}(\omega)$ for larger values of ω. For example, the CCSD and PS(T)-CCSD(2) approaches, at $\omega = 0.4$ yield the errors on the order of 0.715 and 0.168 a.u., respectively, with respect to the CCSDT results. For $\alpha_{ZZ}(\omega) = \alpha_{\parallel}(\omega)$ component these errors are bigger and equal 2.057 and 1.297 for CCSD and PS(T)-CCSD(2), nevertheless the PS(T)-CCSD(2) approach offer improvements upon the CCSD results. The large error of the PS(T)-CCSD(2) approach for larger ω values can be attributed to the lack of the 3^1B_{1u} state (EOM-CCSD transition moment is equal 1.030 a.u.) in the m-space, which is not included by the PS(T)-CCSD(m) $m = 1, 2$.

Table 7.1: The EOM-CCSD, EOM-CCSDT, and CR-EOM-CCSD(T),IA excitation energies (the EOM notation is omitted in the table) and EOM-CCSD transition moments for the N_2 molecule as described by the aug-cc-pVDZ basis set (R_{N-N} = 2.068 a.u.). The $1s$ core orbitals were frozen. The transition moments reported for Π_u and Σ_u^+ states correspond to the x- and z-axis, respectively.

	Excitation energy			Transition moment
State	CCSD	CR-CCSD(T),IA	CCSDT	CCSD
$1^1\Pi_u$	13.475	13.331	13.224	0.894
$2^1\Pi_u$	13.794	13.609	13.611	0.209
$3^1\Pi_u$	14.554	14.187	14.289	0.454
$4^1\Pi_u$	16.741	16.376	16.470	0.350
$1^1\Sigma_u^+$	10.730	10.364	10.560	0.000
$2^1\Sigma_u^+$	13.261	13.116	13.146	0.975
$3^1\Sigma_u^+$	14.907	14.536	14.549	1.030
$4^1\Sigma_u^+$	16.701	16.502	16.431	0.333

The PS(T)-CCSD(3) and PS(T)-CCSD(4) variants lead to systematic improvement of the CCSD and PS(T)-CCSD(2) results for $\alpha_{\|}(\omega)$ (see Fig. 7.1). This can be seen for all ω values. For $\omega = 0.0$ the CCSD and PS(T)-CCSD(m) (m=2,3,4) errors with respect to the CCSDT results are as big as 0.206, 0.164, 0.079, and 0.076 a.u., respectively, whereas for $\omega = 0.4$ we these errors amount to 2.057, 1.297, 0.558, and 0.543 a.u., respectively. In both cases ($\omega = 0.0$ and $\omega = 0.4$) the accuracies of the PS(T)-CCSD(4) and CC3 approaches are comparable. For example, for $\omega = 0.0$ these methods produce 0.076 and -0.094 a.u. of error for $\alpha_{\|}$, while for $\omega = 0.4$ analogous error are equal to 0.543 and -0.540 a.u.

Table 7.2: A comparison of CC frequency-dependent polarizabilities for N_2 system as described by aug-cc-pVDZ basis set (see text for details). The frequency (in Hartrees) is given at the top of each column of values.

	$\alpha_{\perp}(\omega)$					$\alpha_{\parallel}(\omega)$				
Method	0.0	0.1	0.2	0.3	0.4	0.0	0.1	0.2	0.3	0.4
SCF	9.491	-	-	-	-	14.794	-	-	-	-
CCSD	10.004	10.237	11.044	12.934	18.527	14.608	15.002	16.368	19.568	28.963
PS(T)-CCSD(2)	10.038	10.282	11.114	13.075	19.074	14.650	15.057	16.454	19.746	29.723
PS(T)-CCSD(3)	10.057	10.307	11.151	13.143	19.266	14.735	15.165	16.612	20.027	30.462
PS(T)-CCSD(4)	10.066	10.317	11.165	13.164	19.308	14.738	15.169	16.617	20.034	30.477
CC3	10.066	10.305	11.133	13.090	19.080	14.908	15.340	16.847	20.448	31.560
CCSDT	10.054	10.293	11.125	13.097	19.242	14.814	15.237	16.711	20.224	31.020

For the $\alpha_{\perp}$ component the overall situation is slightly different, namely the PS(T)-CCSD(4) approach has a tendency to overestimate the CCSDT results. This trend is apparent for all values of ω and is becoming particularly pronounced for large ω values. For $\omega = 0.0$ and $\omega = 0.4$ PS(T)-CCSD(4) discrepancies reach -0.012 and -0.066 a.u., respectively. This should be compared to -0.012 and 0.162 a.u. of error produced by the CC3 approach.

It is also interesting to analyze how quickly the PS(T)-CCSD(m) results saturate with a growing number (m) of excited states employed by PS(T)-CCSD(m) formalism. For this purpose we performed PS(T)-CCSD(10) calculation employing eight low-lying excited states for dipole allowed symmetries. For $\alpha_{\perp}$ components we included in m-space EOM-CCSD roots with energies between 13.47 and 23.84 eV, whereas for $\alpha_{\parallel}$ EOM-CCSD roots with excitation energies between 10.73 and 19.57 eV falls into the m-space. For ω =0.0, 0.1, 0.2, 0.3, and 0.4 we obtained 10.069, 10.322, 11.170, 13.171, and 19.315 a.u. for $\alpha_{\perp}(\omega)$ and 14.750, 15.184, 16.636, 20.060, and 30.513 a.u. for $\alpha_{\parallel}(\omega)$, respectively. These numbers clearly show that inclusion of the next four excited states in the m-space has little effect on the PS(T)-CCSD(4) results. For example, for $\omega = 0.4$ the differences between PS(T)-CCSD(4) and PS(T)-CCSD(8) results for $\alpha_{\perp}(\omega = 0.4)$ and $\alpha_{\parallel}(\omega = 0.4)$ are as small as 0.007 and 0.033 a.u. (for $\omega = 0.0$ these discrepancies are even smaller and equal to 0.003 and 0.012 a.u. respectively). This relatively fast saturation of the results with the growing dimensionality of the m-space may indicate that in realistic calculations only few important states should be incorporated in the m-space in order to get the reliable results.

Figure 7.2: Errors (with respect to CCSDT) in the static $\alpha_{ZZ}(0)$ polarizability for the N_2 molecule in the aug-cc-pVDZ basis set as a function of N-N stretch.

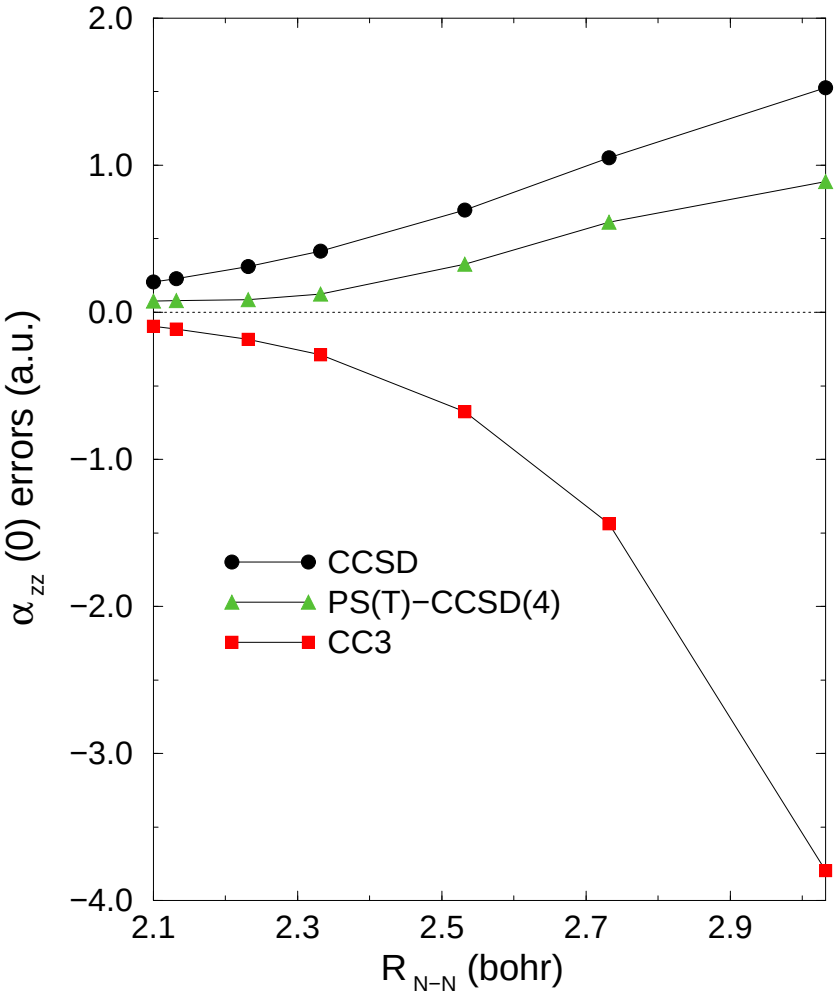

Table 7.3: The EOM-CCSD and CR-EOM-CCSD(T),IA excitation energies and EOM-CCSD transition moments for the $FHCH_3$ molecule with the aug-cc-pVDZ basis set. All core electrons were frozen and C_1 symmetry was used in all EOM-CCSD/CR-EOM-CCSD(T),IA calculations (see text for details).

	Excitation energy		Transition moment
State	EOM-CCSD	CR-EOM-CCSD(T),IA	EOM-CCSD
2^1A	0.956	0.888	0.055
3^1A	0.956	0.888	0.055
4^1A	5.241	4.979	1.495
5^1A	5.657	5.236	0.047
6^1A	5.657	5.236	0.047

7.3.2 Polarizabilities for stretched internuclear geometries

In many processes characterized by small gaps between the ground and the low-lying excited states the calculations of static/dynamic CCSD polarizabilities may be plagued by a large errors due to inadequate description of excitation energies corresponding to these states. This situation mainly occurs when one or more bonds are stretched. In this subsection we study these problems on two examples: (1) the property calculations in the vicinity of the transition state of the $FHCH_3$ system (2) the static polarizabilities for stretched bonds in the N_2 molecule. All calculations were performed with aug-cc-pVDZ basis set [47] with core orbitals kept frozen. The CC3 static polarizabilities were obtained with the ACES2 [45] package.

The high-level description of the molecular properties for transition state can provide very useful information for theoretical description of the laser controlled chemical reactions (see Refs. [48, 49, 50, 51, 52] and references therein). For this reason in this subsection we focus on the $FHCH_3$ molecule, whose static polarizabilities were calculated using MP2 approach along the reaction path of the $F+CH_4$ reaction systems.[48]

The main goal of these calculations was to establish the laser-molecule interactions as a function of the reaction coordinates. Particularly interesting situation occurs for the transition state (TS) geometry for which dipole polarizabilities exhibit significant peak. Our calculations were based on the transition state geometries calculated at the QCISD(T) level of theory using 6-311++G(2df,2dp) basis set. [52] In Table 7.3 we juxtaposed CC results of TS excitation energies and corresponding transition moments calculated at the EOM-CCSD level. The two lowest excited states with degenerate excitation energies (2^1A and 3^1A) are well described by the EOM-CCSD approach. The CR-EOM-CCSD(T) corrections for these states are small: -0.068 eV. In turn, the third excited state (4^1A) is characterized by bigger CR-EOM-CCSD(T) correction (-0.26 eV) and big value of the transition moment. Therefore we expect this state to play a critical role in describing TS properties. Although the CR-EOM-CCSD(T) corrections corresponding to the fourth and fifth excited states are quite big (-0.42 eV) the 5^1A and 6^1A transition moments are rather small. These properties of excited states give us a clear indication what should be included in the m-space. While the differences between CCSD and PS(T)-CCSD(2) static polarizabilities are small (see Table 7.4) the inclusion of the third excited state in the m-space (PS(T)-CCSD(3)) results in a significant change for the $\alpha_{ZZ}(0)$ component. The difference between PS(T)-CCSD(3) and CCSD $\alpha_{ZZ}(0)$ polarizabilities amounts to 1.233 a.u. The enlargement of the m-space by adding 5^1A and 6^1A has minor effect on the static polarizabilities. In summary, this example clearly shows how important is the proper construction of the m-space by including the states with large transition moments in the TS region.

Yet another situation, corresponding to breaking multiple bonds, is illustrated on the N_2 example. All calculations where performed using aug-cc-pVDZ basis set

Table 7.4: Static CCSD and PS(T)-CCSD(3) polarizabilities for $FHCH_3$ system as described by the aug-cc-pVDZ basis set. The z-axis is the F-H-C axis (see Ref. [52] for details).

Method	α_{XX}	α_{YY}	α_{ZZ}
CCSD	18.546	18.546	41.977
PS(T)-CCSD(2)	18.561	18.561	41.977
PS(T)-CCSD(3)	18.561	18.561	43.201
PS(T)-CCSD(5)	18.563	18.563	43.201

with all core orbitals kept frozen. The results for static polarizabilities calculated at several geometries (shown in Table 7.5) ranging from 2.068 bohr to 3.00 bohr were obtained with the CCSD, PS(T)-CCSD(m) ($m = 2, 3, 4$), CC3, and CCSDT approaches. One can see that while the PS(T)-CCSD(m) results are in a reasonable proximity to the CCSDT results, the CC3 results are significantly different from CCSDT ones. This is best seen at larger R_{N-N} distances. For example, at $R_{N-N} = 3.0$ bohr the discrepancy between CC3 and CCSDT $\alpha_{\|}(0)$ polarizabilities amounts to 3.8 a.u. This large difference should be attributed to the poor location of the excitation energies obtained on the CC3 level, which is a consequence of non-negligible doubly-excited contributions to the wavefunctions corresponding to low-lying excited states at stretched geometries. It is interesting to analyze in this context the performance of the PS(T)-CCSD(m) approach for $m = 2, 3, 4$. In all cases we used m-lowest EOM-CCSD states for a given symmetry representation corresponding to a given dipole moment component. At larger R_{N-N} distances we observe a significant increase of the CR-EOM-CCSD(T) corrections, whose values at $R_{N-N} = 3.0$ bohr became as big as $1 - 2$ eV. The inclusion of these large effects in the excitation energies lead to an improvement of the PS(T)-CCSD(m) approaches compared to the CCSD polarizabilities. For example, the $\alpha_{\|}(0)$ CCSDT and PS(T)-CCSD(4) differences for

R_{N-N} =2.068, 2.1, 2.2, 2.3, 2.5, 2.7, and 3.0 bohr are as small as 0.075, 0.078, 0.087, 0.125, 0.327, 0.614, and 0.889 a.u., respectively. These errors should be compared to the CCSD ones: 0.205, 0.227, 0.311, 0.416, 0.694, 1.051, and 1.527 a.u. and CC3 ones: -0.096, -0.113, -0.183, -0.289, -0.675, -1.437, and -3.797 a.u., respectively (see Fig. 7.2). From Table 7.2 one can also see that PS(T)-CCSD(m) series is quickly converging. The best illustration is provided by the $\alpha_{\perp}(0)$ at $R_{N-N} = 2.7$ bohr. While the difference between the PS(T)-CCSD(2) and CCSD results reaches 0.320 a.u., the analogous difference between PS(T)-CCSD(3) and PS(T)-CCSD(2) and PS(T)-CCSD(4) and PS(T)-CCSD(3) are equal 0.008 and 0.003 a.u., respectively, which causes that the PS(T)-CCSD(4) value only slightly overestimates the CCSDT one. In situation where the PS(T)-CCSD(2) result was locate above the CCSDT one by 0.011 a.u. the PS(T)-CCSD(4) is still very close to the CCSDT (difference equals -0.022 a.u.).

7.4 Conclusions

This paper discusses a new approach to correct the location of linear response CCSD poles for the effect of triply-excited configurations. This generally applicable scheme, termed the PS(T)-CCSD(m) formalism, uses the modified resolution of identity of similarity transformed Hamiltonian that naturally occurs in the linear response CCSD equations. In the modified expansion, selected EOM-CCSD excitation energies are corrected by adding the non-iterative corrections due to triples. In our derivations we formulated a simple set of .selection. rules for a given state to be corrected in the spectral resolution of $\bar{H}_N$. Although various non-iterative approaches can be used in this context we were particularly interested in the methods that can provide reliable results for excited states with highly diversified structure. The natural choice was to employ

Table 7.5: A comparison of the CC static polarizabilities as a functions of N-N internuclear stretch. The aug-cc-pVDZ basis set was used and all core electrons were kept frozen in the calculations.

	$R_{N\equiv N}$						
Method	2.068	2.1	2.2	2.3	2.5	2.7	3.0
CCSD							
$\alpha_{\perp}(0)$	10.004	10.096	10.382	10.659	11.170	11.611	12.112
$\alpha_{\parallel}(0)$	14.608	14.931	15.950	16.980	19.035	21.016	23.675
PS(T)-CCSD(2)							
$\alpha_{\perp}(0)$	10.038	10.138	10.447	10.766	11.378	11.931	12.572
$\alpha_{\parallel}(0)$	14.650	14.978	16.019	17.080	19.213	21.123	23.673
PS(T)-CCSD(3)							
$\alpha_{\perp}(0)$	10.057	10.159	10.472	10.772	11.384	11.939	12.578
$\alpha_{\parallel}(0)$	14.735	15.080	16.172	17.267	19.390	21.435	24.281
PS(T)-CCSD(4)							
$\alpha_{\perp}(0)$	10.066	10.166	10.484	10.785	11.403	11.942	12.583
$\alpha_{\parallel}(0)$	14.738	15.080	16.174	17.271	19.402	21.453	24.313
CC3							
$\alpha_{\perp}(0)$	10.066	10.170	10.494	10.820	11.464	12.089	12.951
$\alpha_{\parallel}(0)$	14.909	15.271	16.444	17.685	20.404	23.504	28.999
CCSDT							
$\alpha_{\perp}(0)$	10.054	10.154	10.468	10.777	11.368	11.901	12.522
$\alpha_{\parallel}(0)$	14.814	15.158	16.261	17.396	19.729	22.067	25.202

the CR-EOM-CCSD(T) formalism, which when combined with the PS(T)-CCSD(m) methodology reinstate the correct location of poles for the first order response amplitudes $T^{(1)}(\omega)$. As discussed in Section II we expect essential improvements for the strongly correlated systems, where the correct location of the poles play a pivotal role in obtaining high accuracy for the $T^{(1)}(\omega)$-dependent properties such as dipole polarizabilities (in other situations iterating singly- and doubly-excited amplitudes in the presence of triply- excited cluster may be necessary). Our preliminary studies confirm this premise. The PS(T)-CCSD(m) calculations on the N_2 molecule and open-shell $FHCH_3$ system at transition state geometry convey significant improvement relative to the CCSD results. Moreover, in order to obtain substantial improvements over the CCSD results only few most important excited states need to be included in the m-space. Final accuracies given by the PS(T)-CCSD(m) formalism may be contingent upon the accuracy of the methods used for correcting the EOM-CCSD excitation energies. In the future studies we are planning to combine PS(T)-CCSD(m) approach with other non-iterative approaches such as CCSDR(3) and other.

REFERENCES

[1] J. Paldus and X. Li, *Adv. Chem. Phys.* **110**, 1 (1999).

[2] T.D. Crawford and H. F. Schaefer III, *Rev. Comp. Chem.* **14**, 33 (2000).

[3] P. Piecuch, K. Kowalski, I. S. O. Pimienta and M. J. McGuire, *Int. Rev. Phys. Chem.* **21**, 527 (2002).

[4] R. J. Bartlett and M. Musiał, *Rev. Mod. Phys.* **79**, 291 (2007).

[5] H. J. Monkhorst, *Int. J. Quantum Chem.* **S11**, 421 (1977).

[6] E. Daalgard and H. J. Monkhorst, *Phys. Rev. A* **28**, 1217 (1983).

[7] H. Koch and P. Jørgensen, *J. Chem. Phys.* **93**, 3333 (1990).

[8] O. Christiansen, C. Hättig and P. Jørgensen, *Int. J. Quantum Chem.* **68**, 1 (1998).

[9] R. Kobayashi, H. Koch and P. Jørgensen, *Chem. Phys. Lett.* **249**, 30 (1994).

[10] C. Hättig, O. Christiansen, H. Koch and P. Jørgensen, *Chem. Phys. Lett.* **269**, 428 (1997).

[11] C. Hättig, O. Christiansen, H. Koch and P. Jørgensen, *Chem. Phys. Lett.* **282**, 139 (1998).

[12] O. Christiansen, H. Koch and P. Jørgensen, *Chem. Phys. Lett.* **243**, 409 (1995).

[13] O. Christiansen, A. Halkier, H. Koch, P. Jørgensen and T. Helgaker, *J. Chem. Phys.* **108**, 2801 (1998).

[14] O. Christiansen, H. Koch and P. Jørgensen, *J. Chem. Phys.* **103**, 7429 (1995).

[15] O. Christiansen, H. Koch, P. Jørgensen and J. Olsen, *Chem. Phys. Lett.* **256**, 185 (1996).

[16] H. Koch, O. Christiansen, P. Jørgensen, A.M. Sanchez de Merás and T. Helgaker, *J. Chem. Phys.* **106**, 1808 (1997).

[17] K. Hald and P. Jørgensen, *Phys. Chem. Chem. Phys.* **4**, 5221 (2002).

[18] O. Christiansen, *Theor. Chem. Acta.* **116**, 106 (2006).

[19] M. Kállay and J. Gauss, *J. Mol. Struct. (THEOCHEM)*, **768**, 71 (2006).

[20] Y.S. Lee and R. J. Bartlett, *J. Chem. Phys.* **80**, 4371 (1984).

[21] M. Urban, J. Noga, S. J. Cole and R. J. Bartlett, *J. Chem. Phys.* **83**, 4041 (1985).

[22] J. Noga, R. J. Bartlett and M. Urban, *Chem. Phys. Lett.* **134**, 126 (1987).

[23] O. Christiansen, J. Gauss and J. F. Stanton, *Chem. Phys. Lett.* **292**, 437 (1998).

[24] K. Hald, F. Pawłowski and C. Hättig, *J. Chem. Phys.* **118**, 1292 (2003).

[25] J. Gauss, O. Christiansen and J. F. Stanton, *Chem. Phys. Lett.* **296**, 117 (1998).

[26] F. Pawłowski, P. Jørgensen and C. Hättig, *Chem. Phys. Lett.* **391**, 27 (2004).

[27] O. Christiansen, H. Koch and P. Jørgensen, *J. Chem. Phys.* **105**, 1451 (1996).

[28] J. Geersten, M. Rittby and R. J. Bartlett, *Chem. Phys. Lett.* **164**, 57 (1989).

[29] D. C. Comeau and R. J. Bartlett, *Chem. Phys. Lett.* **207**, 414 (1993).

[30] J. F. Stanton and R. J. Bartlett, *J. Chem. Phys.* **98**, 7029 (1993).

[31] J. F. Stanton and R. J. Bartlett, *J. Chem. Phys.* **99**, 5178 (1993).

[32] K. Raghavachari, G. W. Trucks, J. A. Pople and M. Head-Gordon, *Chem. Phys. Lett.* **157**, 479 (1989).

[33] K. Kowalski and P. Piecuch, *J. Chem. Phys.* **120**, 1715 (2004).

[34] K. Kowalski and P. Piecuch, *J. Chem. Phys.* **113**, 18 (2000).

[35] S. Coussan, Y. Ferro, A. Trivella, M. Rajzmann, P. Roubin, R. Wieczorek, C. Manca, P. Piecuch, K. Kowalski, M. Włoch, S.A. Kucharski and M. Musiał, *J. Phys. Chem. A* **110**, 3920 (2006).

[36] M. Valiev and K. Kowalski, *J. Chem. Phys.* **125**, 211101 (2006).

[37] J. D. Watts and R. J. Bartlett, *Chem. Phys. Lett.* **233**, 81 (1995).

[38] J. D. Watts and R. J. Bartlett, *Chem. Phys. Lett.* **258**, 581 (1996).

[39] S. Hirata, *J. Phys. Chem. A* **107**, 9887 (2003).

[40] S. Hirata, *J. Chem. Phys.* **121**, 51 (2004).

[41] S. Hirata, *Theor. Chem. Acc.* **116**, 2 (2006).

[42] E. J. Bylaska, W. A. de Jong, N. Govind, K. Kowalski, T. P. Straatsma, M. Valiev, D. Wang, E. Apra, T. L. Windus, J. Hammond, P. Nichols, S. Hirata, M.

T. Hackler, Y. Zhao, P.-D. Fan, R. J. Harrison, M. Dupuis, D. M. A. Smith, J. Nieplocha, V. Tipparaju, M. Krishnan, Q. Wu, T. Van Voorhis, A. A. Auer, M. Nooijen, E. Brown, G. Cisneros, G. I. Fann, H. Fruchtl, J. Garza, K. Hirao, R. Kendall, J. A. Nichols, K. Tsemekhman, K. Wolinski, J. Anchell, D. Bernholdt, P. Borowski, T. Clark, D. Clerc, H. Dachsel, M. Deegan, K. Dyall, D. Elwood, E. Glendening, M. Gutowski, A. Hess, J. Jaffe, B. Johnson, J. Ju, R. Kobayashi, R. Kutteh, Z. Lin, R. Littlefield, X. Long, B. Meng, T. Nakajima, S. Niu, L. Pollack, M. Rosing, G. Sandrone, M. Stave, H. Taylor, G. Thomas, J. van Lenthe, A. Wong and Z. Zhang. "NWChem, A Computational Chemistry Package for Parallel Computers, Version 5.1" (2007), Pacific Northwest National Laboratory, Richland, Washington 99352-0999, USA. A modified version.

[43] J. R. Hammond, M. Valiev, W. A. de Jong and K. Kowalski, *J. Phys. Chem. A*, **111**, 5492 (2007).

[44] K. Kowalski and M. Valiev, *J. Phys. Chem. A* **110**, 13106 (2006).

[45] *Aces II*, a quantum chemical program package written by J. F. Stanton, J. Gauss, J .D. Watts, P. G. Szalay, R. J. Bartlett with contribution from A. A. Auer, D. B. Bernholdt, O. Christiansen, M. E. Harding, M. Heckert, O. Heun, C. Huber, D. Jonsson, J. Juselius, W. J. Lauderdale, T. Metzroth, K. Ruud and the integral packages *MOLECULE* (J. Almlöf and P. R. Taylor), Props (P. R. Taylor), and ABACUS (T. Helgaker, H. Å. Jensen, P. Jørgensen and J. Olsen). See also J. F. Stanton, J. Gauss, J. D. Watts, W. J. Lauderdale, R.J. Bartlett, *Int. J. Quantum Chem. Symp.* **26**, 879 (1992) as well as : `http://www.aces2.de` for the current version.

[46] J. R. Hammond and K. Kowalski, *J. Chem. Phys.*, **128**, 224102 (2008).

[47] T. H. Dunning Jr., *J. Chem. Phys.* **90**, 1007 (1989); R. A. Kendall, T. H. Dunning Jr., R. J. Harrison, *J. Chem. Phys.* **96**, 6796 (1992).

[48] A. D. Bandrauk, E.-W. S. Sedik and C.F. Matta, *J. Chem. Phys.* **121**, 7764 (2004).

[49] D. Troya, J. Millàn, I. Banos and M. Gonzàlez, *J. Chem. Phys.* **120**, 5181 (2004).

[50] J. C. Corchado and J. Espinosa-Garcia, *J. Chem. Phys.* **105**, 3152 (1996).

[51] J. F. Castillo, F. J. Aoiz, L. Banares, E. M. Nunez, A. F. Ramos and S. Vazquez, *J. Phys. Chem. A* **109**, 8459 (2005).

[52] Q. Wang, Z. Cai and D. Feng, *J. Mol. Struct. (THEOCHEM)*, **759**, 31 (2006).

CHAPTER 8

C_6 COEFFICIENTS FROM COUPLED-CLUSTER LINEAR RESPONSE THEORY

This chapter will eventually be published in the following article: J. R. Hammond and K. Kowalski, "C_6 coefficients from coupled-cluster linear response theory."

8.1 Introduction

This chapter reports on the extension of our coupled-cluster (CC) linear response codes [1] to the computation of C_6 coefficients from imaginary-frequency polarizabilities using the Casimir-Polder integral. C_6 coefficients quantify the attractive van der Waals (or dispersion) interaction used in the Lennard-Jones potential [2]:

$$V(r) = \left[\left(\frac{A_{12}}{r} \right)^{12} - \left(\frac{C_6}{r} \right)^{6} \right], \tag{8.1}$$

where V is the potential, r is interatomic (intermolecular) distance. The A_{12} term[1] describes the repulsion at short distance while the C_6 is the lowest order term in the expansion of the dispersion interaction. Odd-order terms (C_n for $n = 7, 9, 11, \ldots$) are zero for centrosymmetric species (atoms) or when averaged over all orientations of noncentrosymmetric species (molecules) [3]. The C_6 coefficient is proportional to the

[1] A_{12} is used instead of the conventional nomenclature (C_{12}) since C_{12} represents the dispersion interaction from higher-order multipole polarizabilities, even though the latter is not referred to explicitly in the text.

dipole-dipole polarizability ($\alpha_{i,j} = \langle\langle \mu_i; \mu_j \rangle\rangle$ for $i = x, y, z$) while higher-order terms are proportional to polarizabilities corresponding to higher multipoles (See Ref. [3] for details).

Previously, Stanton implemented this feature using the Aces code and applied it to atoms [4]. Subsequently, Jørgensen and coworkers computed C_6 coefficients from Cauchy moments computed with coupled-cluster response theory [5, 6]. More recently, Korona and coworkers computed C_6 coefficients using an approximate form of CCSD in conjunction with density-fitting [8, 9], while Wheatley computed C_6 coefficients using time-dependent CC theory [10]. This paper reports on the application of CC response theory for computing C_6 coefficients of atoms and molecules using the complete form of the CCSD wavefunction. Numerical issues related to the solution of the linear response equations for imaginary frequencies are investigated. We derive two methods for decoupling the real- and imaginary-components of the response equations and consider the numerical properties of each. Finally, the present implementation has been demonstrated to run on very large supercomputers, enabling the application of the methods described herein to molecules with more than a dozen atoms.

8.2 Theory

An overview of CC theory and its linear response extension can be found in Refs. [11, 13, 12, 14, 15, 1]). In this section, we derive the linear response equations for determinating dynamic polarizabilities for an imaginary frequency and briefly recount the connection between these quantities and C_6 coefficients.

8.2.1 Response equations for a complex frequency

The first-order response amplitudes, $T^{(1)}$, for frequency $\omega \in \Re$ are obtained by solving

$$\langle \Phi^{a_1 \ldots a_n}_{i_1 \ldots i_n} | [\overline{H}, T^{(1)}] | \Phi \rangle - \omega \langle \Phi^{a_1 \ldots a_n}_{i_1 \ldots i_n} | T^{(1)} | \Phi \rangle = - \langle \Phi^{a_1 \ldots a_n}_{i_1 \ldots i_n} | \overline{\mu} | \Phi \rangle. \tag{8.2}$$

For the general case $\omega = \omega_R + i\omega_I$ with $\omega_R, \omega_I \in \Re$, $T^{(1)}$ will be complex. The complex response amplitudes can be decomposed $T^{(1)} = T^{(1)}_R + iT^{(1)}_I$. Under these conditions, the response equations can be separated a real and imaginary components,

$$\begin{aligned} \langle \Phi^{a_1 \ldots a_n}_{i_1 \ldots i_n} | [\overline{H}, T^{(1)}_R] | \Phi \rangle - \omega_R \langle \Phi^{a_1 \ldots a_n}_{i_1 \ldots i_n} | T^{(1)}_R | \Phi \rangle &= - \langle \Phi^{a_1 \ldots a_n}_{i_1 \ldots i_n} | \overline{\mu} | \Phi \rangle \\ &+ \omega_I \langle \Phi^{a_1 \ldots a_n}_{i_1 \ldots i_n} | T^{(1)}_I | \Phi \rangle \qquad (8.3) \\ \langle \Phi^{a_1 \ldots a_n}_{i_1 \ldots i_n} | [\overline{H}, T^{(1)}_I] | \Phi \rangle - \omega_R \langle \Phi^{a_1 \ldots a_n}_{i_1 \ldots i_n} | T^{(1)}_I | \Phi \rangle &= \omega_I \langle \Phi^{a_1 \ldots a_n}_{i_1 \ldots i_n} | T^{(1)}_R | \Phi \rangle. \qquad (8.4) \end{aligned}$$

The real component of the complex response equations (Eq. 8.3) is identical to Eq. 8.2 except for the addition of a second b-term (the linear response equations are of the form $Ax = b$), while the imaginary component (Eq. 8.4) substitutes this b-term in place of the original b-term corresponding to the dipole operator. Thus, very little modification of our real-frequency linear response codes [1, 24, 23, 25] is required to calculate responses for complex frequency. These equations can be decoupled via elimination of the imaginary component from Eqn. 8.3 or the real component in Eqn 8.4. In the matrix notation Eqns. 8.3 and 8.4 are

$$(A - \omega_R) x_R = b + \omega_I x_I \tag{8.5}$$

$$(A - \omega_R) x_I = \omega_I x_R. \tag{8.6}$$

By substituing $x_I = \omega_I (A - \omega_R)^{-1} x_R$ into Eqn. 8.5 we obtain

$$[(A - \omega_R)^2 - \omega_I^2] x_R = (A - \omega_R) b = \tilde{b}. \tag{8.7}$$

Alternatively, by substituing $x_R = \omega_I^{-1} (A - \omega_R) x_I$ into Eqn. 8.5 we obtain

$$[(A - \omega_R)^2 - \omega_I^2] x_I = \omega_I b. \tag{8.8}$$

Once the real (imaginary) component of the response amplitudes are obtained, Eqn. 8.6 (Eqn. 8.5) can be solved to obtain the imaginary (real) component. In Section 8.3, we report the numerical performance of the solution of the response equations using the two decoupling schemes: decoupled via imaginary elimination (Eqns. 8.7 and 8.6) and decoupled via real elimination (Eqns. 8.8 and 8.5). The coupled system of equations (Eqns. 8.5 and 8.6) was numerically insoluble for all even the simplest chemicals systems.

8.2.2 Response function for a complex frequency

The linear response function for a coupled-cluster wavefunction is

$$\langle\langle A; B \rangle\rangle_\omega = \frac{1}{2} \hat{C}^{\pm\omega} \hat{P}_{A,B} \langle \Phi | (1 + \Lambda) \left\{ \left[\overline{A}, T^{(1)}_{B,\omega} \right] + \left[\left[\overline{H}, T^{(1)}_{A,\omega} \right], T^{(1)}_{B,-\omega} \right] \right\} | \Phi \rangle \tag{8.9}$$

where $\hat{C}$ enforces time-reversal symmetry and $\hat{P}$ permutes A and B. Evaluating this quantity requires the evaluation of the Λ amplitudes of gradient theory and the first-order response with respect to operators A and B at both positive and negative frequency.

For a purely imaginary frequency ($\omega_R = 0$), the linear response function can be

reduced to the following contributions from the real and imaginary components of the response amplitudes,

$$\begin{aligned}
\langle\langle A;B\rangle\rangle_{\omega_I} &= \langle\langle A;B\rangle\rangle_R + \langle\langle A;B\rangle\rangle_I && (8.10)\\
\langle\langle A;B\rangle\rangle_R &= \hat{P}_{A,B}\langle\Phi|(1+\Lambda)\left[\overline{A},T^{(1)}_{B,R}\right]|\Phi\rangle \\
&+ \langle\Phi|(1+\Lambda)\left[\left[\overline{H},T^{(1)}_{A,R}\right],T^{(1)}_{B,R}\right]|\Phi\rangle && (8.11)\\
\langle\langle A;B\rangle\rangle_I &= \hat{C}^{\pm\omega_I}\langle\Phi|(1+\Lambda)\left[\left[\overline{H},T^{(1)}_{A,I}\right],T^{(1)}_{B,-I}\right]|\Phi\rangle && (8.12)
\end{aligned}$$

where $T^{(1)}_{O,R}$ is the real component of the response amplitudes with respect to operator O at static frequency and $T^{(1)}_{O,\pm I}$ are the imaginary components of the response amplitudes with respect to operator O at frequency $\pm\omega_I$. The operator $\hat{C}^{\pm\omega_I}$ symmetrizes with respect to ω_I to preserve time-reversal symmetry, while $\hat{P}_{A,B}$ is the interchange operator for property operators A and B. When $\omega_R = 0$, it follows immediately from Eqn. 8.4 that $T^{(1)}_{O,I} = -T^{(1)}_{O,-I}$, so we may simplify Eq. 8.12 as

$$\langle\langle A;B\rangle\rangle_I = -2\cdot\langle\Phi|(1+\Lambda)\left[\left[\overline{H},T^{(1)}_{A,I}\right],T^{(1)}_{B,I}\right]|\Phi\rangle \qquad (8.13)$$

which reduces the number of response amplitudes which need to be computed by one-third.

In the case of dipole polarizabilities, A and B are both dipole moment operators, and the polarizability is given by

$$\alpha_{ij}(i\omega_I) = -\langle\langle\mu_i;\mu_j\rangle\rangle_{\omega_I}. \qquad (8.14)$$

8.2.3 Derivation of the Casimir-Polder relation

The connection between imaginary-frequency dynamic polarizabilities and C_6 coefficients can be derived using simple perturbation theory for long-range intermolecular forces. Our treatment closely follows that of Stone [3], which is based upon the seminal work of London [16, 17], Margenau [18], Longuet-Higgins [19] and Buckingham [20].

The second-order energy in the perturbative expansion of the intermolecular forces between species A and species B includes the induction energy for both A and B as well as the dispersion energy corresponding to simultaneous excitations on both species:

$$E^{(2)} = U^A_{\rm ind} + U^B_{\rm ind} + U^{AB}_{\rm disp} \tag{8.15}$$

where

$$U^A_{\rm ind} = -\sum_{m\neq 0} \frac{\langle 00|H'|m_A 0\rangle\langle m_A 0|H'|00\rangle}{W^A_m - W^A_0} \tag{8.16}$$

$$U^B_{\rm ind} = -\sum_{n\neq 0} \frac{\langle 00|H'|0 n_B\rangle\langle 0 n_B|H'|00\rangle}{W^B_n - W^B_0} \tag{8.17}$$

$$U^{AB}_{\rm disp} = -\sum_{m,n\neq 0} \frac{\langle 00|H'|m_A n_B\rangle\langle m_A n_B|H'|00\rangle}{W^A_m + W^B_n - W^A_0 - W^B_0} \tag{8.18}$$

where H' is the Coulomb interaction between A and B and $H^A_0|m_A n_B\rangle = W^A_n|m_A n_B\rangle$, where H^A_0 is non-interacting Hamiltonian for species A (and similarly for B) [3]. The bra ($|m_A n_B\rangle$) and ket ($|m_A n_B\rangle$) states are formed from the direct-product of non-interaction basis states for A and B, $|m_A\rangle$ and $|n_B\rangle$.

If we consider only the dipole-dipole term in the multipole expansion of the inter-

acting Hamiltonian, H', Eqn. 8.18 becomes

$$U_{\rm disp}^{AB} = -\sum_{m,n\neq 0} \frac{\langle 0_A 0_B|\hat{\mu}_\alpha^A T_{\alpha\beta}\hat{\mu}_\beta^B|mn\rangle\langle mn|\hat{\mu}_\gamma^A T_{\gamma\delta}\hat{\mu}_\delta^B|0_A 0_B\rangle}{W_m^A + W_n^B - W_0^A - W_0^B} \tag{8.19}$$

$$= -T_{\alpha\beta}T_{\gamma\delta}\sum_{m,n\neq 0} \frac{\langle 0_A|\hat{\mu}_\alpha^A|m\rangle\langle m|\hat{\mu}_\gamma^A|0_A\rangle\langle 0_B|\hat{\mu}_\beta^B|n\rangle\langle n|\hat{\mu}_\delta^B|0_B\rangle}{W_m^A + W_n^B - W_0^A - W_0^B} \tag{8.20}$$

$$= -T_{\alpha\beta}T_{\gamma\delta}\sum_{m,n\neq 0} \frac{\omega_m^A\omega_n^B}{\omega_m^A+\omega_n^B}\frac{\langle 0_A|\hat{\mu}_\alpha^A|m\rangle\langle m|\hat{\mu}_\gamma^A|0_A\rangle}{\omega_m^A} \times \frac{\langle 0_B|\hat{\mu}_\beta^B|n\rangle\langle n|\hat{\mu}_\delta^B|0_B\rangle}{\omega_n^B} \tag{8.21}$$

where $m \equiv m_A$, $n \equiv n_B$, $\hat{\mu}_\xi^X$ is the ξ-component ($\xi = x, y, z$) of the dipole operator for species X and $\omega_i^X = W_i^X - W_0^X$ ($X = A, B$).

Eqn. 8.20 is trivially factorizable except for the denominator, $\omega_m^A + \omega_n^B$. However, the Casimir-Polder formula [21],

$$\frac{1}{x+y} = \frac{2}{\pi}\int_0^\infty \frac{xy}{(x^2+z^2)(y^2+z^2)}dz \ , \ (x, y > 0) \ , \tag{8.22}$$

provides a means to factorize the troublesome denominator. Upon application of the Casimir-Polder formula, Eqn. 8.20 becomes

$$= -\frac{2}{\pi}T_{\alpha\beta}T_{\gamma\delta}\int_0^\infty \sum_{m\neq 0} \frac{\omega_m^A\langle 0_A|\hat{\mu}_\alpha^A|m\rangle\langle m|\hat{\mu}_\gamma^A|0_A\rangle}{(\omega_m^A)^2+\nu^2} \times \sum_{n\neq 0} \frac{\omega_n^B\langle 0_B|\hat{\mu}_\beta^B|n\rangle\langle n|\hat{\mu}_\delta^B|0_B\rangle}{(\omega_n^B)^2+\nu^2}\, d\nu \ . \tag{8.23}$$

After identifying the sum-over-states representation of the dipole polarizability,

$$\alpha_{ij}(\nu) = \sum_{m \neq 0} \frac{\omega_n \langle 0|\hat{\mu}_i|n\rangle\langle n|\hat{\mu}_j|0\rangle + \langle 0|\hat{\mu}_j|n\rangle\langle n|\hat{\mu}_i|0\rangle}{\omega_n^2 - \nu^2} \,, \tag{8.24}$$

we have

$$U_{\text{disp}}^{AB} = -\frac{1}{2\pi} T_{\alpha\beta} T_{\gamma\delta} \int_0^\infty \alpha_{\alpha\gamma}^A(i\nu) \alpha_{\beta\delta}^B(i\nu) \, d\nu \,. \tag{8.25}$$

The C_6^{AB} coefficient is the spherically-averaged U_{disp}^{AB}.

8.3 Computational Details

The equations to compute imaginary-frequency response and dynamic polarizabilities were programmed in NWChem [22]. Eqns. 8.7 and 8.6 were implemented using the existing linear response code [1, 23, 25] with a number of modifications, which are described in detail in the next section. It is worth noting that all modifications were high-level; the code to compute the residual from matrix-vector products such as Ax, constant terms such as b or Eqns. 8.11 and 8.12 was already present. The computation of AAx was performed with $y = Ax$ and $r = Ay$, even though in parallel this is not optimal since it unnecessarily requires that the two-electron integrals be communication twice. A new implementation which eliminates this and other performance overhead is under development.

8.3.1 Solution of Response Equations

To solved the linear response equations for a pure-imaginary frequency, the existing DIIS solver was modified to account for the square of the Jacobian in Eqn. 8.7, that is, the preconditioner was $D(\omega_I)^{-2}$ rather than $D(0)^{-1}$, where $D(\omega)$ is a diagonal

matrix with matrix elements defined as $D_i^a(\omega) = (\omega + \epsilon_i - \epsilon_a)$ and $D_{ij}^{ab}(\omega) = (\omega + \epsilon_i + \epsilon_j - \epsilon_a - \epsilon_b)$. For Eqn. 8.6, no such modification was necessary, i.e. $D(0)^{-1}$ was an adequate preconditioner. Of course, if the alternative substitution was employed to decoupled the two sets of equations, the role of the modified preconditioner would apply to Eqn. 8.8 instead.

For both the real and imaginary component of the response equations, one can use the initial guess defined by first-order perturbation theory, although numerical results indicate that this is not necessary for most systems at the CCSD level of theory and improved initial guesses do not reduce the iteration count.

Table 8.1 reports the numerical performance of the solver. The imaginary component of the response equations is relatively easy to solve and its convergence rate does not change over a wide range of frequencies. On the other hand, the real component converges much faster for large values of ω. The reason for this is obvious since $(A^2 - \omega_I^2)$ becomes diagonal as $\omega \to \infty$. Although we do not present results here, the alternative decoupling scheme (Eqns. 8.5 and 8.8) leads to different convergence characteristics and thus an optimal implementation might employ *both* decoupling schemes, with the choice between the two determined by the frequency and bandgap of the system.

8.3.2 Numerical Integration

To obtain C_6 coefficients, the Casimir-Polder integral must be evaluated numerically. Two approaches have been employed for the results herein. First, the trapezoid rule was used to perform the integral using a larger number of grid points. The trapezoid

Table 8.1: Performance of numerical solvers for argon with the q-aug-cc-pVQZ basis set.

	Iterations	
Frequency	Real	Imaginary
CC-LR	20	-
0.0000000	43	0
0.0152284	26	17
1.2988506	19	15
5.8965517	11	15
27.5714286	7	15

rule leads to the following equation for the Casimir-Polder integral,

$$C_6 \approx \frac{3}{\pi} \sum_{i=1}^{N} \frac{f(x_{i+1})^2 + f(x_i)^2}{2 \cdot (x_{i+1} - x_i)}. \tag{8.26}$$

The second approach used was that of Figari and Magnasco [27, 28], in which the imaginary polarizability approximated by a finite set of functions,

$$\alpha(i\omega) \approx \sum_{j=1}^{M} \frac{a_j}{b_j + \omega^2} \tag{8.27}$$

for some number, M, which controls the accuracy of the fit. The Casimir-Polder integral can be evaluated analytically by virtue of the form of the fitting function. An 8-term approximation for imaginary polarizability was determined by least-squares using the Mathematica [29] function `FindFit`. The Casimir-Polder integral was performed analytically using Mathematica.

In the tables, results obtained via the Trapezoid rule are denoted (trap. N), where N is the number of grid points used. Results obtained via fitting and analytic integration are denoted (fit M), where M is the same as in Eqn. 8.27.

8.4 Results

The C_6 coefficients of nobel gas atoms have been considered previously by a number of authors [5, 6, 7]. In Table 8.2, results are given for helium, neon and argon for very large basis sets [26]. In all cases, the computed values are close the experimental ones, although the agreement is not perfect. The errors are most likely due to the omission of triply-excited amplitudes, except in the case of helium, which has only two electrons. For helium, it is not clear why a discrepancy between theory and experiment exists since the basis set should be nearly saturated. For neon and argon, numerical discrepancies exist between the two methods for computing the Casimir-Polder integral; the two values serve as an upper and lower bound for the experimental result.

Table 8.2: Static polarizabilities of the atom and Lennard-Jones coefficients of the dimer for nobel gas atoms with large basis sets. All electrons were correlated for helium, whereas the frozen-core approximation was employed for neon and argon. Pure spherical angular functions used.

		CCSD			DOSD		Experiment	
Atom	Basis	α	C_6 (trap. 100)	C_6 (fit 8)	α	C_6	α	C_6
He	t-aug-cc-pVQZ	1.385	1.447	1.447	1.379[a]	1.458[a]	1.38[b]	1.47[c]
	q-aug-cc-pVQZ	1.385	1.447	1.447				
	t-aug-cc-pV5Z	1.383	1.444	1.443				
	q-aug-cc-pV5Z	1.383	1.444	1.444				
Ne	t-aug-cc-pVQZ	2.680	6.593	6.296	2.669[a]	6.383[a]	2.70[b]	6.4[c]
	q-aug-cc-pVQZ	2.680	6.593	6.296				
	t-aug-cc-pV5Z	2.676	6.564	6.268				
	q-aug-cc-pV5Z	2.676	6.564	6.268				
Ar	q-aug-cc-pVQZ	11.13	65.12	62.16	11.08[a]	64.30[a]	11.07[b]	65[c]

[a] Ref. A. Kumar and W. J. Meath, *Mol. Phys.* **75**, 311 (1992).

[b] Ref. R.R. Teachout and R. T Pack, *At. Data* **3**, 195 (1971).

[c] Ref. A. Dalgarno and W.D. Davision, in *Advanced Atomic and Molecular Physics 2*, edited by D.R. Bates and I. Estermann (Academic, New York, 1966).

8.5 Conclusions

In this chapter, the theory and implementation necessary to compute imaginary-frequency polarizabilities was developed. First, two ways of decoupling the imaginary-frequency response equations were derived. Numerical tests were performed on the scheme that was implemented in NWChem. Unlike past efforts by other groups [30], the methods described here are numerically robust and have been applied to a variety of molecules (water, benzene, guanine and cytosine [31]).

Two numerical integration schemes for the Casimir-Polder integral were tested, but the results were not completely satisfactory. However, given the very fine frequency grid employed for results presented, numerical integration errors should be non-existant. More investigation is necessary to determine if Mathematica is not fitting the imaginary-frequency polarizability correctly or if the trapezoidal quadrature introduces systematic errors. For larger molecules where it is not feasible to compute more than a dozen frequency points, a highly robust numerical integration scheme must be developed.

REFERENCES

[1] J. R. Hammond, M. Valiev, W. A. de Jong and K. Kowalski, *J. Phys. Chem. A* **111**, 5492 (2007).

[2] J. E. Lennard-Jones, *Proc. Roy. Soc.* **A106**, 463 (1924).

[3] A. J. Stone, *The Theory of Intermolecular Forces, The International Series of Monographs on Chemistry* (Clarendon, Oxford, 1996).

[4] J. F. Stanton, *Phys. Rev. A* **49**, 1698 (1994).

[5] C. Hättig, O. Christiansen and P. Jørgensen, *J. Chem. Phys.* **107**, 10592 (1997)

[6] M. Jaszuński, A. Rizzo and P. Jørgensen, *Theor. Chem. Acc.* **106**, 251 (2001).

[7] A. Jiemchooroj, P. Norman and B. E. Sernelius, *J. Chem. Phys.* **123**, 124312 (2005).

[8] T. Korona, M. Przybytek and B. Jeziorski, *Mol. Phys.* **104**, 2303 (2006).

[9] T. Korona and B. Jeziorski, *J. Chem. Phys.* **128**, 144107 (2008).

[10] R. J. Wheatley, *J. Comp. Chem.* **29**, 445 (2008).

[11] J. Cizek, *Adv. Chem. Phys.* **14**, 35 (1969); J. Paldus, J. Cizek and I. Shavitt, *Phys. Rev. A* **5**, 50 (1972).

[12] R. J. Bartlett and M. Musiał, Rev. of Mod. Phys. **79**, 291 (2007).

[13] H. J. Monkhorst, *Int. J. Quantum Chem.* **S11**, 421 (1977).

[14] H. Koch and P. Jørgensen, *J. Chem. Phys.* **93**, 3333 (1990); O. Christiansen, P. Jørgensen and C. Hättig, *Int. J. Quantum Chem.* **68**, 1 (1998).

[15] M. Kállay and J. Gauss, *J. Mol. Struct. (THEOCHEM)* **768**, 71 (2006).

[16] F. London, *Z. Phys* **63**, 245 (1930).

[17] F. London, *Trans. Faraday Soc.* **3**, 8 (1937).

[18] H. Margenau, *Rev. Mod. Phys.* **11**, 1 (1939).

[19] H. C. Longuet-Higgins, *Proc. Roy. Soc. A* **235**, 537 (1956).

[20] A. D. Buckingham, *Adv. Chem. Phys.* **12**, 107 (1967).

[21] H. B. G. Casimir and D. Polder, *Phys. Rev.* **73**, 360 (1948).

[22] E. J. Bylaska, W. A. de Jong, N. Govind, K. Kowalski, T. P. Straatsma, M. Valiev, D. Wang, E. Apra, T. L. Windus, J. Hammond, J. Autschbach, P. Nichols, S. Hirata, M. T. Hackler, Y. Zhao, P.-D. Fan, R. J. Harrison, M. Dupuis, D. M. A. Smith, J. Nieplocha, V. Tipparaju, M. Krishnan, A. Vazquez-Mayagoitia, Q. Wu, T. Van Voorhis, A. A. Auer, M. Nooijen, L. D. Crosby, E. Brown, G. Cisneros, G. I. Fann, H. Fruchtl, J. Garza, K. Hirao, R. Kendall, J. A. Nichols, K. Tsemekhman, K. Wolinski, J. Anchell, D. Bernholdt, P. Borowski, T. Clark, D. Clerc, H. Dachsel, M. Deegan, K. Dyall, D. Elwood, E. Glendening, M. Gutowski, A. Hess, J. Jaffe, B. Johnson, J. Ju, R. Kobayashi, R. Kutteh, Z. Lin, R. Littlefield, X. Long, B. Meng, T. Nakajima, S. Niu, L. Pollack, M. Rosing, G. Sandrone, M. Stave, H. Taylor, G. Thomas, J. van Lenthe, A. Wong and

Z. Zhang. "NWChem, A Computational Chemistry Package for Parallel Computers, Version 5.1.1" (2009), Pacific Northwest National Laboratory, Richland, Washington 99352-0999, USA. A modified version.

[23] J. R. Hammond, K. Kowalski and W. A. de Jong, *J. Chem. Phys.* **127**, 144105 (2007).

[24] K. Kowalski, J. R. Hammond and W.A. de Jong, *J. Chem. Phys.* **127**, 164105 (2007)

[25] J. R. Hammond, W. A. de Jong and K. Kowalski, *J. Chem. Phys.* **128**, 224102 (2008).

[26] T. H. Dunning Jr., *J. Chem. Phys.* **90**, 1007 (1989); R. A. Kendall, T. H. Dunning Jr. and R. J. Harrison, *J. Chem. Phys.* **96**, 6796 (1992); D. E. Woon and T. H. Dunning Jr., *J. Chem. Phys.* **98**, 1358 (1993); D. E. Woon and T. H. Dunning Jr., *J. Chem. Phys.* **100**, 2975 (1994).

[27] G. Figari and V. Magnasco, *Chem. Phys. Lett.* **374**, 527 (2003).

[28] G. Figari and V. Magnasco, *Chem. Phys. Lett.* **452**, 206 (2008).

[29] Mathematica 6, Copyright 1988-2008 Wolfram Research, Inc.

[30] K. Kowalski, personal communication (recounting a conversation with A. Sadlej).

[31] J. R. Hammond, unpublished results.

CHAPTER 9

PARALLEL COMPUTATION OF COUPLED-CLUSTER HYPERPOLARIZABILITIES

This chapter will soon be published in the following article: J. R. Hammond and K. Kowalski, "Parallel computation of coupled-cluster hyperpolarizabilities," *J. Chem. Phys.* Copyright 2009 by the American Institute of Physics.

9.1 Introduction

The rational design of organic nonlinear optical materials is of fundamental interest to chemists due to their applications in telecommunications and other application areas [1]. In order for such rational design to be aided by computational tools, theoretical models which are capable of accurately predicting the measured properties must be available at reasonable computational cost. Numerous factors must be addressed in simulating nonlinear optical materials in their native environment; this paper seeks to address the two factors which rest exclusively within the scope of quantum chemistry: the treatment of electron correlation and the choice of atomic basis set. Other important factors which require careful consideration are the geometry — both the ground-state configuration and fluctuations about it, solvent and the presence of additional chromophores, finite temperature, and the character of the incident light which perturbs the molecule. Within the context of quantum chemistry, none of these factors can be addressed until a satisfactory level of approximation for

the gas-phase electric properties at the equilibrium geometry is available. For non-linear optical properties, finding an computationally tractable approximation which delivers even semi-quantitative results is a significant challenge. In spite of 30 years of progress in the area of *ab initio* molecular property calculations [2, 3, 4, 5, 6], successful application of these methods is far from routine, even for a molecule as simple as HF [7].

In this paper, we apply recently developed parallel quadratic response functionality at the coupled-cluster (CC) level of theory to four prototypical molecules which can be used to benchmark quantum chemical methods in their ability to compute the first hyperpolarizability of a molecule. For computational efficiency, only single and double excitations were included with CC (CCSD). The CCSD model is an excellent compromise in terms of computational cost (relatively speaking, of course) since it includes an iterative treatment of electron correlation which has previously been shown to be quite accurate for linear response electric properties of large molecules [8] but is tractable for molecules with over 1000 orbitals using supercomputers [9], whereas the limit for methods storing triple excitations [10] is around 200 orbitals, even when using a supercomputer [11]. In addition, only static hyperpolarizabilities have been computed to save time and because such data is extremely useful when comparing approximate computational methods since the development of response codes often lags well behind the code developed to calculate the ground-state energy, from which static properties can be calculated using the finite-field technique.

9.2 Theory and computational details

For the sake of general discussion, in this section we present only basic tenets of the CC response theory applied to the third-order electric properties (for more detailed discussion see Refs. [12, 13] and Refs. [14, 15, 16, 17, 18, 19]). The first hyperpolarizability is calculated using the quadratic response function,

$$\begin{aligned}\langle\langle A;B,C\rangle\rangle &= \hat{P}_{ABC}\big\{\langle\Phi|(1+\Lambda)\left[\left[\overline{A},T_B^{(1)}\right],T_C^{(1)}\right]|\Phi\rangle \\ &\quad+\langle\Phi|\Lambda_A^{(1)}\left[\left[\overline{H},T_B^{(1)}\right],T_C^{(1)}\right]|\Phi\rangle \\ &\quad+\langle\Phi|(1+\Lambda)\left[\left[\left[\overline{H},T_A^{(1)}\right],T_B^{(1)}\right],T_C^{(1)}\right]|\Phi\rangle \\ &\quad+\langle\Phi|\Lambda_C^{(1)}\left[\overline{A},T_B^{(1)}\right]|\Phi\rangle\big\}\,, \end{aligned} \tag{9.1}$$

where $\hat{P}$ enforces the appropriate permutation symmetry of the A, B and C components. Evaluating this quantity requires the evaluation of the cluster amplitudes T, the Λ amplitudes (Lagrange multipliers) of gradient theory and the first-order response of both T and Λ with respect to operators A, B and C.

When the dipole moment coincides with the j-axis, we have

$$\beta_{\parallel} = \frac{3}{5}\beta_j = \frac{1}{5}\sum_{i=x,y,z}\left(\beta_{iij}+\beta_{iji}+\beta_{jii}\right)\,, \tag{9.2}$$

or in the general case,

$$\beta_{\parallel} = \frac{3}{5|\mu|}\sum_{i,j=x,y,z}\beta_{iij}\mu_j\,, \tag{9.3}$$

where

$$\beta_{ijk} = \langle\langle\mu_i;\mu_j,\mu_k\rangle\rangle\,. \tag{9.4}$$

For $\omega = 0$, the zeroth-order cluster operator (T), the zeroth-order Lagrange multipliers ($\Lambda^{(0)}$), first-order cluster amplitudes ($T^{(1)}$), and first-order Lagrange multipliers ($\Lambda^{(1)}$) are obtained by solving

$$
\begin{aligned}
0 &= \langle \Phi^{a_1 \ldots a_n}_{i_1 \ldots i_n} | \overline{H} | \Phi \rangle && (9.5)\\
0 &= \langle \Phi | (1+\Lambda) \overline{H} | \Phi^{a_1 \ldots a_n}_{i_1 \ldots i_n} \rangle && (9.6)\\
0 &= \langle \Phi^{a_1 \ldots a_n}_{i_1 \ldots i_n} | [\overline{H}, T^{(1)}_{\gamma}] | \Phi \rangle + \langle \Phi^{a_1 \ldots a_n}_{i_1 \ldots i_n} | \overline{\mu}_{\gamma} | \Phi \rangle && (9.7)\\
0 &= \langle \Phi | \Lambda^{(1)}_{\gamma} \overline{H} | \Phi^{a_1 \ldots a_n}_{i_1 \ldots i_n} \rangle + \langle \Phi | (1+\Lambda) [\overline{H}, T^{(1)}_{\gamma}] | \Phi^{a_1 \ldots a_n}_{i_1 \ldots i_n} \rangle \\
&\qquad + \langle \Phi | (1+\Lambda) \overline{\mu}_{\gamma} | \Phi^{a_1 \ldots a_n}_{i_1 \ldots i_n} \rangle && (9.8)
\end{aligned}
$$

for the excitation manifold ($\Phi^{a_1 \ldots a_n}_{i_1 \ldots i_n}$) used to define the cluster and Λ operators and appropriate components of the dipole moment operator, μ_{γ}, where $\gamma = x, y, z$ in the nonsymmetric case. The generalization of the quadratic response equations to the dynamic case ($\omega \neq 0$) is trivial [19]. As always the similarity transformed Hamiltonian ($\overline{H}$) and dipole moment ($\overline{\mu_{\gamma}}$) operators are defined as follow:

$$
\begin{aligned}
\overline{H} &= \exp(-T) H \exp(T) && (9.9)\\
\overline{\mu_{\gamma}} &= \exp(-T) \mu_{\gamma} \exp(T) && (9.10)
\end{aligned}
$$

where $\gamma = x, y, x$. In CCSD, all cluster and Λ operators used to define zeroth and first order of response include singly and doubly excited components, i.e., $T = T_1 + T_2$, $\Lambda = \Lambda_1 + \Lambda_2$, $T^{(1)}_{\gamma} = T^{(1)}_{\gamma,1} + T^{(1)}_{\gamma,2}$, and $\Lambda^{(1)}_{\gamma} = \Lambda^{(1)}_{\gamma,1} + \Lambda^{(1)}_{\gamma,2}$.

The response equations of Eqn. 9.8 and the quadratic response function (Eqn. 9.1) were implemented as an undocumented feature in NWChem 5.1.1 [20]. Implementation details of the NWChem coupled-cluster response codes were first described in

Ref. [18], while computational issues are discussed in Ref. [8]. One important detail to note with regard to the quadratic response equations (Eq. 9.8) is that the b-vector in the linear equations to be solved contains the two-electron integrals, and is thus expensive to evaluate on the fly, unlike the b-vector corresponding to Eq. 9.7. Thus, the constant terms which comprise the b-vector,

$$\langle\Phi|(1+\Lambda)[\overline{H},T_\gamma^{(1)}]|\Phi_{i_1\ldots i_n}^{a_1\ldots a_n}\rangle + \langle\Phi|(1+\Lambda)\overline{\mu}_\gamma|\Phi_{i_1\ldots i_n}^{a_1\ldots a_n}\rangle \tag{9.11}$$

are formed only once and stored. In solving Eqn, 9.8 we adopted the DIIS solver used in the standard CC calculations with initial guess defined as $y_0^T = D^{-1}b$, where D is a diagonal matrix with matrix elements defined as $D_i^a = (\epsilon_i - \epsilon_a)$ and $D_{ij}^{ab} = (\epsilon_i + \epsilon_j - \epsilon_a - \epsilon_b)$. For PNA, 18 iterations were required to converge the first-order Λ-equations (Eqn. 9.8) for the z-axis to 10^{-7}, which is slightly fewer iterations than the 23 required for the first-order T-equations (Eqn. 9.7). For comparison, 26 and 13 iterations were required to converge the zeroth-order T- and Λ-equations.

Merging all three terms represented in Eqn. 9.8 into a single procedure in the code would eliminate the need for additional storage of the b-vector and minimize the wall time (at the expense of code reuse), but the motivation for this optimization is limited as long as the storage bottleneck remains the fully-transformed two-electron integrals. A code which used AO integrals on-the-fly in the computation of intermediates containing 3- and 4-virtual two-electron integrals would benefit significantly from such an optimization.

The results in this paper were obtained with a modified version of NWChem 5.1.1 [20] which has improved four-index transformation algorithms, allowing the properties of large systems to be calculated quickly and efficiently on parallel com-

puters. The largest coupled-cluster calculations were run on the Chinook supercomputer at PNNL. Each node has 16 GB of memory and two quad-core AMD Barcelona processors. For the CCSD/d-aug-cc-pVTZ calculation of PNA on 256 nodes, the T, Λ, $T^{(1)}$ and $\Lambda^{(1)}$ iterative procedures took approximately 140 s, 290 s, 180 s, and 290 s per iteration, respectively. The four-index transformation, done fully in-core using a spin-free N^5 algorithm, took approximately 7 h, employing four passes on the atomic integral generation to reduce memory usage of the half-transformed intermediate stored in global memory.

Dalton 2.0 [21], supplemented with the CAMB3LYP patch, was used to perform all non-CCSD calculations reported in this paper. The DFT calculations were run in serial workstations, or in the case of PNA, on 512 or $\sim$ 1000 [22] nodes of BlueGene/P, except for CAMB3LYP, which produces erroneous results for the hyperpolarizability when run in parallel.

9.3 Results

In this paper, four common functions — B3LYP [23], PBE [24], PBE0 [25] and CAMB3LYP [26] — are evaluated using CCSD response theory. We limit ourselves to these four functionals due to their ubiquitous use and because they collectively represent three types of functionals: GGA, GGA-hybrid and asymptotically-corrected (AC) GGA-hybrid.

Due to the importance of basis sets in electric property calculations, the basis sets developed by Dunning and coworkers [27], Pople and coworkers [30], Sadlej and coworkers [28, 29] and Roos and coworkers [31] were all considered. The Sadlej basis sets were designed explicitly for electric properties, while the Roos ANO basis sets

have a more general design principle which make them sufficiently flexible to handle such properties. The Dunning series is the most flexible as it contains a systematic way to increase both the ζ-level and the number of diffuse functions. The economical Pople basis sets are evaluated despite their known limitations for correlation energies as well as electric properties. Basis sets were obtained from the NWChem basis set library [20] or the Basis Set Exchange [32].

9.3.1 Water

The hyperpolarizability of water has been the subject of previous studies [33, 34, 4, 35, 36, 37, 39, 40, 38, 41, 42]. Christiansen, et al. [40] considered correlation effects beyond the CCSD level using response theory and compared to density-functional theory while Maroulis [41] used custom basis sets in conjunction with the CCSD(T) method and the finite-field technique (FF). Spelsberg and Meyer [38] performed multi-reference configuration-interaction (MRCI) calculations, which are in excellent agreement with our CCSD results for the static hyperpolarizability. In Table 9.1, we recount the results of Ref. [42] to demonstrate the relevance of our CCSD-LR results. The parallel hyperpolarizability changes dramatically from CCS to CC2 and again from CC2 to CCSD, but the difference between CCSD and CC3 is small. The large basis CCSD(T) result of Maroulis [41] is between CCSD and CC3, although the difference in basis set means the comparison is only semi-quantitative. All these results suggest that the effect of triples reduces the hyperpolarizability. Previous studies affirm the utility of CCSD as a reasonable approximation and an excellent compromise since one cannot approach the complete basis set limit for coupled-cluster methods including triples without significant computational resources, and then only for very small molecules. In addition, the importance of triples suggested by some

Table 9.1: Hyperpolarizabilities of H_2O within the hierarchy of coupled-cluster methods. See the references given for geometry information and other calculation details. All quantities are given in atomic units.

Method	Basis	$\beta_{\parallel}$	Reference
CCS	d-aug-cc-pVTZ	-14.03	[40]
CC2	d-aug-cc-pVTZ	-25.21	[40]
CCSD	d-aug-cc-pVTZ	-17.73	[40]
CC3	d-aug-cc-pVTZ	-17.05	[40]
CCSD(T)	Q1	-17.51	[41]

studies [17, 10] seems exaggerated by the use of small basis sets, as it has been found that the difference between CCSD and CCSDT — at least for polarizabilities — decreases as the basis set is saturated [11].

In Figure 9.1, the convergence in the zeta level of the three unique components of the hyperpolarizability tensor is demonstrated for the Dunning basis sets. The only results which deviate significantly from monotonicity are the triply- and quadruply-augmented cc-pVTZ points for β_{YYZ}. This is most likely due to the destabilization of the valence region by the inclusion of many diffuse functions, which leads to exaggerated polarization. With the exception of the singly augmented series, excellent results are achieved at the triple-zeta level, and owing to its monotonic convergence, the doubly augmented series is most reliable. Thus, we consider the d-aug-cc-pV5Z data to be the reference values for the remainder of this section.

Electric properties of water using based sets in the Pople, Sadlej and Roos families are compared to those of Dunning in Table 9.2. It is immediately clear that the results from the Pople basis sets are highly erroneous, in error for the dipole moment and dipole polarizability by at least 20% in every case, overestimating the former and underestimating the latter. The Pople sets do not accurately reproduce any of

Figure 9.1: Basis set convergence of the three unique tensor components composite and parallel static hyperpolarizability of H_2O.

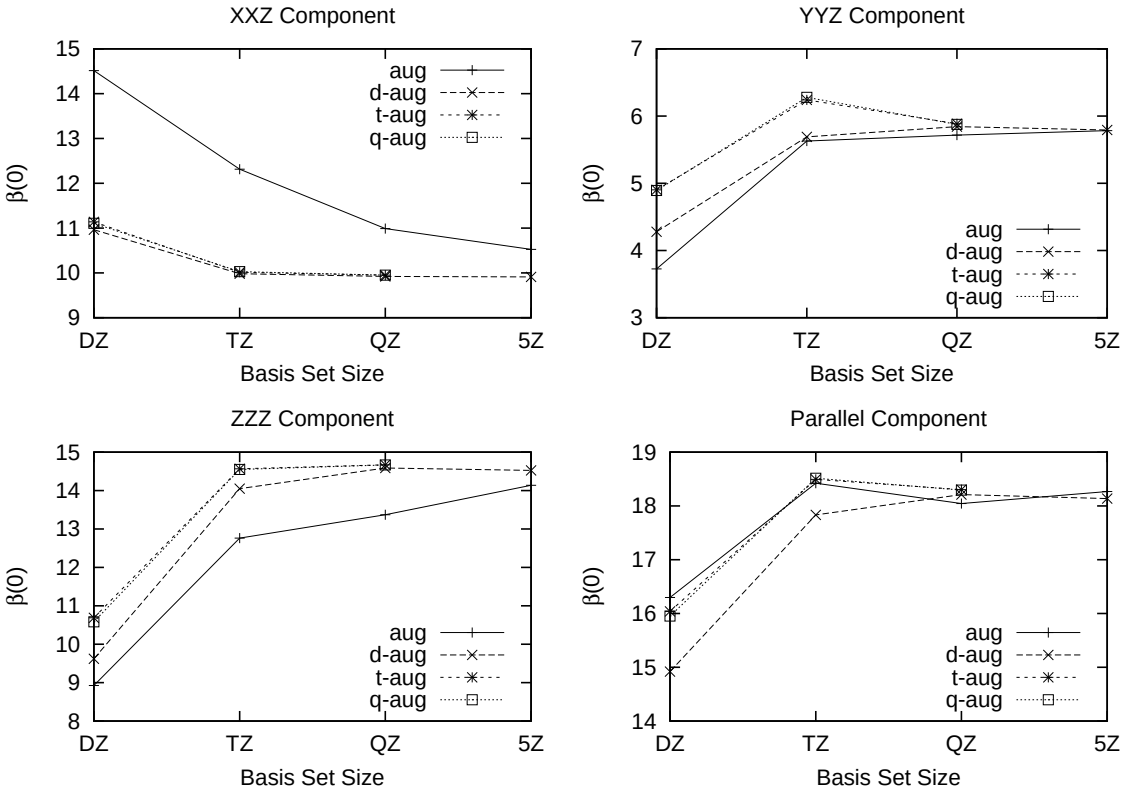

the components of the hyperpolarizability tensor except by coincidence (β_{xxz} with 6-31+G*) or by cancellation of error ($\beta_{||}$ with 6-311++G**).

The Sadlej basis sets, which are specifically designed to do well for electric properties, are more accurate than the Pople sets, but do not reproduce the asymptotic limit of the Dunning series for any of the components. Of the Sadlej bases, POL is best for the dipole moment and polarizability, but is bettered by HYPOL for the hyperpolarizability. The POL set is most comparable to the d-aug-cc-pVDZ set in the Dunning series, despite being approximately two-thirds of the size. The much larger HYPOL set is somewhat comparible to q-aug-cc-pVTZ but with half as many functions, but it underestimates the polarizability anisotropy and overshoots the hyperpolarizability. The very efficient Z2POL and Z3POL basis sets are much preferred to their size-comparible Pople counterparts by virtue of the formers' accuracy for polarizabilities, but their accuracy for the hyperpolarizability is not as impressive.

Finally, we consider the highly-contracted Roos ANO basis sets. If compare the accurate of the Roos DZ and TZ bases to their singly augmented Dunning counterparts of the same size, we see that they are superior for all aspects of the polarizability, but less accurate for the hyperpolarizability. This is natural given their construction and it is likely that if the Roos basis sets were equipped with augmented functions specifically for electric properties through the Dunning augmentation recipe or by using construction employed by Sadlej, that they would produce accurate hyperpolarizabilities as well. It is important to recognize that the high degree of contraction used in the Roos basis sets makes them unappealing for mean-field or MP2 calculations, where the cost of computing the integrals dominates the wall time, whereas for coupled-cluster calculations, they are quite suitable, provided a fully integral-direct approach is avoided.

Table 9.2: Electric properties of H_2O at the CCSD level using various basis sets (spherical, frozen core). All quantities are given in atomic units.

Basis	Rank	μ_z	α_{xx}	α_{yy}	α_{zz}	α_{iso}	α_{ani}	β_{xxz}	β_{yyz}	β_{zzz}	$\beta_{\parallel}$
6-31+G*	23	0.907	7.311	6.273	6.117	6.567	1.124	11.569	3.238	5.821	12.377
6-31++G**	31	0.870	7.790	6.423	6.455	6.889	1.351	16.205	2.750	8.524	16.488
6-311+G*	29	0.949	7.686	6.074	6.026	6.595	1.636	17.092	1.645	9.364	16.861
6-311++G**	37	0.843	8.067	6.691	6.621	7.126	1.413	16.608	2.689	10.421	17.831
POL	42	0.724	10.157	9.559	9.773	9.830	0.525	11.680	3.420	9.934	15.020
HYPOL	87	0.720	10.164	9.727	9.865	9.919	0.387	10.236	6.803	15.782	19.693
Z2POL	30	0.751	10.132	9.769	9.650	9.851	0.435	9.943	7.237	10.318	16.499
Z3POL	30	0.705	10.000	9.959	9.502	9.820	0.478	10.735	9.723	12.713	19.903
Roos ANO DZ	41	0.724	9.979	9.354	9.606	9.646	0.545	15.007	3.433	9.653	16.856
Roos ANO TZ	92	0.725	9.971	9.195	9.484	9.550	0.680	12.222	4.102	10.199	15.914
aug-cc-pVDZ	41	0.729	9.899	8.708	9.066	9.224	1.058	14.514	3.727	8.924	16.299
aug-cc-pVTZ	92	0.727	9.963	9.071	9.416	9.483	0.779	12.314	5.629	12.763	18.424
aug-cc-pVQZ	172	0.731	9.929	9.167	9.495	9.530	0.662	10.989	5.717	13.371	18.046
aug-cc-pV5Z	287	0.733	9.909	9.191	9.514	9.538	0.623	10.525	5.784	14.137	18.268
d-aug-cc-pVDZ	58	0.725	10.079	9.584	9.702	9.788	0.448	10.964	4.279	9.622	14.919
d-aug-cc-pVTZ	126	0.728	9.998	9.374	9.632	9.668	0.544	9.982	5.690	14.049	17.833
d-aug-cc-pVQZ	229	0.732	9.937	9.271	9.570	9.593	0.578	9.922	5.844	14.588	18.212
d-aug-cc-pV5Z	373	0.733	9.915	9.235	9.544	9.565	0.589	9.910	5.794	14.524	18.136
t-aug-cc-pVDZ	75	0.726	10.070	9.592	9.692	9.785	0.437	11.141	4.903	10.686	16.038
t-aug-cc-pVTZ	160	0.728	9.998	9.375	9.641	9.671	0.542	10.016	6.241	14.567	18.494
t-aug-cc-pVQZ	286	0.732	9.937	9.271	9.571	9.593	0.578	9.951	5.886	14.672	18.305
q-aug-cc-pVDZ	92	0.726	10.068	9.597	9.693	9.786	0.432	11.108	4.893	10.585	15.952
q-aug-cc-pVTZ	194	0.728	9.998	9.375	9.641	9.671	0.542	10.029	6.279	14.550	18.514
q-aug-cc-pVQZ	343	0.732	9.938	9.272	9.571	9.594	0.577	9.949	5.877	14.665	18.295

$R_{OH} = 0.9575$Å and $\theta_{HOH} = 104.48°$

9.3.2 Acetonitrile

The nonlinear optical properties of acetonitrile (CH_3CN) has been the subject of many studies [43, 44, 45, 46, 47, 48, 49]. Reis and coworkers [46] revealed the importance of vibrational and solvation effects as well as the effect of triples at the CCSD(T) level. Comparison with experiment found that CCSD/d-aug-cc-pVDZ overestimated the hyperpolarizability with respect to CCSD(T)/d-aug-cc-pVDZ and experiment. Our results demonstrate that larger basis sets move the CCSD results in the direction of experiment (Figure 9.2). Vibrational and solvents effects make up approximately one-third of the parallel hyperpolarizability, thus previous studies of these effects with modest basis sets are quite justified.

In Table 9.3 we report electric properties at the CCSD level for a number of different basis sets, including those in the Pople and Dunning families, as well as the Roos and Sadlej basis sets. The basis set dependence of the dipole moment is small, and the only value which lies outside of 1.54 ± 0.02 a.u. is for the Z3POL basis. Dipole polarizabilities with the Dunning's correlation consistent basis sets are all in the range 38.7 ± 0.2 a.u. and 23.9 ± 0.2, as is the Sadlej pVTZ basis, while the Z3POL and Pople basis sets deviate from this range. Only the α_{xx} component of the Z3POL basis is an outlier, while the Pople basis sets are different by no small amount in both components, which is consistent with previous studies [8]. For the hyperpolarizability components, the Pople basis sets are completely inadequate, if it can be taken for granted that the Dunning series saturates to the proper limit. The β_{xxx} component is off by approximately a factor of two for all four Pople basis sets, while both the Sadlej bases err by at least 25% with respect to the apparent asymptotic value of the Dunning series, ~ -34. The good agreement between the apparent limit of the Dunning series and the Roos ANO TZ basis for the significant

Figure 9.2: Basis set convergence of the three unique tensor components composite and parallel static hyperpolarizability of CH_3CN.

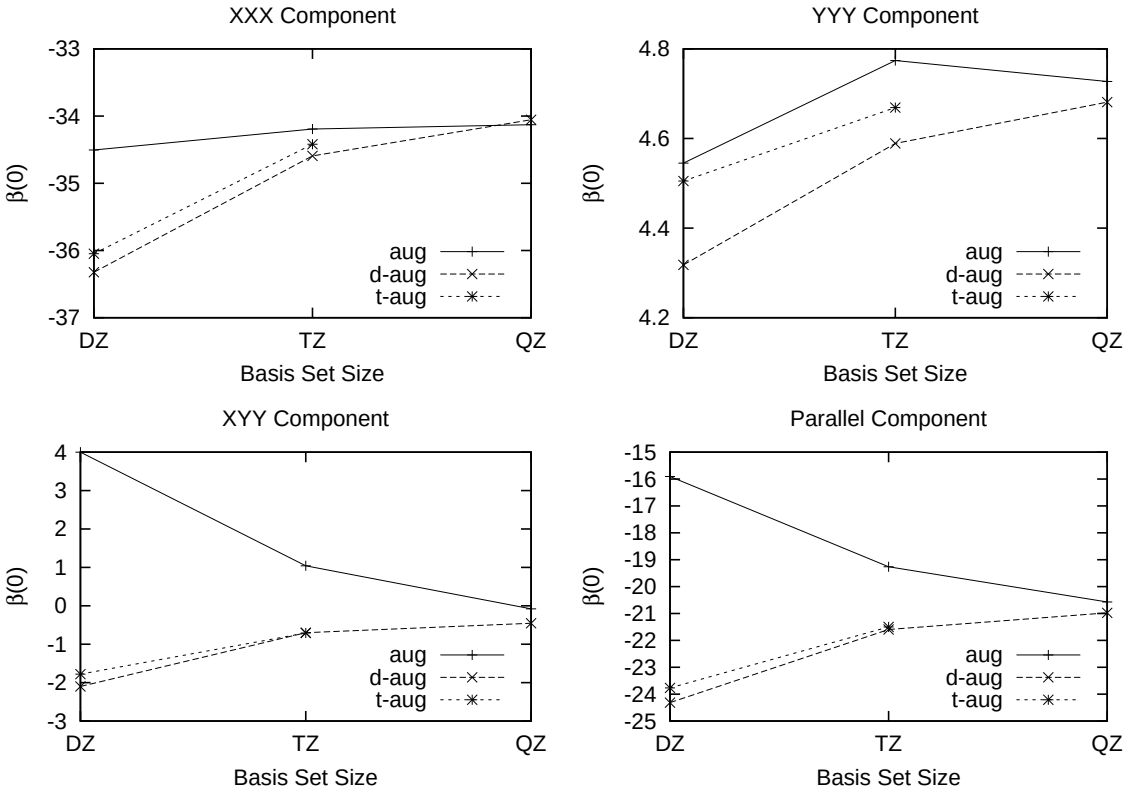

tensor components suggests this limit is correct and a useful standard for evaluating other basis sets. In contrast, the limit value of the Pople basis sets is clearly incorrect; although these basis sets were not designed to be extrapolated, the incorrect limit suggests that there are fundamental shortcomings of these basis sets for correlated calculations of hyperpolarizabilities. While the serious shortcomings of the Pople basis sets for third-order electric properties is not surprising, it is puzzling why the Sadlej pVTZ and Z3POL basis sets are significantly in error for the β_{xxx}, despite their design being specifically for electric properties. It is possible that inclusion of nonlinear response into the construction of these basis sets is necessary. Although not frequently used for nonlinear optical studies, the Roos ANO TZ basis set performs quite well in comparison to Dunning basis sets which contain many more functions. However, the general contraction scheme employed by the Roos basis sets can add significantly to the computational cost of the integral calculation, discouraging the use of such basis sets for integral-direct procedures, either during the SCF step, or in some implementations of CCSD. However, when a fast integral code is used and aggregate memory is sufficient to cache all the integrals, as is the case with NWChem for the present calculations, the additional cost of using such basis sets is not a concern.

The performance of common density-functionals and Hartree-Fock (HF) was evaluated for a variety of basis sets, although we report only the data for d-aug-cc-pVTZ (see Table 9.4). This basis was sufficient to sufficiently converge the electric properties for mean-field calculations. It was critical to use doubly-augmented basis sets but the results were less sensitive to cardinality, as d-aug-cc-pVDZ and d-aug-cc-pVTZ produced similar results in most cases. Of the four functionals considered, CAMB3LYP clearly performed the best (by comparison with CCSD) for the polarizability and hyperpolarizability, although the dipole moment was the worst of the four. The α_{xx}

Table 9.3: Comparison of basis sets for electric properties of CH_3CN at the CCSD level. Pure angular functions were used, as was the frozen core approximation. All quantities are given in atomic units. The x-axis is unique while the y- and z-axes are degenerate. The CCSD iterations did not converge with the t-aug-cc-pVQZ basis set.

Basis	Rank	μ_x	α_{xx}	α_{yy}	β_{xxx}	β_{xyy}	β_{yyy}	$\beta_{\|\|}$
6-31+G*	60	1.558	35.932	19.536	-74.027	6.909	8.776	-36.125
6-31++G**	72	1.534	36.206	20.060	-69.492	8.419	8.974	-31.592
6-311+G*	75	1.545	36.321	20.001	-70.766	8.854	8.875	-31.835
6-311++G**	87	1.518	36.719	20.447	-66.032	10.148	9.125	-27.441
Z3POL	72	1.613	36.347	23.486	-47.580	-1.911	4.152	-30.841
Sadlej pVTZ	99	1.531	38.885	23.993	-43.195	-4.697	5.266	-31.554
Roos ANO DZ	102	1.531	38.905	24.130	-38.369	0.017	4.278	-23.001
Roos ANO TZ	240	1.549	38.596	23.970	-34.336	-0.016	4.774	-20.621
aug-cc-pVDZ	96	1.534	38.772	23.728	-34.504	3.998	4.545	-15.905
aug-cc-pVTZ	207	1.550	38.674	23.955	-34.193	1.043	4.774	-19.264
aug-cc-pVQZ	378	1.556	38.590	23.939	-34.129	-0.080	4.727	-20.574
d-aug-cc-pVDZ	135	1.531	38.805	24.149	-36.323	-2.100	4.318	-24.315
d-aug-cc-pVTZ	282	1.549	38.673	24.032	-34.592	-0.700	4.589	-21.595
d-aug-cc-pVQZ	501	1.556	38.593	23.954	-34.054	-0.455	4.681	-20.978
t-aug-cc-pVDZ	174	1.532	38.810	24.158	-36.048	-1.780	4.505	-23.765
t-aug-cc-pVTZ	357	1.549	38.676	24.034	-34.418	-0.708	4.669	-21.500

component of the polarizability demonstrated a similar trend as for benzene [8], where the PBE functional, which does not include any exact exchange (EE), was the worst of the four, while B3LYP and PBE0, which contain 20% and 25% EE, respectively, performed similarly. The asymptotically corrected CAMB3LYP functional outperformed both of these, although the value of α_{xx} was $\sim$ 1.3 a.u. above the CCSD results with the same basis set. For the largest component of the hyperpolarizability, β_{xxx}, CAMB3LYP was quite close to CCSD, differing by $\sim$ 1.0 au, while the other DFT methods were in error by 17-24%. All four of the functionals were reasonable close for the two smaller components of the hyperpolarizability, β_{xyy} and β_{yyy}, particularly in comparison to the large variance in these components with respect to basis set. As $\beta_{\|}$ is dominated by β_{xxx}, CAMB3LYP is the most accurate for this quantity, and quite close to the CCSD result. The close agreement of PBE is spurious, caused by the large value of β_{xyy} and the small magnitude of the dipole moment relative to the other functionals.

Finally, considering the other wavefunction methods, one sees clearly that the hyperpolarizability component aligned along the molecular axis, β_{xxx} is extremely sensitive to the correlation treatment. The uncorrelated HF and CCS models recover $\sim$ 40% and $\sim$ 20% of the CCSD value, respectively, while the inclusion of doubles at second-order with the CC2 method reduces the difference with CCSD to $\sim$ 5%. These facts makes it even more impressive that CAMB3LYP delivers such excellent results, since KS-DFT is a mean-field treatment whose ability to capture two-body correlation should not be taken for granted.

Table 9.4: Comparison of CCSD and DFT electric properties of CH_3CN with the d-aug-cc-pVTZ basis set. The CCSD results are reported for a variety of basis sets (spherical, frozen core); DFT results are exclusively for the d-aug-cc-pVTZ basis set. All quantities are given in atomic units. The x-axis is unique while the y- and z-axes are degenerate. Due to the different orientations used in NWChem and Dalton, the sign of the dipole moment (μ_x) and one component of the hyperpolarizability tensor (β_{yyy}) for CCSD and the other methods have opposite sign, but this has no effect on $\beta_{\|}$.

Method	μ_x	α_{xx}	α_{yy}	β_{xxx}	β_{xyy}	β_{yyy}	$\beta_{\|}$
PBE	-1.572	41.848	25.089	-28.778	-2.319	-4.047	-20.051
PBE0	-1.600	40.260	24.349	-25.817	-0.365	-4.132	-15.927
B3LYP	-1.595	40.655	24.676	-28.748	-0.722	-5.348	-18.115
CAMB3LYP	-1.614	39.976	24.471	-33.612	-0.700	-5.197	-21.006
HF	-1.679	38.127	23.587	-14.151	2.580	-5.751	-5.395
CCS	-1.679	40.238	25.252	-7.033	3.994	-5.274	0.572
CC2	-1.522	39.529	24.503	-36.491	-1.234	-4.966	-23.376
CCSD	1.549	38.673	24.032	-34.592	-0.700	4.589	-21.595

9.3.3 Chloroform

Two previous studies of chloroform's electric properties include that of Dupuis and coworkers [50], who uses the TDHF method to study the dynamic hyperpolarizability, and that of Eichinger, et al. [48], who compared various DFT methods for the static hyperpolarizability. A related study by Sekino and Bartlett considered the hyperpolarizability of fluoromethane [3].

In Figure 9.3, the convergence of the hyperpolarizability components in the Dunning series is demonstrated. Table 9.5 report data for a larger number of basis sets. The convergence in the zeta and augmentation levels is similar in trend to acetonitrile, showing a significant change as the second set of augmented functions is added, although the changes are on a much larger scale. Convergence in the zeta-level is good for the doubly-augmented series, and there is good agreement between this limit and

the apparent limits of the singly- and triply-augmented series as well as the Roos TZ basis. As for acetonitrile, there are catastrophic errors in the hyperpolarizability obtained with any of the Pople basis sets; the sign of β_{xxx} is similar in magnitude but the opposite sign and the error in $\beta_{\|}$ is over an order of magnitude with respect to d-aug-cc-pVQZ. The Roos DZ and aug-cc-pVDZ bases are an order of magnitude too small for β_{xxx} and quite wrong for $\beta_{\|}$, which is a stark contrast to CH_3CN, where both of these basis sets do reasonably well. Conversely, the Sadlej basis sets POL (Sadlej pVTZ) and Z3POL are much better for $CHCl_3$ than they are for CH_3CN. These trends indicate that molecules which are of similar size but different chemical composition may have very different characters with respect to basis set convergence. In this case, the obvious difference is that chloroform is electron-rich and contains the third-row element chlorine, where as acetonitrile is relatively electron-deficient.

Table 9.6 reports electric properties for four common density functionals and CCSD with d-aug-cc-pVTZ. As for acetonitrile, the CAMB3LYP functional does the best of the four by comparison to CCSD, although the PBE0 and B3LYP functionals produce reasonably accurate results. While CAMB3LYP is worst at reproducing the dipole moment, dipole polarizabilities are nearly identical to CCSD. All the hyperpolarizability components are within $\sim 10\%$ of the CCSD results. As is seen in many molecules, the absence of Hartree-Fock exchange from a density functional results in the overestimation of hyperpolarizabilities by a significant amount, in this case $\sim 20\%$ for PBE.

Figure 9.3: Basis set convergence of the three unique tensor components composite and parallel static hyperpolarizability of $CHCl_3$.

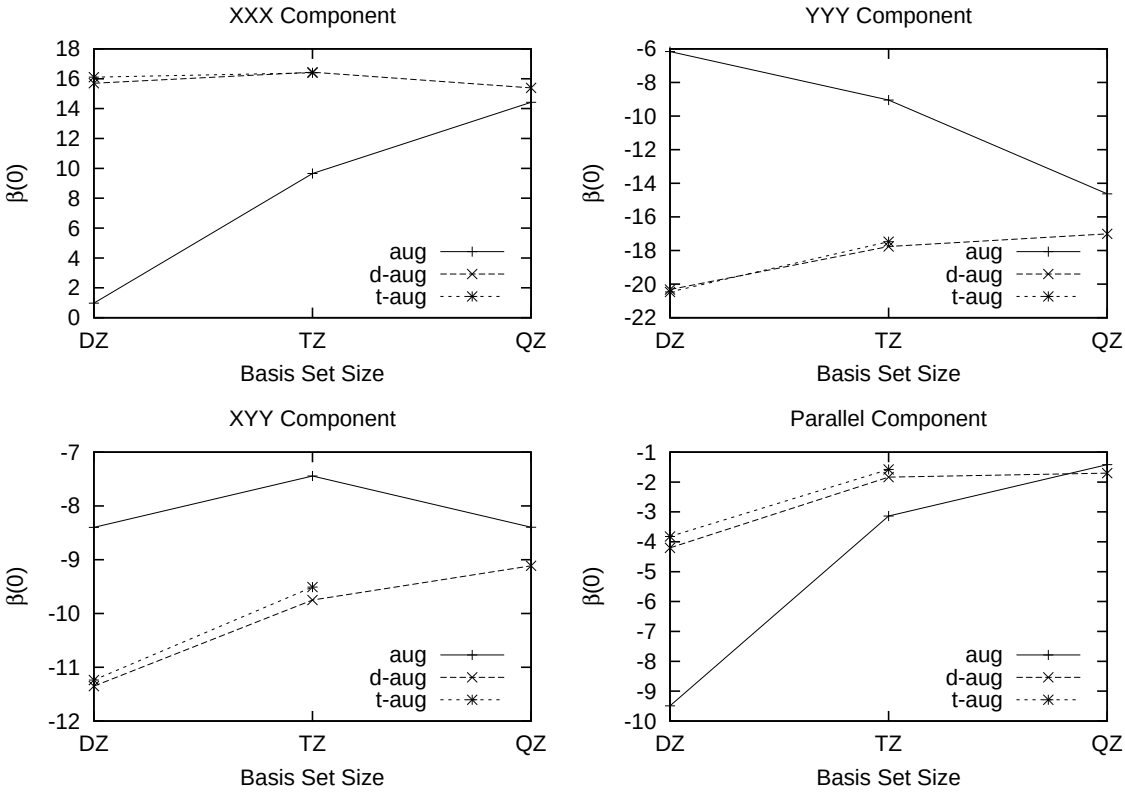

Table 9.5: Comparison basis sets for electric properties of $CHCl_3$ at the CCSD level. Pure angular functions were used, as was the frozen core approximation. All quantities are given in atomic units. The x-axis is unique while the y- and z-axes are degenerate. The CCSD iterations did not converge with the t-aug-cc-pVQZ basis set.

Basis	Rank	μ_x	α_{xx}	α_{yy}	β_{xxx}	β_{xyy}	β_{yyy}	$\beta_{\|\|}$
6-31+G*	86	-0.485	34.448	51.576	-11.568	-14.572	-24.595	-24.427
6-31++G**	90	-0.469	34.632	51.799	-10.351	-16.124	-25.323	-25.559
6-311++G**	123	-0.446	34.849	52.389	-7.596	-15.104	-22.957	-22.682
Z3POL	90	-0.586	39.848	54.435	16.057	-9.999	-19.201	-2.365
Sadlej pVTZ	129	-0.418	45.310	62.681	14.430	-9.936	-19.357	-3.266
Roos ANO DZ	121	-0.410	43.525	61.171	1.722	-12.159	-12.357	-13.557
Roos ANO TZ	257	-0.414	44.902	62.576	14.558	-8.144	-12.284	-1.038
aug-cc-pVDZ	113	-0.417	43.178	60.906	0.978	-8.398	-6.159	-9.491
aug-cc-pVTZ	219	-0.417	44.677	62.263	9.655	-7.444	-9.046	-3.139
aug-cc-pVQZ	378	-0.422	44.840	62.412	14.426	-8.396	-14.631	-1.420
d-aug-cc-pVDZ	153	-0.416	45.153	62.631	15.694	-11.351	-20.326	-4.205
d-aug-cc-pVTZ	292	-0.417	45.125	62.687	16.440	-9.749	-17.763	-1.835
d-aug-cc-pVQZ	494	-0.423	44.899	62.481	15.391	-9.113	-17.007	-1.701
t-aug-cc-pVDZ	193	-0.416	45.193	62.686	16.103	-11.237	-20.467	-3.823
t-aug-cc-pVTZ	365	-0.417	45.127	62.691	16.389	-9.510	-17.477	-1.578

Table 9.6: Comparison of CCSD and DFT electric properties of $CHCl_3$ with the d-aug-cc-pVTZ basis set. All quantities are given in atomic units. The x-axis is unique while the y- and z-axes are degenerate. Due to the different orientations used in NWChem and Dalton, the sign of the dipole moment (μ_x) and one component of the hyperpolarizability tensor (β_{yyy}) for CCSD and the other methods have opposite sign, but this has no effect on $\beta_{\|}$.

Method	μ_x	α_{xx}	α_{yy}	β_{xxx}	β_{xyy}	β_{yyy}	$\beta_{\|}$
B3LYP	0.423	45.710	64.140	20.406	-12.646	21.924	-2.940
CAMB3LYP	0.435	45.057	62.657	18.699	-10.788	19.530	-1.729
PBE0	0.427	44.896	63.028	17.023	-11.210	21.096	-3.233
PBE	0.407	46.629	65.972	22.137	-14.611	27.392	-4.246
HF	0.474	42.837	59.451	13.934	-7.201	13.336	-0.281
CCS	0.474	46.346	63.550	13.373	-8.787	21.061	-2.521
CC2	0.400	46.235	65.441	16.145	-11.473	23.913	-4.081
CCSD	-0.417	45.125	62.687	16.440	-9.749	-17.763	-1.835

9.3.4 para-Nitroaniline

Para-nitroaniline (PNA) is the simplest prototype push-pull chromophore with an aromatic bridge. Previous studies include Refs. [51, 52, 53, 54, 55, 56, 57, 59, 58, 60, 61, 62, 63, 64, 65, 66, 67], which cover a diverse range of topics, including vibrational hyperpolarizabilities, solvent effects, and correlation at lower levels of theory. The only previous study of PNA with CCSD used fairly limited basis sets [42]. In this paper, the hyperpolarizability of PNA has been computed using a variety of large basis sets, including as many as 812 functions; in addition, we compare results for C_{2v} and C_s structures optimized at the B3LYP/cc-pVTZ level. Finally, the utility of four DFT functionals is evaluated using both DZ and TZ basis sets.

Table 9.7: Electric properties of para-nitroaniline at the CCSD level using various basis sets (spherical, frozen core). All quantities are given in atomic units.

Basis	Rank	μ_z	α_{xx}	α_{yy}	α_{zz}	β_{xxz}	β_{yyz}	β_{zzz}	$\beta_{\parallel}$
3-21G*	102	-2.600	18.887	83.660	116.216	-1.593	-71.573	1403.802	798.382
6-31+G*	192	-2.829	50.104	99.215	143.060	-59.613	-114.407	2019.046	1107.016
6-31++G**	216	-2.781	50.429	99.826	143.026	-59.491	-114.041	1974.437	1080.543
6-311+G*	238	-2.840	50.123	99.752	143.452	-63.887	-113.421	1954.214	1066.144
6-311++G**	262	-2.765	50.640	100.515	143.256	-61.702	-112.574	1891.733	1030.474
Z3POL	216	-2.808	54.493	101.656	148.228	-45.327	-94.947	2096.000	1173.435
Sadlej pVTZ	294	-2.711	56.811	105.130	153.008	-58.860	-113.099	1789.563	970.563
Roos ANO DZ	304	-2.725	55.915	104.576	152.121	-57.855	-115.510	1800.087	976.033
aug-cc-pVDZ	284	-2.722	56.303	104.526	152.291	-62.331	-113.264	1822.869	988.364
aug-cc-pVTZ	598	-2.735	55.960	104.519	152.271	-54.466	-117.686	1759.313	952.297
d-aug-cc-pVDZ	398	-2.717	56.907	105.109	153.209	-58.935	-113.991	1782.792	965.920
d-aug-cc-pVTZ	812	-2.734	56.088	104.642	152.424	-52.374	-116.870	1745.828	945.950
t-aug-cc-pVDZ	512	-2.717	56.930	105.138	153.215	-57.946	-114.419	1782.760	966.237

The electric properties of PNA are far less demanding with respect to basis set than smaller molecules, which is consistent with investigations of other large molecular systems, such as aromatic hydrocarbons [8] and water clusters [68]. One can see in Table 9.7 that dipole moment, polarizability and parallel hyperpolarizability are quite similar for all the Dunning basis sets, the Roos ANO DZ basis, and the Sadlej pVTZ (POL) basis set. Data from the Pople sets and Z3POL deviate more so from the d-aug-cc-pVTZ basis, the best quality basis considered. The addition of the second set of diffuse functions makes a small difference for both the DZ and TZ cases and the increase from DZ to TZ at the same augmentation level is larger than either of these changes. It is tenuous to do a formal extrapolation using the Dunning series without a QZ result, but given the trends seen, it appears that the d-aug-cc-pVTZ result provides a reasonably converged $\beta_{\|}$, and given the trends, is most likely an upper bound on the CCSD/CBS result.

The comparison of CCSD to other methods (Table 9.8) is far more interesting. None of the four functionals considered reproduces the CCSD dipole moment to within 5% with the aug-cc-pVTZ basis. The longitudinal polarizabilities (α_{zz}), previously found to be challenging in aromatic molecules [8], are grossly in error for PBE, which contains no HF exchange. The conventional hybrid functionals PBE0 and B3LYP do somewhat better, while CAMB3LYP overcompensates is actually below the CCSD result and is the best of the DFT methods considered. The other polarizability components are less demanding on the functionals and all four are reasonably close to the CCSD results, with PBE closest of the four. All three unique components of the hyperpolarizability tensor appear challenging for DFT, although for practical purposes, the β_{zzz} is much more significant given its magnitude. B3LYP is remarkably close to CCSD for $\beta_{\|}$, due to a near perfect cancellation of error in the three components; it

is also the most accurate of the three conventional functions (GGA or GGA-hybrid). Both PBE and PBE0 are significantly in error for β_{zzz}, but in the opposite direction, and both overestimate β_{yyz} by 20 au. CAMB3LYP underestimates the β_{zzz} by over 200 au, which is the reason that its $\beta_{\|}$ result is the worst of the four functionals. However, none of the DFT methods is as erroneous as HF, CCS or CC2, which err by approximately 300 a.u. for $\beta_{\|}$, with HF and CCS underestimating and CC2 overestimating this value.

The poor performance of CAMB3LYP and the more approximate wavefunction methods (HF, CCS, CC2) is particularly discouraging with respect to modeling larger compounds. Because of the catastrophic errors in DFT for fourth-order electric properties (γ), one is tempted to use HF, which is supposedly qualitatively correct. While HF, CCS and CC2 do not fail for the same reasons that DFT does, errors on the order of 50% are unacceptable if one is to make any comparison to experiment. CAMB3LYP, which partially corrects for the long-range errors in DFT, does not perform as well as the traditional functional upon which it was built (B3LYP), although the former should be more physical with respect to the problems related to electric-field perturbations. It is possible that reparametrizing the asymptotic correction of CAMB3LYP is necessary for larger molecules than the original set used to determine CAMB3LYP's μ, α and β, although related work on this subject pertaining to excited states [69, 70] suggests that reparameterization asymptotically-corrected functionals is not a panacea.

Table 9.8: Comparison of CCSD to other methods for the electric properties of para-nitroaniline with the aug-cc-pVTZ basis set. All quantities are given in atomic units. Due to the different orientations used in NWChem and Dalton, the sign of the dipole moment (μ_x) for CCSD and the other methods have opposite sign; the other properties are not affected. The CCS and CC2 methods were computational intractible with the aug-cc-pVTZ basis.

Basis	μ_z	α_{xx}	α_{yy}	α_{zz}	β_{xxz}	β_{yyz}	β_{zzz}	$\beta_{\parallel}$
aug-cc-pVDZ								
B3LYP	3.098	54.952	102.776	162.876	-64.367	-143.336	1791.496	950.275
CAMB3LYP	2.956	54.476	101.946	154.877	-54.763	-141.278	1606.610	846.341
PBE0	3.085	54.436	101.683	160.051	-54.812	-136.923	1698.357	903.973
PBE	3.025	55.731	104.136	171.203	-67.956	-127.796	1827.082	978.798
HF	3.258	53.726	99.731	141.314	-39.723	-230.316	1206.600	561.936
CCS	3.062	58.052	106.476	146.952	-42.844	-232.313	1233.219	574.838
CC2	2.685	57.384	109.750	168.165	-69.124	-121.020	2324.075	1280.359
CCSD	-2.722	56.303	104.526	152.291	-62.331	-113.264	1822.869	988.364
aug-cc-pVTZ								
B3LYP	2.943	55.296	102.576	159.322	-63.263	-144.326	1796.667	953.447
CAMB3LYP	2.885	54.833	101.633	150.522	-53.453	-138.388	1535.478	806.182
PBE0	2.913	54.554	101.560	155.742	-51.885	-136.830	1681.322	895.564
PBE	2.938	55.955	104.077	168.621	-65.514	-134.214	1910.501	1026.464
HF	2.993	53.946	99.021	133.699	-35.940	-193.975	937.402	424.492
CCSD	-2.735	55.960	104.519	152.271	-54.466	-117.686	1759.313	952.297

Table 9.9: Geometry effects on PNA at the CCSD/aug-cc-pVDZ level.

Basis	$\|\mu\|$	α_{iso}	α_{ani}	$\|\|\beta\|\|_\infty$	$\|\beta_\parallel\|$
C_s [a]	2.57	103.4	80.7	1659.6	891.7
C_{2v} [a]	2.72	104.4	83.1	1822.9	988.4
C_{2v} [b] (Ref. [42])	-	-	-	1919.1	1041.7

[a] B3LYP/cc-pVTZ optimized geometry.
[b] Based upon crystallographic data; see Ref. [42] for details.

It is worth noting the importance of geometry for computed electronic hyperpolarizabilities. The variation in CCSD/aug-cc-pVDZ results with the C_s and C_{2v} optimized geometries is of similar magnitude to the differences between CCSD and the DFT methods. The parallel hyperpolarizability using from Ref [42] using a different C_{2v} geometry also differs from our result by approximately 50 au.

9.4 Conclusions

In this paper, the role of basis set and correlation treatment in computing the electric properties has been explored using a variety of molecules. The wide variety of basis sets considered provides new insight into how best to compromise between computational efficiency and accuracy. For small molecules, the important of very large basis sets is reaffirmed using H_2O. Fortunately, for large molecules, such huge basis sets are not required, provided the one used is properly designed. For medium-sized molecules such as CH_3CN and $CHCl_3$, the d-aug-cc-pVTZ provides very accurate results and is small enough to work with correlated methods as complete as CC3. For the prototypical push-pull chromophore, PNA, the modest Sadlej pVTZ (POL) basis set delivers results close to much larger Dunning basis sets which are computationally intractable at the CCSD level except when using very large computational resources.

As PNA most closely resembles the larger extended systems which are obvious targets for nonlinear optical studies, it is encouraging that a modest basis set is capable of deliver excellent results.

The results also clearly show that basis sets from the Pople family, used ubiquitously by quantum chemists for all kinds of simulation, are incapable of delivering accurate results for optical properties, especially the hyperpolarizability, as clearly demonstrated for CH_3CN and $CHCl_3$. Except for water, the similarly-sized Z3POL basis set is not satisfactory, and is the least accurate of all for PNA. As no basis set smaller than d-aug-cc-pVTZ delivers reliable results for all four cases, it is clear that any quantitative study of nonlinear optical properties must begin with a basis set calibration focusing on the Dunning series, but potentially also including Sadlej and Roos basis sets since their slightly different designs may reveal artifacts in the small Dunning basis sets.

With respect to the treatment of electron correlation, CAMB3LYP is generally superior to conventional GGA and GGA-hybrid functionals and inclusion of HF exchange is important to compute accurate polarizability with DFT. Both of these conclusions are consistent with previous studies. However, as was noted for PNA, CAMB3LYP is not universally more accurate than other DFT methods. Thus, on the basis of the results presented here, the prospect for predictive quantum chemical studies of nonlinear optical materials is rather bleak, as the highly-reliable CCSD method is too expensive for common use and DFT does not appear capable of delivering quantative accuracy even with respect to the loose tolerances of nonlinear optical experimental data. Finally, the contribution of solvent, geometry and vibration which were, for the most part, not considered in this study, are on the order of, or significantly greater than the variations due to basis set and correlation treatment.

Hence, a holistic treatment of nonlinear optical properties of molecules is far from realizable.

REFERENCES

[1] L. R. Dalton, *J. Phys.: Cond. Matt* **15**, R897 (2003).

[2] D. P. Santry and T. E. Raidy, *Theo. Chem. Acc.* **53**, 121 (1979); P. A. Christiansen and E. A. McCullough Jr., *Chem. Phys. Lett.* **63**, 3, 570 (1979); R. S. Watts and A. T. Stelbovic, *Chem. Phys. Lett.* **61**, 351 (1979); D. P. Santry and T. E. Raidy, *Chem. Phys. Lett.* **61**, 473 (1979); R. J. Bartlett and G. D. Purvis III, *Phys. Rev. A* **20**, 1313 (1979).

[3] H. Sekino and R. J. Bartlett, *J. Chem. Phys.* **85**, 976 (1986).

[4] W. A. Parkinson and J. Oddershede, *J. Chem. Phys.* **94**, 7251 (1991).

[5] J. E. Rice and N. C. Handy, *Int. J. Quantum Chem.* **43**, 91 (1992);

[6] H. Sekino and R. J. Bartlett, *J. Chem. Phys.* **98**, 3022 (1993) and references therein.

[7] See P. Rozyczko and R. J. Bartlett, *J. Chem. Phys.* **107**, 10823 (1997) and references therein.

[8] J. R. Hammond, K. Kowalski and W. A. de Jong *J. Chem. Phys.* , **127**, 144105 (2007).

[9] K. Kowalski, J. R. Hammond, W. A. de Jong and A. J. Sadlej, *J. Chem. Phys.* **129**, 226101 (2008).

[10] H. Larsen, J. Olsen, C. Hättig, P. Jørgensen, O. Christiansen and J. Gauss, *J. Chem. Phys.* **111** 1917 (1999).

[11] J. R. Hammond, W. A. de Jong and K. Kowalski, *J. Chem. Phys.* **128**, 224102 (2008).

[12] J. Cizek, Advan. Chem. Phys. **14**, 35 (1969); J. Paldus, J. Cizek and I. Shavitt, *Phys. Rev. A* **5**, 50 (1972).

[13] R. J. Bartlett and M. Musiał, *Rev. of Mod. Phys.* **79**, 291 (2007).

[14] H. J. Monkhorst, *Int. J. Quantum Chem.* **S11**, 421 (1977).

[15] H. Koch and P. Jørgensen, *J. Chem. Phys.* **93**, 3333 (1990); O. Christiansen, P. Jørgensen and C. Hättig, *Int. J. Quantum Chem.* **68**, 1 (1998).

[16] J. Gauss, O. Christiansen and J. F. Stanton, *Chem. Phys. Lett.* **296**, 117 (1998).

[17] M. Kállay and J. Gauss, *J. Mol. Struct. (THEOCHEM)* **768**, 71 (2006).

[18] J. R. Hammond, M. Valiev, W. A. de Jong and K. Kowalski, *J. Phys. Chem. A*, **111**, 5492 (2007).

[19] D. P. O'Neill, M. Kállay and J. Gauss, *J. Chem. Phys.* **127**, 134109 (2007).

[20] E. J. Bylaska, W. A. de Jong, N. Govind, K. Kowalski, T. P. Straatsma, M. Valiev, D. Wang, E. Apra, T. L. Windus, J. Hammond, J. Autschbach, P. Nichols, S. Hirata, M. T. Hackler, Y. Zhao, P.-D. Fan, R. J. Harrison, M. Dupuis, D. M. A. Smith, J. Nieplocha, V. Tipparaju, M. Krishnan, A. Vazquez-Mayagoitia, Q. Wu, T. Van Voorhis, A. A. Auer, M. Nooijen, L. D. Crosby, E. Brown, G. Cisneros, G. I. Fann, H. Fruchtl, J. Garza, K. Hirao, R. Kendall, J. A. Nichols, K.

Tsemekhman, K. Wolinski, J. Anchell, D. Bernholdt, P. Borowski, T. Clark, D. Clerc, H. Dachsel, M. Deegan, K. Dyall, D. Elwood, E. Glendening, M. Gutowski, A. Hess, J. Jaffe, B. Johnson, J. Ju, R. Kobayashi, R. Kutteh, Z. Lin, R. Littlefield, X. Long, B. Meng, T. Nakajima, S. Niu, L. Pollack, M. Rosing, G. Sandrone, M. Stave, H. Taylor, G. Thomas, J. van Lenthe, A. Wong and Z. Zhang. "NWChem, A Computational Chemistry Package for Parallel Computers, Version 5.1.1" (2009), Pacific Northwest National Laboratory, Richland, Washington 99352-0999, USA. A modified version.

[21] *DALTON, a molecular electronic structure program, Release 2.0* (2005), see `http://www.kjemi.uio.no/software/dalton/dalton.html`.

[22] Only 999 of the 1024 nodes in the requested partition could be used due to a limitation in the file naming conventions.

[23] A. D. Becke, Phys. Rev. A 88, 3098 (1988); C. Lee, W. Yang and R. G. Parr, Phys. Rev. B **37**, 785 (1988); A. D. Becke, *J. Chem. Phys.* **98**, 5648 (1993).

[24] J. P. Perdew, K. Burke and M. Ernzerhof, *Phys. Rev. Lett.* **77**, 3865 (1996); **78**, 1396 (1997).

[25] C. Adamo and V. Barone, *J. Chem. Phys.* **110**, 6158 (1998).

[26] T. Yanai, D. P. Tew and N. C. Handy, *Chem. Phys. Lett.* **393**, 51 (2004).

[27] T. H. Dunning Jr., *J. Chem. Phys.* **90**, 1007 (1989); R. A. Kendall, T. H. Dunning Jr. and R. J. Harrison, *J. Chem. Phys.* **96**, 6796 (1992); D. E. Woon and T. H. Dunning Jr., *J. Chem. Phys.* **98**, 1358 (1993); D. E. Woon and T. H. Dunning Jr., *J. Chem. Phys.* **100**, 2975 (1994).

[28] A. J. Sadlej, *Coll. Czech. Chem. Comm.* **53**, 1995 (1988); A. J. Sadlej and M. Urban, *J. Mol. Struct. (THEOCHEM)* **234**, 147 (1991); A. J. Sadlej, *Theor. Chim. Acta* **79**, 123 (1992); A. J. Sadlej, *Theor. Chim. Acta* **81**, 45 (1992); A. J. Sadlej, *Theor. Chim. Acta* **81**, 339 (1992).

[29] Z. Benkova,A. J. Sadlej, R. E. Oakes and S. E. Bell, *J. Comp. Chem.* **26**, 145 (2005).

[30] P. C. Hariharan and J. A. Pople, *Theor. Chimica Acta* **28**, 213 (1973); R. Krishnan, J.S. Binkley, R. Seeger and J.A. Pople, *J. Chem. Phys.* **72**, 650 (1980); M. M. Francl, W. J. Petro, W. J. Hehre, J. S. Binkley, M. S. Gordon, D. J. DeFrees and J. A. Pople, *J. Chem. Phys.* **77**, 3654 (1982); T. Clark, J. Chandrasekhar and P. v. R. Schleyer, *J. Comp. Chem.* **4**, 294 (1983); P. M. W. Gill, B. G. Johnson, J. A. Pople and M. J. Frisch, *Chem. Phys. Lett.* **197**, 499 (1992).

[31] P. O. Widmark, P. A. Malmqvist, B. Roos, *Theor. Chim. Acta.* **77**, 291 (1990); P. O. Widmark, B. J. Persson and B. Roos *Theor. Chim. Acta.* **79**, 419 (1991); R. Pou-Amerigo, M. Merchan, I. Nebot-Gil, P. O. Widmark and B. Roos, *Theor. Chim. Acta.* **92**, 149 (1995).

[32] D. Feller, J. Comp. Chem. **17**, 1571 (1996); K. L. Schuchardt, B. T. Didier, T. Elsethagen, L. Sun, V. Gurumoorthi, J. Chase, J. Li and T.L. Windus, *J. Chem. Inf. Model.* **47**, 1045 (2007).

[33] G. D. Purvis III and R. J. Bartlett, *Phys. Rev. A* **23**, 1594 (1981).

[34] G. Maroulis, *J. Chem. Phys.* **94**, 1182 (1991).

[35] D. M. Bishop, B. Kirtman, H. A. Kurtz and J. E. Rice, *J. Chem. Phys.* **98**, 8024 (1993).

[36] Y. Luo, H. Ågren, O. Vahtras, P. Jørgensen, V. Spirko and H. Hettema, *J. Chem. Phys.* **98**, 7159 (1993).

[37] T. Pluta, J. Noga and R. J. Bartlett, *Int. J. Quantum Chem. Symp.* **S28**, 379 (1994).

[38] D. Spelsberg and W. Meyer, *J. Chem. Phys.* **108**, 1532 (1998).

[39] T. Kobayashi, K. Sasagane and F. Aiga, *J. Chem. Phys.* **110**, 11720 (1999).

[40] O. Christiansen, J. Gauss and J. F. Stanton, *Chem. Phys. Lett.* **305**, 147 (1999). We use the data reported in Ref. [42] for the reasons given in Ref. 18 of that paper.

[41] G. Maroulis, *J. Chem. Phys.* **113**, 1813 (2000).

[42] P. Sałek, T. Helgaker, O. Vahtras, H. Ågren, D. Jonssen and J. Gauss, *Mol. Phys.*, **103**, 439 (2005).

[43] M. Stahelin, C. R. Moylan, D. M. Burland, A. Willetts, J. E. Rice, D. P. Shelton and E. A. Donley, *J. Chem. Phys.* **98**, 5595 (1993); A. Willetts and J. E. Rice, **99**, 426 (1993)

[44] R. Cammi, M. Cossi, B. Mennucci and J. Tomasi, *J. Mol. Struct.* **436**, 567 (1997).

[45] P. Norman, Y. Luo and H. Ågren, *J. Chem. Phys.* **107**, 9535 (1997).

[46] H. Reis, M. G. Papadopoulos and A. Avramopoulos, *J. Phys. Chem. A* **107**, 3907 (2003).

[47] L. Jensen, M. Sward, P. T. van Duijnen, *J. Chem. Phys.* **122**, 034103 (2005).

[48] E. R. Davidson, B. E. Eichinger, B. H. Robinson, *Opt. Mat.* **29**, 360 (2006).

[49] A. Avramopoulos, M. G. Papadopoulos and H. Reis, *J. Phys. Chem. B* **111**, 2546 (2007).

[50] S. P. Karna and M. Dupuis, *Chem. Phys. Lett.* **171**, 201 (1990).

[51] C. Daniel and M. Dupuis, *Chem. Phys. Lett.* **171**, 209 (1990).

[52] S. P. Karna, P. N. Prasad and M. Dupuis, *J. Chem. Phys.* **94**, 1171 (1990).

[53] H. Ågren, O. Vahtras, H. Kock, P. Jørgensen, T. Helgaker, *J. Chem. Phys.* **98**, 6417 (1992).

[54] M. Stähelin, D. M. Burland and J. E. Rice, *Chem. Phys. Lett.* **191**, 245 (1992).

[55] F. Sim, S. Chin, M. Dupuis and J. E. Rice, *J. Chem. Phys.* **97**, 1158 (1993).

[56] Y. Luo, H. Ågren, O. Vahtras and P. Jørgensen, *Chem. Phys. Lett.* **207**, 190 (1993).

[57] M. Tomonari, N. Ookubo, T. Takada, M. W. Feyereisen and J. Almlöf, *Chem. Phys. Lett.* **203**, 603 (1993).

[58] K. V. Mikkelsen, Y. Luo, H. Ågren and P. Jørgensen, *J. Chem. Phys.* **100**, 8240 (1994).

[59] B. Champagne, *Chem. Phys. Lett.* **261**, 57 (1996).

[60] F. L. Huyskens, P. L. Huyskens and A. P. Persoons, *J. Chem. Phys.* **108**, 8161 (1998).

[61] W. Bartkowiak and T. Misiaszek, *Chem. Phys.* **261**, 353 (2000).

[62] H. H. Heinze, F. D. Sala and A. Görling, *J. Chem. Phys.* **116**, 9624 (2002).

[63] C.-K. Wang and Y.-H. Wang, Y. Su and Y. Luo, *J. Chem. Phys.* **119**, 4409 (2003).

[64] H. Reis, A. Grzybowski and M. G. Papadopoulos, *J. Phys. Chem. A* **109**, 10106 (2005).

[65] M. Y. Balakina and S. E. Nefediev, *Int. J. Quantum Chem.* **106**, 2245 (2006).

[66] M. Y. Balakina and S. E. Nefediev, *Comp. Mat. Sci.* **38**, 467 (2007).

[67] K. Y. Suponitsky, S. Tafur and A. E. Masunov, *J. Chem. Phys.* **129**, 044109 (2008)

[68] J. R. Hammond, K. Kowalski and S. S. Xantheas, unpublished results.

[69] A. W. Lange, M. A. Rohrdanz and J. M. Herbert, *J. Phys. Chem. B* **112**, 6304 (2008); M. A. Rohrdanz and J. M. Herbert, *J. Chem. Phys.* **129**, 034107 (2008); M. A. Rohrdanz, K. M. Martins and J. M. Herbert, *J. Chem. Phys. 130*, 054112 (2009).

[70] J. R. Hammond, B. Roux, N. Govind and K. Kowalski, unpublished results.

CHAPTER 10

CALCULATIONS OF MOLECULAR PROPERTIES IN HYBRID COUPLED-CLUSTER AND MOLECULAR MECHANICS APPROACH

This chapter has been previously published in the following article: J. R. Hammond, M. Valiev, W. A. de Jong and K. Kowalski, "Calculations of properties using a hybrid coupled-cluster and molecular mechanics approach," *J. Phys. Chem. A* **111**, 5492 (2007). Copyright 2007 by the American Chemical Society.

10.1 Introduction

The coupled-cluster (CC) methodology [1, 2, 3, 4, 5, 6, 7, 8, 9] has become one of the most widely used tools in quantum chemistry. Over the last two decades numerous variants and extensions were designed to treat not only the energetics of ground and excited states but also to calculate the molecular properties. In contrast to the finite field approaches based on the numerical differentiation of the electronic energy over external field strength, the CC linear response theory (CC-LR)[10, 11] enables us to obtain expressions for static and/or frequency-dependent properties in a compact analytical manner. Different levels of CC theory corresponding to increasing excitation ranks of cluster operators were tested for first-, second-, third- and higher-order properties. Among them, the linear response CC with singles and doubles (CCSD-LR)[12] and with singles, doubles, and triples (CCSDT-LR)[13] approaches providing

different levels of description of correlation effects now have a chance to be used in realistic calculations. In order to save the big numerical overhead associated with full inclusion of triply excited clusters several iterative methods such as CCSDT-n ($n = 1 - 3$) [14, 15] and CC3 [16] have been tested leading to consistent improvements with respect to the CCSD-LR results. Recently, Kállay and coworkers have implemented general order CC [17] including energy derivatives [18] and response functions [19].

In realistic simulations of molecules in solution, electron correlation effects and the effect of the surrounding environment are equally important. For this purpose, one frequently combines the *ab initio* methodology (QM) with classical molecular mechanics (MM). The QM/MM approach [20] was recently extended by Christiansen and coworkers to include linear response functions for CC wavefunctions, [22] and applied to electric moments [21] and to excited states and polarizabilities [23] of liquid water.

Recently, two of the authors developed an efficient multiscale dynamical framework for high-level calculations of finite temperature ground and excited state properties. [24] We illustrated the performance of this approach on the excited states of cytosine base in the native DNA environment using a variant of completely renormalized equation of motion coupled-cluster formalism with singles, doubles and non-iterative triples (CR-EOM-CCSD(T)) [42] method to describe quantum region. For obvious reason the integration of the CCSD property codes with the QM/MM module is also important. Therefore, in this paper, we discuss preliminary results for the dipole moments and static polarizabilties obtained with combined linear response CCSD and MM approches. As a benchmark system for the CCSD/MM simulation we use the Cl_2O molecule in the CCl_4 solution.

Another problem that may heavily impact future QM/MM simulations of molecular properties is the ability of reducing the overall time required by multiple calls to rather expensive *ab initio* procedures for quantum region. In a long-term perspective, the numerical demands of the CC-like approaches can hamper the widespread use of the CC techniques in the context of QM/MM simulations. Several techniques based on the Laplace or Cholesky decomposition [25, 26, 27, 28] of perturbative denominators, methods striving at the reduction of the virtual orbital space [29, 30], or localized approaches [31, 32, 33, 34] are very promising in this matter. Also other class of approaches based on the extrapolation schemes such as correlation energy extrapolation by intrinsic scaling (CEEIS), [35, 36, 37, 38] or extrapolation approaches for second order energies developed by Ayala, Scuseria, and Savin [39] (for rigorous bounds for extrapolated correlation energies see Ref. [40]) seem to be very effective in attaining good estimates of correlation energies. We have recently proposed an approximate scheme based on the asymptotic extrapolation scheme,[41] which allowed us to extrapolate the excitation energies as a function of simple cut-off factor for orbitals energies of correlated unoccupied orbitals for fraction of time required by full calculations. We clearly demonstrated that for the valence excited states the loss of accuracy was on the order of few hundreds of electron volts. We believe that similar arguments can be used in the CC property calculations. However, before going to large scale QM/MM simulations we want to estimate the effectiveness of the AES using simple gas-phase systems.

The organization of this papers is as follows: in Section 2 we give a brief description of the most basic features of linear response theory and asymptotic extrapolation scheme. In Section 3 we discuss the results of our simulations for Cl_2O molecule in the gas-phase and CCl_4 solution.

10.2 Theory

Coupled-cluster response theory [10, 11, 19] was previously described in Chapter 2 (which is based upon the presentation in the journal article associated with this chapter). Here we describe the asymptotic extrapolation scheme in the calculations of molecular properties. We also give a short description of the QM/MM interface we used in our calculations and AES-related issues.

The symmetric formulation of coupled-cluster linear response (see Chapter 2) was implemented for CCSD in the NWChem [46] software suite using the Tensor Contraction Engine.[49, 50, 51]

10.2.1 Asymptotic extrapolation scheme

The time requirements of CC calculations can be significantly reduced by using asymptotic extrapolation schemes introduced in the context of excited state calculations and described in Ref. [41]. We start from noticing that the whole set of correlated spinorbitals (Ω) can be decomposed into two subsets

$$\Omega = \Omega_\tau + \bar{\Omega}_\tau \ , \tag{10.1}$$

where the Ω_τ and $\bar{\Omega}_\tau$ sets are composed of all correlated occupied spinorbitals and correlated virtual orbitals with corresponding orbital energies below the value of τ factor and all virtual orbitals with orbitals energies being greater than the τ parameter respectively. This decomposition induces decomposition of the algebra of operators expressed in the second quantized formalism. Each of these operators X, representing

for example the Hamiltonian or cluster operators, can be decomposed as follows:

$$X = X_\tau + \bar{X}_\tau \ , \tag{10.2}$$

where X_τ represents part of the X operator expressed in terms of spinorbital indices from the set Ω_τ while each term in $\bar{X}_\tau$ contain at least one index from $\bar{\Omega}_\tau$. This leads to the following form of CC equations:

$$Q_\tau[(H_\tau e^{T_\tau})_C + (\bar{H}_\tau e^{T_\tau+\bar{T}_\tau})_C]|\Phi = 0 \tag{10.3}$$

$$\bar{Q}_\tau[(H_\tau e^{\bar{T}_\tau})_C + (\bar{H}_\tau e^{T_\tau+\bar{T}_\tau})_C]|\Phi\rangle = 0 \tag{10.4}$$

where, Q_τ and $\bar{Q}_\tau$ are projection operators on the manifold of excited configurations used to define components T_τ and $\bar{T}_\tau$ ($T = T_\tau + \bar{T}_\tau$) respectively. The $\bar{H}_\tau$ operator in Eqs.(10.3,10.4) should not be confused with similarity transformed Hamiltonian. Using current notation the $\bar{H}_\tau$ operator refers to the part of second quantized electronic Hamiltonian that contains at least one spinorbital index from $\bar{\Omega}_\tau$. Although both sets of equations labeled by Q_τ and $\bar{Q}_\tau$ projections are coupled with respect to amplitudes defining the T_τ and $\bar{T}_\tau$ components, for sufficiently large values of the τ parameter we can anticipate that the most important correlation effects are already included in T_τ part. This enables us to approximate the Q_τ-equations by $((H_\tau + \bar{H}_\tau)\bar{T}_\tau)_C + (\bar{H}_\tau e^{T_\tau})_C$. For example, the approximate formula for doubly excited $\bar{T}_\tau$ amplitudes then becomes

$$\bar{t}^{ij}_{ab} \simeq \frac{1}{\epsilon_i + \epsilon_j - \epsilon_a - \epsilon_b}\langle\Phi^{ab}_{ij}|(\bar{H}_\tau e^{T_\tau})_C|\Phi\rangle. \tag{10.5}$$

Since the orbital energy differences in Eq.(10.5) are on the order of τ ($\epsilon_i+\epsilon_j-\epsilon_a-\epsilon_b = O(\tau)$) the $\bar{T}_\tau$ amplitudes reveal an $\frac{1}{\tau}$ behavior in the asymptotic limit. This simple observation can be easily generalized to Λ and/or $T^{(1)}$ operators ($\Lambda = \Lambda_\tau+\bar{\Lambda}_\tau$, $T^{(1)} = T^{(1)}_\tau+\bar{T}^{(1)}_\tau$), although the $T^{(1)}$ case requires special attention since the operators (such as the dipole moment), having no obvious interpretation in the language of energy differences, are involved in the equations for $T^{(1)}$.

In analogy to the asymptotic schemes used to extrapolate the excitation energies, the same reasoning can be employed in calculating properties. For example, using the bivariational approach,[47] the expectation value for any one-body operator can be written as

$$\langle\rho\rangle = \langle\Phi|(1+\Lambda_\tau+\bar{\Lambda}_\tau)(e^{-(T_\tau+\bar{T}_\tau)}(\rho_\tau+\bar{\rho}_\tau)e^{T_\tau+\bar{T}_\tau})|\Phi\rangle \tag{10.6}$$

Grouping all terms depending on Ω_τ-label creation/annihilation operators (i.e., the Λ_τ, ρ_τ, and T_τ operators) we can rewrite $\langle\rho\rangle$ as

$$\langle\rho\rangle = \langle\rho_\tau\rangle + \bar{\nu}_\tau \ , \tag{10.7}$$

where $\langle\rho_\tau\rangle = \langle\Phi|(1+\Lambda_\tau)(e^{-T_\tau}\rho_\tau e^{T_\tau})|\Phi\rangle$ and $\bar{\nu}_\tau$ decays at least as $\frac{1}{\tau}$ in the asymptotic limit. It is convenient to exploit formula (10.7) in order to extrapolate to the exact value obtained for a given level of theory using full set of correlated spinorbitals. We will use simple functions such as $f(\tau) = a_1 + \sum_{i=1,n}\frac{a_{i+1}}{\tau^{i+1}}$ to find the best fit to several values of $\langle\rho_\tau\rangle$ obtained in calculations for various values of τ.

Another important issue concerns the size-consistency of the AES results. In the general case, the AES does not have to be rigorously size-consistent, even though the extrapolation is based on the sample points that correctly dissociate in the non-

interacting subsystem limit. Another reason for this can be attributed to the τ-dependence of the basic operators. In calculations for a given τ value the T_τ and $T_\tau^{(1)}$ operators do not have to lead to size-consistent results even though they are obtained from explicitly connected equations (the equations for Λ_τ include some disconnected but linked terms, which in calculating the properties, when the HF reference is employed, are fully contracted to connected operators such as $e^{-T_\tau}\rho_\tau e^{T_\tau}$ leading to connected property-diagrams). In order to arrive at the size-consistency of approximate CC approaches one has to be able to separately localize the set of occupied and unoccupied orbitals in the non-interacting subsystems limit (for exhaustive discussion of related issues see Ref. [48]). Since approaches such as the CCSD, CCSDT, etc. are invariant under the rotations of occupied and unoccupied orbitals this localization does not have to be done explicitely. However, by cutting off all virtual orbitals above some τ threshold we may define virtual Ω_τ space, which in non-interacting subsystems limit cannot be localized. The control of localization properties for all Ω_τ spaces used by AES can be hard to achieve for larger systems. In such cases the rigorous size-consistency may be only approximately restored in the extrapolation process.

10.3 Computational details

All linear response codes as well as the second quantized expressions for static polarizabilities were automatically generated by TCE [49, 50, 51]. Calculations for the Λ_{CCSD} operator and the CCSD dipole moments were performed using code implemented by Hirata [49]. In all codes a new and more efficient way of handling two-electron integrals and related offset-tables was used [52].

Table 10.1: Optimized ground-state energies and geometries obtained with the B3LYP and CCSD(T) approaches using the aug-cc-pVTZ basis set (Cartesian representation of d functions was used in calculations).

Method	Total Energy	R_{O-Cl}	$\alpha_{Cl-O-Cl}$
B3LYP	-995.598665	1.71437	112.60327
CCSD(T)	-994.486282	1.71399	110.84889

In the gas-phase calculations for the Cl_2O molecule we used Sadlej's (POL1) [54] and aug-cc-pVXZ (X=D,T,Q) basis sets [55]. In all calculations all core electrons were kept frozen and Cartesian representation of the angular-momentum functions was used for the POL1 and aug-cc-pVXZ, (X=D,T,Q) basis sets. We optimized ground-state geometry with the B3LYP and CCSD(T) approaches using aug-cc-pVTZ basis set. As seen from Table 10.1, the equilibrium value of R_{O-Cl} is nearly the same for both approaches discussed in the Table 10.1. The more substantial differences occur for the Cl-O-Cl angle. While the CCSD(T) method predicts its value to be 110.849 degree, the B3LYP value is significantly different and equals 112.603 degree. Since the first and second order properties may be sensitive to such geometry changes we decided to use the CCSD(T) equilibrium geometry in all gas-phase calculations presented here (see Tables 10.2 and 10.3).

Table 10.2: Extrapolated values of the CCSD polarizabilities and dipole moment of the Cl_2O molecule obtained with asymptotic extrapolation scheme (AES). Two functions were used in extrapolation $f_1(\tau) = x_1 + \frac{x_2}{\tau}$ and $f_2(\tau) = x_1 + \frac{x_2}{\tau} + \frac{x_3}{\tau^2}$. Versions (A) and (B) refer to five $\{\tau_2, \tau_3, \tau_4, \tau_5, \tau_6\}$ and six points $\{\tau_1, \tau_2, \tau_3, \tau_4, \tau_5, \tau_6\}$ extrapolation schemes, respectively. The aug-cc-pVQZ basis set was used (Cartesian representation of d functions was employed) and all core orbitals were kept frozen. The energy of highest molecular orbital is equal to 226.088907 Hartree.

Property	$\tau_1 = 1.5$	$\tau_2 = 2.0$	$\tau_3 = 2.5$	$\tau_4 = 3.0$	$\tau_5 = 3.5$	$\tau_6 = 4.0$	$f_1^{(A)}$	$f_1^{(B)}$	$f_2^{(A)}$	$f_2^{(B)}$	full CCSD
α_{XX}	53.979	54.046	53.932	54.016	53.977	53.972	53.920	53.970	54.252	53.873	53.457
α_{YY}	29.675	29.725	29.458	29.361	29.318	29.317	28.856	29.052	29.752	28.603	28.646
α_{ZZ}	32.540	32.611	32.472	32.413	32.401	32.383	32.149	32.286	32.573	31.941	31.783
μ	-0.174	-0.183	-0.184	-0.207	-0.206	-0.205	-0.236	-0.228	-0.232	-0.251	-0.237

Table 10.3: The CCSD dipole moments and polarizabilities obtained for the Cl_2O molecule for the LR-CCSD(T),IB equilibrium geometry. All core orbitals were kept frozen.

Basis set	α_{XX}	α_{YY}	α_{ZZ}	$\Delta\alpha$	$\bar{\alpha}$	μ
POL1	53.711	29.167	32.102	23.216	38.327	-0.228
aug-cc-pVDZ	52.364	27.002	30.233	23.911	36.533	-0.223
aug-cc-pVTZ	53.272	28.300	31.479	23.544	37.962	-0.237
aug-cc-pVQZ	53.457	28.646	31.783	23.401	37.462	-0.237

The description of the effect of the environment on the molecular system is an extremely difficult task. Usually this is achieved within combined QM/MM formalism, which requires inclusion of the correlation effects for the quantum region as well as description of interaction between QM and MM parts. The QM/MM formalism has been implemented using CC theory by Christiansen and coworkers [23, 56, 57, 58] including linear response functions, and two of the authors [24] which included a temperature dependent formalism for calculating excitation energies. The QM/MM Hamiltonian used in this work,

$$H = H_{QM} + H_{QM/MM} + H_{MM} \tag{10.8}$$

is optimized including static charges, but the complete linear response function of Christiansen and coworkers [22] has not been used because the QM charge density response is not included (column four in Table I. of Ref. [23]). In the absence of this term, a simple way to increase the accuracy of this approach is to include the first solvation shell within the QM part of the calculation. While this computationally expensive, it is likely to be as accurate, if not more so, than treating the first solvation shell using polarizable force fields with more terms in the response function.

Our system was composed of a Cl_2O embedded in a cubic box in 215 CCl_4 molecules. The quantum region consisted of the Cl_2O molecule with the rest of the system treated at the molecular mechanics level using Amber force field parameters [59]. After the initial QM/MM DFT optimization of the entire system the solvent(CCl_4) was brought to equilibrium over the course of 3.8 ns QM/MM molecular dynamics simulation at constant temperature and pressure (298.15 K,1.025×10^5 Pa) with 15 Å cutoff. During this dynamical run the QM region was represented by a set of fixed effective charges. These were updated approximately every 0.5 ns by means of QM/MM electrostatic potential fitting using DFT/B3LYP level of theory and POL1 basis set [54]. After the solvent equilibration, the entire system was optimized once more using multi-region QM/MM optimization at DFT/B3LYP level of theory. This gave rise to a final structure for the QM/MM coupled-cluster property calculations. Two types of calculations were performed to asses the influence of the solvent. The first one ignored the presence of solvent altogether (gas phase), and the second included all the solvent charges on the system (a total of 1075) using the same geometry structure of the Cl_2O molecule.

10.4 Results

This section is divided into two parts: the first part deals with the effectiveness of AES in calculating molecular properties in the gas-phase using various basis sets, the second part reports the results of our combined CC/MM formalism. Since the Cl_2O has recently attracted a considerable amount of attention and was a subject of experimental studies in the the CCl_4 solution [53] we think it is worthwhile to use our combined CC/MM formalism to model the experimental conditions and es-

timate the effect of the surrounding environment on the dipole moments and static polarizabilities of Cl_2O molecule.

Table 10.2 summarizes our calculations for dipole moments, static polarizabilities, polarizability anisotropy ($\Delta\alpha$), and average polarizability ($\bar{\alpha}$). One can notice that the POL1 results, which was specially designed for molecular properties, are very close to the results obtained with the aug-cc-pVQZ basis set, although the aug-cc-pVQZ basis set is almost three times bigger than the POL1 basis set. For example, the absolute values of discrepancies between POL1 and aug-cc-pVQZ basis set results amount to 0.254, 0.521, and 0.319 a.u. for α_{XX}, α_{YY}, and α_{ZZ}, respectively. The agreement between predicted dipole values is much better. The POL1 and aug-cc-pVQZ differ by only 0.009 a.u. At the same time the differences between the aug-cc-pVDZ (the dimension of the aug-cc-pVDZ basis set (83) is roughly the same as the the dimension of the POL1 basis set (94)) are much larger. The 1.644 a.u. of difference for α_{YY} calculated in aug-cc-pVDZ and aug-cc-pVQZ once again emphasizes the efficiency of the POL1 basis set in describing molecular properties.

The efficiency of the AES can be easily evaluated by analyzing Table 10.3 that summarizes different extrapolation schemes. At the very core of the AES lies the reduction of the overall numerical cost by using possibly small values of the τ parameter. At the same time chosen τ values (or sample points) should be big enough to guarantee the proper asymptotic behaviour of the τ-dependet properties. Sometimes the simultaneous fulfilment of these two conflicting needs may be quite a challenging task. In our studies we used the following values of τ: $\tau_1 = 1.5$, $\tau_2 = 2.0$, $\tau_3 = 2.5$, $\tau_4 = 3.0$, $\tau = 3.5$, and $\tau = 4.0$. For each point the overall cost of the CCSD properties calculations is significantly reduced compared to the full CCSD counterpart. To be more specific, for $\tau_1 = 1.5$ only 87 virtual orbitals are correlated, which results in

about 140-fold speed-up of the CCSD calculations (total number of virtual orbitals is equal to 298), whereas for $\tau_6 = 4.0$, 158 virtual orbitals are used in calculations resulting in almost 13-fold speed-up of the CCSD part. Also the choice of the trial function used for extrapolation plays a critical role. We used two, probably the most rudimentary forms of the trail functions: $f_1(\tau) = x_1 + \frac{x_2}{\tau}$ and $f_1(\tau) = x_1 + \frac{x_2}{\tau} + \frac{x_3}{\tau^2}$ that reflect the asymptotic, $\frac{1}{\tau}$ behaviour of the τ-expansion. In order to explore the impact of low values of τ parameter we decided to employ two sets of τ points. The first set (A) is composed of $[\tau_2, \tau_3, \tau_4, \tau_5, \tau_6]$ while the second set (B) contains all six τ values, i.e., $[\tau_1, \tau_2, \tau_3, \tau_4, \tau_5, \tau_6]$ including τ_1. These choices of the sample points are also consistent with our general observation that contrary to the valence excited states case, [41] in order to get reliable results for molecular properties one has to apply the AES to the sequence of single point calculations corresponding to larger values of the τ parameter. This poorer convergence properties of the AES may be a consequence of the fact that the observables involved in property calculations, such as dipole moments are not directly related to the energy differences, which in turn may lead to slower convergence of corresponding $\frac{1}{\tau}$-expansion.

The results of the $f_1(\tau)$ and $f_2(\tau)$ extrapolations based on (A) and (B) sets of sample points (defining the $f_1(\tau)^{(A)}$, $f_1(\tau)^{(B)}$, $f_2(\tau)^{(A)}$, $f_2(\tau)^{(B)}$ schemes) are collected in Table 10.3. Of all approaches shown in this table, the performance of the $f_2(\tau)^{(B)}$ seems to be the most accurate regarding the achieved accuracies for the polarizabilities. For example, the $f_2(\tau)^{(B)}$ absolute errors with respect to the full CCSD results amount to 0.416, 0.043, and 0.158 a.u. for α_{XX}, α_{YY}, and α_{ZZ}, respectively. By going from the $f_2(\tau)^{(B)}$ scheme to the $f_2(\tau)^{(A)}$ one can clearly demonstrate the importance of the sampling of small τ values in situations when the maximum value of the τ parameter (in our case this is the $\tau_6 = 4.0$ point)

still provides significant reduction of the full CCSD cost. The $f_2(\tau)^{(A)}$ errors are considerably bigger than the $f_2(\tau)^{(B)}$ ones and equal 0.795, 1.106, and 0.790 a.u. for α_{XX}, α_{YY}, and α_{ZZ}, respectively. None of the $f_1(\tau)$ schemes cannot compete with the $f_2(\tau)^{(B)}$ version regarding accuracies for static polarizabilities. The situation is slightly different for dipole moment, which seems to be the best described by the $f_1(\tau)^{(A)}$, $f_1(\tau)^{(B)}$ variants despite of the irregular behaviour of the CCSD dipole moment as a function of τ parameter. The corresponding errors with respect to the full CCSD calculations of 0.001 and 0.009 a.u. respectively. While the polarizabilities values vary monotonically for $\tau \geq 3.0$ (which may be the first indication of working in the $\frac{1}{\tau}$ regime for polarizabilities) the same is not true for dipole moments which reveal oscillatory behaviour in the $[\tau_3, \tau_4, \tau_5]$ interval. For this reason larger values of τ need to be used in order to get more reliable picture. Yet another issue concerns level of theory employed. While in the excited-state calculations the EOM-CCSD excitation energies supplemented with the non-iterative corrections due to triples were the subject of the extrapolation procedures, in the present studies all quantities of interest were obtained on the singles and doubles elvel. Summarizing this part of discussion one should conclude that there is possible to obtain reliable AES results for molecular properties provided that the set of sample points is correctly defined until undesired oscillatory behavior of a given property is eliminated.

As seen from Table 10.4 the effect of the environment is estimated to be rather small. The most prone to external perturbation seems to be the α_{XX} component of polarizability tensor (for simplicity we brought the polarizability tensor to diagonal form). While the corresponding difference between gas-phase (using solution structure) and solution values of α_{XX} amounts to 0.134 a.u., the remaining differences for α_{YY} and α_{ZZ} are significantly smaller and are equal to 0.062 and 0.006 a.u.,

Table 10.4: The CCSD polarizabilities (α_{XX}, α_{YY}, α_{ZZ}), average polarizabilities ($\bar{\alpha}$), and polarizability anisotropy ($\Delta\alpha$) obtained for solution and the gas-phase using POL1 basis set. In all calculations all core electrons were kept frozen and cartesian representation of d orbitals was employed (see text for details). Δ-rows correspond to differences between gas-phase and solution values of corresponding quantities.

environment (geometry)	α_{XX}	α_{YY}	α_{ZZ}	$\bar{\alpha}$	$\Delta\alpha$
solution	55.497	29.247	32.351	39.065	24.785
vacuum (vacuum)	55.705	29.314	32.371	39.130	25.003
vacuum (solution)	55.631	29.309	32.357	39.099	24.939
Δ(vacuum)	0.208	0.067	0.020	0.065	0.218
Δ(solution)	0.134	0.062	0.006	0.034	0.154

respectively. For $\bar{\alpha}$ and $\Delta\alpha$ the shifts are on the order of 0.03 and 0.15 a.u. It is also interesting to analyze the results obtained for the true gas structure. One can immediately see that these results are invariably above the solution structure ones, which is best reflected by comparing the $\Delta(gas.struct.)$ and $\Delta(sol.struct.)$ discrepancies. For example, the α_{XX} component of polarizability tensor reveal the most visible effect due to geometry relaxation on the order of 0.074 a.u. (estimated as a difference between corresponding $\Delta(gas.struct.)$ and $\Delta(sol.struct.)$). Since the correlation effects for the ground state are are rather mild we do not expect triply excited clusters to change these values significantly.

10.5 Conclusions

The effect of CCl_4 solvent on the dipole polarizability of Cl_2O has been computed using a QM/MM approach. It was found that the solvent effects were very small and are less than the basis set dependence of the polarizability. Hence, it would seem that the application of QM/MM to this problem was not necessary and that other factors

Figure 10.1: Schematic representation of the Cl_2O molecule in CCl_4 solution.

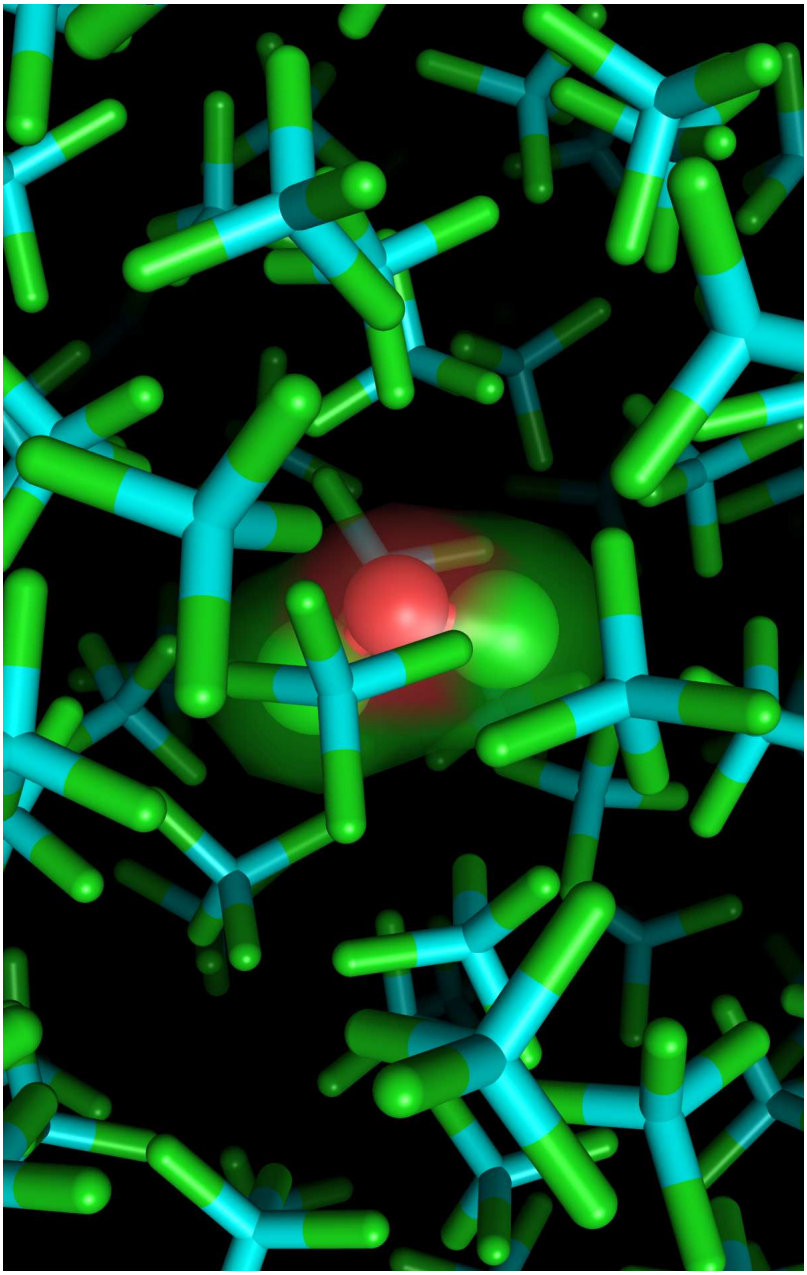

require a more thorough treatment before introducing solvent effects. There are two possibilities to consider: (1) solvent is not important or (2) the QM/MM treatment we chose to use was insufficient to capture the solvent effects happening.

First, it is unlikely that solvent effects in the system under investigation are significantly larger than reported. Tetrachloromethane is a highly-polarizable non-polar solvent whereas oxygen dichloride is less polarizable and has a dipole moment of approximately 0.8 debye (for comparison, water has a dipole moment of $\sim$1.85 debye). A physical principle which frequently leads to enhanced polarization is charge-transfer (CT); in this instance, solvent stabilization or destabilization of the CT state can change the polarizability greatly. This effect is not occurring to any significant degree in our system due to the size and bonding character of oxygen dichloride.

The second issue of whether the QM/MM treatment employed is sufficient for this system is less easily answered. The QM/MM methodology implemented in NWChem is such that the electrostatic interactions between the QM and MM regions of the system are treated at the SCF level. The MM region manifests itself as a collection of point charges surrounding the QM region which perturb the molecular integrals used in the SCF iterations. The orbitals resulting from the SCF procedure are the only means by which the MM region affects the calculation. The CC procedure does not see any partial charges directly, rather it is merely using the orbitals and electron-integrals which know about the partial charges. Another effect which is missing is the polarizability of the solvent itself, since the force field used is a non-polarizable one. The response function used in this work thus excludes terms which couple QM dipoles with MM induced-dipoles as well the interactions between the MM charges and the post-SCF QM charge density. If electron correlation changes the charge density significantly, the latter term will be significant.

For the chemical system considered here, there is no evidence that the terms neglected from the QM/MM response function used are large. However, there are other scenarios where such a treatment will not be sufficient. For example, nonlinear optical properties of large chromophores with significant CT-character (i.e. para-nitroaniline, see Chapter 9) will be problematic, as will any system solvated by water or another polar solvent. Given the importance of solvent in nonlinear optical materials and aqueous chemistry in general, having a QM/MM module which is capable of treating arbitary-order couplings (arbitary-order response densities coupled to arbitrary-order multipoles) is highly desirable. The work presented here is a first step in that direction.

REFERENCES

[1] F. Coester, *Nucl. Phys.* **7**, 421 (1958).

[2] F. Coester and H. Kümmel, *Nucl. Phys.* **17**, 477 (1960).

[3] J. Čížek, *J. Chem. Phys.* **45**, 4256 (1966); J. Čížek and J. Paldus, *Int. J. Quantum Chem.* **5**, 359 (1971).

[4] J. Paldus, J. Čížek and I. Shavitt, *Phys. Rev. A* **5**, 50 (1972).

[5] J. Paldus, in *New Horizons of Quantum Chemistry*, edited by P.-O. Löwdin and B. Pullman (Reidel, Dordrecht, 1983), pp. 31-60; R. J. Bartlett, C. E. Dykstra and J. Paldus, in *Advanced Theories and Computational Approaches to the Electronic Structure of Molecules*, edited by C.E. Dykstra (Reidel, Dordrecht, 1984), pp. 127-159.

[6] R.J. Bartlett, in *Modern Electronic Structure Theory,* edited by D.R. Yarkony (World Scientific, Singapore, 1995), Vol. 1, pp. 1047-1131.

[7] J. Paldus and X. Li, *Adv. Chem. Phys.* **110**, 1 (1999).

[8] T. D. Crawford and H. F. Schaefer III, *Rev. Comp. Chem.* **14**, 33 (2000).

[9] R. J. Bartlett, in *Theory and Applications of Computational Chemistry: The First Forty Years*, edited by C. E. Dykstra, G. Frenking, K. S. Kim and G. E. Scuseria (Elsevier, 2005), pp. 1191-1221.

[10] H. J. Monkhorst, *Int. J. Quantum Chem.* **S11**, 421 (1977); E. Dalgaard and H.J. Monkhorst, Phys. Rev. A **28**, 1217 (1983).

[11] H. Koch and P. Jørgensen, *J. Chem. Phys.* **93**, 3333 (1990); O. Christiansen, C. Hättig and P. Jørgensen, *Int. J. Quantum Chem.* **68**, 1 (1998).

[12] R. Kobayashi, H. Koch and P. Jørgensen, *Chem. Phys. Lett.* **249**, 30 (1994); C. Hättig, O. Christiansen, H. Koch and P. Jørgensen, *Chem. Phys. Lett.* **269**,428 (1997); C. Hättig, O. Christiansen and P. Jørgensen, *Chem. Phys. Lett.* **282**, 139 (1998).

[13] H. Larsen, J. Olsen, C. Hättig, P. Jørgensen, O. Christiansen and J. Gauss, *J. Chem. Phys.* **111**, 1917 (1999).

[14] Y. S.Lee, R. J. Bartlett, *J. Chem. Phys.* **80**, 4371 (1984); Y. S. Lee, S. A. Kucharski, *J. Chem. Phys.* **81**, 5906 (1984).

[15] J. Noga, R. J. Bartlett, M. Urban, *Chem. Phys. Lett.* **134**, 126 (1987).

[16] O. Christiansen, H. Koch and P. Jørgensen, *J. Chem. Phys.* **103**, 7429 (1995); H. Koch, O. Christiansen, P. Jørgensen, A. M. Sanchez de Merás and T. Helgaker, *J. Chem. Phys.* **106**, 1808 (1997); K. Hald, F. Pawłowski, P. Jørgensen and C. Hättig, *J. Chem. Phys.* **118** 1292 (2003).

[17] M. Kállay and P. R. Surján, *J. Chem. Phys.* **115**, 2945 (2001).

[18] M. Kállay, J. Gauss and P. G. Szalay, *J. Chem. Phys.* **119**, 2991 (2003); M. Kállay and J. Gauss, *J. Chem. Phys.* **120**, 6841 (2004); M. Kállay, J. Gauss and P. G. Szalay, *J. Chem. Phys.* **121**, 9257 (2004).

[19] M. Kállay and J. Gauss, *J. Mol. Struct. (THEOCHEM)* **768**, 71 (2006).

[20] J. Noell and K. Morokuma, *Chem. Phys. Lett.* **36**, 465 (1975); A. Warshel and M. Levitt, *J. Mol. Biol.* **103**, 227 (1976); U. C. Singh and P. A. Kollman, *J. Comp. Chem.* **7**, 718 (1986); M. J. Field, P. A. Bash and M. Karplus, *J. Comp. Chem.* **11**, 700 (1990); M. A. Thompson, *J. Phys. Chem.* **100**, 14492 (1996).

[21] J. Kongsted, A. Osted, K. V. Mikkelsen and O. Christiansen, *Chem. Phys. Lett.* **364**, 379 (2002).

[22] J. Kongsted, A. Osted, K. V. Mikkelsen and O. Christiansen, *Mol. Phys.* **100**, 1813 (2002).

[23] J. Kongsted, A. Osted, K. V. Mikkelsen and O. Christiansen, *J. Chem. Phys.* **118**, 1620 (2003).

[24] M. Valiev and K. Kowalski, *J. Chem. Phys.* **125**, 211101 (2006).

[25] J. Almlöf, *Chem. Phys. Lett.* **181**, 319 (1991).

[26] P. Constans, P.Y. Ayala and G.E. Scuseria, *J. Chem. Phys.* **113**, 10451 (2000).

[27] H. Koch, A. Sánches de Merás, *J. Chem. Phys.* **113**, 508 (2000).

[28] H. Koch, A. Sánches de Merás, T.B. Pedersen, *J. Chem. Phys.* **118**, 9481 (2003).

[29] L. Adamowicz and R. J. Bartlett, *J. Chem. Phys.* **86**, 6314 (1987).

[30] L. Adamowicz, R. J. Bartlett, A.J. Sadlej, *J. Chem. Phys.* **88**, 5749 (1988).

[31] M. Schütz, H.-J. Werner, *Chem. Phys. Lett.* **318**, 370 (2000).

[32] M. Schütz, *J. Chem. Phys.* **113**, 9986 (2000).

[33] M. Schütz, *J. Chem. Phys.* **116**, 8772 (2002).

[34] N. Flocke and R. J. Bartlett, *J. Chem. Phys.* **121**,10935 (2004).

[35] L. Bytautas and K. Ruedenberg, *J. Chem. Phys.* **121**, 10905 (2004).

[36] L. Bytautas and K. Ruedenberg, *J. Chem. Phys.* **121**, 10919 (2004).

[37] L. Bytautas and K. Ruedenberg, *J. Chem. Phys.* **121**, 10852 (2004).

[38] L. Bytautas and K. Ruedenberg, *J. Chem. Phys.* **122**, 154110 (2005).

[39] P. Y. Ayala, G. E. Scuseria and A. Savin, *Int. J. Quantum Chem.* **307**, 227 (1999).

[40] S. Iyengar, G. E. Scuseria and A. Savin, *Int. J. Quantum Chem.* **79**, 222 (2000).

[41] K. Kowalski and M. Valiev, *J. Phys. Chem. A* **110**, 13106 (2006).

[42] K. Kowalski and P. Piecuch, *J. Chem. Phys.* **120**, 1715 (2004).

[43] G. D. Purvis, III and R. J. Bartlett, *J. Chem. Phys.* **76**, 1910 (1982).

[44] E. A. Salter, G. W. Trucks and R. J. Bartlett, *J. Chem. Phys.* **90**, 1752 (1989).

[45] P.-O. Löwdin, *J. Mol. Spec.*, **13**, 326 (1964).

[46] E. Aprà, T. L. Windus, T. P. Straatsma, E. J. Bylaska, W. de Jong, K. Kowalski, S. Hirata, M. Valiev, D. Wang, M. T. Hackler, Y. Zhao, R. J. Harrison, M. Dupuis, D. M. A. Smith, J. Nieplocha, V. Tipparaju, M. Krishnan, A. A. Auer, E. Brown, G. Cisneros, G. I. Fann, H. Fruchtl, J. Garza, K. Hirao, R. Kendall, J. A. Nichols, K. Tsemekhman, K. Wolinski, J. Anchell, D. Bernholdt, P. Borowski, T. Clark, D. Clerc, H. Dachsel, M. Deegan, K. Dyall, D. Elwood, E. Glendening, M. Gutowski, A. Hess, J. Jaffe, B. Johnson, J. Ju, R. Kobayashi, R. Kutteh, Z.

Lin, R. Littlefield, X. Long, B. Meng, T. Nakajima, S. Niu, L. Pollack, M. Rosing, G. Sandrone, M. Stave, H. Taylor, G. Thomas, J. van Lenthe, A. Wong and Z. Zhang, *NWChem, A Computational Chemistry Package for Parallel Computers, Version 5.0* (2006), Pacific Northwest National Laboratory, Richland, Washington 99352-0999, USA. A modified version.

[47] J. S. Arponen, *Ann. Phys. 151*, 311 (1983).

[48] K. Jankowski and K. Kowalski, *J. Chem. Phys.* **111**, 2940 (1999).

[49] S. Hirata, *J. Phys. Chem. A 107*, 9887 (2003).

[50] S. Hirata, *J. Chem. Phys. 121*, 51 (2004).

[51] S. Hirata, *Theor. Chem. Acc. 116*, 2 (2006).

[52] K. Kowalski and W. A. de Jong, in preparation.

[53] A. P. Esposito, P. J. Reid, K. W. Rousslang, *J. Photochem. Photobiol.* **129**, 9 (1999).

[54] A. J. Sadlej, *Coll. Czech. Chem. Comm.* **53**, 1995 (1988).

[55] T. H. Dunning Jr., *J. Chem. Phys.* **90**, 1007 (1989); D. E. Woon and T. H. Dunning Jr., *J. Chem. Phys.* **98**, 1358 (1993).

[56] J. Kongsted, A. Osted, K.V. Mikkelsen, P.-O. Åstrand and O. Christiansen, *J. Chem. Phys.* **121**, 8435 (2004).

[57] K. Aidas, J. Kongsted, A. Osted, K. V. Mikkelsen and O. Christiansen, *J. Phys. Chem. A* , **109**, 8001 (2005).

[58] A. Osted, J. Kongsted, K.V. Mikkelsen, P.-O. Åstrand and O. Christiansen, *J. Chem. Phys.* **124**, 124503 (2006).

[59] T. Fox and P.A. Kollman, *J. Phys. Chem. B* **102**, 8070 (1998).

CHAPTER 11

AUTOMATIC TUNING OF MULTIDIMENSIONAL ARRAYS KERNELS USED IN COUPLED-CLUSTER CALCULATIONS

11.1 Introduction

Many numerical algorithms, particularly those of quantum many-body theory, rely heavily upon procedures called tensor contractions. Tensor contractions (TC) are the multi-dimensional generalization of matrix multiplication (MM). Whereas in MM, one has only a single internal (contracted) index and the two external indices of the matrix,

$$C_j^i = \sum_k \; A_k^i \; B_j^k \; , \tag{11.1}$$

a tensor contraction may have an arbitary number of both. One simple example from quantum chemistry is

$$R_{i,j}^{a,b} = \sum_{c,d} \; V_{c,d}^{a,b} \; T_{i,j}^{c,d} \; . \tag{11.2}$$

While Eqn. 11.2 is isomorphic to MM upon fusion of the three pairs of indices, other similar contractions with permuted indices are not. An example of a TC that cannot be performed with MM alone is

$$R_{i,j}^{a,b} = \sum_{k,c} \; \tilde{V}_{c,j}^{k,b} \; T_{i,k}^{a,c} \, , \tag{11.3}$$

presuming that we are utilizing the straightforward layout of these objects in memory. That the objects R and T in Eqns. 11.2 and 11.3 are the same, the best one can do is to choose a layout which is optimal for the most expensive TC and use a sub-optimal ordering for the other. Alternatively, one can change the memory layout sub-optimally-ordered tensors via a transpose-like operation. A much more complex approach is to use Morton-ordering [1] (also known as Z-ordering), or more generally, hierarchical tiling [2], to improve the performance of all tensor contractions, but then it is not possible to use existing implementations of MM, such as BLAS.

The complexity introduced by the transposition of indices in TCs presents a significant challenge to programmers. If one hand-codes procedures which are not MM, then a significant performance loss is incured, as MM kernels are perhaps the most optimized in all numerical computation. Alternatively, one can retain the use of fast MM kernels by realigning the memory layout such that operations like Eqn. 11.3 can be performed with MM.

The transformation of Eqn. 11.3 to a form which is consistent with matrix multi-

plication is as follows:

$$T^{a,c}_{i,k} \rightarrow T1(i,k,a,c) \tag{11.4}$$

$$\tilde{V}^{k,b}_{c,j} \rightarrow V1(c,j,k,b) \tag{11.5}$$

$$R^{a,b}_{i,j} \rightarrow R1(i,j,a,b) \tag{11.6}$$

$$T2(i,a,k,c) = T1(i,k,a,c) \tag{11.7}$$

$$V2((k,b),(c,j)) = V1((c,j),(k,b)) \tag{11.8}$$

$$V3(k,c,b,j) = V2(k,b,c,j) \tag{11.9}$$

$$R2((i,a),(b,j)) = \text{SUM}[(k,c)]\ V3((k,c),(b,j)) * T2((i,a),(k,c)) \tag{11.10}$$

$$R1(i,j,a,b) = R2(i,a,b,j) \tag{11.11}$$

where the matrix dimensions used in the matrix transpose and multiplication calls are denoted with parentheses. Row-major ordering (the last index is stride-1) is presumed throughout. Equations 11.7, 11.9 and 11.11 correspond to tensor transpose (TT) operations. Since matrix transpose is not a standard BLAS operation, Eqn. 11.10 will be treated as another TT. However, when a vendor BLAS library (i.e. IBM's ESSL) contains a matrix transpose procedure, it should be used instead if the performance justifies it.

For a rank-n tensor, there are $n!$ possible permutations of the indices, and writing fast code for each of these procedures by hand is impractical for $n > 4$. The automatic generation of code for these procedures is the subject of this chapter.

11.2 Background

The target application for this project was the coupled-cluster codes within TCE module of the quantum chemistry package NWChem [3]. Because most of the code within the TCE module was written by a code generator, it employs a simple structure which is easily modified. The TCE module also has few, if any, manually optimized procedures and thus suffers in performance with respect to the best hand-written packages. In the particular case of TT, four subroutine calls, `tce_sortN` (`N=2,4,6,8`), were used to perform every associated array permutation. Nearly identical sort-acculuate calls (`tce_sortaccN`, `N=2,4,6,8`) have use the same code except with "`+=`" instead of "`=`". Replacing these procedure with faster ones would result in increased performance throughout the code.

Is it not unreasonable to question the utility of optimizing permutations at all. The permutation of a n-d array requires N^n floating-point operations (flops), where N is the rank of each dimension, whereas contracting an n-d array with an m-d array over k indices requires N^{m+n-k} flops. However, the number of memory operations (mops) required to permute a 4-d array or contract two 4-d arrays over 2 indices is $C{\cdot}N^4$ where C is 2 for permutation (1 read, 1 write) and 3 for contraction (2 reads, 1 write). On modern processors, mops are so expensive that some have said that flops can almost be ignored. MM achieves a large percentage of machine peak by obscuring memory latency through data reuse, which is possible because flops/mops is large. Since the performance of permutations is entirely memory-bandwidth, it is unreasonable to expect a large percentage of peak performance. At the same time, improper implementation of these procedures can be extraordinarily expensive. Unlike MM, the flow of data during permutation is necessarily not optimal since at

least half of the mops will not be stride-1.

If we assume flops are free and that performance is determined by the number and type of mops occuring, then permutation, not MM will be the more expensive procedure of the two. Since theoretical analyses are rarely quantitative, the relative cost of the two procedures has been measured using profiling techniques. Both the GNU profiler gprof [4] and TAU [5] were used to profile the code to ensure correct measurements. TAU profiling results are not reported as they do not differ significantly from those of gprof.

11.3 Results

All results are for a single water molecular at the equilibrium geometry. Calculations were performed without point-group symmetry using spherical angular functions. The tile size for the virtual orbitals (VO) was no greater than 32. For the cc-pVDZ, cc-pVTZ and cc-pVQZ basis sets, there were 2, 4 and 8 VO tiles with average dimension 19, 26.5 and 27.5, respectively. Using a larger tile size favors `dgemm` performance, while smaller favors `tce_sortN`.

11.3.1 Profiling of CCSD within NWChem

First it was established empirically that the tensor transpose operation is a significant portion of the was time, as predicted by the aforementioned theoretical analysis. In Table 11.1, the results of profiling are given for computing the CCSD ground-state energy. When computing the CCSD energy, the coupled-cluster equations (described in previous chapters) are solved iteratively. The energy evaluation two orders less expensive than the iterative procedure and does not contribute significantly to the

Table 11.1: Profile (`gprof`) of the NWChem TCE module CCSD code for computing the ground-state energy.

	Matrix multiplication dgemm		Tensor transpose tce_sort4 & tce_sortacc4	
Basis	Time (s)	% of Total	Time (s)	% of Total
cc-pVDZ	0.40	27.59	1.49	29.65
cc-pVTZ	8.70	30.87	34.15	37.22
cc-pVQZ	154.46	38.54	108.47	27.07

computational cost. The data given in Table 11.1 shows that MM and transpose both contribute significantly to wall time. However, the fraction of the wall time devoted to MM grows with the basis set, so it is not entirely clear that the optimality of the transpose will matter for larger systems. It should be noted that the MM implementation used was from NETLIB. A high-performance BLAS library such as GotoBLAS [6] or ATLAS [7] would greatly decrease the time spent on MM operations.

As should be clear from previous chapters, computating the ground-state energy is but one of many possible tasks for a coupled-cluster code. In Table 11.2, profiling information is given for the evaluation of all steps necessary to compute the hyperpolarizability using the method described in Chapter 8. The number of difficult transposes required for the solution of the $\Lambda^{(0)}$, $T^{(1)}$ and $\Lambda^{(1)}$ equations is significantly larger than required just for $T^{(0)}$, which is affirmed by the data. The relative amount of time spend in the transpose operations is approximately 50% greater than that spent in MM for the cc-pVQZ basis set, and while the overall trend in the basis set is the same as Table 11.1, rate of which MM increases and transpose decrease is much less.

Table 11.2: Profile (`gprof`) of the NWChem TCE module CCSD code for computing the hyperpolarizability.

	dgemm		tce_sort4 & tce_sortacc4	
Basis	Time (s)	% of Total	Time (s)	% of Total
cc-pVDZ	5.78	28.18	11.08	54.03
cc-pVTZ	111.10	28.44	192.45	49.26
cc-pVQZ	1389.05	29.16	2137.17	44.87

11.3.2 Autotuning transpose kernels

It was determined that the primary reason transpose operations are slow is that they access memory in a suboptimal way, that is, strided access rather than sequential (stride-1) access. While it is not possible to eliminate strided access, it is possible to minimize the cost of strided access by rearranging the loops such that the stride distance is minimal. If the stride distance is small enough that cache reuse occurs, a significant performance increase will result.

While it is possible to determine optimal loop ordering using mathematical analysis, a much cruder approach — exhaustive sampling — is sufficient in this case. In addition, sampling includes all possible hardware-specific factors which may not be available for integration into a performance modeling used in the analytic approach. To determine the optimal loop-ordering for the 4-d transpose problem, a code-generator was developed which would produce source code for all possible implementations (24) for each of the 24 transposes, for a total of 576 cases. Source code was generated in both Fortran 77 and ANSI C since the former is known to be more amenable to compiler optimization, while the latter allows a more complete set of compiler pragmas and is the language of choice of people who would further hand-tune these kernels. A master program was instrumented to compile the source

code into binary form using a variety of possible compiler flags to determine the effect of available optimization options. Some of the optimizations sampled for the Intel compilers were loop-unrolling, auto-vectorization and auto-parallelization; compiler pragmas were also explored as a means to explicitly control unrolling and vectorization. The master program built a self-contained binary for each possible transpose which, when executed, performed the timing and printed a complete table of results then identified the optimal loop-ordering. It also prints the compiler flags which were used to generate the code to prevent data rot.

Table 11.3 shows the best improvement obtained with the automatically-generated code as compared to the original implementation within NWChem by So Hirata. Four cases were considered: regular 4-d arrays of rank 20, 32 and 60 plus an irregular array. The speed-up for the rank 20 case is significantly better than the others because both the input and output array (1,250 KB each) fit into cache on the machine tested (Intel Core2Duo, 4 MB L3 cache). For larger dimensions, the arrays do not fit into cache. This clearly indicates that L3 cache-blocking will significantly improve the transpose performance, although finding the optimal code with that additional level of complexity becomes harder. Instead of performing an exhaustive search over just the space of loop-orderings or compiler options, an exhaustive search for the cache-blocking case involves exploring the tensor product space of blocking sizes and loop-orderings for each level of blocking. The dimensionality here is too large to consider by brute force, and a space-pruning algorithm must be employed to make the solution achievable in a reasonable amount of time.

In addition to the 4-d case, exhaustive search was used to find the best implementation of the subset of 6-d transpose-accumulate operations used in CCSD(T). Because of memory constraints imposed by the use triple-excitation amplitudes, dimensions

Table 11.3: Best improvement relative to the original implementation by the ANSI C automatically-generated implementation of the transpose operations for a 4-d array. The Intel 10.1 compiler flags used were `-O3 -xT -march=core2 -mtune=core2 -funroll-loops -align`.

Transpose	20^4	32^4	60^4	irregular
1234	7.250	2.500	1.946	3.769
1243	7.667	2.345	2.257	2.733
1324	5.000	1.828	1.861	2.667
1342	5.250	2.379	2.173	2.923
1423	7.000	2.448	2.272	2.929
1432	5.250	2.000	2.372	3.154
2134	5.250	2.000	1.967	2.583
2143	8.334	2.586	2.108	2.786
2314	5.250	2.000	2.028	2.583
2341	5.000	2.267	2.179	3.000
2413	7.000	2.571	2.390	2.857
2431	5.000	1.889	2.756	3.385
3124	5.250	1.862	1.966	2.538
3142	5.000	3.233	2.216	3.000
3214	5.250	2.143	2.104	2.833
3241	7.000	1.971	2.219	2.571
3412	5.000	1.838	2.208	2.692
3421	6.334	1.976	2.281	2.429
4123	6.333	2.655	2.228	2.875
4132	4.750	1.944	2.202	3.000
4213	5.250	2.821	2.326	2.786
4231	5.250	2.195	2.299	3.077
4312	4.750	1.973	2.120	3.308
4321	4.500	1.767	2.163	3.077

irregular $= 41 \times 17 \times 24 \times 39$

of the arrays are much smaller. Due to the smaller stride length, cache-blocking is less important and the performance improvement realized just by finding the optimal loop-ordering (among $6! = 720$ possibilities) is quite good. The performance improvement realized in preliminary attempts ranges from a factor of 3 to a factor of 12. This is the subject of ongoing research.

11.4 Conclusions

Tensor operations, which compose the overwhelming majority of quantum chemistry codes, require optimal implementations to take advantage of high-performance computers. It was demonstrated that tensors transpose is a significant contribution to the wall time for coupled-cluster calculations and that a very simple approach decrease the time devoted to these operations by a factor of two. The successful approach employed here did not employ cache-blocking or many other possible optimization techniques which will further improve the performance

Ultimately, this project demonstrates that the artificial seperation of transpose and MM in the implementation of tensor contractions is wholly inappropriate. The original motivation for it was to take advantage of vendor-optimized BLAS libraries, but developments in autotuning over the past 10 years clearly indicate that it is possible to generate tensor contraction kernels directly. The advantage is not only with respect to performance, but also in terms of mathematical elegance. The many-body formalism of coupled-cluster theory is multidimensional and flattening the data structures used in such codes into matrices just to use BLAS should not be tolerated.

REFERENCES

[1] G. M. Morton, "A Computer Oriented Geodetic Data Base and a New Technique in File Sequencing," IBM technical report (1966).

[2] L. Carter, J. Ferrante, S. Flynn Hummel, B. Alpern and K.S. Gatlin, UCSD Tech Report CS96-508, November 1996; L. Carter, J. Ferrante and S. Flynn Hummel, *Int. Par. Proc. Symp.*, April 1995; L. Carter, J. Ferrante and S. Flynn Hummel, *SIAM Conf. on Par. Proc. for Sci. Comp.*, February 1995.

[3] E. J. Bylaska, W. A. de Jong, N. Govind, K. Kowalski, T. P. Straatsma, M. Valiev, D. Wang, E. Apra, T. L. Windus, J. Hammond, J. Autschbach, P. Nichols, S. Hirata, M. T. Hackler, Y. Zhao, P.-D. Fan, R. J. Harrison, M. Dupuis, D. M. A. Smith, J. Nieplocha, V. Tipparaju, M. Krishnan, A. Vazquez-Mayagoitia, Q. Wu, T. Van Voorhis, A. A. Auer, M. Nooijen, L. D. Crosby, E. Brown, G. Cisneros, G. I. Fann, H. Fruchtl, J. Garza, K. Hirao, R. Kendall, J. A. Nichols, K. Tsemekhman, K. Wolinski, J. Anchell, D. Bernholdt, P. Borowski, T. Clark, D. Clerc, H. Dachsel, M. Deegan, K. Dyall, D. Elwood, E. Glendening, M. Gutowski, A. Hess, J. Jaffe, B. Johnson, J. Ju, R. Kobayashi, R. Kutteh, Z. Lin, R. Littlefield, X. Long, B. Meng, T. Nakajima, S. Niu, L. Pollack, M. Rosing, G. Sandrone, M. Stave, H. Taylor, G. Thomas, J. van Lenthe, A. Wong and Z. Zhang. "NWChem, A Computational Chemistry Package for Parallel Computers, Version 5.1.1" (2007), Pacific Northwest National Laboratory, Richland, Washington 99352-0999, USA. A modified version.

[4] gprof. Jay Fenlason and Richard Stallman. Copyright 1988, 92, 97, 98, 99, 2000, 2003 Free Software Foundation, Inc.

[5] TAU: The TAU Parallel Performance System. S. Shende and A. D. Malony. *International Journal of High Performance Computing Applications*, Volume 20 Number 2 Summer 2006. Pages 287-331.

[6] `http://www.tacc.utexas.edu/resources/software/`

[7] `http://math-atlas.sourceforge.net/`

CHAPTER 12

CONCLUSIONS

In the previous chapters, a number of applications of coupled-cluster (CC) response theory were presented. These are briefly reviewed here and the overarching themes are highlighted.

In Chapters 3 and 4, the role of electron correlation and basis set were evaluated for the polarizabilities of aromatic hydrocarbons ranging from benzene to C_{60}. For benzene, a relatively modest level of theory — CCSD/aug-cc-pVTZ — was found to reproduce the experimental dynamic polarizability. Exhaustive calibration of the basis set and use of the approximate triples model CC3 validate that this result is "the right answer for the right reason."[1] Based upon the benchmarking of benzene, the CCSD/Sadlej pVTZ model was applied to larger polyacenes and those results compared to DFT. Errors associated with approximate DFT exchange were quantified and explained. Finally, the CCSD approximation in conjunction with a compact but appropriate basis set was applied to the C_{60} fullerene. The CC2 model was found to be inadequate but some DFT methods produced results close to CCSD, which was nearly within the experimental error bars.

One motivation for studying aromatic hydrocarbons is many types of nanostructures have similar chemical properties. Realistic nanostructures cannot be modeled with high-level quantum chemical models but by systematically benchmarking smaller systems, it should be possible to understand what low-level models are appropriate

[1]This quote is frequently attributed to Ernest Davidson.

and how they can be improved. In the case of nanographene and larger fullerenes, the results for polyacenes demonstrate that the role of exchange must be considered carefully. In the polyacene study, PBE0 was the best exchange-correlation functional considered, although the scope of comparative study for DFT was somewhat limited.

The study of water clusters in Chapter 5 was based upon a hierarchy of models; high-level calculations were performed on the monomer and small clusters, while larger systems were treated using the most accurate model possible, CCSD/aug-cc-pVDZ. The basis set dependence seen for water clusters was similar to aromatic hydrocarbons: aug-cc-pVDZ and Sadlej pVTZ are excellent basis sets for the computational cost, while Pople basis sets should not be used for polarizabilities. Where computations were feasible, higher-order correlations in water clusters were found to be non-negligible but also small enough that the use of CCSD for large systems was justified. Of all the DFT approximations considered, PBE0 was the best, having reproduced CCSD quite effectively for polarizabilities and out-performed all other functionals for reproducing CCSD(T) binding energies. However, the most surprising result was that MP2 reproduced CCSD(T) binding energies almost perfectly, which has significant consequences for many aspects of computational modeling of water. The full scope of these is not yet known but will the subject of future research.

A far more exhaustive study of computational models for determining polarizabilities was the subject of Chapter 6. Using the CCSDT model and very large basis sets, it was shown that the experimental polarizability could be reproduced to the available precision. While neon is a very simple system, this result is one affirmation of the underlying hypothesis of quantum chemistry: computation can reproduce experiment when the space of modeling approximations can be exhausted. The second key result of Chapter 6 was that spin-contamination introduced by a UHF reference

can falsely present itself as higher-order correlation. While it is not always necessary (see the case of NO) a spin-pure reference is strongly recommended for computing polarizabilities.

For polarizability computations, two important conclusions emerged: (1) saturating the basis set with CCSD is more useful than higher-order CC methods with limited basis sets, and (2) larger systems ($N_{\mathrm{atom}} \gtrsim 10$) display less basis set dependence than small molecules ($N_{\mathrm{atom}} \lesssim 3$). Chapter 9 was an important test of the generality of these conclusions since hyperpolarizabilies should have more basis set dependence and require a higher-level correlation treatment than polarizabilities. The importance of basis set saturation for small molecules was affirmed for HF and H_2O in the hyperpolarizability study. For PNA, basis set effects were similar to benzene, such that double- and triple-zeta basis sets appear to be sufficiently converged such that further saturation is not necessary until other effects are adequately addressed. Further study is required to understand higher-order correlation, particularly since these effects will be more important for dynamic hyperpolarizabilities, which were not considered.

For numerous examples presented in previous chapters, the modeling approach which combines a hierarchy of correlation models based upon the CC ansatz with the hierarchy of correlation-consistent basis sets developed by Dunning is found to systematically converge to experimentally-determined electric-field properties. That is this approach can now be employed for much larger chemical systems due its parallel implementation within a freely-available software package opens the door for synergy between theory and experiment over a much larger set of problems.

CHAPTER 13

FINAL THOUGHTS

This thesis describes the kind of progress in computational chemistry that can be made when the numerical methods of interest are implemented on supercomputers. Despite advancing the capability of certain quantum chemical methods by at least an order of magnitude, the pace at which computer technology moves provides no opportunity to relish this progress.

In 2003, the fastest computer in world was Earth Simulator in Japan, which was LINPACK-rated at 35.9 teraflops/s, twice that of the second-fastest computer, ASCI Q at Los Alamos National Laboratory. Earth Simulator was displaced from the top spot on the Top500 list [1] by the 71 teraflops/s BlueGene/L at Lawrence Livermore National Laboratory in the fall of 2004. Despite increasing its performance to 596 teraflops/s, BlueGene/L was replaced at the top in the summer of 2008 when Roadrunner at Los Alamos National Laboratory broke the petaflops/s barrier with a LINPACK rating of 1026 teraflops/s. As of November 2008, Earth Simulator is only the 73rd fastest computer in the world and it is arguably the least economical, as it uses over 3 megawatts of electricity, more than all but one other computer on the Top500 list. An even more striking historical comparison is that the fastest computer in the world in 1999, the 2 teraflops/s ASCI Red at Sandia National Laboratory, is rivaled in performance by desktop workstation equipped with two state-of-the-art video cards.

What does this have to do with chemistry? Ground-breaking theoretical advances

(i.e. Jarzynski Inequality [2]) are truly rare but the scope of precise experimental techniques is growing rapidly. Experimental techniques once applied only to small molecules are now used to study complex quantum phenomena in biological systems of tremendous complexity. In order for the synergy between theory (including computation) and experiment to continue, computational chemistry must be able to take advantage of the exponential growth in computing power which has been occurring since the dawn of the computer age. Due to the polynomial but nonlinear cost of accurate quantum chemical methods, even a linear increase in experimentally-treatable systems leads to a hopeless situation in which simulation of experiments takes an ever-increasing amount of time to simulate the same observable quantities. Massively-parallel algorithms effectively turn a supercomputer into a time machine. A petaflops/s computer performs nearly one million times as many operations as a desktop computer over the same period of time. Hence, a simulation which would have otherwise taken 1000 years takes only a day or two if a good parallel algorithm exists.

Assuming the exponential growth in computing power continues, the fastest computer in the world will run at one exaflops/s around my 40th birthday (2021). A parallel trend in commodity computing means that at that time, every scientist will have their own petaflops/s computer, that is, a computer as capable as the two most powerful supercomputers on earth in 2009. All areas of chemistry will be transformed by this level of computing power. State-of-the-art simulations today provide accuracy equal to (and occasionally greater than) experiment for small molecule thermochemistry as well as many electric-field properties. Physical phenomena not directly accessible via accurate experimental techniques can be elucidated by simulation, although widespread application of the necessary methods is not possible due insufficient com-

puter time. The process by which the state-of-the-art techniques of today become the college homework problems of 20 years from now will transform the chemical sciences by providing every laboratory chemist with a computational resource capable of resolving difficult spectra and revealing mechanisms not observable in a test tube.

The transformational impact of ever more powerful computers is not limited to physical chemistry. The same software technology [3] that enabled my coupled-cluster property code also powers a massively-parallel genome-sequencing code [4], despite having very different algorithmic characteristics. While such examples might still seem like the exception rather than the rule, thinking of parallel computation is a special case is completely backwards. In 2009 in the United States, it is effectively impossible to purchase a computer which is not parallel (i.e., serial). Every new computer and video game console runs a multicore processor while standard appliances and automobiles contain processors with significant performance [5, 6]. Multicore processors for cell phones will soon be the norm [7]. Each American possesses in their home enough computing power to solve non-trivial scientific problems. This capability has already been exploited by projects such as SETI [8], BOINC [9], Folding@Home [10] and Einstein@Home [11], which exploit massive arrays of personal computers to solve scientific problems amenable to loosely-coupled parallelism.

As computing power grows in individual machines, and while these simultaneously become more connected, the opportunity to solve important scientific problems increases, but only if scientific algorithms advance as well. It would be tragic if consumer computing technology of the future is still used primarily for social networking and games. While photorealistic video games or Facebook with real-time-video may excite some, the electrical power consumption of such uses of computers can hardly be justified. By most standards, video games and social networking have no lasting

value, while the environmental consequences of electrical power generation by current technology last hundreds of years. In contrast, sequencing ones own genome and searching for genetic indicators of serious diseases using an idle video game console would be a good use of such computing resources since the moral value of preserving human life is not widely disputed. In the event that a disease indicator is discovered, ones laptop, personal digital assistant or cell phone[1] could embark upon a quest to find a high-efficacy, low-toxicity pharmaceutical compound to disable the relevant protein binding site [12].

My vision for the future may seem far-fetched, or at least unrelated to my thesis. However, my linear response property code has already been applied to one aspect of the drug design problem [13] and I began porting NWChem for graphics processors earlier this year. It is my hope that future students in the field of computational science will be just as likely to perform their research with a parent's cell phone or sibling's video game console accessed remotely as it is for them to employ government-owned supercomputers.

The central goal of thesis was to push the frontier of accurate quantum chemical simulation of molecular properties in multiple directions (accuracy, molecule size, time-to-solution) using state-of-the-art supercomputers. In addition to the immediate impact of the chemical data produced, the way in which the data was generated demonstrates facets of two relatively new paradigms in computational chemistry — massive parallelism and automatic code generation — which must soon become normative if chemists are to realize the next-generation of computer technology.

[1] It is unlikely they will be distinct for much longer.

REFERENCES

[1] `http://www.top500.org`.

[2] C. Jarzynski, *Phys. Rev. Lett.* **78**, 2690 (1997).

[3] J. Nieplocha, R. Harrison and R. Littlefield, *J. Supercomputing* **10**, 197 (1996).

[4] C. Oehmen and J. Nieplocha, *IEEE Trans. on Par. and Dist. Sys.*, **17**, 740 (2006).

[5] Because of the rate of growth of semiconductor fabrication capabilities, it is impossible to purchase processors slower than a certain rate, hence the fuel-injection system on a Lexus might only require a 50 KHz chip but a 100 MHz one is used instead because the former is not available and the latter's cost is nominal.

[6] The Intel XScale processor for cell phones circa 2003 (312-MHz CPU and 4MB) was faster than my first computer circa 1993.

[7] "ST-Ericsson Collaborates With ARM to Demonstrate the World's First Symmetric Multi Processing Mobile Platform Technology on Symbian OS," press release (16 February 2009).

[8] E. Korpela, D. Werthimer, D. Anderson, J. Cobb and M. Leboisky, *Comp. Sci. & Eng.* **3** (1), 78 (2001).

[9] D. P. Anderson, *Proc. 5th IEEE/ACM Int. Work. on Grid Comp.*, 4 (2004)

[10] S. M. Larson, C. D. Snow, M. Shirts and V. S. Pande, arXiv:0901.0866v1 (http://arxiv.org/abs/0901.0866).

[11] B. Abbott, et al., *Phys. Rev. D* **79**, 022001 (2009).

[12] D. C. Young, *Computational Drug Design: A Guide for Computational and Medicinal Chemists*, (Wiley, 2009).

[13] J. R. Hammond and J.-F. Truchon, in preparation.

APPENDIX A

SUPPLEMENTAL INFORMATION FOR CHAPTER 6

Most of this numerical data corresponds to the figures in Chapter 6. Additional benchmark results are included for posterity. See Chapter 6 for details.

Table A.1: Complete data for Ne. The frequency is given in Hartrees at the top of each column.

	CCSD				CC3				CCSDT			
Basis	0.0	0.1	0.2	0.3	0.0	0.1	0.2	0.3	0.0	0.1	0.2	0.3
aug-cc-pVDZ	2.003	2.020	2.077	2.187	1.981	1.998	2.053	2.158	1.983	2.000	2.055	2.161
aug-cc-pVTZ	2.433	2.454	2.525	2.661	2.421	2.443	2.512	2.647	2.423	2.445	2.515	2.650
aug-cc-pVQZ	2.598	2.623	2.704	2.860	2.594	2.619	2.700	2.856	2.595	2.621	2.702	2.858
aug-cc-pV5Z	2.643	2.670	2.757	2.927	2.643	2.671	2.758	2.928	2.644	2.671	2.759	2.930
d-aug-cc-pVDZ	2.705	2.735	2.830	3.018	2.676	2.705	2.798	2.978	2.679	2.708	2.801	2.982
d-aug-cc-pVTZ	2.697	2.727	2.823	3.011	2.691	2.721	2.816	3.003	2.693	2.722	2.818	3.006
d-aug-cc-pVQZ	2.679	2.709	2.803	2.989	2.680	2.709	2.804	2.989	2.680	2.710	2.805	2.991
d-aug-cc-pV5Z	2.667	2.696	2.790	2.974	2.670	2.699	2.793	2.978	2.670	2.699	2.794	2.979

Table A.2: Complete data for HF.

Basis	Frequency (a.u.)	CCSD		CC3		CCSDT	
		$\alpha_\perp$	$\alpha_\parallel$	$\alpha_\perp$	$\alpha_\parallel$	$\alpha_\perp$	$\alpha_\parallel$
aug-cc-pVDZ	0.0	4.339	6.283	4.293	6.220	4.296	6.225
	0.1	4.442	6.407	4.392	6.343	4.397	6.348
	0.2	4.833	6.827	4.770	6.755	4.776	6.762
	0.3	6.188	7.732	6.032	7.642	6.053	7.653
aug-cc-pVTZ	0.0	4.901	6.353	4.890	6.328	4.892	6.331
	0.1	5.010	6.479	4.999	6.454	5.002	6.458
	0.2	5.414	6.904	5.402	6.879	5.407	6.884
	0.3	6.689	7.819	6.667	7.795	6.686	7.804
aug-cc-pVQZ	0.0	5.080	6.341	5.088	6.329	5.088	6.332
	0.1	5.195	6.467	5.204	6.456	5.204	6.459
	0.2	5.615	6.889	5.628	6.882	5.630	6.886
	0.3	6.884	7.796	6.911	7.798	6.926	7.805
aug-cc-pV5Z	0.0	5.121	6.329	-	-	-	-
	0.1	5.239	6.455	-	-	-	-
	0.2	5.669	6.876	-	-	-	-
	0.3	6.951	7.779	-	-	-	-
d-aug-cc-pVDZ	0.0	5.288	6.456	5.234	6.396	5.237	6.400
	0.1	5.421	6.588	5.363	6.525	5.366	6.530
	0.2	5.913	7.030	5.838	6.959	5.844	6.966
	0.3	7.478	7.983	7.308	7.895	7.329	7.906
d-aug-cc-pVTZ	0.0	5.255	6.401	5.255	6.378	5.255	6.381
	0.1	5.384	6.530	5.385	6.508	5.385	6.511
	0.2	5.860	6.965	5.861	6.943	5.863	6.948
	0.3	7.312	7.903	7.307	7.884	7.323	7.892
d-aug-cc-pVQZ	0.0	5.197	6.356	5.211	6.344	5.210	6.347
	0.1	5.322	6.483	5.338	6.472	5.337	6.475
	0.2	5.782	6.909	5.803	6.902	5.803	6.906
	0.3	7.157	7.827	7.194	7.829	7.208	7.836
d-aug-cc-pV5Z	0.0	5.171	6.335	-	-	-	-
	0.1	5.295	6.461	-	-	-	-
	0.2	5.747	6.884	-	-	-	-
	0.3	7.092	7.794	-	-	-	-

Table A.3: Complete data for N_2.

Basis	ω (a.u.)	CCSD		CC3		CCSDT	
		$\alpha_\perp$	$\alpha_\parallel$	$\alpha_\perp$	$\alpha_\parallel$	$\alpha_\perp$	$\alpha_\parallel$
aug-cc-pVDZ	0.0	10.003	14.610	10.065	14.910	10.050	14.814
	0.1	10.236	15.004	10.304	15.341	10.293	15.237
	0.2	11.043	16.370	11.132	16.848	11.125	16.711
	0.3	12.933	19.568	13.090	20.448	13.097	20.224
	0.4	18.528	28.957	19.085	31.552	19.243	31.020
aug-cc-pVTZ	0.0	10.126	14.578	10.213	14.860	10.187	14.753
	0.1	10.365	14.965	10.460	15.286	10.434	15.169
	0.2	11.189	16.302	11.315	16.768	11.289	16.612
	0.3	13.089	19.390	13.317	20.279	13.295	20.012
	0.4	18.563	28.141	19.355	30.854	19.434	30.1507
aug-cc-pVQZ	0.0	10.108	14.541	10.2008	14.823	10.179	14.714
	0.1	10.349	14.926	10.459	15.248	10.430	15.128
	0.2	11.180	16.256	11.328	16.728	11.297	16.566
	0.3	13.101	19.320	13.366	20.223	13.337	19.956
	0.4	18.619	27.917	19.529	30.694	19.581	29.961
d-aug-cc-pVDZ	0.0	10.192	14.740	10.274	15.039	10.257	14.944
	0.1	10.440	15.138	10.530	15.475	10.513	15.370
	0.2	11.300	16.515	11.419	16.993	11.403	16.855
	0.3	13.322	19.724	13.532	20.607	13.526	20.378
	0.4	19.508	29.229	20.268	31.873	20.390	31.324
d-aug-cc-pVTZ	0.0	10.153	14.604	10.246	14.888	10.219	14.781
	0.1	10.397	14.994	10.499	15.316	10.471	15.199
	0.2	11.238	16.337	11.376	16.807	11.346	16.650
	0.3	13.193	19.442	13.443	20.336	13.416	20.067
	0.4	18.957	28.282	19.868	31.029	19.920	30.328
d-aug-cc-pVQZ	0.0	10.481	15.831	10.109	14.548	-	-
	0.1	10.694	16.221	10.351	14.935	-	-
	0.2	11.409	17.556	11.185	16.266	-	-
	0.3	12.970	20.553	13.118	19.336	-	-
	0.4	16.877	28.179	18.750	27.969	-	-

Table A.4: Complete data for CO (frozen core).

Basis	ω (a.u.)	CCSD		CC3		CCSDT	
		$\alpha_\perp$	$\alpha_\parallel$	$\alpha_\perp$	$\alpha_\parallel$	$\alpha_\perp$	$\alpha_\parallel$
aug-cc-pVDZ	0.000	11.618	15.820	11.685	15.575	11.663	15.642
	0.100	12.100	16.342	12.194	16.101	12.168	16.169
	0.200	14.169	18.219	14.423	18.006	14.371	18.079
	0.300	32.238	23.164	38.041	23.151	37.489	23.219
aug-cc-pVTZ	0.000	11.825	15.712	11.895	15.506	11.865	15.569
	0.100	12.320	16.224	12.417	16.027	12.380	16.091
	0.200	14.443	18.059	14.700	17.904	14.631	17.970
	0.300	35.318	22.807	43.023	22.890	41.944	22.940
aug-cc-pVQZ	0.000	11.832	15.639	11.908	15.444	11.877	15.509
	0.100	12.330	16.148	-	-	12.396	16.028
	0.200	14.468	17.967	-	-	-	-
	0.300	35.959	22.650	-	-	-	-
aug-cc-pV5Z	0.000	11.819	15.604	-	-	-	-
	0.072	12.068	15.861	-	-	-	-
d-aug-cc-pVDZ	0.000	11.913	15.907	11.980	15.668	11.959	15.734
	0.100	12.415	16.435	12.509	16.201	12.483	16.268
	0.200	14.555	18.334	14.810	18.129	14.759	18.201
	0.300	33.072	23.333	39.112	23.337	-	-
d-aug-cc-pVTZ	0.000	11.877	15.718	11.951	15.516	11.919	15.579
	0.100	12.377	16.234	-	-	12.441	16.104
	0.200	14.523	18.078	-	-	14.717	17.992
	0.300	35.661	22.850	-	-	-	-
d-aug-cc-pVQZ	0.000	11.838	15.634	-	-	-	-
	0.100	12.338	16.143	-	-	-	-
	0.200	14.482	17.964	-	-	-	-
	0.300	36.078	22.651	-	-	-	-
d-aug-cc-pV5Z	0.000	11.823	15.604	-	-	-	-
	0.072	12.072	15.861	-	-	-	-

Table A.5: Complete data for CN (frozen core).

	ROHF Reference				UHF Reference			
	CCSD		CCSDT		CCSD		CCSDT	
ω (a.u.)	$\alpha_\perp$	$\alpha_\parallel$	$\alpha_\perp$	$\alpha_\parallel$	$\alpha_\perp$	$\alpha_\parallel$	$\alpha_\perp$	$\alpha_\parallel$
d-aug-cc-pVDZ								
0.00	16.319	26.398	16.304	26.349	15.878	25.587	16.211	26.267
0.01	16.472	26.458	16.448	26.412	15.982	25.637	16.346	26.329
0.02	17.017	26.641	16.957	26.605	16.335	25.789	16.821	26.520
0.03	18.377	26.963	18.207	26.944	17.118	26.056	17.965	26.852
0.04	22.851	27.449	22.128	27.460	18.994	26.454	21.364	27.358
d-aug-cc-pVTZ								
0.00	16.355	26.127	16.311	26.163	15.821	25.249	16.208	26.081
0.01	16.518	26.185	16.466	26.226	15.924	25.297	16.352	26.141
0.02	17.103	26.366	17.019	26.419	16.274	25.444	16.864	26.330
0.03	18.598	26.681	18.420	26.758	17.050	25.700	-	-
0.04	23.913	27.157	-	27.274	18.910	26.082	-	-
d-aug-cc-pVQZ								
0.00	16.305	25.963	-	-	15.795	24.598	-	-
0.01	16.466	26.021	-	-	15.965	25.403	-	-
0.02	17.043	26.197	-	-	16.336	24.854	-	-
0.03	18.512	26.507	-	-	17.179	25.796	-	-
0.04	23.653	26.973	-	-	18.476	25.989	-	-

Table A.6: Complete data for NO (frozen core). When a basis set is listed instead of a frequency, $\omega = 0.0$ and the given basis set was employed for subsequent dynamic calculations. The basis sets aug-cc-pVXZ and d-aug-cc-pVXZ are abbreviated aXZ and daXZ, respectively.

Basis/	ROHF Reference				UHF Reference			
	CCSD		CCSDT		CCSD		CCSDT	
ω (a.u.)	$\alpha_\perp$	$\alpha_\parallel$	$\alpha_\perp$	$\alpha_\parallel$	$\alpha_\perp$	$\alpha_\parallel$	$\alpha_\perp$	$\alpha_\parallel$
aDZ	9.123	15.096	9.153	14.944	9.118	15.073	9.152	14.942
0.050	9.186	15.239	9.219	15.088	9.181	15.215	9.218	15.085
0.100	9.391	15.704	9.433	15.555	9.385	15.677	9.432	15.552
0.150	9.802	16.641	9.867	16.498	9.794	16.604	9.866	16.494
aTZ	9.508	15.155	9.558	15.026	9.502	15.131	9.556	15.023
0.050	9.574	15.293	9.627	15.166	9.568	15.268	-	-
0.100	9.787	15.741	9.850	15.622	9.779	15.713	-	-
0.150	10.206	16.633	10.296	16.532	10.196	16.595	-	-
aQZ	9.600	15.174	-	-	-	-	-	-
0.050	9.669	15.312	-	-	-	-	-	-
0.100	9.889	15.759	-	-	-	-	-	-
0.150	10.324	16.646	-	-	-	-	-	-
a5Z	9.753	15.644	-	-	-	-	-	-
0.072	9.919	16.054	-	-	-	-	-	-
a6Z	9.609	15.172	-	-	-	-	-	-
0.072	9.756	15.465	-	-	-	-	-	-
daDZ	9.844	15.546	9.892	15.408	9.835	15.521	9.891	15.406
0.050	9.922	15.699	9.973	15.562	9.913	15.673	9.972	15.560
0.100	10.177	16.199	10.240	16.067	10.166	16.169	10.238	16.064
0.150	10.707	17.228	10.803	17.108	10.690	17.188	10.800	17.103
daTZ	9.707	15.319	-	-	9.699	15.295	-	-
0.050	9.780	15.463	-	-	9.771	15.437	-	-
0.100	10.016	15.929	-	-	10.006	15.899	-	-
0.150	10.493	16.863	-	-	10.479	16.823	-	-
daQZ	9.656	15.226	-	-	-	-	-	-
0.050	9.727	15.367	-	-	-	-	-	-
0.100	9.958	15.822	-	-	-	-	-	-
0.150	10.421	16.730	-	-	-	-	-	-
da5Z	9.607	15.508	-	-	-	-	-	-
0.072	9.752	15.840	-	-	-	-	-	-
da6Z	9.630	14.761	-	-	-	-	-	-
0.072	9.783	15.049	-	-	-	-	-	-

Table A.7: Complete data for O_2 (frozen core).

	ROHF Reference				UHF Reference			
	CCSD		CCSDT		CCSD		CCSDT	
Frequency	$\alpha_\perp$	$\alpha_\parallel$	$\alpha_\perp$	$\alpha_\parallel$	$\alpha_\perp$	$\alpha_\parallel$	$\alpha_\perp$	$\alpha_\parallel$
aug-cc-pVDZ								
0.000	7.531	15.035	7.520	15.121	7.532	15.021	7.521	15.115
0.100	7.665	15.746	7.656	15.888	7.667	15.732	7.656	15.881
0.200	8.141	18.936	8.135	19.435	8.142	18.918	8.135	19.423
aug-cc-pVTZ								
0.000	8.038	15.192	8.050	15.234	8.040	15.177	8.050	15.228
0.100	8.188	15.894	8.203	15.983	8.190	15.878	8.203	15.977
0.200	8.714	19.034	8.740	19.429	8.714	19.012	8.740	19.419
aug-cc-pVQZ								
0.000	8.171	15.245	8.197	15.271	-	-	-	-
0.100	8.332	15.947	-	-	-	-	-	-
0.200	8.892	19.079	-	-	-	-	-	-
aug-cc-pV5Z								
0.000	8.173	15.247	-	-	-	-	-	-
0.100	8.336	15.950	-	-	-	-	-	-
0.200	8.908	19.075	-	-	-	-	-	-
aug-cc-pV6Z								
0.000	8.172	15.249	-	-	-	-	-	-
d-aug-cc-pVDZ								
0.000	8.349	15.520	8.354	15.599	8.352	15.505	8.354	15.593
0.100	8.527	16.251	8.533	16.385	8.530	16.235	8.534	16.378
0.200	9.163	19.524	9.177	20.016	9.166	19.503	9.177	20.0003
d-aug-cc-pVTZ								
0.000	8.257	15.380	8.284	15.424	8.260	15.364	8.285	15.418
0.100	8.429	16.094	8.460	16.186	8.431	16.077	8.460	16.179
0.200	9.036	19.280	9.084	19.678	9.037	19.257	9.083	19.667
d-aug-cc-pVQZ								
0.000	8.216	15.296	-	-	-	-	-	-
0.100	8.385	16.004	-	-	-	-	-	-
0.200	8.980	19.156	-	-	-	-	-	-
d-aug-cc-pV5Z								
0.000	8.191	15.270	-	-	-	-	-	-
0.100	8.358	15.975	-	-	-	-	-	-
0.200	8.948	19.112	-	-	-	-	-	-

APPENDIX B

SUPPLEMENTAL INFORMATION FOR CHAPTER 9

The following data was not included in Chapter 9 nor in the submitted version of the corresponding journal article. It is included here for posterity. See Chapter 9 for details.

Table B.1: Electric properties of HF at the CCSD level using various basis sets (spherical, frozen core). All quantities are given in atomic units.

Basis	Rank	μ_z	α_{xx}	α_{zz}	β_{xxz}	β_{zzz}	$\beta_{\parallel}$
Roos ANO DZ	32	0.713	4.634	6.369	2.761	15.678	12.721
Roos ANO TZ	69	0.706	5.054	6.407	1.555	11.802	8.947
aug-cc-pVDZ	32	0.703	4.339	6.283	1.706	12.144	9.333
aug-cc-pVTZ	69	0.706	4.908	6.360	2.393	11.589	9.825
aug-cc-pVQZ	126	0.709	5.094	6.355	1.972	10.501	8.667
aug-cc-pV5Z	207	0.710	5.139	6.347	1.886	10.100	8.323
aug-cc-pV6Z	316	0.711	5.158	6.343	1.870	9.952	8.215
d-aug-cc-pVDZ	45	0.701	5.288	6.457	0.687	8.632	6.004
d-aug-cc-pVTZ	94	0.705	5.263	6.409	1.520	9.771	7.687
d-aug-cc-pVQZ	167	0.709	5.212	6.369	1.581	9.774	7.761
d-aug-cc-pV5Z	268	0.710	5.190	6.352	1.601	9.794	7.797
d-aug-cc-pV6Z	401	0.711	5.181	6.346	1.607	9.785	7.800
t-aug-cc-pVDZ	58	0.702	5.306	6.444	0.783	8.931	6.298
t-aug-cc-pVTZ	119	0.705	5.261	6.418	1.695	9.857	7.948
t-aug-cc-pVQZ	208	0.709	5.211	6.371	1.676	9.790	7.886
t-aug-cc-pV5Z	329	0.710	5.189	6.353	1.628	9.786	7.825
t-aug-cc-pV6Z	486	0.711	5.181	6.346	1.616	9.785	7.810
q-aug-cc-pVDZ	71	0.702	5.307	6.440	0.825	9.033	6.410
q-aug-cc-pVTZ	144	0.705	5.261	6.419	1.716	9.825	7.955
q-aug-cc-pVQZ	249	0.709	5.211	6.372	1.652	9.807	7.867
q-aug-cc-pV5Z	390	0.710	5.189	6.353	1.619	9.798	7.822

$R_{HF} = 1.7328795$ bohr

TITLE: Coupled-cluster response theory: parallel algorithms and novel applications

NAME: Jeffrey Richard Hammond

ADVISOR: Dr. Karl F. Freed, Henry J. Gale Distinguished Service Professor of Chemistry, The University of Chicago

COMMITTEE MEMBERS: Dr. Aaron Reuven Dinner, Assistant Professor of Chemistry, The University of Chicago; Dr. Gregory Steven Engel, Assistant Professor of Chemistry, The University of Chicago; Dr. Karol Kowalski, Senior Research Scientist, Pacific Northwest National Laboratory.

ABSTRACT

The parallel implementation of coupled-cluster response theory within NWChem and its subsequent application to novel chemical problems is reported. Linear-response dipole polarizabilities of polyacenes, the 60-carbon buckyball, and larger water clusters were computed with coupled-cluster singles and doubles (CCSD) and compared to density-functional results. The complete treatment of coupled-cluster response theory including up to triples (CCSDT) was applied to diatomic molecules using large basis sets and this method was used to evaluate a newly-developed perturbative approximation for triples. Hyperpolarizabilities and Lennard-Jones coefficients were implemented at the CCSD level of theory by extending the linear response code in two different ways. Benchmark hyperpolarizabilities are reported for molecules as large as para-nitroaniline using large basis sets. Tensor transpose algorithms are shown to

be an important component in a coupled-cluster property code and automatic code generation successfully identified faster algorithms for these.